Ultraviolet Radiation Exposure in Cannabis Farms

Maximilian J. Chmielinski

A dissertation
submitted in partial fulfillment of the
requirements for the degree of

Doctor of Philosophy

University of Washington

2023

Reading Committee:
Christopher Simpson, Chair
Michael Yost
Martin Cohen

Program Authorized to Offer Degree:

Environmental and Occupational Health Sciences

University of Washington

Abstract

Ultraviolet Radiation Exposure in Cannabis Farms

Maximilian J. Chmielinski

Chair of Supervisory Committee:

Dr. Christopher Simpson

Department of Environmental and Occupational Health Sciences

Laws permitting growth and possession of cannabis for medicinal and recreational use are currently changing rapidly in the United States (U.S.) and internationally (Carliner *et al.*, 2017; Caulkins *et al.*, 2018; Mahamad and Hammond, 2019). While cultivation and use of cannabis is still considered illegal by the U.S. federal government, multiple U.S. states have passed laws legalizing recreational or medical use of marijuana (Carliner *et al.*, 2017). Canada has also recently legalized cannabis (Mahamad and Hammond, 2019). These changes have led to a dramatic expansion of the legal cannabis industry, which now employs approximately 420,000 workers in U.S., and job-growth is among the fastest of any industry in the U.S. (Borchardt, 2017; Barcott *et al.*, 2022). The scale and growth of the industry stands in juxtaposition with federal laws that continue to criminalize cannabis farming, and the contrast impacts the occupational health of a large, novel, and growing group of agricultural workers. A direct impact of cannabis criminalization is the lack of research that has investigated the occupational hazards faced by workers in this emerging industry (Simpson, 2017).

Many cannabis farms grow their crop using artificial lighting, the sun, or a combination of both throughout a crop cycle. The lamps used may emit ultraviolet radiation (UV), and UV overexposure causes a range of negative health outcomes (IARC, 2012). Currently, no studies have investigated UV overexposure in this industry, with most existing publications still limited to exploratory overviews of potential occupational hazards (Martyny *et al.*, 2013; CDPHE, 2017, 2019). However, research investigating specific occupational hazards has begun to trickle into the literature, with some investigated occupational topics including exposure to mold (Green *et al.*, 2018; Couch, Burton, Victory, Green, Lemons, Nayak and Donald H Beezhold, 2019) and exposure to particulate matter and volatile organic compounds (Silvey *et al.*, 2020).

In this thesis, we address three issues related to UV exposure in cannabis farms. In chapter 2 – we summarize measurements of UV exposure in five cannabis farms, including indoor, outdoor and shade house facilities. Lamp emission testing was performed at each facility and worker exposures to UV radiation (UVR) was measured for 87 work-shifts. Observations of worker activities and use of personal protective equipment in association with the UVR exposure measurements were recorded. For lamp emission measurements, at three feet from the center of the lamp in the 180 to 400nm range, the average irradiances were $4.09x10^{-4}$, $6.95x10^{-8}$, $6.76x10^{-9}$, $3.96x10^{-9}$, $1.98x10^{-9}$ effective W/cm^2 for germicidal lamps, metal halide lamps, high pressure sodium lamps, fluorescent lamps, and light emitting diodes, respectively. The average UVR exposure measured on the workers was $2.91x10^{-3}$ effective J/cm^2 (range: $1.54x10^{-6}$, $1.57x10^{-2}$ effective J/cm^2). Thirty percent of the work-shifts monitored exceeded the American Conference for Governmental Industrial Hygienists threshold limit value of 0.003 effective J/cm^2. Exposures were highest for workers who spent all or part of their work-shift outdoors, and solar radiation was the primary source of the workers' UVR exposure for most of the work-shifts that exceeded the threshold limit values. Outdoor workers can reduce their UVR

exposures by wearing appropriate personal protective equipment. Although the artificial lighting used in the cannabis production facilities included in this study did not contribute substantially to the measured UV exposures, in many cases the lamp emissions would generate theoretical exposures at three feet from the center of the lamp that would exceed the TLV. Therefore, employers should choose low UVR emitting lamps for indoor grow operations and should use engineering controls (e.g., door-interlocks to de-energize lamps) to prevent worker exposure to UVR from germicidal lamps.

In chapter 3 we developed a wearable spectroradiometer to address the limitation of spectral mismatch inherent in all available broadband dosimeters. We developed a microcontroller system and platform that allows for researchers to mount and deploy the Ocean Insight Flame-S Spectroradiometer as a wearable device for measurement of UV and visible wavelengths (300 to 700 nm). The platform validation consisted of comparing measurements from a solar simulator at three different intensities taken under platform control with measurements taken with the spectrometer controlled by a personal computer running the software provided by the spectroradiometer manufacturer. Three Mann–Whitney U-Tests (two-tailed, 95% CI), one for each intensity condition, compared the central tendency between the total spectral power (TSP), the integral of a spectrum measurement, measured under both control schemas. An additional analysis of per pixel agreement and overall platform stability was performed. The three Mann–Whitney tests returned no significant difference between the set of TSPs for each filter condition. These results demonstrate that the spectroradiometer takes measurements of equivalent accuracy under both control schemas and can be deployed as a wearable device for the measurement of wavelength resolved UV and visible radiation.

In Chapter 4 we developed and evaluated a vegetative radiative transfer model (VRTM) for predicting worker exposure to non-ionizing radiation – as a surrogate for exposure to UV radiation - in an indoor

cannabis farm. The model uses morphological characteristics of the crop, manufacturer provided lamp emissions data, and dimensional measurements of the grow room and hedgerows to predict irradiance. A linear regression comparing model predictions with the measurements taken by a visible light spectroradiometer had slopes within 23% of unity and R^2 values above 0.88 for visible (400 to 700nm), blue (400 to 500nm), green (500 to 600nm), and red (600 to 700nm) wavelength bands. The excellent agreement between the model and the measured irradiance in the cannabis farm grow room supports the potential of using VRTMs to predict irradiance and worker exposure in agricultural settings. Because there is no mechanistic difference between visible and other non-ionizing wavelengths of radiation in regards to mechanisms of radiative transfer, the model developed herein for visible wavelengths of radiation should be generalizable to other radiation bands including infrared and UVR.

Contents

Chapter 1

A. Background

A.1. Fundamental Principles

Ultraviolet radiation (UVR) or 'broadband' UVR is optical radiation that occupies the 100 - 400 nm wavelengths of the electromagnetic spectrum. UVR is further subdivided into UVA (315 - 400 nm), UVB (280 - 315 nm), and UVC (100 - 280 nm). Upon exposure, these three subdivisions of UVR differentially affect human health, with exposure to UVC causing the most rapid onset of skin and eye damage. However, solar UVB is the most common cause of most UVR induced injuries because UVB can readily permeate through the atmosphere, whereas solar UVC cannot. Broadband UV power per unit area is properly referred to as 'irradiance' and UVR energy (the time-integral of irradiance) is referred to as 'radiant energy' (IARC, 2012).

A.2. Non-Ionizing Radiation Sources in Agriculture

A.2.a. Solar Radiation

The American Society for Testing and Materials (ASTM) publishes the extraterrestrial solar spectrum as standard E490 (ASTM, 2014). This spectrum is based on data from satellites, space shuttle missions, high-altitude aircraft, rocket soundings, ground-based solar telescopes, and modeled spectral irradiance. The Upper Atmosphere Research Satellite (UARS)/ATLAS-2 spectral measurements form the basis for the ASTM spectrum between 119.5 and 379.5 nm. The UARS spectrum values are averages from two different instruments: the Solar Ultraviolet Spectral Irradiance Monitor (SUSIM) and the Solar Stellar Irradiance Comparison Experiment (SOLSTICE) (Woods *et al.*, 1996). These data were obtained in April 1993 during a period of moderate solar activity and were scaled by a factor of 0.96843 to match spectrum data published by Neckel *et al.* (1984) over the 330 to 410 nm range.

The ASTM standard presents the solar spectral irradiance in tabular form for wavelengths between 119.5 nm to 1000000 nm, and Figure A-1 presents a graph of the published values in the UV range.

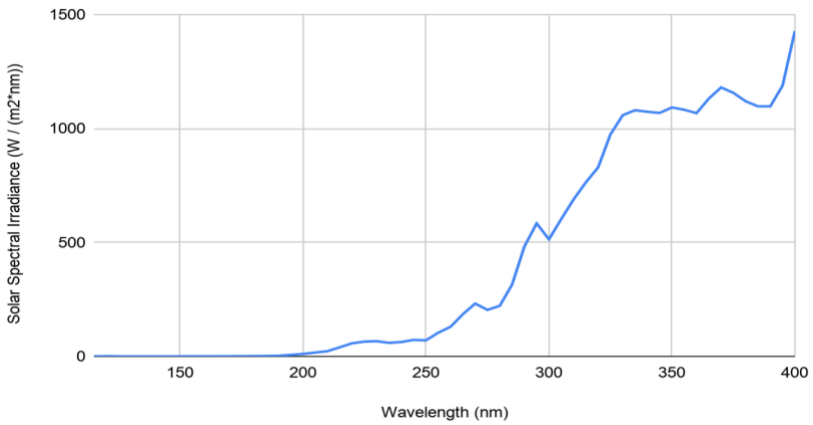

Figure A-1 The ASTM E490 (ASTM, 2014) *solar spectrum below 400 nm.*

The total irradiance uncertainty in the SUSIM spectral measurements for the 180 to 410 nm range was 5.3%. The SOLSTICE device used three spectrometer channels to measure the solar spectrum between 119 to 420 nm. The middle UV channel measured the range between 170 to 320 nm (resolution = 0.2 nm) and had an irradiance measurement uncertainty of 5.7%. The near UV channel measured the range between 280 to 420 nm an irradiance uncertainty of 7.9% (Woods *et al.*, 1996).

The solar spectrum variability is dependent on wavelength and period of interest. Solar irradiance research has typically structured monitoring periods to match the 27-day solar rotational period or the 11-year solar cycle. The magnitude of the 27-day solar rotational variability is usually no more than one third of the solar cycle variability. Observations of solar cycle 22 (1986-1996) are the basis for creating reference spectra of the solar UV irradiance for use in comparative aeronomic studies. From these reference spectra, the solar cycle variability at wavelengths above 160 nm is 15% or less (Woods and Rottman, 2002).

Atmospheric Gas Interaction

As UV passes through earth's atmosphere, it is subject to many absorption and scattering processes. Stratospheric oxygen and ozone absorb all UVC radiation and prevent it from reaching earth's surface. Stratospheric ozone differentially absorbs wavelengths of UVB, with the highest absorption at shorter wavelengths. The consequence of radiation absorption by ozone is that less than 3% of erythemal radiation reaches the earth's surface (Kerr and Fioletov, 2008) (Refer to section A.4.d for definition of erythemal radiation).

Other naturally occurring absorbers of UVB radiation include sulfur dioxide (SO_2) and nitrogen dioxide (NO_2). Large volcanic eruptions emit enough SO_2 to cause significant absorption, up to 50%, of erythemal UV radiation (Krueger *et al.*, 1995). Forest fires are also a source of SO_2 and NO_2. However, any elevated levels of SO_2 or NO_2 from these natural sources are generally short-lived and not widespread (Fioletov *et al.*, 1998). NO_2 also occurs naturally in the stratosphere (Brewer, Mcelroy and Kerr, 1973; Noxon, 1975), but absorption of erythemal UV radiation by stratospheric NO_2 is negligible (<1%) (Kerr and Fioletov, 2008).

Anthropomorphically generated gases that absorb UV include ozone, NO_2, SO_2, chlorine compounds, bromine compounds, and volatile organic compounds. Anthropomorphically generated gases seldom

reach concentrations necessary to cause a discernible effect on UV irradiance at the earth's surface, however, detectable effects may occur near emission sources such as in urban areas (Koronakis *et al.*, 2002; Chubarova *et al.*, 2011).

Solar Zenith Angle

An increasing solar zenith angle (sza) decreases the UV irradiance at earth's surface because the surface UV is proportional to the cosine of the sza and because a large sza increases the length of the atmospheric optical pathway. A long optical pathway increases the spatial contact between the UV and atmospheric gases, thus increasing the total atmospheric absorption of UV (Kerr and Fioletov, 2008).

Molecular Effects

Rayleigh scattering is the scattering of radiation by molecules smaller than the wavelength of the radiation. The amount of Rayleigh scattering depends on wavelength, and there is considerably more Rayleigh scattering at shorter wavelengths. Consequently, the ratio of diffuse (scattered) to direct UV is larger in the UVB than in UVA (Kerr and Fioletov, 2008).

Aerosols

Aerosols originate from natural and anthropomorphic sources. Natural causes include volcanoes (Kerr and Fioletov, 2008), forest fires (Fioletov *et al.*, 2001) and deserts (di Sarra *et al.*, 2002). Manufactured sources include emissions from power plants, factories, biomass burning (Kirchhoff *et al.*, 2001), automobiles, and aircraft (Kerr and Fioletov, 2008). Aerosols in the atmosphere cause UV scattering and absorption. The wavelength dependence and angular distribution of scattering depend on the shape, size distribution, refractive index, and physical state of the suspended particles. Absorption processes depend on the chemical and physical properties of the particles. Notable aerosols include black carbon, sulfates, nitrates, and mineral dust. Black carbon originates from virtually all combustion processes and has large scattering and absorption effects. In contrast to black carbon's absorption effect, the aerosols of nitrates, mineral dust, and sulfates primarily have a scattering effect on solar radiation (Dickerson, Stenchikov and Civerolo, 1997).

Clouds

UV absorption and scatter due to clouds is highly variable, and depends on cloud thickness, height, composition, and homogeneity. Heavy cumulonimbus clouds can reduce surface UV irradiance by as much as 95% (Fioletov *et al.*, 2010). Overcast conditions always reduce surface UVR (Josefsson and Landelius, 2000) and partly cloudy conditions reduce surface UVR if they obscure the sun (Schwander *et al.*, 2002). However, partly cloudy conditions where the sun is not obscured may increase the surface UV by as much as 25% due to an increase in the diffuse component of total UV radiation (Sabburg and Wong, 2000).

A.2.b. Supplemental and Artificial Lighting

Growing plants indoors use a wide array of optical sources including incandescent lamps (INC), high-pressure sodium lamps (HPS), metal halide lamps (MH), fluorescent lamps (FL), including compact fluorescent lamps (CFL), and light emitting diodes (LEDs). The selection of an appropriate supplemental light source depends on the spectral distribution, intensity, energy efficiency, expected lifetime, annual hours of operation, and operational costs (Kozai, Fujiwara and Runkle, 2016).

Farms inside warehouses rely exclusively on artificial lighting from lamps to provide the energy needed for plant photosynthesis. Farms in greenhouses primarily utilize lamps to provide supplemental lighting to increase crop production during periods of low solar radiation. This is especially true at high latitudes, during darker months of the year and on overcast days, because the amount of solar radiation reaching plants in greenhouses may not be sufficient to sustain adequate fruit yields. Supplemental lighting (SL) placed above the inner canopy of a crop stand can improve the light environment, thereby increasing photosynthesis and yield. In addition to increased fruit production, SL can improve product quality, enable earlier or year-round production, and sustain a more stable workforce (Heuvelink *et al.*, 2006).

A.2.c. Lamp Emissions

Farms select lamp types based on emitted spectra. MH and HPS lamps emit a considerable amount of their radiation in the photosynthetically active radiation (PAR; 400-700 nm) wavelength range. PAR is desirable because it is the portion of the light spectrum that plants utilize for photosynthesis. MH lamps produce a cool-white light with almost as much blue as red light, whereas the light emitted by HPS lamps is yellowish orange with much less blue. HPS lamps have been widely used for greenhouse overhead lighting because they have been the most economically viable mass- produced light source available that can provide adequate intensity and spectrum for plant growth (Huché-Thélier *et al.*, 2016).

INCs primarily emit radiation in the red (600-700 nm) and far-red (700–800 nm) wavelength ranges, however, this accounts for only about 8% of the total energy emitted (Thimijan and Heins, 1983). Incandescent lamps became popular because of their low purchase cost, but global trends of increased energy standards have considerably reduced their prevalence. CFLs are more efficient than INC lamps and are capable of emitting radiation across the PAR range, however, they emit little far-red radiation, which is required to accelerate flowering in some long-day crops (Kozai, Fujiwara and Runkle, 2016).

A light-emitting diode (LED) is a semiconductor that emits light when electrical current flows through it. The energy required for electrons to cross the semiconductor band gap in the semiconductor determines the color of the emitted radiation. Depending on semiconductor material, individual LEDs can emit light in a narrow band of wavelengths (typically ~100 nm band) from 215 to 800 nm. As the wavelengths become shorter, because of the larger band gap of these semiconductors, the operating voltage of the LED increases. LEDs are very energy efficient relative to other lamps and this energy efficiency, together with incentives provided by power utilities, has motivated farms to rapidly adopt the technology (Kozai, Fujiwara and Runkle, 2016).

Table A-1 Spectral characteristics of incandescent lamps, compact fluorescent lamps, high pressure sodium lamps, and blue+red+far red, red+white, red+white+far red, cool white, and warm-W light emitting diodes. This table is directly reproduced from Kozai et al. 2016.

% of photon flux	INC	CFL	HPS	LED[1]	LED[2]	LED[3]	LED[4]	LED[5]
400 – 500 nm	3	14	5	11	6	6	20	12
500 – 600 nm	14	37	51	2	14	13	46	39
600 – 700 nm	30	42	38	60	78	36	30	43
700 – 800 nm	54	7	6	27	1	44	4	6

1. TotalGrow Day & Night Management Light
2. Philips GreenPower LED flowering DR/W
3. Philips GreenPower LED flowering DR/W/FR
4. Philips model 9290002296
5. Philips model 9290002204

The table above does not include spectral characteristics of MH lamps. These lamps emit radiation characterized by unevenly distributed spectral lines across the PAR range (Flesch, 2006).

Huché-Thélier *et al.* (2016) published a highly cited review on the effects of blue light and UV radiation on plant physiological response. The review concluded that controlled UV and blue light inputs can influence the development of a crop's physiology, and proposed that the refinement of the UV and blue light inputs could lead to the creation of higher value crops.

A.3. Radiation Propagation in Horticulture

Radiation propagation in horticulture (and all settings) is governed by radiative transfer, (RT) the physical phenomenon of energy transfer in the form of electromagnetic radiation (Chandrasekhar, 1960). The equation of RT describes how absorption, emission, and scattering affect radiation propagation through a space. The general form of the RT equation is:

$$\frac{dI}{ds} = E + A$$

Equation A-1

Where dI is the change in radiant energy, ds is the path length, E represents the extinction component, and A represents the energy contributions from the emissions of the source itself and scattering. The extinction component takes the following form:

$$E = \sigma(P) * I_\lambda(P, \vec{r})$$

Equation A-2

Where $\sigma(P)$ is the extinction coefficient at location P, and $I_\lambda(P, \vec{r})$ the wavelength-dependent radiance at location P in direction $\vec{r}$. The energy contributions are described as the integral over all incident directions $\overrightarrow{r'}$:

$$A = \int_0^{4\pi} I_\lambda(P, \overrightarrow{r'})\, \Gamma(\overrightarrow{r'}, \vec{r}) dr'$$

Equation A-3

Where $I_\lambda(P, \overrightarrow{r'})$ is the emissions of the source itself at location P in direction $\vec{r}$ and $\Gamma(\overrightarrow{r'}, \vec{r})$ is the scattering phase function (Chandrasekhar, 1960).

A.3.a. Application of Radiative Transfer to Vegetation Canopies

Application of the RT function to vegetation canopies requires defining the spatial and optical properties of a volume dV within the canopy of interest. However, defining the spatial and optical properties of dV is not a straightforward task because considerable variation exists in the morphological and optical characteristics of a canopy's phytoelements (Myneni, Ross and Asrar, 1989). Over the years, researchers have developed several different methodologies to define dV (Kuusk *et al.*, 2018).

Vegetation radiative transfer models typically attempt to derive various optical properties from physiological characteristics of a plant canopy. Frequently used characteristics are the leaf area density distribution (L_D), leaf angle distribution (s), the leaf area index (L_I), and the leaf absorptivity (a). The leaf area density distribution is a ratio of the one-sided leaf area to a volume within the canopy (m^2/m^3). The leaf angle distribution is the mathematical description of the angular orientation of the leaves in the vegetation. According to Campbell and Norman (2000), a spherical leaf angle distribution is a good approximation to real plant canopies. The leaf area index is the one-sided green leaf area per unit ground surface area. The leaf absorptivity is the fraction of the incident irradiance absorbed by a single leaf. At the top of the canopy, the L_I=0, and with increasing depth into the canopy, L_I increases. A popular model that takes inputs of L_I, L_D, and s are the light distribution equations by Campbell and Norman (2000).

Light Distribution Equations

Campbell's work synthesizes the work published in Goudriaan *et al.* (1977), Goudriaan *et al.* (1988), Campbell *et al.* (1986), and Campbell *et al.* (1990). The Campbell and Norman (2000) model represents the canopy as a 3D object with various optical properties derived from the s, the L_D, and the L_I.

The Campbell equations take one more input that is not morphological but is a direct property of the plant: leaf optical absorptivity (α). This property typically has a value of approximately 0.8 for photosynthetically active radiation (Goudriaan, 1977).

The model published in Campbell and Norman (2000) model calculates the fraction of incident beam radiation that penetrates the canopy as:

$$\tau_b(\psi) = \exp\left(a * L_I * K(s, \psi)\right)$$

Equation A-4

Where $K(s, \psi)$ is the extinction coefficient, L_I is the leaf area index at the depth of interest, α is the wavelength specific leaf optical absorptivity, and ψ is the angle of the incoming radiation measured from vertical.

Computation of the extinction coefficient depends on the leaf angle distribution. The following formula approximates an ellipsoidal leaf angle distribution, which generalizes a spherical leaf angle distribution, but allows the sphere to be flattened or elongated:

$$K\,(s,\psi) = \frac{\sqrt{s^2+sin^2(\psi)}}{s+1.774(s+1.182)^{-0.733}}$$

Equation A-5

Where *s* is the ratio of average projected areas of canopy elements on horizontal and vertical surfaces. The *s* parameter value is unity for a spherical leaf angle distribution, zero for a vertical distribution, and approaches infinity for a horizontal leaf distribution.

Finally, the Campbell and Norman (2000) model uses the Goudriann *et al.* (1988) description of a canopy's reflection coefficient. The reflection of a deep canopy is proportional to the extinction coefficient and the leaf optical absorptivity.

$$\rho_i = \frac{1 - \sqrt{a}}{1 + \sqrt{a}}$$

Equation A-6

Studies have used the Campbell and Norman (2000) equations to model photosynthetically active radiation interception for maize (Stewart *et al.*, 2003; Wang *et al.*, 2015), fruit trees (Annandale *et al.*, 2004; Oyarzun, Whiting and Sto, 2007), willow tree canopy (Mottus and Sulev, 2006), vineyards (Pieri, 2010; Parry *et al.*, 2019), row crops (Colaizzi, Evett, *et al.*, 2012; Colaizzi, Schwartz, *et al.*, 2012), and tomatoes (Xu and Wei, 2019). Only one study, Xu *et al.* (2019), modeled radiation generated by artificial sources.

Xu *et al.* (2019) applied Goudriaan and Campbell's work to represent a non-uniform leaf area density distribution for hedgerows. This application defined the leaf area density distribution as a horizontal and vertical component. The following function describes the horizontal leaf area density distribution:

$$L_{DH}(L_I, x) = L_I * \frac{\pi}{2W} * \sin\left(\frac{x\pi}{W}\right)^u$$

Equation A-7

Where W is the width of the hedgerow, x is the horizontal position defined from [0,W], and *u* is a horizontal density distribution modifier defined from [0,1]. The *u* parameter is not an original part of the Xu et al. (2019) equations, and was added due to suspicions that intense cannabis pruning may flatten the L_D distribution in cannabis farms.

The function describing the vertical leaf area density distribution is:

$$L_{DV}(L_I, z, v) = \frac{L_I * \left(\frac{H}{v/H}\right)^2 * \left({}^{z}/_{H}\right)^2}{{}^{1}/_{2} * \sqrt{{}^{1}/_{2} * \sqrt{\frac{\pi}{\left(\frac{H}{v/H}\right)^2}} * \operatorname{erf}\left(\sqrt{\left(\frac{H}{v/H}\right)^2}\right) - e^{-\left(\frac{H}{v/H}\right)^2}}} * e^{-\left(\frac{H}{v/H}\right)^2 * \left(\frac{z}{v/H}\right)^2}$$

Equation A-8

Where H is the height of the canopy, v is the height at which the vertical density reaches its maximum, and z is the vertical position defined from the bottom of the hedgerow to the top of the hedgerow. Note, the lower bound of z may not be equal to zero.

The relationships presented by the two formulas are difficult to visualize, so Figure A-2 presents graphical representations of them for clarity.

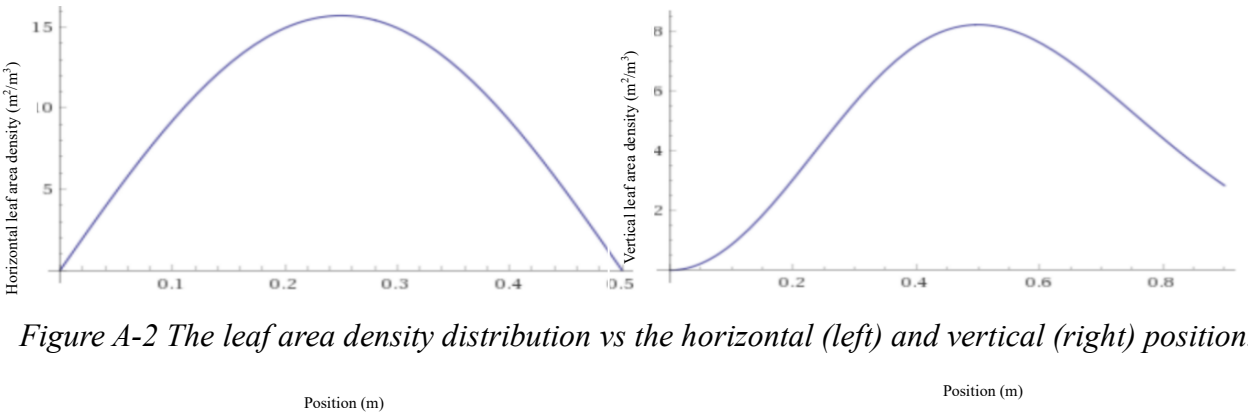

Figure A-2 The leaf area density distribution vs the horizontal (left) and vertical (right) position.

Figure A-2 presents plots of the two equations for a typical cannabis canopy with a width of 0.5 m, a height of 0.9 m, a height at which the vertical density reaches its maximum at 0.5 m, and the canopy starting at a height of zero.

A.4. The Metrics of UV Exposure Measurement

A.4.a. Terminology

Radiometric units allow the characterization of UVR intensity. The terms radiance (W/m^2*sr) and radiant intensity (W/sr) pertain to radiant flux emitted by a source into a given solid angle. The terms dose (J/m^2) and dose rate (W/m^2) pertain to the energy (radiant energy) and power (irradiance), respectively, striking a unit surface area of an irradiated object (Jagger, 1985). The terms ‘fluence’, ‘exposure dose’, and ‘dose’ refer to the radiant energy delivered to a given area in a given time (IARC, 2012). A unit of dose is different from a unit of effective dose. Effective dose is a dose weighted in accordance with its capacity to bring about a particular biological effect (IARC, 2012). Since not all wavelengths of UVR are equally effective in producing a biological effect, weighting functions that define the relative biological effectiveness of different wavelengths have been developed. The term for this type of function is an “action spectrum”.

A.4.b. Biological Dose and Action Spectra

The biologically effective dose is the integral of the biologically effective irradiance with respect to time. To calculate biologically effective irradiance, henceforth termed effective irradiance (units: effective Watt/m^2), one must multiply the unweighted UV irradiance by the action spectrum of interest for each wavelength within the action spectrum (Sliney, 1972). Application of an action spectrum is mathematically represented by the following equation (ICNIRP, 2004; ACGIH, 2023).

$$E_{eff} = \sum E_{\lambda} S(\lambda) \Delta\lambda$$

Equation A-9

Where:
E_{eff} = effective irradiance in W/m^2
E_{λ} = spectral irradiance at wavelength λ, in W/(m^2*nm)
S(λ) = relative spectral effectiveness (unitless) of the action spectrum at wavelength λ
Δλ = bandwidth in nanometers of the calculation or measurement intervals

A.4.c. ICNIRP Action Spectrum

The International Commission on Non-Ionizing Radiation Protection (ICNIRP) developed the most widely used action spectrum by considering the risks of acute and chronic injury to both the eye and skin. This action spectrum is sometimes referred to as the actinic action spectrum (ICNIRP, 2004) and is used in exposure guidelines published by both the ICNIRP themselves and was previously used by the American Conference of Governmental Industrial Hygienists (ACGIH). In 2020, ACGIH updated their action spectrum to address concerns of excessive safety margins in UV-C wavelengths (ACGIH, 2020). These spectra are illustrated in Figure A-3.

The ICNIRP guidelines on incoherent optical radiation and the ACGIH broadband UV threshold limit values (TLVs) both refer to incoherent ultraviolet radiation with wavelengths between 180 and 400 nm. These two guidelines represent conditions under which it is believed that nearly all healthy workers may be repeatedly exposed without acute adverse health effects such as erythema and photokeratitis. Both guidelines limit human exposure of the eye and skin to 3 effective mJ/cm^2 per day, however, as of 2020 the ICNIRP and ACGIH no longer use identical action spectra to compute broadband effective irradiance (ICNIRP, 2004; ACGIH, 2020; ACGIH, 2023). In 2020, the ACGIH added two separate TLVs for the skin and eyes for use when the eyes are protected and skin exposure is the only concern (ACGIH, 2020).

Both the ICNIRP guidelines and ACGIH TLVs contain guidelines for unweighted radiant exposure to broadband UVA (315-400 nm). The UVA guidelines protect the eyes from thermal injury resulting from rapid delivery of radiant energy to ocular tissues (ICNIRP, 2004; ACGIH, 2023). Like the broadband UV guidelines, they represent conditions under which nearly all healthy workers may be repeatedly exposed without acute adverse health effects. The ICNIRP UVA guidelines are specific to ocular exposure and limit ocular exposure to unweighted radiant UVA exposure of 10,000 J/m^2 for periods of up to 30,000s. The ACGIH guideline also limits ocular exposure to 10,000 J/m^2 but for periods of up to 1,000s and sets a maximum irradiance limit of 10 W/m^2 (ICNIRP, 2004; ACGIH, 2023). The more conservative ICNIRP guideline reflects a concern for potential photochemical effects in the lens of the eye for lengthy exposures while the ACGIH guideline moderates thermal effects (ICNIRP, 2007).

All ICNIRP UV guidelines specify that in no case is the irradiance to be averaged over an area greater than 1 mm for pulsed sources or 3.5 mm for continuous sources. Furthermore, the field of view of the detector should be 180° for measurements to be used for skin hazard assessment and should be limited to 80° (± 40° from the normal) for measurements to be used for eye hazard assessment (ICNIRP, 2004). The ACGIH TLVs state that "sources may subtend an angle less than 80 degrees at the detector, but those sources that subtend a greater angle need to be measured over an angle of 80 degrees" (ACGIH, 2023).

A.4.d. CIE Action Spectrum

Another action spectrum frequently used in regulations and research is the standard erythema action spectrum. This spectrum was originally published by Mckinley and Diffey in 1987 and adopted as the International Commission on Illumination (CIE) standard in 1998 (CIE, 1999). It provides a representation of the erythema-inducing effectiveness of wavelengths in the UV part of the spectrum. The output of the application of the CIE action spectrum is termed erythemal radiation or irradiance. Figure A-3 presents this action spectrum, along with a comparison to the action spectrum used by ICNIRP/ACGIH.

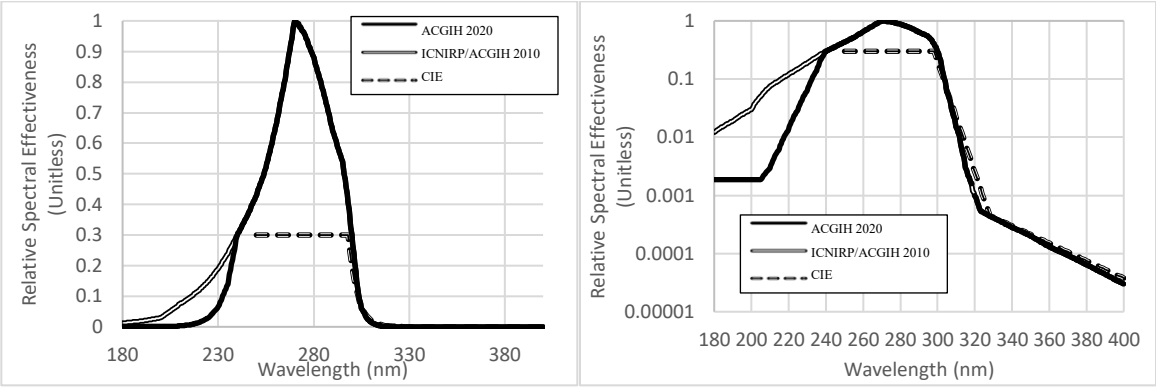

Figure A-3 Comparison of the ICNIRP/ACGIH 2010, ACGIH 2020, and CIE functions presented in linear (left) and log (right) scales.

All three action spectra are measures of the relative effectiveness of UV radiation on target organs (eyes and skin for the action spectra used by ICNIRP/ACGIH and skin in the case of the erythemal action spectrum) and do not allow the interpretation of "safe" conditions. However, one can determine "safe" conditions using action spectra in conjunction with an accumulated energy limit such as the TLV.

The accumulated energy limit typically used with the erythemal action spectrum is the standard erythemal dose (SED). The SED is equivalent to 100 J/m^2 and is independent of skin type (Diffey, 2002). Another unit that uses the erythemal action spectrum is the minimal erythemal dose (MED). The MED represents the minimum radiant energy, weighted to the erythemal action spectrum, needed to induce an erythemal skin response, minimal erythema (sunburn or redness caused by engorgement of capillaries). Unfortunately, the unit of MED is person specific and varies both between individuals and even within the same individual on different days or body sites, with typical values ranging from 150 J/m^2 to 600 J/m^2. The lack of a consistent baseline decreases the value of the MED for interstudy comparisons.

A.5. UV Measurement Instrumentation

Ultraviolet (UV) exposure measurement is typically performed using one of three types of devices: spectrometers, spectroradiometers, or broadband UV devices. A spectrometer is a device that can measure a light's spectral distribution, or the distribution of radiant energy by wavelength. With the addition of an appropriate calibration, a spectrometer can perform as a spectroradiometer, which is a device that measures the absolute irradiance at each wavelength. In contrast, broadband devices provide a single measure of UV intensity aggregated across a range of wavelengths - they do not provide wavelength specific values (Diffey, 2002). Miniaturization of the technology powering broadband radiometers has allowed construction of devices that can be deployed as personal electronic dosimeters (ICNIRP, 2007). Other types of broadband devices include polysulfone film dosimeters (Jackson, 1980), polyphenylene oxide film dosimeters (Wainwright, Parisi and Schouten, 2013), and *bacillus subtilis* spore film dosimeters (Quintern *et al.*, 1997). When selecting a UV measurement device, one must consider factors related to the spectra and propagation pathway of the radiation(s) of interest in choosing an appropriate measurement instrument.

A.5.a. Polysulfone Film Dosimeters

Polysulfone film is a thermoplastic polymer that degrades when exposed to ultraviolet radiation. As degradation occurs, the absorption spectrum of the polysulfone film in the UV region changes. The process of measuring this change uses a monochromatic radiation source and spectroradiometer. The monochromatic radiation source needs to emit radiation of known intensity and wavelength, usually at 330 nm (Wainwright, Parisi and Schouten, 2013). This change in absorption is one of two variables used to construct a calibration curve.

The other variable is the known erythemal radiant dose, a value sourced by co-location of the polysulfone film dosimeters with a calibrated radiometer or spectroradiometer. These calibrations are only accurate for the specific source used to calibrate the polysulfone film dosimeter, and they assume that the spectral output from the calibration source is stable.

A co-location is necessary because polysulfone film has a spectral response to UV which does not perfectly emulate the erythemal action spectrum. Figure A-4 shows this imperfect agreement, taken from the "Manual for Polysulfone Dosimeters" by Geiss *et al.* (2003).

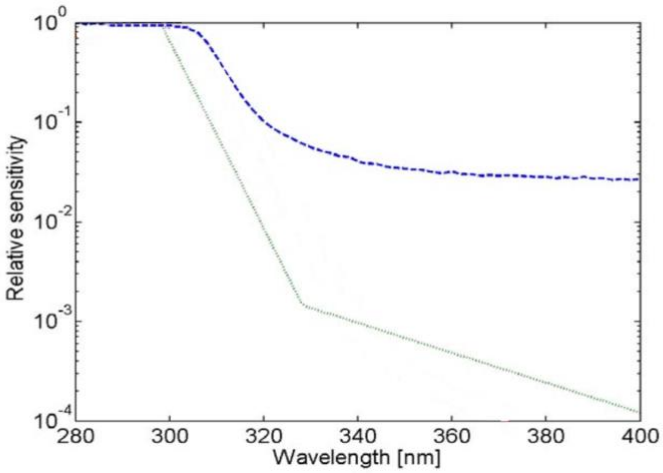

Figure A-4 The relative sensitivity of polysulfone film (blue line) charted alongside the CIE erythemal action spectrum (grey line) (Geiss and Rembges, 2003). *As shown in the figure above, the normalized polysulfone response is greater than that of the erythemal action spectrum, at all wavelengths >~310nm.*

A.5.b. Spore Film Dosimeters

Spore film dosimeters use *Bacillus subtilis* spores mounted on film to measure UV exposure. The core components of this type of dosimeter are a diffuser, optical filter, an aperture stop, and a sheet of spore film with a transparent polyester plastic sheet that immobilizes the spores on the sporefilm. The spore film consists of several sections of *Bacillus subtilis* dried spores, referred henceforth as 'zones'. A single dosimeter's spore film contains two types of zones: measurement zones and calibration zones.

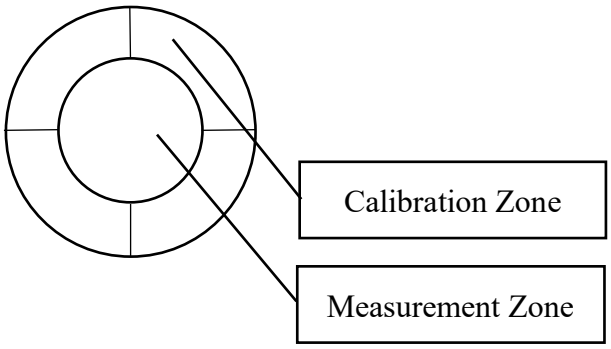

Figure A-5 2D image of a polyester plastic sheet that houses Bacillus subtilis spores.

Prior to use, an aperture stop covers the dosimeter's measurement zones. Then, the dosimeter receives known UV effective doses from calibrated UV sources, and since the aperture stop covers the measurement zones, only the calibration zones receive this known UV radiance. The irradiance causes partial inactivation of the calibration zone spores. Then, a calibration technician removes the aperture stop uncovering the measurement zone and uses a separate aperture stop to cover the calibration zones.

During dosimeter deployment, received UV irradiance causes inactivation of some of the spores on the measurement zone. After the measurement period, a calibration technician transfers the spores from all

zones to an incubation medium and allows the spores to germinate. The technician then stains the proteins synthesized during spore germination and determines the bacterial optical density via photometry. A plot of the optical densities from the calibration zones and the known radiant exposure doses forms the calibration curve, which allows determination of UV dose received by the measurement zone (Quintern *et al.*, 1997).

The response of *Bacillus subtilis* spore film roughly matches the erythemal action spectrum between 300 to 340 nm, but spore film tends to overestimate UV exposure at wavelengths below 300 nm and to underestimate UV exposure at wavelengths above 340 nm. Figure A-6 shows a chart of the spore film response, plotted alongside the erythemal action spectrum. This chart is reproduced from Cockell *et al.* (2002).

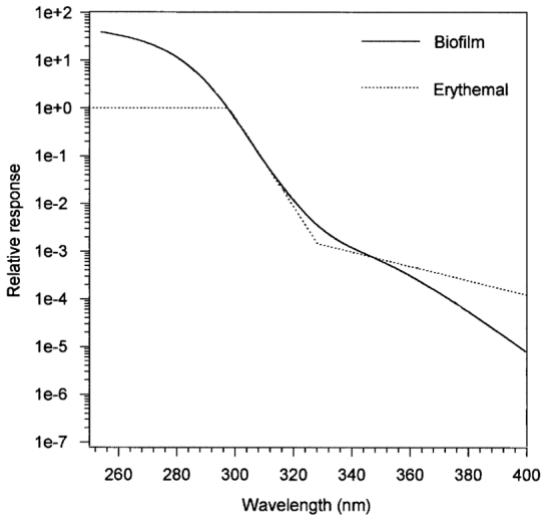

Figure A-6 The action spectrum for inactivation of Bacillus subtilis spores used in the DLR-Biofilm dosimeters and the standard CIE erythemal action spectrum (here normalized to 1 at 297 nm) (Cockell et al., 2002).

To correct for the bias outside of the 300 to 340 nm range, studies typically calibrate *Bacillus subtilis* spore film dosimeters against a spectroradiometer (Thieden, Ågren and Wulf, 2000; Cockell *et al.*, 2001; Antoine *et al.*, 2007; Serrano *et al.*, 2009, 2013; Serrano, Cañada and Moreno, 2010; M.-A. A. Serrano *et al.*, 2014; M.-A. Serrano *et al.*, 2014; Ysasi *et al.*, 2014). As with the polysulfone film dosimeters, these calibrations are only accurate for the specific source used to calibrate the polysulfone film dosimeter, and they assume that the spectral output from the calibration source is stable.

A.5.c. Electronic UV Dosimeters

Electronic broadband UV measurement instruments measure UV irradiance by converting radiant energy into an electrical current and then measuring this new current with an ammeter (Wilson and Lyall, 1986). These instruments include radiometers, small electronic dosimeters and actinometers, although the latter's primary purpose is to count photons (Taylor, 1971). Electronic broadband devices usually consist of input optics, a photodetector, an ammeter, and a data extraction mechanism.

An electronic broadband device's measurement process begins when radiant energy enters the input optics of the device. Common input optic components include diffusers and optical filters (Nicholas G.

Reed *et al.*, 2009). Diffusers allow the capture of photons traveling at angles not incident to the entrance aperture's normal axis (ILT, 2019), and adapt the device's *angular* response function to conform to a specific health protective criterion. Optical filters selectively transmit radiant energy of selected wavelengths and allow the device to measure in accordance with a wavelength-specific *spectral* response function (Madsen and Zhao, 1999). Once past the optical filter, radiation photons hit a photodetector, which then converts the radiant energy to electrical current. An ammeter measures this electrical current and sends it to a visual display, a local memory system, or both. Designers of broadband devices often engineer the collective system response so that the system response emulates that of an action spectrum of interest (Madsen and Zhao, 1999).

A.5.d. UV Spectrometers

UV spectrometers measure the radiant energy distribution of UV radiation by wavelength. These devices typically consist of an entrance slit, a diffraction grating, and a photosensitive device. The entrance slit controls the amount and the angle of the radiation entering the spectrometer. The dispersive grating causes the UV to disperse into its spectral components. The spectrum then falls onto the photosensitive element, which converts the UV irradiance into electric current. Finally, an ammeter measures the electric current and sends it to a visual display, a local memory system, or both (AZOM, 2016).

A spectrometer's key performance specifications are its sensitivity, signal to noise ratio, spectral scatter, linearity, wavelength resolution, wavelength accuracy, and dynamic range. Sensitivity is the relative efficiency of detection of the optical signal as a function of wavelength. The signal to noise ratio is defined as the average over time of the peak optical signal divided by the RMS noise of the peak signal over the same time. Radiation with wavelengths outside the bandpass of the spectrometer's specific wavelength setting that contributes to the output signal is called spectral scatter. Linearity means that a given change in optical signal will result in a proportional change of the electrical output of the detector. Spectral resolution is a measure of the spectrometer's ability to resolve features in the electromagnetic spectrum. Wavelength accuracy is a tolerance to the true wavelength value of a measured wavelength value. Finally, dynamic range is defined as the full-scale signal divided by the minimum resolvable signal.

There exist two general implementations of the spectrometer design. One implementation comprises of a monochromator with an entrance slit, a rotating grating, an exit slit, and a single channel photodetector and the other comprises of an entrance slit, a fixed grating, and a multi-channel photodetector array. The former implementation scans through the spectral features of the optical signals with a step-by-step mechanical rotation of the diffraction grating. During rotation, the grating guides a spectral subset of total optical signal through the exit slit and onto the photodetector. Resolving the spectral components is possible because of the known relationship between each angle of rotation and a narrow subset of wavelengths. The second type of spectrometer design has a fixed grating that passively disperses the spectral components onto the surface of a multi-channel photodetector array comprised of thousands of tiny photodiodes called pixels. Resolving the spectral components is possible because of the known relationship between the position of each pixel and the overlap location where a known subset of the spectrum wavelengths fall (HORIBA, 2020).

The two implementations have different relative advantages and disadvantages. A spectrometer with a monochromator and a single channel photodetector can achieve higher spectral wavelength resolution

and optical throughput due to the ability to achieve higher spectral dispersion with the rotating grating. Additionally, the exit slit drastically decreases amount of the spectral scatter present in the measurement. However, the need to mechanically rotate the grating prevents simultaneous measurement of all wavelengths in an optical signal. Thus, spectrometers with monochromators cannot measure dynamic optical environments. Spectrometers with a fixed grating and multi-channel photodetector simultaneously measure all wavelengths of an optical signal, allowing their use in dynamic optical environments. However, they generally have lower spectral resolution, lower throughput, and higher spectral scatter (HORIBA, 2020).

Two common types of multi-channel photodetector arrays used in fixed grating spectrometers are the charge coupled device (CCD) and the complementary metal–oxide–semiconductor (CMOS). Both designs consist of pixel arrays, and the key difference is in how the devices read the optically induced charge out of pixels. A CCD uses a shift register to perform either a one- or two-dimensional shift of charges off pixels. The shifting then moves the charges serially to an output node amplifier. A CMOS has the capability to read out each pixel's charge without the use of a shift register. Historically, CCD photodetector arrays outperformed CMOS photodetector arrays, especially in sensitivity. However, recent developments in lithography have allowed the manufacture of CMOS photodetector arrays with specifications matching those of CCD photodetector arrays (Meroli, 2012).

Thermal and vibrational fluctuations may ruin the wavelength accuracy of the spectrometer both during and post measurement. Temperature and dark current are exponentially related, and measurement in high temperature environments will cause large dark currents at the detector. Post measurement, thermal fluctuations may cause deformation in the material of the spectrometer housing and diffraction grating, and this deformation can cause focal shift in spectrometer system. Vibrations at specific mechanical resonance of the grating will cause the spectra will blur during measurement. Post measurement, vibration may cause changes in the relative geometry of the optical bench, causing focal shift in the system (Scheeline, 2017).

Application of an action spectrum to a spectroradiometer measurement can be done by multiplying the measured irradiance at each wavelength by that wavelength's specific weighting factor. Computer software usually performs this multiplication.

A.6. Optical Calibration of Electronic Broadband Instruments

A full calibration of an electronic broadband instrument allows for the quantification of fourteen device performance characteristics. The Joint ISO/CIE International Standard ISO/CIE 19476:2014(E) terms these characteristics 'quality indices' and though they primarily apply to electronic broadband instruments, they equally apply to other types of UV measurement devices. The quality indices describe a device's initial adjustment, spectral mismatch, short-wavelength range response, long-wavelength range response, directional response, linearity, display-unit, fatigue, temperature dependence, humidity test, modulated radiation, polarization response, spatial response, and the range change. Of the fourteen, the most critical are the directional response and spectral mismatch (CIE, 2016).

A.6.a. Spectral Mismatch

The spectral mismatch index describes the deviation of the relative spectral responsivity of the radiometer head from the designated action spectrum using the designated reference spectrum source, which is an idealized spectrum of a real source or a theoretical spectral distribution. The value of the spectral mismatch index is specific to each optical source measured.

A.6.b. Directional Response Index

The directional response index describes the deviation from the ideal cosine law of the responsivity of the radiometer head to radiation incident at angles other than normal to the reference plane of the head (CIE, 2016).

A.6.c. Primary Calibration

A primary calibration is necessary if the UV radiometer is to act as a reference device or where low uncertainties are required. A primary calibration is the process of determining a device's effective irradiance responsivity, which is the quotient of the radiometer head output signal by the true signal weighted to an action spectrum of interest. To determine the effective irradiance responsivity, the absolute spectral responsivity must be known. The absolute spectral responsivity equals the monochromatic detector input divided by the detector output for each wavelength. Methods CIE 63-1984 and CIE 202:2011 allow the determination of the absolute spectral responsivity using a tunable monochromatic source.

The following equation takes the absolute spectral responsivity ($s_{0,E}$) along with several other radiometer characteristics to compute the effective irradiance responsivity.

$$s_{E,\mathrm{act,R}} = s_{0,E} \cdot \frac{\int_{\lambda_{\mathrm{s,Sensor}}}^{\lambda_{\mathrm{l,Sensor}}} E_{\lambda,\mathrm{R,rel}}(\lambda)\, s_{\mathrm{rel}}(\lambda)\,\mathrm{d}\lambda}{\int_{\lambda_{\mathrm{s,Act.}}}^{\lambda_{\mathrm{l,Act.}}} E_{\lambda,\mathrm{R,rel}}(\lambda)\, A_{\mathrm{act}}(\lambda)\,\mathrm{d}\lambda},$$

Equation A-10

Where:

$s_{E,\mathrm{act,R}}$	is the effective irradiance responsivity
$E_{\lambda,\mathrm{R,rel}}(\lambda)$	is the relative spectral irradiance distribution of the reference
$A_{\mathrm{act}}(\lambda)$	is the action spectrum under consideration with $A_{act}(\lambda) = 0$ in the out of bound regions
$s_{\mathrm{rel}}(\lambda)$	is the relative spectral responsivity function of the UV radiometer
$s_{0,E}$	is the absolute value of the irradiance responsivity measured in ($A \cdot W{-}1 \cdot m^2$) of the UV radiometer at a chosen suitable wavelength

Performance of a primary calibration requires sophisticated optical infrastructure and technical expertise. Therefore, if low uncertainty is not needed, research teams frequently choose to calibrate a radiometer with a secondary calibration. A secondary calibration is the process of generating a measurement conversion factor for a specific optical source spectrum. The product of the raw radiometer measurement and the conversion factor is the actual irradiance value.

A.6.d. Secondary Calibration

Joint ISO/CIE International Standard ISO/CIE 19476:2014(E) provides two secondary calibration procedures: direct comparison between the device under test (DUT) and a primary calibrated reference radiometer or DUT measurement of a reference spectrum source. The former procedure requires taking measurements of a stabilized source at an identical location with both the DUT and the primary calibrated reference radiometer. The selected location must cause the distance between the source and the location of measurement to exceed the radiometric limiting distance of both devices. A measurement taken at a distance exceeding the radiometric limiting distance allows treatment of the optical source as a point.

For the second procedure in which the DUT is calibrated via measurement of a reference spectrum source, that source must match the spectrum of the optical source of measurement. and measurements must be made at distances that exceed the radiometric limiting distance.

ASTM International, an organization formerly known as the American Society for Testing and Materials, publishes two other broadband radiometer calibration methods: (ASTM)-G130 and ASTM-E824. The former details a calibration procedure for a broadband ultraviolet radiometer using a scanning or a linear-diode-array spectroradiometer as the primary reference instrument. The latter details a procedure for transferring a calibration from a reference radiometer to the broadband ultraviolet radiometer under test.

A.7. Optical Calibration of Spectrometers

The most cited spectroradiometer calibration procedure is the ASTM G138 method. This method generates a spectral response function for each wavelength over the calibrated range.

A.7.a. ASTM G138 Physical Setup

This calibration method requires installing a standard of spectral irradiance, input optics, a monochromator, and the spectroradiometer under test on an optical bench in a temperature-controlled environment.

The standard of spectral irradiance is typically a lamp with a known spectral irradiance over the wavelength values of interest but can also be a narrow band monochromatic source. The emissions of this standard should be traceable to a national standards laboratory or other appropriate entity. Additionally, the standard lamp must receive power from a stable DC power supply and this power supply must have an installed calibrated current shunt and voltmeter to accurately monitor the current provided to the device.

The input optics must capture and guide incident radiation such that it evenly fills the entrance slit of the monochromator. Additionally, the G138 method requires the installation of long-pass and short pass filters for stray light testing of the monochromator.

Wavelength Offset Calibration
Prior to generating a spectral response function, the full setup must undergo a wavelength offset calibration. To fix the offset, one would illuminate the input with a wavelength calibration source, select an emission line of known wavelength, scan and locate the emission line output signal, and compensate for the offset.

Dark Noise Measurement
Dark noise is the output signal when no irradiance enters the inlet. A technician needs to measure this value to subtract it value from the output signal generated by an optical measurement.

Spectral Scatter Measurement
Testing for spectral scatter requires setting the monochromator to a wavelength setting at a point where a short or long pass filter transmission is zero, but the wavelength is near the filter cut-off wavelength. Measured signals between 10 to 90% of the unfiltered signal indicate that the setup has spectral scatter.

Generation of the Slit Scattering Function
The slit scattering function describes the responsivity of the setup as a function of a measurement wavelength λ_i and the setup wavelength setting λ_o. Ideally, the responsivity should be zero unless the measurement wavelength and the setup wavelength are equivalent. The G138 method requires measurement and reporting of the slit scattering function but does not use this function to adjust the spectral response function in any way.

A.7.b. Spectral Irradiance Calibration

Once a technician has completed the setup preparation, the spectral irradiance calibration can begin. This process involves setting the monochromator to transmit narrow band of optical radiation to the spectroradiometer detector and recording the output signal for each wavelength to be calibrated. Once completed, the technician may compute the spectral response function for each selected wavelength according to the following equation:

$$K(\lambda) = S(\lambda)[R(\lambda) - i(\lambda)]$$

Equation A-11

Where

$S(\lambda)$ = the known spectral irradiance of the standard lamp (W/m^2)
$R(\lambda)$ = the detector flux readings taken during the calibration scan (amps)
$i(\lambda)$ = the dark current reading (amps)

A.7.c. Other Spectroradiometer Calibration Methods

The other commonly referenced calibration is NIST 150-2E published by the National Voluntary Laboratory Accreditation Program (NVLAP). The document describes the requirements for lab accreditation of technical competency to perform optical calibration and measurement, and it references various National Bureau of Standards measurement services that share considerable overlap with the ASTM G138 method. Relevant NBS services include the procedure documents for spectral irradiance and radiance calibration of a measurement device.

A.8. Health Outcomes of UV Exposure

UV exposure causes negative health outcomes in skin, eyes, and the immune system (Lucas, 2010). Differential health outcomes result from acute and chronic UV exposure. The most common outcome of acute UV exposure is sunburn (erythema) on the skin and photokeratitis on the eye. Chronic exposure to UV can lead to the development of multiple types of cancer on both the skin and the eye. Table A-2 presents the adverse health outcomes associated with UVR exposure, organized by target organ and whether the effect results from acute or chronic UV exposure.

Table A-2 Health outcomes of UV exposure (Lucas, 2010).

Target Organ	Acute	Chronic
Skin	Sunburn, photodermatoses	Cutaneous malignant melanoma cancer of the lip, basal cell carcinoma, squamous cell carcinoma, photoaging
Eye	Photokeratitis, retinopathy	Climatic droplet keratopathy, pterygium pinguecula, corneal and conjunctival squamous cell carcinoma, cataracts (cortical, sub-capsular, nuclear)
Immune System	Suppression of cell-mediated immunity, increased susceptibility to infection, prophylactic immunization impairment	Suppression of cell-mediated immunity, increased susceptibility to infection, prophylactic immunization impairment

A.8.a. Health Outcomes of UV Exposure on the Skin

Sunburn

Erythema is the reddening of skin that occurs approximately three to five hours after UV exposure, reaches a maximum severity in eight to twenty-four hours, and then fades over three days (IARC, 2012). Erythema manifests differentially depending on the exposure wavelength, as described by the CIE action spectrum (Lucas, 2010).

Photodermatoses

Photodermatoses are a range of skin diseases that include solar urticaria, photoallergic contact dermatitis, actinic prurigo, polymorphic light eruption and hydroa vacciniforme. Solar urticaria is a rare outbreak of urticaria or hives thought to be caused by a photo allergy (Botto and Warshaw, 2008). Photoallergic contact dermatitis is a rare condition resulting from sun-exposure that consists of an itchy rash with an appearance like dermatitis (Kerr and Ferguson, 2010). Actinic prurigo is a rare photodermatosis characterized as a firm, raised and itchy area of the skin (Pile and Crane, 2020). Polymorphous light eruption is the most common photodermatosis, and appears as a red, tiny bumps or slightly raised patches of skin (Herbert, 2007). Finally, hydroa vacciniforme is a rare chronic photodermatosis characterized by characterized by recurrent fluid-filled blisters.

Cancer of the Lip

Cancer of the lip describes cancer at the vermilion border of the lip and the adjacent mucous membrane but excludes cancer of skin adjacent to the lip. There is some evidence for UVR exposure as a causal risk factor for this disease, including: most occur on the lower lip which has a higher sun exposure than the upper lip; incidence is higher in men than women and higher in white populations than in black or Asian populations; incidence is lower in migrants from areas of low UVR to areas of high UVR (compared to those born in the area of high UVR) and higher in rural than urban dwellers and in those

with outdoor occupations. However, according to a meta-analysis, the evidence is insufficient to conclude there exists a causal link between UV exposure and cancer of the lip (Lucas, 2010).

Photoaging

Photoaging refers to skin damage caused by chronic UV exposure. Studies have repeatedly shown that chronic UV exposure causes photoaging (Engel, Johnson, and Haynes, 1988; Singer *et al.*, 1994; Bernstein *et al.*, 1996; Kambayashi *et al.*, 2001). Symptoms of photoaging include skin dyspigmentation, emergence of spider veins, loss of skin elasticity, and the deepening of wrinkles (CDA, 2020).

Cutaneous Malignant Melanoma

Chronic UV exposure causes cutaneous malignant melanoma (CMM), a potentially lethal form of skin cancer (Shenenberger, 2012). A large body of literature supports the causation of CMM by UVR exposure (Lucas, 2010). Studies have found a relationship between an increase in the incidence of CMM and living at lower latitudes (Østerlind *et al.*, 1988; Langford, Bentham, and McDonald, 1998) and having a history of intermittent heavy sun exposure and sunburns (Østerlind *et al.*, 1988). CMM incidence is low in populations of dark-skinned individuals, and the incidence increases in older adults (Lucas, 2010). Finally, CMM incidence is highest at body locations expected to have the most solar exposure (shoulder, neck), relative to other body locations (Lucas, 2010).

Squamous Cell Carcinoma

SCC is a common skin cancer arising from the squamous cells of the epithelium (Firnhaber, 2012). The World Health Organization (Lucas, 2010) concluded that there is a causal link between the incidence of squamous cell carcinoma (SCC) and UV exposure. Many studies provide evidence supporting the causal relationship. Stern *et al.* (1999) concluded that SCC incidence decreases with increasing latitude. Hoy *et al.* (1996) compared rates of SCC incidence for different population groups and found higher incidence of SCC in groups with light complexion. Fartasch *et al.* (2012) showed that population groups with high lifetime and occupational sun exposure are at increased risk of SCC incidence. Lekalakala *et al.* (2015) found that black albinos in sub-Saharan Africa have about a 1000x higher risk of developing squamous cell carcinoma of the skin than the general population. Finally, SCC incidence is highest at body locations expected to have the most solar exposure (shoulder, neck), relative to other body locations (Lucas, 2010).

Basal Cell Carcinoma

Basal cell carcinoma (BCC) is the most common skin cancer in humans (Sehgal *et al.*, 2014), and Lucas *et al.* (2010) confirmed a causal link between excessive UVR exposure and BCC incidence. Like CMM and SCC, BCC incidence is highest at body locations expected to have the most solar exposure (shoulder, neck), relative to other body locations (Armstrong and Kricker, 2001). Factors related to UV exposure that increase the risk of BCC incidence include a history of sunburn and UV induced skin damage including loss of skin elasticity, freckles, and high lifetime, occupational, and intermittent UV exposure (Kricker *et al.*, 1995).

A.8.b. Health Outcomes of UV Exposure on the Eye

Photokeratitis

Photokeratitis is a painful eye condition caused by acute UVB and UVC exposure, akin to a sunburn of the cornea and conjunctiva (Cullen, 2002). The initial symptoms of photokeratitis are due to lost or damaged epithelial cells leading to a gritty feeling in the eye with photophobia and tearing (Yam and Kwok, 2014).

Retinopathy

Retinopathy is retinal damage caused by intense and acute UV exposure, usually sourced by the sun (Baisakhiya and Chaudhry, 2013). Persons who experience acute retinopathy usually recover vision loss over weeks or months, but some cases will have permanent visual impairment (Atmaca, Idil and Can, 1995).

Climatic Droplet Keratopathy

Climatic droplet keratopathy (CDK) is characterized by the haziness and opalescence of the cornea (María-Antonia Serrano, Javier Cañadab *et al.*, 2011). Yam *et al.* (2014) concluded that there was sufficient evidence that UVA and UVB exposure are associated with increase in CDK incidence.

Pterygium

Pterygium is an abnormal pinkish tissue growth on the cornea (Serra *et al.*, 2018). Many studies support a causal link between pterygium increased incidence and UV exposure (DeV., 1965; Moran and Hollows, 1984; Mackenzie *et al.*, 1992).

Pinguecula

A pinguecula is a raised white to yellowish lesion on the conjunctiva which does not cross onto the cornea (Eltis, 2011). According to Yam *et al.* (2014), a relationship between UVR exposure and pinguecula may exist (Taylor *et al.*, 1989), the evidence is yet insufficient to prove a causal link.

Corneal and Conjunctival Squamous Cell Carcinoma

Ocular surface squamous cell carcinoma is a cancer on the surface of the eye that appears as a white or yellow-pink nodule on the front eye surface (Gichuhi and Sagoo, 2016). Many studies have shown solar UVR to be a factor in the incidence of ocular surface SCC (Newton *et al.*, 1996; Pola, Masanganise and Rusakaniko, 2003; Pe'er, 2005).

Cataract

A cataract is a loss of lens transparency in the lens of the eye (Alshamrani, 2018). Numerous studies have investigated the relationship between cataract formation and UV exposure, with some concluding there is a significant positive association (Hiller, Giacometti, and Yuen, 1977; Taylor, 1980) and others concluding there is no significant association (Chatterjee, Milton and Thyle, 1982; Perkins, 1985; Collman *et al.*, 1988).

A.8.c. Other Health Outcomes of UV Exposure

Immunoresponse

Multiple studies have provided evidence that UVR exposure, especially UVB exposure, has local and systemic effects on cell-mediated immunity. Locally, UVR exposure suppresses the immune response to abnormal cells, allowing the proliferation of skin cancers (Selgrade, Repacholi and Koren, 1997;

Ponsonby, Lucas and van der Mei, 2005). Garssen *et al.* (1999) demonstrated UV exposure causes suppression of the T helper cell type 1 immune response, causing systemic effects on the immune system that may lead to the development of autoimmune disorders (Ponsonby, Lucas and van der Mei, 2005). However, a review by Hart *et al.* (2018) concluded more experimental work is required to determine the nature of UVR induced immunosuppression.

Experimental animal models (Kripke and Fisher, 1976; Garssen *et al.*, 1999; Norval, 2006) and clinical studies (Yoshikawa *et al.*, 1990; Garssen *et al.*, 1998) have provided evidence that UVR exposure increases susceptibility to infection. Garssen *et al.* (1998) has shown evidence that acute UVR exposure may cause re-activation of latent herpes labialis infection and Jackson *et al.* (2000) has shown evidence that chronic UVR exposure may cause increased incidence of viral warts caused by latent papilloma infection. Some studies have also suggested that UVR exposure may cause disruption in the development of prophylactic immunization (Damian, Barnetson and Halliday, 2001; Sleijffers *et al.*, 2001).

Vitamin D Production

UVB absorption in the epidermis and dermis causes production of Vitamin D3, which is beneficiaal to health. Numerous studies have linked vitamin D deficiency with a large number of diseases including colon cancer (Pereira, Larriba and Muñoz, 2012), prostate cancer (Gilbert *et al.*, 2012), breast cancer (Chen *et al.*, 2010), heart disease (Welles *et al.*, 2014), multiple sclerosis (Ascherio, Munger and Simon, 2010), type I diabetes (Pittas and Dawson-Hughes, 2010), rheumatoid arthritis (Song, Bae and Lee, 2012), and even infectious diseases such as tuberculosis (Talat *et al.*, 2010) and influenza (Urashima *et al.*, 2010). Some locations with low solar irradiance have used lamp emitted UV exposure to stimulate vitamin D production to overcome vitamin D deficiency (Chandra *et al.*, 2007).

CIE has published an action spectrum characterizing the wavelength dependent effectiveness of UV mediated conversion between 7-dehydrocholesterol (7-DHC) and pre-vitamin D production in human skin. This action spectrum is similar to the erythemal action spectrum at wavelengths greater than 297 nm (Bouillon *et al.*, 2006).

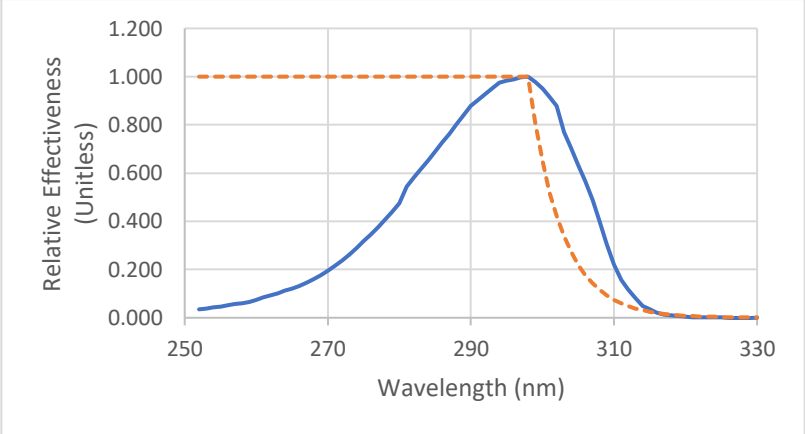

Figure B-7 The action spectrum of UV mediated conversion of 7-DHC to previtamin D (solid line) and the CIE erythemal action spectrum (dashed line) (Bouillon et al., 2006).

A.8.d. UV Exposure Interactions with Exogenous Agents

UV exposure may interact with a variety of exogenous agents, resulting in several effects. Medical practitioners have used UV exposure in combination with topical and oral psoralens to a treat psoriasis, mycosis, fungoides, vitiligo, and atopic dermatitis (Kang *et al.*, 2022). Kerr *et al.* (2010) presented a review of photoallergic contact dermatitis resulting from UV exposure interactions with organic UV filters (sunscreens) and non-steroidal anti-inflammatory drugs (NSAIDs). A comprehensive review of drug induced photosensitivity found evidence implicating numerous drug types, including antibiotics, antifungals, diuretics, anti-inflammatory drugs, calcium channel antagonists, psoralens, psychoactive drugs, retinoids, and photodynamic therapy agents (Dawe and Ibbotson, 2014).

B. Cannabis

Cannabis sativa and *cannabis indica* are annual, dioeciously flowering, fast growing, plants. The genus is believed to have originated in the eastern Tibetan plateau (McPartland, Hegman and Long, 2019) and its morphology is characterized by erect angular stems, branched taproots, and palmate leaves with seven lobes. Cannabis reproduction may occur through seeds or cloning. Seed, or sexual, reproduction results from the cross pollination of male and female plants, while cloning reproduction occurs when a parent plant clipping gets replanted. Cannabis farms typically clone female plants as this method ensures genetic stability across sequential crop cycles and the homogenous female crop prevents crop fertilization, an event that reduces the quality of a crop's flowers (Farag and Kayser, 2017).

The first stage of a cannabis life cycle is the germination stage, which lasts 3 to 7 days and is triggered by seed exposure to water. Farms may skip the germination stage by cloning and start a crop at the second stage, the seedling stage. This stage lasts two to three months, followed by an approximately one-month vegetative growth stage where the plant grows most of its biomass. The vegetative growth stage ends when a plant's light environment changes from long daily photoperiods (18 to 24 hours) to shorter photoperiods (12 hours) (Farag and Kayser, 2017). The flowering stage lasts between two to three months.

B.1. The Cannabis Industry

Washington state divides the cannabis industry into cannabis production, processing, and retail. Cannabis production consists of growing and harvesting a cannabis crop. Cannabis processing consists of various intermediary steps that transform the crop plant matter into a final product. Cannabis retail consists of selling the final cannabis product to the end consumer (WASAO, 2018).

B.1.a. Cannabis Cultivation

Cannabis cultivation is structured around bringing a crop from clone (or seedling) to harvest. A farm begins a crop cycle by planting clones originating from a previous harvest or from mother plants, which are plants perpetually kept in the vegetative state to use as a source of clippings from one crop to the next. The clones are placed in an indoor area of the farm designated as a plant nursery. Once the plants reach a farm specific size, approximately 8 inches tall, farm workers relocate the crop to an indoor grow room or an outdoor growing area. The farm triggers a crop's flowering stage by exposing the crop to a light schedule with a 12-hour day / night cycle. A crop's flowering stage ends at harvest when farm workers cut the plants at their base and move the biomass to other areas of the farm for crop pre-processing (Green, 2010; Farag and Kayser, 2017; WASAO, 2018).

Pre-processing methods include cannabis drying, manicuring, and curing. Farms apply some or all pre-processing methods to their crop prior to shipment to cannabis processors. Cannabis drying involves placing the product in a dark room with a temperature between 18 and 25 °C and humidity between 45 and 55% (Hawes and Cohen, 2013). Cannabis manicuring involves farm workers removing all biomass other than the buds and stem from the product. Cannabis curing is usually the last pre-processing step and involves placing the product in an airtight container and letting it sit in a dark area at room temperature. The cannabis industry has not reached a consensus of the optimum durations for the drying and curing steps (Lazarjani *et al.*, 2021; Green, 2010). After pre-processing, farms will group

the buds into product lots, collect quality assurance lot samples, and send those samples to laboratories for chemical testing. If a lot's samples pass Washington state's cannabis quality standards, the farm may ship the cultivated product to processors (WASAO, 2018).

The cannabis Industry has yet to reach consensus on the spectral profile and intensity of the radiation that farms should supply their crop. One study provides some evidence that farms have started to consolidate to the use of high-pressure sodium (HPS) lamps during the flowering stage of growth. However, this same study found that farms deployed a variety of lamps during the vegetative growth stage (Sweet, 2016).

B.1.b. Cannabis Processing

Cannabis processing refers to the component of the cannabis industry that converts the cannabis biomass to intermediary or final products. Examples of intermediary products include hash oil, kief, wax, which are intended for further refinement to end products. Examples of final products include joints, edibles, and topical products intended for use by the end consumer (WASAO, 2018).

Many cannabis intermediate products require the biomass to undergo some form of extraction method to isolate the desired compounds, usually cannabinoids, flavonoids, and/or terpenes. Solvent based methods are commonly used in the industry, and the solvents used range from hydrocarbons such as ethanol and butane to vegetable fats and supercritical carbon dioxide. Non-solvent based methods exist, but the industry does not employ them due to issues at scale (Lazarjani *et al.*, 2021).

Cannabis processors send their intermediary products to other cannabis processors and their final product to cannabis retailors.

B.1.c. Cannabis Retail

Cannabis retail is the component of the industry at which point the end consumer may purchase the product (WASAO, 2018).

B.1.d. Cannabis Quality Assurance Testing

Washington state requires quality assurance product testing. Testing procedures include water activity, potency analysis, presence of foreign matter, presence of microbiological contaminants, presence of mycotoxins, presence of pesticides, and presence of residual solvents (WAC, 2022).

B.2. Occupations in the Cannabis Industry

The cannabis industry consists of a diverse set of occupations across all three segments of the industry. All three segments employ various transportation, administrative, and maintenance roles. Roles specific to the cannabis cultivation segment are cultivators, trimmers, and farm managers, all of which may experience UV exposure. Cultivators plant, transplant, water, clean, apply pesticides, and otherwise directly interact with the crops. Trimmers handle preprocessing tasks such as trimming, packaging and grouping lots. Farm workers frequently typically operate as both cultivators and trimmers. Farm managers oversee farm operations and typically lead teams of cultivators during day-to-day operations.

Roles specific to the cannabis processing segment are extraction technicians, edible producers, and laboratory technicians. Extraction technicians plan and execute various extraction methods to extract cannabinoids, flavonoids, and terpenes from the plant biomass. Edible producers cook, bake, package, bottle, and label marijuana infused products.

A role specific to the cannabis retail sector is the budtender, a sales representative that sells cannabis and cannabis infused products to customers (CDPHE, 2017).

C. The State of Research of Occupational Health in the Cannabis Industry

C.1.a. Scope and Purpose

The purpose of this section is to undertake a comprehensive review of previous research that investigated occupational health issues in the cannabis industry.

C.1.b. Generation of Search Queries

Studies captured in this literature search investigated or discussed "hazards" within the "cannabis" industry that impacted "workers." These three criteria formed the basis for search queries submitted to Clarivate's Web of Science and Google Scholar.

Web of Science Search Query

ALL=((hazard OR safety OR health OR exposure*) AND (cannabis OR marijuana OR sativa) AND (worker* OR employee* OR occupation* OR grower* OR cultivat* OR process*))*

Google Scholar Search Query

The query input into google scholar is below.

(hazard OR safety OR health OR exposure*) AND (cannabis OR marijuana OR sativa) AND (worker* OR employee* OR occupation* OR grower* OR cultivat* OR process* OR facility)*

C.1.c. Results

Web of Science returned 5777 results and Google Scholar returned 25,600 results. The titles of the first thousand results from each engine were screened for relevance, and if the title indicated that the article was relevant, the abstract would be read. If the abstract indicated that study was relevant, the study was included in the literature review. Excluded studies included those that covered occupational hazards in non-cannabis hemp industries, and those that investigated consumption of cannabis while at work in non-cannabis industry occupations. The filtering process identified thirty-six studies.

Twenty-one of the thirty-six studies measured an environmental variable(s) or conducted worker interviews/questionaries, twelve reviewed the current state of literature, and three were editorials or commentaries. Of the former twenty-one publications, ten measured an agent in the ambient environment, three utilized some form of biomonitoring, thirteen utilized worker surveys (questionaries and/or interviews), and three utilized both questionnaires and environmental measurement methods. Of the ten studies that measured an environmental variable, four tested for endotoxin, four tested for THC, four tested for volatile organic compounds (VOCs), six tested for fungal spores, three tested for bacteria, two tested for particle matter, and one tested for ergonomic issues related to cannabis trimming. Studies that used surveys generally structured questions to qualitatively identify occupational health issues in the cannabis industry as well as external forces that interact with those issues. External forces touched on by the publications include those of demographic, gender, social, political, regulatory, and cultural nature. Table C-1 presents a list of the twenty-one studies that measured a variable(s) and a description of the measurement and variable.

Table C-1 A list of the twenty-one studies that measured a variable(s) and a description of the measurement and variable.

Reference	Type	Variable(s)
(Couch *et al.* 2019)	Measurement	Environmental sampling for airborne endotoxin concentrations
(Couch, Grimes, *et al.*, 2019)	Measurement	Surface wipes of THC, cannabidiol, and cannabinol. Environmental air samples for VOCs, endotoxins, and fungal diversity
(Evoy and Kincl, 2020)	Measurement	Qualitative analysis of Oregon State pesticide testing data to generate list of pesticides used in industry
(Green *et al.*, 2018)	Measurement	Qualitative and quantitative personal and environmental air sampling of airborne bacteria and fungi
(Martyny *et al.*, 2013)	Measurement	Surface sampling for THC, environmental air sampling for fungal spores, VOCs, CO2, CO, and THC
(Root *et al.*, 2020)	Measurement	Environmental sampling of airborne fungal spores
(Sack *et al.*, 2020)	Measurement	Worker survey for of respiratory, ocular, nasal, and dermal symptoms; measurement of spirometry, fractional exhaled nitrogen oxide (FeNO), and skin prick testing
(Silvey, 2019)	Measurement	Environmental air sampling for particle number concentration, particle mass concentration, cumulative size distribution, and VOCs
(Silvey *et al.*, 2020)	Measurement	Environmental air sampling for particle number concentration, particle mass concentration, cumulative size distribution, and VOCs
(Couch *et al.*, 2017)	Measurement	Survey of occupational tasks that the workers performed, use of PPE, experienced sensitization symptoms related to working with cannabis, musculoskeletal
(Victory *et al.*, 2018)	Measurement	Survey of work, safety, and health concerns. Measurement of manual hand forces during destemming, measurement of repetitive motion of the hand and fingers in trimming. Environmental and personal air samples for endotoxin, fungal diversity, and bacterial diversity, surface wipe samples for THC
(Beckman *et al.*, 2023)	Survey	Worker survey for of respiratory, dermal, musculoskeletal symptoms; reporting of mold, pesticide, thermal hazards; unsanitary living conditions; Reporting of different and contrasting worker vs management lived experience
(Beckman, Langer and Schenker, 2023)	Survey	Worker survey for eye, nasal, respiratory, and dermal symptoms; Demographic characteristics
(Brown *et al.*, 2020)	Survey	Worker survey for demographics, perceived job hazards, confidence to change workplace practices post safety training, knowledge, training relevancy and quality, intent to change behavior, as well as barriers and resources.
(Ehrlich, Simpson, and Busch Isaksen, 2020)	Survey	Worker survey of health concerns resulting from social, economic, regulatory, political, and cultural forces; Cultural forces include race, gender, educational, and other individual factors.
(Majano, 2020)	Survey	Worker survey of issues related to sexual harassment.
(Otanez and Grewal, 2021)	Survey	Transcripts of interviews with cannabis industry workers and occupational health and safety trainers on occupational issues in the cannabis industry. Topics mentioned include airborne mold exposure, respiratory health, pandemic disruptions, cultural stigmas associated with cannabis, labor / management relationship, and issues caused by federal regulations
(Trask, Koehncke and Trask, 2021)	Survey	Worker survey on opinions related to implementations of occupational health and safety
(Walters, Fisher and Tenney, 2018)	Survey	Worker survey on occupation, job tasks, general well-being, occupational health and safety, cannabis use, and tobacco use.
(Ghodsian, 2019)	Survey, Measurement	Worker survey for respiratory, ocular, nasal and dermal health symptoms as well as health history, cannabis use history, tobacco smoking status, and occupational exposure to dusts, gases, and other respiratory hazards; measurement of spirometry, fractional exhaled nitrogen oxide (FeNO) and skin prick testing (SPT) for sensitization to cannabis / hemp and other common allergens.
(Kenleigh, 2022)	Survey, Measurement	Worker survey for respiratory, ocular, nasal and dermal health symptoms as well as health history, cannabis use history, tobacco smoking status, and occupational exposure to dusts, gases, and other respiratory hazards; measurement of spirometry, fractional exhaled nitrogen oxide (FeNO) and skin prick testing (SPT) for sensitization to cannabis / hemp and other common allergens.

Editorials and commentaries on occupational health research in the cannabis industry include Stone *et al.* 2014, Simpson 2020, and Schenker *et al.* 2023. Review papers on occupational health research in the cannabis industry include Davidson *et al.*, 2018; Eykelbosh, 2018; Reed *et al.*, 2018; Couch *et al.*, 2020; Decuyper *et al.*, 2020; Howard and Osborne, 2020; Phalen, 2020; Russell, 2020; Schenker and Langer, 2021; Monticelli *et al.*, 2022; Sack, Simpson, and Pacheco, 2023.

C.1. Occupational Health in the Cannabis Industry

Cannabis industry workers may encounter many biological, chemical, and physical hazards during work.

C.1.a. Biological Hazards

Identified biological hazards consist of exposure to molds, bacteria, and sensitizers. Mold is a ubiquitous hazard due to the shared appreciation that both cannabis plants and mold have for warm and humid environmental conditions. Research has shown that indoor cannabis farms may have large airborne fungal spore concentrations relative to outdoor air (Martyny *et al.*, 2013; Root *et al.*, 2020) and that the number of identified airborne fungal species is very large (Howard and Osborne, 2020; Root *et al.*, 2020). Also, the species concentrations can rapidly change during plant relocation (Martyny *et al.*, 2013). Mold related endotoxins and endotoxins released by the outer cell walls of gram-negative bacteria might become an airborne hazard during the harvest and processing stages (Couch *et al.*, 2019). Even in an outdoor cannabis facility in the US, the cannabis workers were exposed to a variety of bacteria especially Acinetobacter species as well as the cannabis plant pathogen, *botrytis cinerea* during harvesting, bud-stripping, and hand-trimming processes (Green *et al.*, 2018).

Research has examined allergic sensitization to cannabis dust. A study of workers at a Washington State cannabis farm showed a high proportion of employees with work-aggravated allergic symptoms (Sack *et al.*, 2020; Kenleigh, 2022). Dermal sensitization usually manifests as dermatitis (urticaria) and respiratory allergens can cause itchy, runny or congested nose, sneezing, or coughing and wheezing (Majmudar, Azam and Finch, 2006; Williams, Thompstone and Wilkinson, 2008). Investigations of adult cannabis allergies have found that type I hyper-sensitivity mechanisms involving allergen-specific IgE anti-bodies are predominant (Herzinger *et al.*, 2011).

C.1.b. Chemical Hazards

The chemical occupational risk factors in the cannabis industry include exposures to carbon dioxide (CO_2), carbon monoxide (CO), volatile organic compounds (VOCs), pesticides, fertilizers, disinfectants, and cleaning chemicals (CDPHE, 2017; Simpson, 2020).

Some farms pump supplemental CO_2 into indoor grow rooms to accelerate plant growth (Chandra *et al.*, 2011), however, this action has the potential to create oxygen deficient atmospheres (Martyny *et al.*, 2013). Other oxygen deficient atmospheres may result from improper handling of dry ice during extraction processes or in environments with combustion-powered equipment. Environments with combustion powered equipment also have the potential to have carbon monoxide exposures (Martyny *et al.*, 2013).

Cannabis farm workers, processors, retailors, and even potentially end consumers have the risk of exposure to pesticides and fungicides (Stone, 2014; Eykelbosh, 2018; Evoy and Kincl, 2020; Howard and Osborne, 2020). However, state level quality assurance and quality control regulations reduce the likelihood of exposure to groups outside of those working at cannabis farms (WAC, 2022).

Cannabis cultivars produce and emit a wide range of VOCs. Workers' exposure to tetrahydrocannabinol (THC) may result in changes to mood, memory, or disorientation (Couch *et al.*, 2017). During cannabis

decarboxylation and grinding of dried cannabis material, elevated job-specific concentrations of volatile organic compounds (VOCs) such as terpenes, diacetyl, and 2,3-pentanedione were measured (Couch *et al.*, 2020; Silvey *et al.*, 2020). Inorganic fertilizers used for promoting plant growth and flower development are a corrosive and/or irritant hazard, which can severely damage body tissues while organic fertilizers may expose workers to biological hazards (Davidson *et al.*, 2018).

Disinfectants and cleaning chemicals can cause respiratory tract, eye and skin irritation while improper mixing of chemicals and resulting fumes can lead to lung damage. Indoor air quality in the warm, humid environment enclosed areas may be affected by ozone produced in the reaction of nitrogen oxides and volatile organic compounds such as terpenes released from the marijuana plant. Ozone used for odor control can contribute to the decrease of lung function while terpenes and nitric oxide reaction products are linked to eye, skin, and mucous irritation (CDPHE, 2017). Apart from physiological health effects due to increased concentrations of ozone, terpenes and their oxidation products, some health effects may be associated with odor. These include annoyance, problems with sleeping, nausea, and headache (Monticelli *et al.*, 2022).

C.1.c. Physical Hazards

The cannabis industry shares many physical hazards with other agricultural industries. Examples include slips, trips and falls, electrical, noise, vehicles, heavy machinery, confined spaces.

Physical hazards specific to the cannabis industry include the ergonomic hazards associated with the repetitive motions of cannabis trimming, explosion and fire hazards associated with extraction processes, workplace violence hazards, and sexual harassment (CDPHE, 2017). The cannabis industry operates in regulatory and cultural conditions that may exacerbate workplace violence risks. The federal illegality of the cannabis industry drives farms, processers, and retailors to operate almost exclusively in cash, consequently creating cash stockpiles at each business locations (CDPHE, 2017). These stockpiles put a target on the businesses for robbery and the associated physical hazards, and unfortunately many reports have documented instances of armed robbery in states where the cannabis industry may operate (Saldanha, 2022; ABC 7 News, 2023). A 2020 master's thesis on sexual harassment in the cannabis industry argues that the culture of secrecy fostered pre-legalization helped establish a 'culture of silence' that is effective at hiding sexual harassment abuses in the workplace (Majano, 2020).

D. Review of Ultraviolet Radiation Exposure Measurement

D.1. Literature Search

D.1.a. Scope and Purpose

The purpose of this section is to undertake a comprehensive review of previous research that investigated human UV exposure using UV measurement devices.

D.1.b. Generation of Search Queries

Studies captured in this literature search performed some form of "measurement," defined a "population of interest," and considered "UV" "exposure," the outcome variable. These four criteria formed the basis for search queries submitted to Scopus and Google Scholar.

Scopus Search Query
TITLE-ABS-KEY((Ultraviolet OR UV) AND (Expos OR Dos* OR Irradiance OR Radiant* OR "Action Spectrum" OR Erythem* OR SED OR MED OR Intensit*) AND (Measure* OR Spectro* OR Radiometer* OR ICNIRP OR CIE OR ACGIH OR photodiode OR sensor OR detector) AND (Work* OR Farm* OR Job OR Agricult* OR Employ* OR Occupation* OR child* OR group OR population))*

Google Scholar Search Query
Google scholar only accepts queries of 260 characters or less, therefore, the query input to google scholar had to have less terms than that of the input to Scopus. Terms chosen for removal include those that specified weighting by an action spectrum because studies having these terms would also have the terms with the root expos*, dos*, or irradiance. The query input into google scholar is below.

(Ultraviolet OR UV) AND (Expos OR Dos* OR Irradiance OR Radiant* OR Intensit*) AND (Measure* OR Spectro* OR Radiometer* OR photodiode OR sensor OR detector) AND (Work* OR Farm* OR Job OR Agricult* OR Employ* OR Occupation* OR child* OR group OR population)*

Scopus returned 20,081 results and Google Scholar returned 6,630 results. The process of identifying relevant studies included reading the title of each result to determine whether the article was relevant to this literature review. If the title indicated that the article was relevant, the abstract would be read, and if the abstract indicated that study was relevant, the study was included in the literature review. The filtering process identified 187 studies that met the four inclusion criteria.

D.2. UV Exposure Introduction

Studies measuring UV exposure published measurement values as either accumulated radiant energy or irradiance, and unfortunately direct comparison between the two is impossible. To allow comparison, the following sections contain tables that present minimum, maximum, and central tendency values converted into units of irradiance. This section describes the process of conversion assumptions.

Results originally presented as accumulated radiant energy per session were converted into irradiance by dividing the published value by the length of the monitoring session. Sometimes, studies did not publish each monitoring session duration, instead only publishing the average session duration. If this was the case, results were converted from their original units into irradiance by dividing the value by the average session length. However, dividing by the average session length may bias the converted irradiance by underestimating the minimum and overestimating the maximum.

Results presented as accumulated radiant energy over a day were converted into irradiance by computing the average irradiance over a 24-hour period. Results presented in units of SED were converted into units of effective radiant energy in J/m^2 by multiplying by 100 J/m^2. Results presented in units of MED were converted into units of effective radiant energy in J/m^2 by multiplying the published value by the person specific effective radiant value usually published in the article. If the article did not publish a conversion value, the conversion used a value of 200 J/m^2. Finally, all irradiance values presented over an area other than square centimeters were converted to square centimeters.

D.3. Dosimetric Monitoring of Occupational Solar UV Exposure

The literature search identified forty-one studies that directly measured occupational exposure to solar radiation. A few other studies performed UV exposure measurement as part of the validation process for UV exposure models. Section D.6 titled “Estimates of Occupational Solar UV Exposure” provides an overview of these studies.

D.3.a. Study Subjects

Past efforts have investigated solar UV exposure in a wide variety of occupations. Commonly studied occupations include agricultural workers (Sisto *et al.*, 2009; Alois W Schmalwieser *et al.*, 2010; Siani *et al.*, 2011; Liljendahl *et al.*, 2013; Bodekær *et al.*, 2014, 2015; Nardini, Neri and Paroncini, 2014), construction workers (Gies and Wright, 2003; Antoine *et al.*, 2007; Serrano, Cañada and Moreno, 2013; Wolska, 2013; Grandahl *et al.*, 2018), and lifeguards (Gies *et al.*, 1995, 2009; Moehrle and Garbe, 2000; Serrano *et al.*, 2009; Liljendahl *et al.*, 2013).

D.3.b. UV Measurement Devices

Studies used various personal dosimetry devices to measure UV exposure. Devices included polysulfone film dosimeters (Challoner *et al.*, 1976; Leach *et al.*, 1978; O. Larko and Diffey, 1983; Wong *et al.*, 1992; Gies *et al.*, 1995, 2009; Kimlin, Parisi and Wong, 1998; A. V Parisi, Meldrum, Kimlin, *et al.*, 2000; Vishvakarman, Wong and Boreham, 2001; Gies and Wright, 2003; Siani *et al.*, 2008, 2011; Sisto *et al.*, 2009; Liljendahl *et al.*, 2013; Downs, Harrison and Parisi, 2015; Peters *et al.*,

2019), *Bacillus subtilis* spore film (Moehrle and Garbe, 2000; Cockell *et al.*, 2001, 2002; Thieden, Ågren and Wulf, 2001; Moehrle *et al.*, 2003; Antoine *et al.*, 2007; Serrano *et al.*, 2009; Feister, Meyer and Kirst, 2013; Serrano, Cañada and Moreno, 2013; Cheng *et al.*, 2015) and electronic dosimeters (Cockell *et al.*, 2001, 2002; Thieden, Peter A Philipsen, *et al.*, 2004; Thieden, Philipsen and Wulf, 2006; Antoine *et al.*, 2007; Sisto *et al.*, 2009; Alois W Schmalwieser *et al.*, 2010; Feister, Meyer and Kirst, 2013; Wolska, 2013; Bodekær *et al.*, 2014; Nardini, Neri and Paroncini, 2014; Peters *et al.*, 2016, 2019; Grandahl *et al.*, 2017, 2018).

Researchers mounted UV dosimeters at a variety of body locations including on the top of the head (Wong *et al.*, 1992; Vishvakarman, Wong and Boreham, 2001; Siani *et al.*, 2011; Feister, Meyer and Kirst, 2013; Cheng *et al.*, 2015; Peters *et al.*, 2016), face (Wong *et al.*, 1992; Moehrle *et al.*, 2003; Antoine *et al.*, 2007; Siani *et al.*, 2008; Alois W Schmalwieser *et al.*, 2010; Nardini, Neri and Paroncini, 2014) , on the neck (Wong *et al.*, 1992; Cockell *et al.*, 2001; Antoine *et al.*, 2007; Downs, Parisi and Igoe, 2014; Nardini, Neri and Paroncini, 2014), chest (Challoner *et al.*, 1976; Leach *et al.*, 1978; O. Larko and Diffey, 1983; Gies *et al.*, 1995; Vishvakarman, Wong and Boreham, 2001; Cockell *et al.*, 2002; Gies and Wright, 2003; Feister, Meyer and Kirst, 2013; Peters *et al.*, 2016), arm (Sisto *et al.*, 2009; Siani *et al.*, 2011; Nardini, Neri and Paroncini, 2014; Cheng *et al.*, 2015), back (Vishvakarman, Wong and Boreham, 2001; Antoine *et al.*, 2007; Sisto *et al.*, 2009; Feister, Meyer and Kirst, 2013), and wrist (Thieden, Ågren and Wulf, 2001; Thieden, Peter A Philipsen, *et al.*, 2004; Elisabeth Thieden, Peter A Philipsen, *et al.*, 2005; E. Thieden *et al.*, 2005; Thieden, Philipsen and Wulf, 2006; Gies *et al.*, 2009; Siani *et al.*, 2011; Bodekær *et al.*, 2014; M.-A. Serrano *et al.*, 2014; Peters *et al.*, 2016, 2019; Grandahl *et al.*, 2017, 2018).

D.3.c. Ambient Solar UV Measurements

Concurrently with personal exposure measurements, some studies measured or acquired ambient solar UV irradiance data. The studies that took ambient measurements used either a radiometer (Gies *et al.*, 1995; Kimlin, Parisi and Wong, 1998; A. V Parisi, Meldrum, Kimlin, *et al.*, 2000; Thieden, Ågren and Wulf, 2001; Thieden, Peter A Philipsen, *et al.*, 2004; Elisabeth Thieden, Peter A Philipsen, *et al.*, 2005; E. Thieden *et al.*, 2005; Thieden, Philipsen and Wulf, 2006; Siani *et al.*, 2008, 2011; Serrano *et al.*, 2009; Sisto *et al.*, 2009; Alois W Schmalwieser *et al.*, 2010; Serrano, Cañada and Moreno, 2013; Bodekær *et al.*, 2014; M.-A. Serrano *et al.*, 2014; Downs, Harrison and Parisi, 2015; Downs *et al.*, 2016), spectroradiometer (Nardini, Neri and Paroncini, 2014; Peters *et al.*, 2016), a polysulfone film dosimeter (Challoner *et al.*, 1976; Gies *et al.*, 1995, 2009; Vishvakarman, Wong and Boreham, 2001; Downs, Parisi and Igoe, 2014; Peters *et al.*, 2019), a spore film dosimeter (Antoine *et al.*, 2007), an allyl diglycol carbonate dosimeter (CR-39)(Wong *et al.*, 1992), an electronic dosimeter (Cockell *et al.*, 2002; Siani *et al.*, 2011), or acquired the data from a local meteorological data source (LMDS) (Cockell *et al.*, 2001; Antoine *et al.*, 2007; Feister, Meyer and Kirst, 2013; Liljendahl *et al.*, 2013; Bodekær *et al.*, 2014). Table D-1 contains a summary of study methodologies for studies investigating solar UV exposure in occupational groups.

Table D-1 Studies that measured solar UV exposure in occupational groups using dosimetry. The table contains the type of study subjects, the position of the dosimeters, the type of dosimeter, and the ambient UV measurement device.

Citation	Subjects	Dosimetric Position	Dosimeter	Ambient UV Instrument
(Antoine *et al.*, 2007)	Construction	neck, shoulder, back, face	Spore film, electronic dosimeters	Spore film, LMDS
(Bodekær *et al.*, 2014)	Agricultural	wrist	Electronic dosimeters	LMDS
(Bodekær *et al.*, 2015)	Agricultural	wrist	Electronic dosimeters	Electronic dosimeter, LMDS, Radiometer
(Challoner *et al.*, 1976)	Gardeners, Lab techs	chest	Polysulfone film	Polysulfone film
(Cheng *et al.*, 2015)	Mountaineers	top of head, armpit	Spore film	None
(Cockell *et al.*, 2001)	Arctic researchers	neck	Spore film, electronic dosimeters	LMDS
(Cockell *et al.*, 2002)	Scientists	chest	Spore film	Electronic dosimeters
(Downs, Parisi and Igoe, 2014)	Teachers	neck	Polyphenylene oxide film	Polyphenylene oxide film
(Downs, Harrison and Parisi, 2015)	Teachers	Not stated	Polysulfone film	Radiometer
(Downs *et al.*, 2016)	Teachers	shoulder	Polysulfone film	Radiometer
(Feister, Meyer and Kirst, 2013)	Seafarers	top of head, shoulder, chest and back	Spore film, electronic dosimeters	LMDS
(Gies *et al.*, 1995)	Multiple Occupations	chest, shoulder	Polysulfone film	Polysulfone film, Radiometer
(Gies and Wright, 2003)	Construction	chest	Polysulfone film	None
(Gies *et al.*, 2009)	Lifeguards	wrist	Polysulfone film	polysulfone film
(Grandahl *et al.*, 2017)	Outdoor workers	wrist	Electronic dosimeters	None
(Grandahl *et al.*, 2018)	Multiple	wrist	Electronic dosimeters	None
(Kimlin, Parisi and Wong, 1998)	Outdoor workers	shoulder	Polysulfone film	Radiometer
(O. Larko and Diffey, 1983)	Outdoor Workers, Indoor Workers	chest	Polysulfone film	None
(Leach *et al.*, 1978)	Indoor workers	chest	Polysulfone film	Polysulfone film
(Liljendahl *et al.*, 2013)	Lifeguards and agricultural workers	shoulder	Polysulfone film	LMDS
(Moehrle and Garbe, 2000)	lifeguards and mountaineers	shoulder, face	Spore film	None
(Moehrle *et al.*, 2003)	Mountaineers	face	Spore film	None
(Nardini, Neri and Paroncini, 2014)	Agriculture	arm, face, neck	Electronic dosimeter	spectrometer
(A. V Parisi, Meldrum, Kimlin, *et al.*, 2000)	Outdoor workers, home workers	shoulder	Polysulfone film	Radiometer
(Peters *et al.*, 2016)	Outdoor workers	wrist, chest, top of head	Electronic dosimeters	Spectroradiometer
(Peters *et al.*, 2019)	Outdoor workers	wrist, shoulder, head	Polysulfone film	Polysulfone film
(Alois W Schmalwieser *et al.*, 2010)	Agriculture	face	Electronic dosimeters	Radiometers
(Serrano *et al.*, 2009)	Gardeners and lifeguards	shoulder	Spore film	Radiometer
(Serrano, Cañada and Moreno, 2013)	Construction	shoulder, chest	Spore film	Radiometer
(M.-A. Serrano *et al.*, 2014)	Environmental enforcement agents	shoulder, wrist	Spore film	Radiometer
(Siani *et al.*, 2008)	Ski instructors	face	Polysulfone film	Radiometer
(Siani *et al.*, 2011)	Agriculture	chest, top of head, shoulder, arm, back, face, wrist, neck	Polysulfone film	Radiometer, electronic dosimeters
(Sisto *et al.*, 2009)	Agriculture	arm, back	Polysulfone film, electronic dosimeter	Radiometer
(Thieden, Ågren and Wulf, 2001)	Indoor workers	wrist	Spore film	Radiometer
(Thieden, Peter A Philipsen, *et al.*, 2004)	Indoor workers, gardeners	wrist	Electronic dosimeters	Radiometer
(E. Thieden *et al.*, 2005)	Gardeners	wrist	Electronic dosimeter	Radiometer
(Thieden, Philipsen and Wulf, 2006)	Indoor workers	wrist	Electronic dosimeter	Radiometer
(Elisabeth Thieden, Peter A Philipsen, *et al.*, 2005)	Indoor workers, gardeners, rangers	wrist	Electronic dosimeter	Radiometer
(Vishvakarman, Wong and Boreham, 2001)	Teachers, Postal Worker	head, chest, back, leg, shoulder	Polysulfone film	Polysulfone film
(Wolska, 2013)	Multiple	shoulder	Electronic dosimeters	None
(Wong *et al.*, 1992)	Multiple	face, neck, top of head	CR-39	Polysulfone film, CR-39

'None' - the study did not use any calibration instrumentation specified by the column title.

'No mention' - the study did not mention any calibration whatsoever for either the wearable or ambient device(s).

'Unspecified' - the study explicitly stated use of a calibrated device but provided no information on the calibration procedure.

D.3.d. Calibration

All studies monitoring with polysulfone film dosimeters directly stated or implied that the research team built a calibration curve as described in section A.5.a and most used solar radiation as the optical reference. However, two studies (Leach *et al.*, 1978; Downs, Harrison and Parisi, 2015) did not specify the optical reference used to construct the calibration curve, and a single study (O. Larko and Diffey, 1983) used known emissions from a xenon arc lamp (solar simulator) to build the calibration curve. The research teams used either calibrated radiometers (Challoner *et al.*, 1976; Vishvakarman, Wong and Boreham, 2001; Siani *et al.*, 2011; Peters *et al.*, 2019) or spectroradiometers (Challoner *et al.*, 1976; Gies *et al.*, 1995, 2009; Kimlin, Parisi and Wong, 1998; A. V Parisi, Meldrum, Kimlin, *et al.*, 2000; Gies and Wright, 2003; Siani *et al.*, 2008; Sisto *et al.*, 2009; Liljendahl *et al.*, 2013; Downs *et al.*, 2016) to measure the irradiance from their optical source in order to construct their calibration curves.

Studies calibrated their wearable electronic devices using a variety of methods. Ten studies used solar radiation as the calibration reference (Cockell *et al.*, 2001; Thieden, Peter A Philipsen, *et al.*, 2004;

Antoine *et al.*, 2007; Sisto *et al.*, 2009; Alois W Schmalwieser *et al.*, 2010; Bodekær *et al.*, 2014; Peters *et al.*, 2016; Grandahl *et al.*, 2017, 2018) and two studies used a quartz tungsten halogen lamp (QTHL) (Wolska, 2013). Four studies calibrated their electronic wearable devices through intercomparison with a radiometer (Thieden, Peter A Philipsen, *et al.*, 2004; Antoine *et al.*, 2007; Alois W Schmalwieser *et al.*, 2010; Bodekær *et al.*, 2014) or spectroradiometer (Cockell *et al.*, 2001; Sisto *et al.*, 2009; Peters *et al.*, 2016; Grandahl *et al.*, 2017, 2018). Finally, some studies do not mention the calibration of the dosimetric device at all (Leach *et al.*, 1978; Moehrle *et al.*, 2003; Elisabeth Thieden, Peter A Philipsen, *et al.*, 2005; E. Thieden *et al.*, 2005; Thieden, Philipsen and Wulf, 2006; Serrano *et al.*, 2009; Cheng *et al.*, 2015).

Studies also calibrated their ambient UV measurement devices using a variety of methods. The most common method was intercomparison with a spectroradiometer (Challoner *et al.*, 1976; Gies *et al.*, 1995, 2009; Vishvakarman, Wong and Boreham, 2001; Siani *et al.*, 2008; Serrano *et al.*, 2009; Downs, Parisi and Igoe, 2014; M.-A. Serrano *et al.*, 2014; Peters *et al.*, 2016). One study (Serrano *et al.*, 2009) used both a spectroradiometer and a radiometer and another (Alois W Schmalwieser *et al.*, 2010) used only a radiometer as the intercomparison device. Five studies mentioned that calibration of the ambient device occurred but did not specify the procedure or instrumentation used (Parisi, Meldrum, Kimlin, *et al.*, 2000; Thieden, Ågren and Wulf, 2001; Cockell *et al.*, 2002; Thieden, Peter A Philipsen, *et al.*, 2004; Siani *et al.*, 2011). Finally, some studies included in this section omit any mention of calibration for the ambient UV device (Leach *et al.*, 1978; Moehrle *et al.*, 2003; Elisabeth Thieden, Peter A Philipsen, *et al.*, 2005; E. Thieden *et al.*, 2005; Thieden, Philipsen and Wulf, 2006; Nardini, Neri and Paroncini, 2014; Cheng *et al.*, 2015). A full summary of the calibration instrumentation is provided in Table D-2 below.

Table D-2 Summaries of the calibration instrumentation for the studies included in this section.

Citation	Calibration Light	Dosimeter	Intercomparison Device(s)
(Antoine *et al.*, 2007)	Solar	Spore film, electronic dosimeters	Radiometer
(Bodekær *et al.*, 2014)	Solar	Electronic dosimeters	Radiometer
(Bodekær *et al.*, 2015)	Solar	Electronic dosimeters	Spectroradiometer
(Challoner *et al.*, 1976)	Solar	Polysulfone film	Spectroradiometer, radiometer
(Cheng *et al.*, 2015)	No mention	Spore film	No mention
(Cockell *et al.*, 2001)	Solar	Spore film, electronic dosimeters	Spectroradiometer
(Cockell *et al.*, 2002)	Solar	Spore film	Radiometer, Spectroradiometer
(Downs, Parisi and Igoe, 2014)	Solar	Polyphenylene oxide film	Spectroradiometer
(Downs, Harrison and Parisi, 2015)	Unspecified	Polysulfone film	Unspecified
(Downs *et al.*, 2016)	Solar	Polysulfone film	Spectroradiometer
(Feister, Meyer and Kirst, 2013)	QTHL, Solar	Spore film, electronic dosimeters	Manufacturer
(Gies *et al.*, 1995)	Solar	Polysulfone film	Spectroradiometer
(Gies and Wright, 2003)	Solar	Polysulfone film	Spectroradiometer
(Gies *et al.*, 2009)	Solar	Polysulfone film	Spectroradiometer
(Grandahl *et al.*, 2017)	Solar	Electronic dosimeters	Spectroradiometer
(Grandahl *et al.*, 2018)	Solar	Electronic dosimeters	Spectroradiometer
(Kimlin, Parisi and Wong, 1998)	Solar	Polysulfone film	Spectroradiometer
(O. Larko and Diffey, 1983)	Xenon arc lamp	Polysulfone film	Xenon Arc
(Leach *et al.*, 1978)	No mention	Polysulfone film	No mention
(Liljendahl *et al.*, 2013)	Solar	Polysulfone film	Spectroradiometer
(Moehrle and Garbe, 2000)	Unspecified UV lamps	Spore film	Manufacturer
(Moehrle *et al.*, 2003)	No mention	Spore film	No mention
(Nardini, Neri and Paroncini, 2014)	No mention	Electronic dosimeter	No mention
(A. V Parisi, Meldrum, Kimlin, *et al.*, 2000)	Solar	Polysulfone film	Spectroradiometer
(Peters *et al.*, 2016)	Solar	Electronic dosimeters	Spectroradiometer
(Peters *et al.*, 2019)	Solar	Polysulfone film	Radiometer
(Alois W Schmalwieser *et al.*, 2010)	Solar	Electronic dosimeters	Radiometer
(Serrano *et al.*, 2009)	Solar	Spore film	No mention
(Serrano, Cañada and Moreno, 2013)	Solar	Spore film	Spectroradiometer
(M.-A. Serrano *et al.*, 2014)	Solar	Spore film	Spectroradiometer
(Siani *et al.*, 2008)	Solar	Polysulfone film	Spectroradiometer
(Siani *et al.*, 2011)	Solar	Polysulfone film	Radiometer
(Sisto *et al.*, 2009)	Solar	Polysulfone film, electronic dosimeter	Spectroradiometer, manufacturer
(Thieden, Ågren and Wulf, 2001)	Solar	Spore film	Radiometer
(Thieden, Peter A Philipsen, *et al.*, 2004)	Solar	Electronic dosimeters	Radiometer
(E. Thieden *et al.*, 2005)	No mention	Electronic dosimeter	No mention
(Thieden, Philipsen and Wulf, 2006)	No mention	Electronic dosimeter	No mention
(Elisabeth Thieden, Peter A Philipsen, *et al.*, 2005)	No mention	Electronic dosimeter	No mention
(Vishvakarman, Wong and Boreham, 2001)	Solar	Polysulfone film	Radiometer
(Wolska, 2013)	QTHL	Electronic dosimeters	Manufacturer
(Wong *et al.*, 1992)	Solar	Radiometer, polysulfone film	Spectrometer, radiometer

D.3.e. Units and Health Weighting of Original Publication

Studies published UV exposure measurements in units of effective irradiance or effective radiant exposure. Studies that used the CIE erythemal action spectrum published their results as either effective irradiance (Sisto *et al.*, 2009), effective radiant exposure (Challoner *et al.*, 1976; Gies *et al.*, 1995; Liljendahl *et al.*, 2013), SED per day (Thieden, Ågren and Wulf, 2001; Bodekær *et al.*, 2014; Peters *et al.*, 2016), SED per monitoring session (A. V Parisi, Meldrum, Kimlin, *et al.*, 2000; Cockell *et al.*, 2001; Gies and Wright, 2003; Moehrle *et al.*, 2003; Thieden, Peter A Philipsen, *et al.*, 2004; Antoine *et al.*, 2007; Gies *et al.*, 2009; Serrano *et al.*, 2009; Siani *et al.*, 2011; Serrano, Cañada and Moreno, 2013; M.-A. Serrano *et al.*, 2014; Nardini, Neri and Paroncini, 2014; Grandahl *et al.*, 2017, 2018), accumulated radiant exposure over a multi-day period of time (Wong *et al.*, 1992; Alois W Schmalwieser *et al.*, 2010), or in MED per some time period (Moehrle and Garbe, 2000; Cheng *et al.*, 2015). Studies that used the ACGIH action spectrum published results in units of either effective irradiance (Feister, Meyer and Kirst, 2013) or effective accumulated irradiance (Downs, Harrison and Parisi, 2015; Downs *et al.*, 2016). One study (O. Larko and Diffey, 1983) predates publication of the ACGIH and CIE action spectra, and published the results weighted to biologically effective UV-B

doses (UVBE), The study defines UVBE as equivalent to that of a hypothetical dose of monochromatic 297 nm radiation which produces the same erythemal effect as solar radiation received by each film badge worn in the study.

D.3.f. Summary of Published Results

Table D-3 presents the minimum, maximum, and central tendency statistics converted from the original units of publication into units of effective irradiance using the procedure described previously. If the study originally published a single value of central tendency, the table presents only this single value. If the study did not present a single value of central tendency, but instead presented values of central tendency for each subject group, the table presents the converted minimum and maximum of these central tendency statistics as well as the number of subject groups.

Table D-3 The published minimum, maximum, and values of central tendency from the studies that measured solar UV exposure in occupational settings.

Citation	Subjects	Health Weighting	Units as Published	Mean Session Length (min)	Min Published Value (W/cm^2)	Max Published Value (W/cm^2)	Cent Tend Min (W/cm^2)	Cent Tend Max (W/cm^2)	Mean or Median (# of Groups)	Group Type
(Antoine *et al.*, 2007)	Construction	CIE	SED	1440	0.00E+00	1.05E-05	1.38E-06	3.31E-06	mean (of 3)	Mountaineers divided by altitude
(Bodekær *et al.*, 2014)	Agricultural	CIE	SED	1440	5.79E-08	7.52E-07	1.27E-07	1.74E-07	mean (of 4)	Farmers, Spouses, Boys, Girls,
(Bodekær *et al.*, 2015)	Agricultural	CIE	SED	1440	1.62E-07	3.13E-07	NP	NP	N/A	
(Challoner *et al.*, 1976)	Gardeners, Lab techs	CIE*	mJ/cm^2	1440	NP	NP	2.66E-09	2.34E-07	mean (of 4)	patient types 1 and 2, lab techs, gardeners
(Cheng *et al.*, 2015)	Mountaineers	CIE	MED	1440	4.63E-07	1.76E-06	6.02E-07	1.20E-06	median (of 4)	Base camp sherpas and expeditioners, above base camp sherpas and expeditioners
(Cockell *et al.*, 2001)	Arctic researchers	CIE	SED	60	5.56E-08	1.53E-06	NP	NP	N/A	
(Cockell *et al.*, 2002)	Scientists	CIE	SED	1440	0.00E+00	2.89E-06	4.32E-07	1.70E-06	mean (of 2)	Two days in December
(Downs, Parisi and Igoe, 2014)	Teachers	ACGIH	J/m^2	1440	6.37E-08	3.76E-07	1.33E-07	1.33E-07	mean	
(Downs, Harrison and Parisi, 2015)	Teachers	ACGIH	J/m^2	1440	0.00E+00	3.23E-07	NP	NP	N/A	
(Downs *et al.*, 2016)	Teachers	ACGIH	J/m^2	1440	2.31E-09	3.24E-08	1.27E-08	1.27E-08	median	
(Feister, Meyer and Kirst, 2013)	Seafarers	ACGIH	W/cm^2	IRR	NP	5.00E-06	NP	NP	N/A	
(Gies *et al.*, 1995)	Multiple Occupations	CIE	J/m^2	1440	1.28E-07	1.58E-06	3.70E-07	1.06E-06	mean (of 6)	Shoulder and chest of PE teachers, grounds staff, and lifeguards
(Gies and Wright, 2003)	Construction	CIE	SED	60	1.67E-07	1.78E-05	5.47E-06	5.47E-06	median	
(Gies *et al.*, 2009)	Lifeguards	CIE	SED	2880	NP	1.84E-06	1.91E-07	1.91E-07	median	
(Grandahl *et al.*, 2017)	Outdoor workers	CIE	SED	720	1.62E-07	1.18E-06	NP	NP	N/A	
(Grandahl *et al.*, 2018)	Multiple	CIE	SED	1440	NP	NP	3.47E-08	5.56E-07	median (of 17)	17 different occupations
(Kimlin, Parisi and Wong, 1998)	Outdoor workers	CIE	MED	30	NP	NP	5.56E-06	6.67E-05	mean (of 6)	Outdoor workers, school children, and home workers in Brisbane and Toowoomba
(O. Larko and Diffey, 1983)	Outdoor Workers, Indoor Workers	UVBE	J/cm^2	43830	2.66E-08	6.46E-07	7.61E-08	5.70E-07	geometric mean (of 6)	
(Leach *et al.*, 1978)	Indoor workers	CIE	mJ/cm^2	10080	0.00E+00	2.91E-07	NP	NP	N/A	
(Liljendahl *et al.*, 2013)	Lifeguards and agricultural workers	CIE	J/m^2	1440	3.25E-07	1.48E-06	6.94E-07	6.94E-07	mean	
(Moehrle and Garbe, 2000)	lifeguards and mountaineers	CIE	MED	1440	2.89E-08	4.94E-06	2.05E-07	3.44E-06	mean (of 3)	Children, lifeguards, mountain guides
(Moehrle *et al.*, 2003)	Mountaineers	CIE	SED	600	1.67E-07	6.72E-06	1.83E-06	1.83E-06	mean	
(Nardini, Neri and Paroncini, 2014)	Agriculture	CIE	SED	240	2.71E-07	1.59E-06	NP	NP	N/A	
(A. V Parisi, Meldrum, Kimlin, *et al.*, 2000)	Outdoor workers, home workers	CIE	SED	1440	1.16E-07	1.27E-06	2.31E-07	9.26E-07	median (of 36)	Outdoor workers, school children, and home workers in Brisbane and Toowoomba from six days
(Peters *et al.*, 2016)	Outdoor workers	CIE	SED	1440	1.16E-09	2.22E-06	1.25E-07	1.25E-07	mean	
(Peters *et al.*, 2019)	Outdoor workers	CIE	SED	1440	0.00E+00	3.07E-06	7.06E-07	7.06E-07	mean	
(Alois W Schmalwieser *et al.*, 2010)	Agriculture	CIE	SED	1440	NP	1.64E-06	3.46E-07	3.46E-07	mean	
(Serrano *et al.*, 2009)	Gardeners and lifeguards	CIE	SED	60	1.31E-06	4.14E-06	4.78E-07	1.32E-06	mean (of 2)	Gardeners, lifeguards
(Serrano, Cañada and Moreno, 2013)	Construction	CIE	SED	60	2.78E-07	7.11E-06	1.89E-06	1.89E-06	median	
(M.-A. Serrano *et al.*, 2014)	Environmental enforcement agents	CIE	SED	2880	1.74E-08	8.62E-07	3.59E-07	3.59E-07	median	
(Siani *et al.*, 2008)	Ski instructors	Unweighted	% of total ambient	1440	NP	NP	NP	NP	N/A	
(Siani *et al.*, 2011)	Agriculture	CIE	SED	555	4.50E-07	7.12E-06	6.01E-07	4.35E-06	median (of 6)	2 body location measurements from 3 days
(Sisto *et al.*, 2009)	Agriculture	CIE	W/m^2	IRR	NP	1.50E-05	NP	NP	N/A	
(Thieden, Ågren and Wulf, 2001)	Indoor workers	CIE	SED	1440	2.31E-09	8.68E-07	8.10E-08	3.24E-07	mean (of 2)	Working and holiday periods
(Thieden, Peter A Philipsen, *et al.*, 2004)	Indoor workers, gardeners	CIE	SED	1440	1.16E-08	7.75E-07	2.89E-07	3.70E-07	median (of 2)	Northern and Southern Europe
(E. Thieden *et al.*, 2005)	Gardeners	CIE	SED	60	2.78E-07	2.58E-06	6.11E-07	9.44E-07	median (of 4)	Work and day off for Ireland and Denmark workers
(Thieden, Philipsen and Wulf, 2006)	Indoor workers	CIE	SED	1440	NP	2.48E-07	NP	NP	N/A	
(Elisabeth Thieden, Peter A Philipsen, *et al.*, 2005)	Indoor workers, gardeners, rangers	CIE	SED	1440	NP	NP	NP	NP	N/A	
(Vishvakarman, Wong and Boreham, 2001)	Teachers, Postal Worker	CIE	kJ/m^2	525600	NP	NP	4.09E-07	1.23E-06	mean (of 8)	Postal worker's chest, hands, and back and PE teacher's vertex (hat), chest, shoulder, thigh, and back
(Wolska, 2013)	Multiple	CIE	SED	60	5.56E-08	2.08E-05	5.56E-08	1.04E-05	median (of 10)	Ten different occupations
(Wong *et al.*, 1992)	Multiple	CIE	mJ/cm^2	7200	1.62E-07	1.76E-06	NP	NP	N/A	

NP - the study did not publish this data; IRR - originally presented as irradiance; * This study weighted its results using the erythema action spectrum obtained by Mackenzie & Bell (1973)

Of the studies that focused on occupational exposure to solar radiation, more studies used the CIE action spectrum (n = 34) than the ACGIH action spectrum (n = 4). Of the studies using the CIE action spectrum, the published irradiance values ranged from zero to 6.67E-05 effective W/cm^2. The studies with the top nine maximum CIE weighted irradiance measurements all investigated UV exposure of study subjects working in agriculture or construction (A. V Parisi, Meldrum, Kimlin, *et al.*, 2000; Gies and Wright, 2003; Moehrle *et al.*, 2003; Thieden, Peter A Philipsen, *et al.*, 2004; Antoine *et al.*, 2007; Gies *et al.*, 2009; Sisto *et al.*, 2009; Alois W Schmalwieser *et al.*, 2010; Siani *et al.*, 2011; Serrano, Cañada and Moreno, 2013; Grandahl *et al.*, 2017). The lowest maximum CIE weighted irradiance was 2.48E-07 effective W/cm^2, from a study investigating indoor workers in Denmark. The ACGIH action spectrum was used in four studies investigating UV exposure of teachers and seafarers. Of these, seafarers had the highest maximum irradiance measured using the ACGIH action spectrum, with a value of 5.00E-06 effective W/cm^2 (Feister, Meyer and Kirst, 2013).

Studies published accumulated radiant energy as either accumulated over the duration of the occupational task or accumulated over the course of a day. A two tailed unpaired t-test of unequal variance at the 95% confidence level did not find a significant difference between the means of the maximum accumulated radiant energy of the two groups. [p=0.06]. The converted mean irradiance of the studies that published accumulated exposures over the duration of an occupational task was (1.27E-05 effective W/cm^2 (n=12). The converted mean irradiance of the studies that published accumulated exposures over a day was 1.95E-06 effective W/cm^2 (n=22). The lack of a statistically significant difference between the two groups may imply that the studies publishing daily exposures may have taken measurements over a shift and simply labeled these results as "daily" exposure.

D.4. Dosimetric Monitoring of Non-Occupational Solar UV Exposure

The literature search identified fifty-five studies that performed dosimetric monitoring of non-occupational UV exposure to solar radiation. A few other studies performed UV exposure measurement in non-occupational settings as part of the validation process for UV exposure models. Section D.7 titled “Estimates of Non-Occupational Solar UV Exposure” provides an overview of these studies.

D.4.a. Study Subjects

The most common study subject researched by the studies included in this section was children (M. G. Kimlin, A. V. Parisi *et al.*, 1998; Roy *et al.*, 1998; A. V Parisi and Kimlin, 1999; Moise *et al.*, 1999; Moise, Gies and Harrison, 1999; Moehrle *et al.*, 2000; Parisi and Wong, 2000; Kimlin and Parisi, 2001b; Boldeman *et al.*, 2004; Thieden, Peter A. Philipsen, *et al.*, 2004; Elisabeth Thieden, Peter A. Philipsen, *et al.*, 2005; Elisabeth Thieden, Peter A Philipsen, *et al.*, 2005; Ono, Munakata and Watanabe, 2005; Boldemann *et al.*, 2006; María-Antonia Serrano, Javier Cañadab *et al.*, 2011; Liljendahl *et al.*, 2012; María-Antonia Serrano Javier Cañada *et al.*, 2012; Serrano *et al.*, 2013; Bodekær *et al.*, 2014; Vanos *et al.*, 2017; Kimlin *et al.*, 2019). Other common study subjects included a child’s parent (Liljendahl *et al.*, 2012; Bodekær *et al.*, 2014; Kimlin *et al.*, 2019), adult members of a population typically “described by age and/or nationality” (DBAN)(Boldeman *et al.*, 2004; Thieden, Peter A Philipsen, *et al.*, 2004; Chodick *et al.*, 2008; Thieden *et al.*, 2013, 2019; Guo *et al.*, 2014; Xiang *et al.*, 2015; Køster *et al.*, 2017), vacation goers (Siani *et al.*, 2009; Petersen *et al.*, 2015),

patients (Challoner *et al.*, 1976; Idorn *et al.*, 2013, 2014; Schmid *et al.*, 2013), and sport participants (Herlihy *et al.*, 1994; A. V Parisi, Meldrum, Kimlin, *et al.*, 2000; Moehrle *et al.*, 2000; Moehrle, Korn and Garbe, 2000; Thieden, Peter A Philipsen, *et al.*, 2004; Thieden, Peter A. Philipsen, *et al.*, 2004; Elisabeth Thieden, Peter A Philipsen, *et al.*, 2005; Kimlin *et al.*, 2006; Downs *et al.*, 2009; A W Schmalwieser *et al.*, 2010; Serrano, Cañada and Moreno, 2010, 2011; M.-A. A. Serrano *et al.*, 2014; Ysasi *et al.*, 2014; Casale *et al.*, 2015; Cheng *et al.*, 2015).

D.4.b. UV Measurement Devices

Study subjects most commonly wore dosimeters on the wrist (Herlihy *et al.*, 1994; Diffey and Saunders, 1995; Thieden, Ågren and Wulf, 2000; Thieden, Peter A Philipsen, *et al.*, 2004; Thieden, Peter A. Philipsen, *et al.*, 2004; Elisabeth Thieden, Peter A. Philipsen, *et al.*, 2005; Elisabeth Thieden, Peter A Philipsen, *et al.*, 2005; María-Antonia Serrano, Javier Cañadab *et al.*, 2011; Serrano, Cañada and Moreno, 2011; Idorn *et al.*, 2013, 2014; Petersen *et al.*, 2013, 2015; Thieden *et al.*, 2013, 2019; Bodekær *et al.*, 2014; Guo *et al.*, 2014; M.-A. A. Serrano *et al.*, 2014; Ysasi *et al.*, 2014; Xiang *et al.*, 2015; Køster *et al.*, 2017; Vanos *et al.*, 2017; Cust *et al.*, 2018; Kimlin *et al.*, 2019). Researchers also commonly mounted dosimeters on the shoulder (Herlihy *et al.*, 1994; Diffey and Saunders, 1995; M. G. Kimlin, A. V. Parisi *et al.*, 1998; Roy *et al.*, 1998; Moise *et al.*, 1999; Moise, Gies and Harrison, 1999; A. V Parisi, Meldrum, Kimlin, *et al.*, 2000; Moehrle, Korn and Garbe, 2000; Parisi and Wong, 2000; Thieden, Ågren and Wulf, 2000; Kimlin and Parisi, 2001b; Boldeman *et al.*, 2004; Boldemann *et al.*, 2006; Chodick *et al.*, 2008; María-Antonia Serrano, Javier Cañadab *et al.*, 2011; Serrano, Cañada and Moreno, 2011; María-Antonia Serrano Javier Cañada *et al.*, 2012; Petersen *et al.*, 2013; Serrano *et al.*, 2013; Weihs *et al.*, 2013; Idorn *et al.*, 2014; M.-A. A. Serrano *et al.*, 2014; Wainwright, Parisi and Downs, 2017; Cust *et al.*, 2018), chest (Challoner *et al.*, 1976; Herlihy *et al.*, 1994; Knuschke and Barth, 1996; Moise *et al.*, 1999; Moise, Gies and Harrison, 1999; Munakata, 1999; Parisi and Wong, 2000; Thieden, Ågren and Wulf, 2000; Siani *et al.*, 2009; A W Schmalwieser *et al.*, 2010; Schmid *et al.*, 2013; Weihs *et al.*, 2013), face (Herlihy *et al.*, 1994; Moehrle, Korn and Garbe, 2000; Weihs *et al.*, 2013), arm (Diffey and Saunders, 1995; Munakata, 1999; Moehrle *et al.*, 2000; Thieden, Ågren and Wulf, 2000; Ono, Munakata and Watanabe, 2005; Downs *et al.*, 2009; Liljendahl *et al.*, 2012; Weihs *et al.*, 2013; Cheng *et al.*, 2015), and the top of the head (Thieden, Ågren and Wulf, 2000; Kimlin *et al.*, 2006; Serrano, Cañada and Moreno, 2010, 2011; Ysasi *et al.*, 2014; Cheng *et al.*, 2015). Table D-4 contains a summary of study methodologies for studies investigating solar UV exposure in non-occupational settings.

Table D-4 This table contains the study subject groups, location of dosimeters, the type of dosimeter, and the type of ambient UV instrument used in the studies included in this section.

Citation	Subjects	Dosimeter Position	Dosimeter	Ambient UV Instrument
(Bodekær *et al.*, 2014)	Children, Parents	wrist	Electronic dosimeters	LMDS
(Bodekær *et al.*, 2015)	Children, Parents	wrist	Electronic dosimeters	Electronic dosimeter, LMDS, Radiometer
(Boldeman *et al.*, 2004)	Children	shoulder	Spore film	LMDS
(Boldemann *et al.*, 2006)	Children	shoulder	Polysulfone film	polysulfone film
(Casale *et al.*, 2015)	Sports activities	top of head	Polysulfone film, Poly-dimethyl phenylene oxide (PPO) film	Radiometer
(Challoner *et al.*, 1976)	Geriatric patients	chest	Polysulfone film	Polysulfone film
(Cheng *et al.*, 2015)	Sports activities	top of head, armpit	Spore film	None
(Chodick *et al.*, 2008)	DBAN	shoulder	Polysulfone film	polysulfone film
(Cust *et al.*, 2018)	DBAN	wrist	Polysulfone film	None
(Diffey and Saunders, 1995)	Authors	arm, wrist	Electronic dosimeter	Unspecified
(Downs *et al.*, 2009)	Sports activities	arm, back, top of head	Polysulfone film	Spectroradiometer
(Roy *et al.*, 1998)	Children	shoulder	Polysulfone film	Radiometer
(Guo *et al.*, 2014)	DBAN	wrist	Unspecified wearable dosimeter	Unspecified
(Herlihy *et al.*, 1994)	Sports activities	face, wrist, chest, shoulder, back, leg	Polysulfone film	Spectroradiometer
(Idorn *et al.*, 2013)	Hospital patients	wrist	Electronic dosimeters	None
(Idorn *et al.*, 2014)	Hospital patients	wrist	Electronic dosimeters	None
(M. G. Kimlin, A. V. Parisi *et al.*, 1998)	Children	shoulder	Polysulfone film	Radiometer
(Kimlin and Parisi, 2001)	Children	shoulder	Polysulfone film	Radiometer
(Kimlin *et al.*, 2006)	Sports activities	top of head, hand, leg	Polysulfone film	Radiometer
(Kimlin *et al.*, 2019)	Children, Parents	wrist	Polysulfone film	polysulfone film
(Knuschke and Barth, 1996)	Elderly, "Normal people"	chest	Polysulfone film	None
(Køster *et al.*, 2017)	DBAN	wrist	Electronic dosimeter	Radiometer
(Liljendahl *et al.*, 2012)	Children, Parents	arm	Spore film	None
(Moehrle, Korn and Garbe, 2000)	Sports activities	shoulder, face	Spore film	None
(Moehrle *et al.*, 2000)	Children, Sport activities	head, arm, leg, neck	Polysulfone film	None
(Moise *et al.*, 1999)	Children	chest, shoulder	Polysulfone film	polysulfone film, Radiometer
(Moise, Gies and Harrison, 1999)	Children	shoulder, chest	Polysulfone film	polysulfone film
(Munakata, 1999)	Authors	chest, arm	Spore film	spore film
(Ono, Munakata, and Watanabe, 2005)	Children	arm	UV-coloring labels	LMDS
(A. V Parisi and Kimlin, 1999)	Children	face, arm	Polysulfone film	Radiometer
(A. V Parisi, Meldrum, Kimlin, *et al.*, 2000)	Sports activities	shoulder	Polysulfone film	Radiometer
(Parisi and Wong, 2000)	Children	chest, shoulder	Spectrum evaluator	None
(Petersen *et al.*, 2013)	Vacationists	wrist	Electronic dosimeter	None
(Petersen *et al.*, 2015)	Vacationists	wrist	Electronic dosimeters	electronic dosimeters
(A W Schmalwieser *et al.*, 2010)	Sports activities	chest	Electronic dosimeters	Radiometer
(Schmid *et al.*, 2013)	Patients	chest	Polysulfone film	None
(Serrano, Cañada and Moreno, 2010)	Sports activities	top of head	Spore film	Radiometer
(Serrano, Cañada and Moreno, 2011)	Sports activities	top of head, wrist	Spore film	Radiometer
(María-Antonia Serrano, Javier Cañadab *et al.*, 2011)	Children	wrist, shoulder	Spore film	spore film
(María-Antonia Serrano Javier Cañada *et al.*, 2012)	Children	shoulder, wrist	Spore film	Radiometer
(Serrano *et al.*, 2013)	Children	shoulder	Spore film	LMDS
(M.-A. A. Serrano *et al.*, 2014)	Sports activities	shoulder, wrist	Spore film	Radiometer
(Siani *et al.*, 2009)	vacationists	chest	Polysulfone film	Radiometer
(Thieden, Ågren and Wulf, 2000)	Researchers	top of head, shoulder, chest, arm, wrist	Spore film	Radiometer
(Thieden, Peter A Philipsen, *et al.*, 2004)	DBAN, Sport Activities	wrist	Electronic dosimeters	Radiometer
(Thieden, Peter A. Philipsen, *et al.*, 2004)	Children, Sport activities	wrist	Electronic dosimeter	Radiometer
(Elisabeth Thieden, Peter A. Philipsen, *et al.*, 2005)	Children, DBAN	wrist	Electronic dosimeter	Radiometer
(Thieden *et al.*, 2013)	DBAN	wrist	Electronic dosimeter	Radiometer
(Elisabeth Thieden, Peter A Philipsen, *et al.*, 2005)	Children, DBAN, Sports activities	wrist	Electronic dosimeter	Radiometer
(Thieden *et al.*, 2019)	DBAN	wrist	Electronic dosimeter	Radiometer
(Vanos *et al.*, 2017)	Children	wrist	Electronic dosimeters	pyranometer
(Wainwright, Parisi and Downs, 2017)	Unspecified	shoulder	Polyphenylene oxide film	Radiometer
(Weihs *et al.*, 2013)	Unspecified	face, shoulder, arm, chest, thighs, and leg	Electronic dosimeter	Radiometer
(Xiang *et al.*, 2015)	DBAN	wrist	Polysulfone film	LMDS
(Ysasi *et al.*, 2014)	Sports activities	top of head, wrist	Spore film	Radiometer

Table D-4 contains twenty studies that used polysulfone film dosimeters (Challoner *et al.*, 1976; Herlihy *et al.*, 1994; Knuschke and Barth, 1996; Roy *et al.*, 1998; A. V Parisi and Kimlin, 1999; Moise *et al.*, 1999; Moise, Gies and Harrison, 1999; A. V Parisi, Meldrum, Kimlin, *et al.*, 2000; Moehrle *et al.*, 2000; Kimlin and Parisi, 2001b; Boldemann *et al.*, 2006; Kimlin *et al.*, 2006, 2019; Chodick *et al.*, 2008; Downs *et al.*, 2009; Siani *et al.*, 2009; Schmid *et al.*, 2013; Casale *et al.*, 2015; Xiang *et al.*, 2015; Cust *et al.*, 2018). Studies also commonly used *Bacillus subtilis* spore film dosimeters (Munakata, 1999; Moehrle, Korn and Garbe, 2000; Thieden, Ågren and Wulf, 2000; Boldeman *et al.*, 2004; Serrano, Cañada and Moreno, 2010, 2011; María-Antonia Serrano, Javier Cañadab *et al.*, 2011; Liljendahl *et al.*, 2012; María-Antonia Serrano Javier Cañada *et al.*, 2012; Serrano *et al.*, 2013; M.-A. A. Serrano *et al.*, 2014; Ysasi *et al.*, 2014; Cheng *et al.*, 2015), spectroradiometers (Herlihy *et al.*, 1994; Downs *et al.*, 2009), and electronic dosimeters (Diffey and Saunders, 1995; Thieden, Peter A Philipsen, *et al.*, 2004; Thieden, Peter A. Philipsen, *et al.*, 2004; Elisabeth Thieden, Peter A. Philipsen, *et al.*,

2005; Elisabeth Thieden, Peter A Philipsen, *et al.*, 2005; A W Schmalwieser *et al.*, 2010; Idorn *et al.*, 2013, 2014; Petersen *et al.*, 2013, 2015; Thieden *et al.*, 2013, 2019; Weihs *et al.*, 2013; Bodekær *et al.*, 2014; Casale *et al.*, 2015; Køster *et al.*, 2017; Vanos *et al.*, 2017). A popular type of electronic dosimeter was the SunSaver, which had a silicon carbide photodiode and took measurements weighted to the CIE action spectrum (Thieden, Peter A Philipsen, *et al.*, 2004; Petersen *et al.*, 2013, 2015; Bodekær *et al.*, 2014; Idorn *et al.*, 2014; Thieden *et al.*, 2019). Poly-dimethyl phenylene oxide (PPO) film dosimeters (Casale *et al.*, 2015) and UV-coloring labels (Ono, Munakata, and Watanabe, 2005) were each used by a single study. A single study did not specify the type of dosimeter (Guo *et al.*, 2014).

Some studies acquired ambient UV irradiance measurements from a local data source (Boldeman *et al.*, 2004; Ono, Munakata, and Watanabe, 2005; Serrano *et al.*, 2013; Bodekær *et al.*, 2014; Guo *et al.*, 2014; Xiang *et al.*, 2015). Two studies (Diffey and Saunders, 1995) (Guo *et al.*, 2014) did not specify how they acquired ambient UV irradiance measurements, one study (Vanos *et al.*, 2017) used a pyranometer, and some studies did not acquire measurements of ambient UV at all (Knuschke and Barth, 1996; A. V Parisi, Meldrum, Kimlin, *et al.*, 2000; Moehrle *et al.*, 2000; Moehrle, Korn and Garbe, 2000; Liljendahl *et al.*, 2012; Idorn *et al.*, 2013, 2014; Petersen *et al.*, 2013; Schmid *et al.*, 2013; Cheng *et al.*, 2015; Cust *et al.*, 2018).

All studies using polysulfone dosimeters calibrated the devices by the method described in section A.5.a. The studies using spore film dosimeters hinted that the manufacturer calibrated the devices, but only one study performed intercomparison with a radiometer at the study site study (Thieden, Ågren and Wulf, 2000). Some studies calibrated their wearable electronic devices through intercomparison with another UV measurement instrument (Diffey and Saunders, 1995; Thieden, Peter A Philipsen, *et al.*, 2004; A W Schmalwieser *et al.*, 2010; Idorn *et al.*, 2013; Petersen *et al.*, 2013, 2015; Weihs *et al.*, 2013; Bodekær *et al.*, 2014; Køster *et al.*, 2017; Vanos *et al.*, 2017), although notably quite a few studies did not mention any calibration for the wearable electronic device (Thieden, Peter A. Philipsen, *et al.*, 2004; Elisabeth Thieden, Peter A. Philipsen, *et al.*, 2005; Elisabeth Thieden, Peter A Philipsen, *et al.*, 2005; Thieden *et al.*, 2013, 2019) Not a single study included in this section specified whether the calibration procedures conformed to the standard methods detailed in section A.6., however, a few studies did mention wavelength specific calibration akin to a primary calibration (Knuschke and Barth, 1996; A. V Parisi and Kimlin, 1999; A. V Parisi, Meldrum, Kimlin, *et al.*, 2000; Serrano, Cañada and Moreno, 2011; Serrano *et al.*, 2013; M.-A. A. Serrano *et al.*, 2014). Finally, some studies did not mention calibration at all (Moehrle *et al.*, 2000; Thieden, Peter A. Philipsen, *et al.*, 2004; Elisabeth Thieden, Peter A. Philipsen, *et al.*, 2005; Elisabeth Thieden, Peter A Philipsen, *et al.*, 2005; Ono, Munakata and Watanabe, 2005; Serrano, Cañada and Moreno, 2010; María-Antonia Serrano, Javier Cañadab *et al.*, 2011; Liljendahl *et al.*, 2012; María-Antonia Serrano Javier Cañada *et al.*, 2012; Thieden *et al.*, 2013, 2019; Ysasi *et al.*, 2014; Xiang *et al.*, 2015; Cust *et al.*, 2018). A full summary of the calibration instrumentation is provided in Table D-5 below.

Table D-5 The calibration instrumentation for the studies included in this section.

Citation	Optical Source	Dosimeter	Wearable Comparison Device(s)
(Bodekær *et al.*, 2014)	Solar	Electronic dosimeters	Radiometer
(Bodekær *et al.*, 2015)	Solar	Electronic dosimeters	Spectroradiometer
(Boldeman *et al.*, 2004)	Solar	Spore film	Radiometer
(Boldemann *et al.*, 2006)	Solar	Polysulfone film	Unspecified
(Casale *et al.*, 2015)	Solar	Polysulfone film, PPO film	Radiometer, Spectroradiometer
(Challoner *et al.*, 1976)	Solar	Polysulfone film	Spectroradiometer, radiometer
(Cheng *et al.*, 2015)	Unknown	Spore film	Manufacturer
(Chodick *et al.*, 2008)	Solar	Polysulfone film	LMDS
(Cust *et al.*, 2018)	No mention	Polysulfone film	No mention
(Diffey and Saunders, 1995)	Solar	Electronic dosimeter	Spectroradiometer
(Downs *et al.*, 2009)	Solar	Polysulfone film	Spectroradiometer
(Roy *et al.*, 1998)	Solar	Polysulfone film	Radiometer
(Guo *et al.*, 2014)	Unspecified	Unspecified wearable dosimeter	Unspecified
(Herlihy *et al.*, 1994)	Solar	Polysulfone film	Spectroradiometer
(Idorn *et al.*, 2013)	Solar	Electronic dosimeters	Spectroradiometer
(Idorn *et al.*, 2014)	Solar	Electronic dosimeters	Spectroradiometer
(M. G. Kimlin, A. V. Parisi *et al.*, 1998)	Solar	Polysulfone film	Spectroradiometer
(Kimlin and Parisi, 2001)	Solar	Polysulfone film	Radiometer
(Kimlin *et al.*, 2006)	Solar	Polysulfone film	Radiometer
(Kimlin *et al.*, 2019)	Solar	Polysulfone film	Spectroradiometer
(Knuschke and Barth, 1996)	monochromatic radiation	Polysulfone film	Spectroradiometer, primary
(Køster *et al.*, 2017)	Solar	Electronic dosimeter	Radiometer
(Liljendahl *et al.*, 2012)	No mention	Spore film	Manufacturer
(Moehrle, Korn and Garbe, 2000)	Calibrated UV lamps	Spore film	Manufacturer
(Moehrle *et al.*, 2000)	N/A	Polysulfone film	No mention
(Moise *et al.*, 1999)	Solar	Polysulfone film	Spectroradiometer
(Moise, Gies and Harrison, 1999)	Solar	Polysulfone film	Spectroradiometer
(Munakata, 1999)	Solar	Spore film	Manufacturer
(Ono, Munakata, and Watanabe, 2005)	N/A	UV-coloring labels	No mention
(A. V Parisi and Kimlin, 1999)	Solar	Polysulfone film	Spectroradiometer, primary
(A. V Parisi, Meldrum, Kimlin, *et al.*, 2000)	Solar	Spectrum evaluator	Unspecified
(Parisi and Wong, 2000)	Solar	Polysulfone film	Spectroradiometer, primary
(Petersen *et al.*, 2013)	Solar	Electronic dosimeter	Radiometer
(Petersen *et al.*, 2015)	Solar	Electronic dosimeters	Spectroradiometer, primary
(A W Schmalwieser *et al.*, 2010)	Solar	Electronic dosimeters	Radiometer
(Schmid *et al.*, 2013)	No mention	Polysulfone film	No mention
(Serrano, Cañada and Moreno, 2010)	No mention	Spore film	No mention
(Serrano, Cañada and Moreno, 2011)	Solar	Spore film	Manufacturer, primary
(María-Antonia Serrano, Javier Cañadab *et al.*, 2011)	No mention	Spore film	No mention
(María-Antonia Serrano Javier Cañada *et al.*, 2012)	No mention	Spore film	No mention
(Serrano *et al.*, 2013)	Solar	Spore film	Manufacturer, primary
(M.-A. A. Serrano *et al.*, 2014)	Solar	Spore film	Manufacturer, primary
(Siani *et al.*, 2009)	Solar	Polysulfone film	Unspecified
(Thieden, Ågren and Wulf, 2000)	Solar	Spore film	Manufacturer, Radiometer
(Thieden, Peter A Philipsen, *et al.*, 2004)	Solar	Electronic dosimeters	Radiometer
(Thieden, Peter A. Philipsen, *et al.*, 2004)	No mention	Electronic dosimeter	No mention
(Elisabeth Thieden, Peter A. Philipsen, *et al.*, 2005)	No mention	Electronic dosimeter	No mention
(Thieden *et al.*, 2013)	No mention	Electronic dosimeter	No mention
(Elisabeth Thieden, Peter A Philipsen, *et al.*, 2005)	No mention	Electronic dosimeter	No mention
(Thieden *et al.*, 2019)	No mention	Electronic dosimeter	No mention
(Vanos *et al.*, 2017)	Solar	Electronic dosimeters	Pyranometer
(Wainwright, Parisi and Downs, 2017)	Solar	Polyphenylene oxide film	Radiometer
(Weihs *et al.*, 2013)	Solar	Electronic dosimeter	Radiometer
(Xiang *et al.*, 2015)	No mention	Polysulfone film	No mention
(Ysasi *et al.*, 2014)	Solar	Spore film	No mention

D.4.c. Summary of Published Results

The studies included in this section published results in many different units. To allow direct comparison, Table D-6 presents the results as converted into units of W/cm^2 with the conversion done according to the description in section D.2.

Table D-6 Dosimetric measurements of non-occupational exposure to UV radiation.

Citation	Subjects	Health Weighting	Units as Published	Session Length (min)	Min (W/cm^2)	Max (W/cm^2)	Cent Tend Min (W/cm^2)	Cent Tend Max (W/cm^2)	Mean or Median (# of Groups)	Group Type
(Bodekær *et al.*, 2014)	Children, Parents	CIE	SED	1440	5.79E-08	7.52E-07	1.27E-07	1.74E-07	mean (of 4)	Four subject groups
(Bodekær *et al.*, 2015)	Children, Parents	CIE	SED	1440	1.62E-07	3.13E-07	NP	NP	N/A	
(Boldeman *et al.*, 2004)	Children	CIE	J/m^2 per day	1440	1.92E-07	2.77E-07	2.31E-07	2.31E-07	mean	
(Boldemann *et al.*, 2006)	Children	CIE	J/m^2	1440	8.56E-08	3.38E-07	NP	NP	N/A	
(Casale *et al.*, 2015)	Sports activities	CIE	kJ/m^2	240	4.65E-06	2.42E-05	8.06E-06	1.48E-05	Published min and max	
(Challoner *et al.*, 1976)	Geriatric patients	CIE*	mJ/cm^2	1440	NP	NP	2.66E-09	2.34E-07	mean (of 4)	Four subject groups
(Cheng *et al.*, 2015)	Mountaineers	CIE	MED	1440	4.63E-07	1.76E-06	6.02E-07	1.20E-06	median (of 4)	Four subject groups
(Chodick *et al.*, 2008)	DBAN	CIE	J/m^2	480	2.43E-06	1.34E-05	7.64E-06	7.81E-06	mean (of 2)	Northern and southern regions average daily ambient UVR dose
(Cust *et al.*, 2018)	DBAN	CIE	SED	60	8.33E-07	4.17E-06	1.67E-06	1.67E-06	median	
(Diffey and Saunders, 1995)	Authors	CIE	MED	60	5.56E-08	1.28E-05	5.56E-08	2.28E-06	median (of 3)	Three activities
(Downs *et al.*, 2009)	Sports activities	CIE	SED	133	0.00E+00	6.60E-06	2.51E-07	4.01E-06	mean (of 6)	Three measurement locations for two seasons
(Roy *et al.*, 1998)	Children	CIE	SED	1440	6.94E-09	1.33E-06	1.44E-07	4.86E-07	median (of 6)	Two subject groups for three locations
(Guo *et al.*, 2014)	DBAN	CIE	SED	1440	NP	NP	NP	NP	N/A	
(Herlihy *et al.*, 1994)	Sports activities	CIE	MED	60	NP	NP	3.11E-06	1.49E-05	mean (of 7)	Seven different activities
(Idorn *et al.*, 2013)	Hospital patients	CIE	SED	1440	2.31E-08	3.13E-07	9.26E-08	1.50E-07	median (of 3)	Three subject groups
(Idorn *et al.*, 2014)	Hospital patients	CIE	SED	1440	9.26E-08	1.85E-07	NP	NP	N/A	
(M. G. Kimlin, A. V. Parisi *et al.*, 1998)	Children	CIE	MED	30	NP	NP	5.56E-06	6.67E-05	mean (of 6)	Three groups from two cities
(Kimlin and Parisi, 2001)	Children	CIE	MED	1440	NP	NP	2.31E-07	4.86E-07	mean (of 6)	Two groups with three measurement days
(Kimlin *et al.*, 2006)	Sports activities	CIE	MED	1440	6.48E-08	9.00E-05	2.18E-07	4.17E-07	mean (of 4)	Four measurement locations
(Kimlin *et al.*, 2019)	Children, Parents	CIE	MED	1440	1.53E-06	7.15E-06	4.92E-06	4.99E-06	mean (of 2)	Two locations
(Knuschke and Barth, 1996)	Elderly, "Normal people"	CIE	MED	20160	0.00E+00	1.14E-06	NP	NP	N/A	
(Køster *et al.*, 2017)	DBAN	CIE	SED	1440	6.94E-08	2.31E-07	1.39E-07	1.39E-07	median	
(Liljendahl *et al.*, 2012)	Children, Parents	CIE	SED	462	2.71E-05	5.01E-04	1.26E-04	2.30E-04	N/A	
(Moehrle, Korn and Garbe, 2000)	Sports activities	CIE	MED	1440	2.89E-08	4.94E-06	2.05E-07	3.44E-06	mean (of 3)	Three subject groups
(Moehrle *et al.*, 2000)	Children, Sport activities	CIE	MED	60	3.47E-06	1.67E-05	2.34E-06	2.34E-06	mean	
(Moise *et al.*, 1999)	Children	CIE	SED	1440	NP	2.38E-06	4.63E-08	1.04E-07	median (of 2)	Two subject groups
(Moise, Gies and Harrison, 1999)	Children	CIE	J/m^2	1440	NP	2.38E-06	4.51E-08	1.06E-07	median (of 2)	Two subject groups
(Munakata, 1999)	Authors	OTHER	SID	1440	NP	NP	NP	NP	mean (of 3)	Three European sites
(Ono, Munakata, and Watanabe, 2005)	Children	CIE	J/m^2	1440	NP	NP	3.21E-08	1.97E-07	mean (of 20)	Four seasons for five locations
(A. V Parisi and Kimlin, 1999)	Sports activities	CIE	SED	1440	1.16E-07	1.27E-06	2.31E-07	9.26E-07	median (of 36)	Three subject groups from two cities on six different days
(A. V Parisi, Meldrum, Kimlin, *et al.*, 2000)	Children	CIE	mW/cm^2	IRR	NP	NP	2.70E-06	5.40E-06	mean (of 2)	Two body measurement locations
(Parisi and Wong, 2000)	Children	CIE	MED	15	1.11E-05	3.33E-05	NP	NP	N/A	
(Petersen *et al.*, 2013)	Vacationists	CIE	SED	1440	9.26E-08	3.73E-06	1.09E-06	1.09E-06	mean	
(Petersen *et al.*, 2015)	Vacationists	CIE	SED	60	NP	NP	8.33E-07	6.67E-06	mean (of 7)	Seven different activities
(A W Schmalwieser *et al.*, 2010)	Sports activities	CIE	UVI	IRR	NP	1.15E-05	NP	NP	N/A	
(Schmid *et al.*, 2013)	Patients	CIE	MED	1440	1.62E-08	1.20E-07	3.94E-08	7.41E-08	mean (of 3)	Three subject types
(Serrano, Cañada and Moreno, 2010)	Sports activities	CIE	SED	60	NP	NP	3.58E-06	7.11E-06	mean (of 6)	Six different days
(Serrano, Cañada and Moreno, 2011)	Sports activities	CIE	SED	1440	NP	NP	1.76E-07	6.16E-07	mean (of 3)	Three different sports
(María-Antonia Serrano, Javier Cañadab *et al.*, 2011)	Children	CIE	SED	1440	1.52E-07	2.44E-07	NP	NP		
(María-Antonia Serrano Javier Cañada *et al.*, 2012)	Children	CIE	SED	60	2.25E-06	5.11E-06	3.14E-06	3.14E-06	median	
(Serrano *et al.*, 2013)	Children	CIE	SED	60	4.44E-07	3.33E-06	1.36E-06	1.36E-06	median	
(M.-A. A. Serrano *et al.*, 2014)	Sports activities	CIE	SED	60	7.78E-07	3.61E-06	8.68E-07	1.69E-06	mean (of 3)	Three different sports
(Siani *et al.*, 2009)	vacationists	CIE	J/m^2	114	1.46E-06	6.98E-06	2.98E-06	3.78E-06	median (of 3)	Three subject types
(Thieden, Ågren and Wulf, 2000)	Researchers	CIE	SED	300	NP	NP	3.67E-06	3.22E-05	mean (of 7)	Seven measurement conditions
(Thieden, Peter A Philipsen, *et al.*, 2004)	DBAN, Sport Activities	CIE	SED	1440	1.16E-08	7.75E-07	2.89E-07	3.70E-07	median (of 2)	Northern and Southern Europe
(Thieden, Peter A. Philipsen, *et al.*, 2004)	Children, Sport activities	CIE	SED	1440	NP	4.51E-06	NP	NP	N/A	
(Elisabeth Thieden, Peter A. Philipsen, *et al.*, 2005)	Children, DBAN	CIE	SED	1440	NP	NP	5.79E-08	2.31E-07	median (of 6)	Six subject types
(Thieden *et al.*, 2013)	DBAN	CIE	SED	174240	2.39E-08	1.28E-06	1.47E-07	1.47E-07	mean	
(Elisabeth Thieden, Peter A Philipsen, *et al.*, 2005)	Children, DBAN, Sports activities	CIE	SED	1440	NP	NP	NP	NP	N/A	
(Thieden *et al.*, 2019)	DBAN	CIE	SED	1440	NP	NP	1.18E-07	1.18E-07	mean	
(Vanos *et al.*, 2017)	Children	CIE	J/m^2	IRR	1.50E-06	4.60E-06	NP	NP	N/A	
(Wainwright, Parisi and Downs, 2017)	Unspecified	CIE	SED	1400	0.00E+00	1.07E-06	1.19E-07	5.95E-07	mean (of 4)	Four Seasons
(Weihs *et al.*, 2013)	Unspecified	NONE	% of total ambient	1	NP	NP	NP	NP	N/A	
(Xiang *et al.*, 2015)	DBAN	CIE	J/m^2	1440	NP	4.17E-08	NP	NP	N/A	
(Ysasi *et al.*, 2014)	Sports activities	CIE	SED	60	3.61E-07	2.06E-06	1.22E-06	1.22E-06	mean	

IRR - originally presented as irradiance.

NP - the study did not publish this data.

*Weighted using the Mackenzie & Frain-Bell (1973) erythemal spectrum

Table D-6 presents the minimum, maximum, and central tendency statistics converted from the original units of publication into units of effective irradiance. If the study originally published a single value of central tendency, the table presents only this single value. If the study did not present a single value of central tendency, but instead presented values of central tendency for each subject group, the table presents the converted minimum and maximum of these central tendency statistics as well as the number of subject groups.

Most of the studies in this section published measurements weighted to the CIE action spectrum (n = 53). Of these, the highest published irradiance is 5.01E-04 effective W/cm^2 (Liljendahl, 2012). This study investigated UV exposure of children and adults during outdoor recreation with spore dosimeters mounted on the left forearm. Twenty-one studies investigated UV exposure in children, and of those that published central tendency values (n=15), the median of the minimum and maximum of the central tendency values were 2.31E-07 (σ=3.22E-05) and 4.86E-07 (σ=6.02E-05) effective W/cm^2, respectively. Of the rest of the studies listed in Table E-6, the next most prevalent subject group was persons engaging in sport activities (n=16), and of the studies that only investigated this group (n=12), the median of the minimum and maximum central tendency values were 6.02E-07 (σ=2.43E-06) and 1.69E-06 (σ=5.44E-06) effective W/cm^2, respectively.

A two tailed unpaired t-test of unequal variance did not reveal a significant difference between the mean of the maximum published energy values accumulated over the period of time specific to the activity of interest (3.73E-05 effective W/cm^2, n=21) when compared to the mean of the maximum published accumulated radiant energy accumulated over a period of time labeled as “daily exposure” (4.42E-06 effective W/cm^2, n=29). (p=0.18) The lack of a statistically significant difference between the two groups may imply that the studies publishing daily exposures may have taken measurements over the activity period of time and simply labeled these results as "daily" exposure.

D.5. Dosimetric Monitoring of UV Exposure from Artificial Light Sources

The literature search identified five studies that used dosimetry to measure human UV exposure to emissions from artificial light sources. Many more studies estimated human exposure to UV emissions from optical sources without using dosimetry, and section D.8. covers these studies.

D.5.a. Study Subjects

The studies included in this section mounted dosimeters on a variety of subject groups. Diffey *et al. (*1986) mounted polysulfone film dosimeters on the shoulders of twenty-five subjects employed at a control station where they inspect paintwork on bodies of freshly-sprayed cars under compact fluorescent lamps. First *et al.* (2005) mounted electronic dosimeters in the middle of the chest approximately one inch below the top of the breastbone on a variety of subject groups that reside near germicidal lamps. These subject groups included office workers, shelter workers, nurses at a tuberculosis (TB) isolation hospital ward, TB patients at the same hospital, and a grade schoolteacher. Miller *et al.* (2006) placed a radiometer on the back of a tanning bed user for a spot measurement of the UV irradiance at the beginning of a tanning bed session. Finally, two studies mounted dosimeters on welders. A single study mounted polysulfone film badges to the cheeks of a welder, to the outside of his

protective mask, and to the cuffs of his overalls. (Shehade *et al.*, 1987) Another study mounted an electronic dosimeter on a subject's wrist. (Zamanian *et al.*, 2015) Table D-7 presents a summary of the five studies that used dosimetry.

Tbale D-7 Studies that directly measured UV exposure to emissions from artificial optical sources.

Citation	Subjects	Dosimeter Position	Dosimeter	Optical Source
(Diffey *et al.*, 1986)	Factory workers	shoulder	Polysulfone film	CFL
(First *et al.*, 2005)	Multiple	chest	Electronic dosimeter	Germicidal lamp
(Miller *et al.*, 2006)	Tanning bed user	back	Electronic dosimeter	Tanning Lamp
(Shehade *et al.*, 1987)	Welders	face, legs	Polysulfone film	Welding Arc
(Zamanian *et al.*, 2015)	Welders	wrist	Electronic dosimeter	Welding Arc

D.5.b. Ambient UV Measurement

Only First *et al.* (2005) reported taking measurements of ambient UV in the study's environment of interest. His research team surveyed hospital offices with an IL 1700 radiometer meter to find points of maximum irradiance at a height from the floor of approximately 173 cm, (95% of male eye height), a level chosen to assure maximum protection of room occupants.

D.5.c. Calibration

Diffey *et al.* (1986) calibrated the polysulfone dosimeters using the radiation emitted from the same model of CFL lamp under which the study subjects worked and developed correction factors using measurements taken by an Optronic model 742 spectroradiometer. One study also mentioned developing a correction factor for the polysulfone film dosimeters they used, but the publication did not specify how the research team developed the correction factor (Shehade *et al.*, 1987). First *et al.* (2005) stated that the instrument's underwent manufacturer calibration prior to the beginning of the study and that the research team frequently calibrated the instruments against an unspecified reference instrument throughout the study period. Miller *et al.*, (2006) calibrated his radiometer for the emission spectra of all tanning lamps encountered during the study period using an Optronic Laboratories Model 754 spectroradiometer. Finally, Zamanian *et al.* (2015) did not mention any calibration procedure. Table D-8 summarizes each study's calibration procedure.

Table D-8 The calibration instrumentation for the studies included in this section.

Citation	Cal Optical Source	Dosimeter	Wearable Comparison Device(s)
(Diffey *et al.*, 1986)	CFL	Polysulfone film	Spectroradiometer
(First *et al.*, 2005)	Unspecified	Electronic dosimeter	Unspecified
(Miller *et al.*, 2006)	Standard lamp	Radiometer	Spectroradiometer
(Shehade *et al.*, 1987)	Unspecified	Polysulfone film	Unspecified
(Zamanian *et al.*, 2015)	No mention	Electronic dosimeter	No mention

D.5.d. Units and Health Weighting of Original Publication

Four studies included in this section weighted measurements with the ACGIH action spectrum (Diffey *et al.*, 1986; Shehade *et al.*, 1987; First *et al.*, 2005; Zamanian *et al.*, 2015) and only Miller *et al.* (2006) published measurements weighted to the CIE spectrum. First *et al.* (2005) and Zamanian *et al.* (2015) published measurements in units of effective irradiance, while the other three published effective radiance values. Two studies published effective radiance values equal to the UV radiance accumulated over a period of eight hours (Diffey *et al.*, 1986; Shehade *et al.*, 1987). Finally, Miller *et al.* (2006) used

the dosimetric measurements to set the exposure period to control the accumulated UV dose that a tanning bed user received, however, the article did not publish the length of the exposure period.

D.5.e. Summary of Published Results

Table D-9 presents the minimum, maximum, and central tendency statistics converted from the original units of publication into units of effective irradiance. If the study originally published a single value of central tendency, the table presents only this single value. If the study did not present a single value of central tendency, but instead presented values of central tendency for each subject group, the table presents the converted minimum and maximum of these central tendency statistics as well as the number of subject groups.

Table D-9 Summary of dosimetric measurements of exposure to artificial UV sources.

Citation	Subjects	Optical Source	Health Weighting	Units as Published	Session Length (min)	Min (W/cm^2)	Max (W/cm^2)	Cent Tend Min (W/cm^2)	Cent Tend Max (W/cm^2)	Mean or Median (# of Groups)
(Diffey *et al.*, 1986)	Factory workers	CFL	ACGIH	J/m^2	480	NP	1.39E-08	NP	NP	N/A
(First *et al.*, 2005)	Multiple	UVGL	ACGIH	$\mu W/cm^2$	IRR	3.00E-08	3.70E-07	NP	NP	N/A
(Miller *et al.*, 2006)	Tanning bed users	Tanning Lamp	CIE	J/m^2	NP	NP	NP	NP	NP	N/A
(Shehade *et al.*, 1987)	Welders	Welding	ACGIH	J/m^2	480	4.27E-07	1.34E-05	NP	NP	N/A
(Zamanian *et al.*, 2015)	Welders	Welding	ACGIH	$\mu W/cm^2$	IRR	1.00E-09	1.27E-06	3.62E-07	3.62E-07	mean

NP - the study did not publish this data,
IRR - originally presented as irradiance.
NC - not convertible into units of irradiance.

The only study included in this section that weighted measurements to the CIE action spectrum did not publish the duration of exposure periods. Therefore, conversion from the accumulated effective UV radiance into effective UV irradiance is impossible. Of the studies that used the ACGIH action spectrum, the largest and second largest converted effective irradiance values came from studies that measured UV exposure in welders, with both at least an order of magnitude larger than the converted effective irradiance values of the study subjects from the other studies.

D.6. Estimates of Occupational Solar UV Exposure

This review found thirty studies that estimated solar UV exposure in occupational groups without using human dosimetry. Most of these (n=24) used an empirical model to relate measurements of direct solar UV irradiance into UV exposure, and of these, twelve used exposure ratios to convert direct UV irradiance into estimates of exposure (Rosenthal *et al.*, 1991; Diffey, 1992; Airey *et al.*, 1997; Duncan *et al.*, 1997; A. Parisi and Kimlin, 1999; Guy and Diab, 2002; Vishvakarman and Wong, 2003a, 2003b; Dadvand *et al.*, 2011; Wright *et al.*, 2013; Feister *et al.*, 2015). Several studies developed their own exposure factors by mounting dosimeters on manikins and placing the manikins in the occupational environment (Airey, Wong, and Fleming, 1995; Airey *et al.*, 1997; A. V. Parisi *et al.*, 2000; Verdebout, 2010; Giménez *et al.*, 2015). Some studies did not use exposure ratios for various reasons including: selection of the vertex of the head as the body site of exposure (M G Kimlin *et al.*, 2002), defining UV exposure as the amount of radiant UV intensity measured in a workers' environment (Parisi and Wong,

1997; A. Parisi and Kimlin, 1999; Guy and Diab, 2002; Weaver, 2008; de Paula Corrêa and C.M. Pires, 2013; Wright *et al.*, 2013; Makgabutlane and Wright, 2015; Rafieepour *et al.*, 2015; Beck, Balanay and Johnson, 2017), defining the UV exposure as an arbitrary fraction of ambient UV measurements (Wright *et al.*, 2013) and calculating UV irradiance at a body site directly using radiative transfer equations (Vernez *et al.*, 2011; Regili *et al.*, 2016). A single study used an empirical model to translate historical dosimetric measurements into estimates of UV exposure (Wittlich *et al.*, 2016).

Other common model inputs include diffuse UV irradiance (Parisi and Wong, 1997; M G Kimlin *et al.*, 2002; Verdebout, 2010; Vernez *et al.*, 2011; Regili *et al.*, 2016), behavioral factors (Rosenthal *et al.*, 1991; Airey *et al.*, 1997; Parisi and Wong, 1997; Kimlin and Parisi, 1999; Parisi *et al.*, 1999; M. G. Kimlin *et al.*, 2002; Vishvakarman and Wong, 2003b, 2003a; Weaver, 2008; Vernez *et al.*, 2011; de Paula Corrêa and C.M. Pires, 2013; Feister *et al.*, 2015; Makgabutlane and Wright, 2015; Wittlich *et al.*, 2016), geographic location factors (Duncan *et al.*, 1997; M. G. Kimlin *et al.*, 2002; Dadvand *et al.*, 2011; Feister *et al.*, 2015; Wittlich *et al.*, 2016), and clothing protection factors (Duncan *et al.*, 1997; M. G. Kimlin *et al.*, 2002; Feister *et al.*, 2015; Wittlich *et al.*, 2016). Two studies measured ambient solar UV at locations and orientations selected by anticipating the location(s) of worker UV exposure (Chorley *et al.*, 2014, 2016; Schennetten, Meier and Scheibinger, 2019). This and subsequent proposal sections will refer to this practice as “location by anticipation” (LBA). Three studies used mechanistic models that solved radiative transfer equations to compute UV irradiance at a simulated surface, either a 3D representation of a person (Vernez *et al.*, 2011; Regili *et al.*, 2016) or a UV radiative field (Verdebout, 2010). Table D-10 provides an overview of how each study estimated UV exposure from various inputs.

Table D-10 A summary of the exposure models used by various studies to estimate UV exposure in occupational settings.

Citation	Model Class	Model Inputs	Exposure Site	Subject Types
(Airey, Wong, and Fleming, 1995)	Empirical	DIR, DMM	face	Outdoor Worker
(Airey *et al.*, 1997)	Empirical	DIR, DMM, TIME, ER, BEH	face	Agricultural
(Beck, Balanay, and Johnson, 2017)	Empirical	DIR, TIME	radiant intensity	Groundskeepers
(Chorley *et al.*, 2014)	LBA	N/A	eye	Pilots
(Chorley *et al.*, 2016)	LBA	N/A	eye	Pilots
(de Paula Corrêa and C.M. Pires, 2013)	Empirical	DIR, TIME	radiant intensity	Outdoor Workers
(Dadvand *et al.*, 2011)	Empirical	DIR, TIME, ER, GEO	face	Indoor Worker
(Diffey, 1992)	Empirical	DIR, TIME, ER	face	Indoor workers
(D. Duncan *et al.*, 1997)	Empirical	DIR, TIME, ER, CPL, GEO	eye	Multiple
(Feister *et al.*, 2015)	Empirical	DIR, TIME, ER, BEH, GEO	vertex of head, shoulder, chest, back	Sailors
(Giménez *et al.*, 2015)	Empirical	DIR, DMM	face, top of head, neck	Construction
(Guy and Diab, 2002)	Empirical	DIR, TIME, ER	radiant intensity	Multiple
(Kimlin, Parisi and Wong, 1999)	Empirical	DIR, TIME, ER, BEH, CPL	head	Home Workers
(M G Kimlin *et al.*, 2002)	Empirical	DIR, IND, TIME, BEH, GEO	vertex of head	Outdoor Workers, Home Workers
(Makgabutlane and Wright, 2015)	Empirical	DIR, TIME	radiant intensity	Outdoor Workers
(Parisi and Wong, 1997)	Empirical	DIR, IND, ENV	radiant intensity	Agricultural
(A. Parisi and Kimlin, 1999)	Empirical	DIR, TIME	radiant intensity	Outdoor workers
(Parisi *et al.*, 1999)	Empirical	DIR, ER, BEH, CPL	neck, hand, arm, shoulder, back, leg	Multiple
(A. V. Parisi *et al.*, 2000)	Empirical	DIR, DMM, TIME, ER	top of head, face	Indoor Worker
(Rafieepour *et al.*, 2015)	Empirical	DIR, TIME	radiant intensity	Outdoor workers
(Regili *et al.*, 2016)	Mechanistic	DIR, IND, ENV	entire human surface	Unspecified
(Rosenthal *et al.*, 1991)	Empirical	DIR, TIME, ER, CPL, BEH	face, eye	Watermen
(Schennetten, Meier and Scheibinger, 2019)	LBA	N/A	eye	Pilots
(Verdebout, 2010)	Mechanistic	DIR, DMM, TIME, IND, ENV	shoulders, face, ears, neck	Indoor Worker
(Vernez *et al.*, 2011)	Mechanistic	DIR, IND, ENV, BEH, TIME	neck, back, shoulders, hand, chest, face, vertex of head	None Specified
(Vishvakarman and Wong, 2003a)	Empirical	DIR, TIME, ER, BEH	check, hand, back	Postal Worker
(Vishvakarman and Wong, 2003b)	Empirical	DIR, TIME, ER, BEH	hands, neck	Multiple
(Weaver, 2008)	Empirical	DIR	radiant intensity	Outdoor Worker
(Wittlich *et al.*, 2016)	Empirical	DOS, TIME, BEH, CPL, GEO, ENV	face, vertex of head, neck, shoulder, back, chest, foot	Multiple
(Wright *et al.*, 2013)	Empirical	DIR, TIME, ER	radiant intensity	Outdoor Worker

DIR: direct solar irradiance, IND: diffuse UV irradiance, DMM: dosimetric manikin measurements, MEI: values of measurements taken in the environment of interest, TIME: exposure duration, ER: exposure ratio, CPL: clothing protection factors, GEO: geographic location factors, BEH: behavioral factors, ENV: environmental influence factors, DOS: dosimetric measurements

Eight of the studies listed in Table D-10 estimated UV dose at the face (Rosenthal et al., 1991; Diffey, 1992; Airey et al., 1997; A. V. Parisi et al., 2000; Verdebout, 2010; Dadvand et al., 2011; Vernez et al., 2011; Wittlich et al., 2016). Other common body locations that studies selected for estimating UV dose include the eyes (Rosenthal et al., 1991; Duncan et al., 1997; Chorley et al., 2014, 2016), shoulder (Parisi et al., 1999; Wittlich et al., 2016), chest (Vishvakarman and Wong, 2003a; Feister et al., 2015; Wittlich et al., 2016), back (Vishvakarman and Wong, 2003b; Vernez et al., 2011; Feister et al., 2015; Wittlich et al., 2016), and top of the head (Kimlin, Parisi and Wong, 1999; A. V Parisi, Meldrum, Wong, et al., 2000; M G Kimlin et al., 2002; Vernez et al., 2011; Feister et al., 2015; Wittlich et al., 2016).

The studies listed in Table D-10 estimated UV exposure in several occupations. Common occupations included agricultural workers (Airey et al., 1997; Duncan et al., 1997), indoor workers (Diffey, 1992; A. V. Parisi et al., 2000; Guy and Diab, 2002; Vishvakarman and Wong, 2003b; Dadvand et al., 2011), marine workers (Rosenthal et al., 1991; Feister et al., 2015), and unspecified outdoor workers (Duncan et al., 1997; Guy and Diab, 2002; M G Kimlin et al., 2002; Wright et al., 2013; Makgabutlane and Wright, 2015).

Twenty-two of the studies listed in Table D-10 published quantitative estimates of UV exposure. Seventeen weighted estimates using the CIE action spectrum (Diffey, 1992; Airey et al., 1997; Parisi and Wong, 1997; A. Parisi and Kimlin, 1999; Parisi et al., 1999; A. V. Parisi et al., 2000; Guy and Diab, 2002; Vishvakarman and Wong, 2003b, 2003a; Verdebout, 2010; Dadvand et al., 2011; Vernez et al., 2011; de Paula Corrêa and C.M. Pires, 2013; Wright et al., 2013; Chorley et al., 2014; Makgabutlane and Wright, 2015; Wittlich et al., 2016), three weighted estimates using the ACGIH action spectrum (Weaver, 2008; Beck, Balanay and Johnson, 2017; Schennetten, Meier and Scheibinger, 2019). Three studies published unweighted estimates (M G Kimlin et al., 2002; Rafieepour et al., 2015; Schennetten, Meier and Scheibinger, 2019). The periods of exposure for the modeled scenarios were either sub-daily (Kimlin, Parisi and Wong, 1999; Verdebout, 2010; Giménez et al., 2015), daily (Airey et al., 1997; Parisi et al., 1999; Vernez et al., 2011; Wright et al., 2013; Wittlich et al., 2016) or yearly (Diffey, 1992; A. V. Parisi et al., 2000; Guy and Diab, 2002; M G Kimlin et al., 2002; Vishvakarman and Wong, 2003a, 2003b; Dadvand et al., 2011).

Table D-11 presents the minimum, maximum, and central tendency statistics converted from the original units of publication into units of effective irradiance. If the study originally published a single value of central tendency, the table presents only this single value. If the study did not present a single value of central tendency, but instead presented values of central tendency for each subject group, the table presents the converted minimum and maximum of these central tendency statistics as well as the number of subject groups.

Table D-11 Published estimates of estimated UV exposure occupational exposure in units of W/cm^2.

Ref #	Occupation	Health Weighting	Unit as Published	Mean Session Length (min)	Min (W/cm^2)	Max (W/cm^2)	Cent Tend Min (W/cm^2)	Cent Tend Max (W/cm^2)	Mean or Median (# of Groups)	Group Type
(Airey, Wong, and Fleming, 1995)	Outdoor Worker	N/A	ER	N/A	NP	NP	NP	NP	N/A	
(Airey *et al.*, 1997)	Agricultural	CIE	J/cm^2	1440	9.84E-05	1.67E-04	1.10E-04	1.10E-04	mean	
(Beck, Balanay, and Johnson, 2017)	Groundskeepers	ACGIH	uW/cm^2	IRR	0.00E+00	8.00E-05	1.40E-06	1.16E-05	mean (of 9)	Nine different exposure conditions
(Chorley *et al.*, 2014)	Pilots	CIE	mW/m^2	IRR	0.00E+00	2.00E-06	NP	NP	N/A	
(Chorley *et al.*, 2016)	Pilots	Unweighted	J/m^2	IRR	4.82E-06	2.28E-04	NP	NP	N/A	
(de Paula Corrêa and C.M. Pires, 2013)	Outdoor Workers	CIE	UVI	IRR	0.00E+00	3.50E-06	NP	NP	N/A	
(Dadvand *et al.*, 2011)	Indoor Worker	CIE	SED	525600	NP	NP	1.16E-06	3.21E-06	mean (of 6)	Participants from six cities
(Diffey, 1992)	Indoor workers	CIE	MED	525600	NP	NP	5.90E-08	9.96E-08	mean	
(Duncan *et al.*, 1997)	Multiple	N/A	ER	N/A	NP	NP	NP	NP	N/A	
(Feister *et al.*, 2015)	Sailors	N/A	N/A	N/A	NP	NP	NP	NP	N/A	
(Giménez *et al.*, 2015)	Construction	CIE	SED per hour	60	1.69E-06	1.92E-05	2.36E-06	1.73E-05	mean (of 15)	Five body positions for a spring, summer, and winter periods
(Guy and Diab, 2002)	Multiple	CIE	MED	525600	1.53E-06	3.12E-06	NP	NP	N/A	
(Kimlin, Parisi and Wong, 1999)	Home Workers	CIE	MED	60	0.00E+00	6.94E-06	NP	NP	N/A	
(M G Kimlin *et al.*, 2002)	Outdoor Workers, Home Workers	Unweighted	J/cm2	525600	NP	NP	3.84E-04	8.77E-04	mean (of 4)	Two scenarios for home and outdoor workers
(Makgabutlane and Wright, 2015)	Outdoor Workers	CIE	UVI	IRR	0.00E+00	1.17E-05	NP	NP	N/A	
(Parisi and Wong, 1997)	Agricultural	CIE	uW/cm^2	IRR	0.00E+00	3.20E-07	2.31E-07	2.31E-07	mean (of 2)	Two days, both with 5 mJ/cm2
(A. Parisi and Kimlin, 1999)	Outdoor worker	CIE	MED	1440	0.00E+00	3.78E-05	4.44E-06	6.67E-06	mean (of 7)	Seven different exposure conditions
(Parisi *et al.*, 1999)	Multiple	CIE	J/m^2	28908000	8.07E-09	4.04E-07	NP	NP	N/A	
(A. V. Parisi *et al.*, 2000)	Indoor Worker	CIE	SED	525600	NP	NP	7.96E-07	2.54E-06	mean (of 9)	Nine different body positions
(Rafieepour *et al.*, 2015)	Outdoor workers	Unweighted	W/m^2	IRR	5.00E-03	7.70E-02	NP	NP	N/A	
(Regili *et al.*, 2016)	Unspecified	N/A		N/A	NP	NP	NP	NP	N/A	
(Rosenthal *et al.*, 1991)	Watermen	N/A		N/A	NP	NP	NP	NP	N/A	
(Schennetten, Meier and Scheibinger, 2019)	Pilots	ACGIH	W/cm^2	IRR	NP	1.00E-07	NP	NP	N/A	
(Verdebout, 2010)	Indoor Worker	CIE	kJ/m^2	220	0.00E+00	1.52E-05	NP	NP	N/A	
(Vernez *et al.*, 2011)	None Specified	N/A	J/m^2	1440	4.63E-07	4.05E-06	NP	NP	N/A	
(Vishvakarman and Wong, 2003a)	Postal Worker	CIE	kJ/m^2	525600	4.79E-07	1.40E-06	NP	NP	N/A	
(Vishvakarman and Wong, 2003b)	Multiple	CIE	kJ/m^2	525600	1.01E-07	1.23E-06	NP	NP	N/A	
(Weaver, 2008)	Outdoor Worker	ACGIH	uW/cm^2	IRR	0.00E+00	3.30E-06	NP	NP	N/A	
(Wittlich *et al.*, 2016)	Multiple	CIE	SED	1440	2.08E-07	9.61E-07	NP	NP	N/A	
(Wright *et al.*, 2013)	Outdoor Worker	CIE	SED	1440	0.00E+00	1.74E-06	NP	NP	N/A	

NP - the study did not publish this data,
IRR - originally presented as irradiance,

Of the eighteen studies using the CIE action spectrum, the published irradiance values ranged from zero to 1.67E-04 effective W/cm^2, with the highest estimated irradiance coming from a study that estimated UV exposure in agricultural workers (Airey *et al.*, 1997). The lowest maximum UV irradiance values came from a study measuring solar UV irradiance inside a greenhouse and calling those measurements "exposure" (Parisi and Wong, 1997). However, that study also published values of ambient UV outside the greenhouse, and the conversion of those irradiance values put the maximum irradiance measured at 2.22E-05 effective W/cm^2.

A two tailed unpaired t-test of unequal variance did not reveal a significant difference between the mean of the maximum published energy values accumulated over the period of time specific to the occupational task (8.41E-06 effective W/cm^2, n=7) when compared to the mean of the maximum published radiant energy accumulated over a "daily" time period of time not specific to the occupational task (2.00E-05 effective W/cm^2, n=11). (p=.47) The lack of a statistically significant difference between the two groups may imply that the studies publishing daily exposures may have

taken measurements over the activity period of time and simply labeled these results as "daily" exposure.

Most studies in Table E-11 listed some or all the following factors as contributors to variability in the exposure estimates: aerosol content, cloud cover, accuracy of exposure ratio inputs, location, clothing, occupation, behavior, ground reflectance, shade, and time of year.

D.6.a. Validation of UV Exposure Estimates

Only a few studies described validation between measured and predicted values. Airey *et al.* (1995) stated that significant differences can occur between UVB dose measurements performed on rotating head form models and those that use humans engaged in normal activity, and suggested head angle as a potential factor. The estimates predicted by Diffey *et al.* (1992) were in “good agreement” with those obtained by personal monitoring (Challoner *et al.*, 1976; Leach *et al.*, 1978; O Larko and Diffey, 1983). Estimates generated by the Feister *et al.* (2015) showed systematic differences between predicted exposure doses and measured/satellite based daily erythemal exposure of 1 to 3% for clear days and around 30% for cloudy days. Rosenthal *et al.* (1991) discussed the need to further validate the model but did not detail any existing validation efforts. Verdebout *et al.* (2010) and Vernez *et al.* (2011) compared UV exposure estimates to values measured by dosimeters mounted on a manikin. Verdebout *et al.* 2010 performed a linear regression on the measured and modeled values and found that the least mean square proportionality function with a slope of 1.077 and a correlation coefficient of 0.95. Vishvakarman *et al.* (2003a) compared UV exposure estimates to values measured by dosimeters mounted on chest, hand, and back of Australia post mail delivery personnel and found that most of the estimates were within 20% of the measured value, with the worst case being a 35% difference. Vernez *et al.* (2011) stated that half of the predictions fell within a 17% range of the measurements and 75% within a 40% range of the measurements.

D.7. Estimates of Non-Occupational Solar UV Exposure

The literature search identified twenty studies that estimated solar UV exposure in non-occupational groups without performing human dosimetry. All studies included in this section used an empirical model to translate measurements of direct solar UV effective irradiance into UV effective irradiance exposure (Diffey, 1992, 2008; Jokela *et al.*, 1995; Parisi and Wong, 1998; Kimlin and Parisi, 1999, 2001; Moise, Büttner and Harrison, 1999; A. V Parisi, Kimlin, *et al.*, 2000; A. V Parisi, Meldrum, Wong, *et al.*, 2000; Parisi and Kimlin, 2000; M. G. Kimlin *et al.*, 2002; Moehrle, Soballa and Korn, 2003; Vishvakarman and Wong, 2003b; Wright, Coetzee and Ncongwane, 2011; de Paula Corrêa and C.M. Pires, 2013; Wright *et al.*, 2013; Ysasi *et al.*, 2018). Seven studies measured the radiant UV intensity present in an environment of interest and defined those measurement values as UV exposure (Parisi and Wong, 1998; Kimlin and Parisi, 1999; A. V Parisi, Kimlin, *et al.*, 2000; Parisi and Kimlin, 2000; M. G. Kimlin *et al.*, 2002; Moehrle, Soballa and Korn, 2003; Ysasi *et al.*, 2018). Five studies mounted dosimeters on manikins and placed those manikins in the environment of interest, and then published dosimeter UV measurements as estimates of human UV exposure for a defined group (Parisi and Wong, 1998; A. V Parisi, Kimlin, *et al.*, 2000; A. V Parisi, Meldrum, Wong, *et al.*, 2000; Moehrle, Soballa and Korn, 2003; Logue and Zlotoff, 2015). One study used survey data alone to estimate lifetime ocular exposure to UVB (McCarty *et al.*, 1996).

Nine studies presented converted inputs of direct UV irradiance into estimates of exposure using exposure ratios. The remaining studies did not use exposure ratios for various reasons, including: defining UV exposure as the measured amount of ambient UV, defining the UV exposure as an arbitrary fraction of ambient UV measurements (Wright *et al.*, 2013), and defining UV exposure as the amount of ambient UV present in the subject's environment (Jokela *et al.*, 1995; Kimlin and Parisi, 1999; Moise, Büttner and Harrison, 1999; Parisi and Kimlin, 2000; M. G. Kimlin *et al.*, 2002; Downs *et al.*, 2008; Wright, Coetzee and Ncongwane, 2011; de Paula Corrêa and C.M. Pires, 2013; Ysasi *et al.*, 2018).

Other common model inputs include values of measurements taken in the environment of interest (Parisi and Wong, 1998; Kimlin and Parisi, 1999; A. V Parisi, Kimlin, *et al.*, 2000; Parisi and Kimlin, 2000; M. G. Kimlin *et al.*, 2002; Moehrle, Soballa and Korn, 2003; Ysasi *et al.*, 2018), behavioral factors (McCarty *et al.*, 1996; A. V Parisi, Meldrum, Wong, *et al.*, 2000; Vishvakarman and Wong, 2003b), geographic location factors (McCarty *et al.*, 1996), and clothing protection factors (McCarty *et al.*, 1996; A. V Parisi, Meldrum, Wong, *et al.*, 2000; Kimlin and Parisi, 2001). Table D-12 provides an overview of model inputs, the location of estimated exposure, and the study subjects.

Table D-12 A summary of the exposure models used by various studies to estimate UV exposure in non-occupational settings.

Citation	Model Inputs	Exposure Site	Subject Types
(de Paula Corrêa and C.M. Pires, 2013)	DIR, TIME	radiant intensity	Children
(Diffey, 1992)	DIR, TIME, ER	face	Children
(Diffey, 2008)	DIR, TIME, ER	face	DBAN
(Downs *et al.*, 2008)	DIR, IND, TIME	radiant intensity	Children
(Jokela *et al.*, 1995)	DIR, IND	radiant intensity	DBAN
(Kimlin and Parisi, 1999)	DIR, MEI	radiant intensity	Car occupants
(Kimlin and Parisi, 2001)	DIR, TIME, ER, CPL	shoulder	Children
(M. G. Kimlin *et al.*, 2002)	DIR, MEI	radiant intensity	Car occupants
(Logue and Zlotoff, 2015)	DOS	face	Phone users
(McCarty *et al.*, 1996)	TIME, ER, CPL, GEO, BEH	eye	Melbourne Visual Impairment Subjects
(Moehrle, Soballa and Korn, 2003)	DIR, MEI	face, top of head, arm, ear	Car occupants
(Moise, Büttner and Harrison, 1999)	DIR, TIME	radiant intensity	Children
(Parisi and Wong, 1998)	DIR, MEI	face, arm, shoulder	Car occupants
(A. V Parisi, Meldrum, Wong, *et al.*, 2000)	DIR, TIME, ER, BEH, CPL	Hand, arm, shoulder, leg, neck, back	Children
(Parisi and Kimlin, 2000)	DIR, MEI	radiant intensity	Car occupants
(A. V Parisi, Kimlin, *et al.*, 2000)	DIR, MEI	shoulder, arm	Sports activities
(Vishvakarman and Wong, 2003)	DIR, TIME, ER, BEH	hands, neck	Children
(Wright, Coetzee and Ncongwane, 2011)	DIR, ER	radiant intensity	Children
(Wright *et al.*, 2013)	DIR, TIME, ER	radiant intensity	Children
(Ysasi *et al.*, 2018)	DIR, MEI	radiant intensity	Car occupants

DIR: direct solar irradiance, IND: diffuse UV irradiance, DMM: dosimetric manikin measurements, MEI: values of measurements taken in the environment of interest, TIME: exposure duration, ER: exposure ratio, CPL: clothing protection factors, GEO: geographic location factors, BEH: behavioral factors, ENV: environmental influence factors, DOS: dosimetric measurements, DBAN: Described by age and nationality

Out of the twenty studies listed in Table D-12, five estimated UV dose at the face (Diffey, 1992, 2008; Parisi and Wong, 1998; Moehrle, Soballa and Korn, 2003; Logue and Zlotoff, 2015). Other common body locations that studies selected for estimating UV dose include the eyes (McCarty *et al.*, 1996), shoulder (Parisi and Wong, 1998; A. V Parisi, Kimlin, *et al.*, 2000; A. V Parisi, Meldrum, Wong, *et al.*, 2000; Kimlin and Parisi, 2001), and top of the head (Moehrle, Soballa and Korn, 2003). Finally, four studies mounted dosimeters on anatomically representative manikins and placed those manikins in the

environment of interest (Parisi and Wong, 1998; A. V Parisi, Kimlin, *et al.*, 2000; A. V Parisi, Meldrum, Wong, *et al.*, 2000; Moehrle, Soballa and Korn, 2003).

The studies listed in Table D-12 investigated UV exposure in several subject groups. Common subject groups included children (Diffey, 1992; Moise, Büttner and Harrison, 1999; A. V Parisi, Meldrum, Wong, *et al.*, 2000; Kimlin and Parisi, 2001; Vishvakarman and Wong, 2003b; Downs *et al.*, 2008; Wright, Coetzee and Ncongwane, 2011; de Paula Corrêa and C.M. Pires, 2013; Wright *et al.*, 2013) and car occupants (Parisi and Wong, 1998; Kimlin and Parisi, 1999; Parisi and Kimlin, 2000; M. G. Kimlin *et al.*, 2002; Moehrle, Soballa and Korn, 2003).

D.7.a. Model Estimates

Eighteen of the twenty studies included in this section published quantitative estimates of UV exposure. Of these, seventeen weighted estimates using the CIE action spectrum (Diffey, 1992, 2008; Parisi and Wong, 1998; Moise, Büttner and Harrison, 1999; A. V Parisi, Kimlin, *et al.*, 2000; A. V Parisi, Meldrum, Wong, *et al.*, 2000; Kimlin and Parisi, 2001; Moehrle, Soballa and Korn, 2003; Vishvakarman and Wong, 2003b; Downs *et al.*, 2008; Wright, Coetzee and Ncongwane, 2011; de Paula Corrêa and C.M. Pires, 2013; Wright *et al.*, 2013; Ysasi *et al.*, 2018). Two studies (McCarty *et al.*, 1996; Logue and Zlotoff, 2015) published unweighted values and a single study (McCarty *et al.*, 1996) published estimates in units of Melbourne Sun years (MSY).

Table D-13 presents the minimum, maximum, and central tendency statistics converted from the original units of publication into units of effective irradiance. If the study originally published a single value of central tendency, the table presents only this single value. If the study did not present a single value of central tendency, but instead presented values of central tendency for each subject group, the table presents the converted minimum and maximum of these central tendency statistics as well as the number of subject groups.

Table D-13 A summary of modeled estimates of non-occupational UV exposure.

Citation	Subject Group	Health Weighting	Unit as Published	Mean Session Length (min)	Min (W/cm^2)	Max (W/cm^2)	Cent Tend Min (W/cm^2)	Cent Tend Max (W/cm^2)	Mean or Median (# of Groups)	Group Type
(de Paula Corrêa and C.M. Pires, 2013)	Children	CIE	UVI	IRR	0.00E+00	3.50E-06	NP	NP	N/A	
(Diffey, 1992)	Children	CIE	MED	525600	NP	NP	5.90E-08	9.96E-08	mean	
(Diffey, 2008)	DBAN	CIE	SED	1440	NP	NP	3.47E-09	8.10E-07	median (of 10)	Five time periods for northern Europe and Florida
(Downs *et al.*, 2008)	Children	CIE	SED	40	1.25E-06	3.00E-05	5.00E-06	2.00E-05	mean (of 2)	Summer and winter
(Jokela *et al.*, 1995)	DBAN	CIE	KJ/m^2	525600	7.99E-07	1.90E-06	1.37E-06	1.78E-06	Mean (of 2)	Two cities
(Kimlin and Parisi, 1999)	Car occupants	CIE	W/m^2	IRR	1.78E-10	1.80E-07	NP	NP	N/A	
(Kimlin and Parisi, 2001)	Children	CIE	MED	1440	NP	NP	2.31E-07	4.86E-07	mean (of 6)	Two groups with three measurement days
(M. G. Kimlin *et al.*, 2002)	Car occupants	CIE	W/m^2	IRR	0.00E+00	6.00E-06	NP	NP	N/A	
(Logue and Zlotoff, 2015)	Phone users	Unweighted	uW/cm^2	60	NP	NP	1.10E-03	2.90E-03	mean (of 12)	Reflections off twelve handheld devices
(McCarty *et al.*, 1996)	Melbourne Visual Impairment Subjects	Melbourne Sun Years	Melbourne Sun Years	N/A	NP	NP	NP	NP	N/A	
(Moehrle, Soballa and Korn, 2003)	Car occupants	CIE	MED	60	5.56E-07	1.18E-04	5.56E-07	1.25E-05	mean (of 6)	Six different window setups
(Moise, Büttner and Harrison, 1999)	Children	CIE	SED	7200	NP	NP	1.14E-06	1.14E-06	mean	
(Parisi and Wong, 1998)	Car occupants	CIE	mJ/cm^2	360	1.02E-08	1.44E-07	NP	NP	N/A	
(A. V Parisi, Meldrum, Wong, *et al.*, 2000)	Children	CIE	J/m^2	525600	NP	NP	2.76E-07	3.81E-07	mean (of 3)	Three different body sites
(Parisi and Kimlin, 2000)	Car occupants	Unweighted	J/cm^2	525600	6.08E-05	1.96E-04	NP	NP	N/A	
(A. V Parisi, Kimlin, *et al.*, 2000)	Sports activities	CIE	MED	480	0.00E+00	1.25E-06	NP	NP	N/A	
(Vishvakarman and Wong, 2003)	Children	CIE	kJ/m^2	525600	1.01E-07	1.23E-06	NP	NP	N/A	
(Wright, Coetzee and Ncongwane, 2011)	Children	CIE	SED	1440	1.16E-09	4.48E-07	NP	NP	N/A	
(Wright *et al.*, 2013)	Children	CIE	SED	1440	0.00E+00	1.74E-06	NP	NP	N/A	
(Ysasi *et al.*, 2018)	Car occupants	CIE	J/m^2	330	0.00E+00	1.99E-06	NP	NP	N/A	

NP - the study did not publish this data,
IRR - originally presented as irradiance.

Of the seventeen studies using the CIE action spectrum, the published irradiance values ranged from zero to 1.18E-04 effective W/cm^2, with the highest estimated irradiance coming from a study that estimated the UV exposure inside a car (Moehrle, Soballa and Korn, 2003). The lowest maximum UV irradiance value was 1.44E-07 effective W/cm^2, also from a study that investigated UV exposure inside a car.

A two tailed unpaired t-test of unequal variance did not reveal a significant difference between the mean of the maximum published energy values accumulated over the period of time specific to the

occupational task (2.01E-05 effective W/cm^2, n=8) when compared to the mean of the maximum published radiant energy accumulated over a “daily” time period (9.15E-07 effective W/cm^2, n=9). (p=.22) The lack of a statistically significant difference between the two groups may imply that the studies publishing daily exposures may have taken measurements over a shift and simply labeled these results as "daily" exposure.

D.7.b. Model Variability

The majority of the studies included in this section defined UV exposure as the amount of ambient UV present in the subject’s environment (Jokela *et al.*, 1995; Kimlin and Parisi, 1999; Moise, Büttner and Harrison, 1999; Parisi and Kimlin, 2000; M. G. Kimlin *et al.*, 2002; Downs *et al.*, 2008; Wright, Coetzee and Ncongwane, 2011; de Paula Corrêa and C.M. Pires, 2013; Ysasi *et al.*, 2018) and all of these studies mentioned that behavioral factors will impact an individual’s UV exposure, with commonly discussed factors including time spent indoors and clothing choice. Other commonly discussed factors included aerosol content, cloud cover, accuracy of exposure ratio inputs, occupation, ground reflectance, shade, and time of year.

D.7.c. Validation of UV Exposure Estimates

Of the studies listed in Table D-13, only a single study (Diffey, 1992) compared model estimates to dosimetric measurements, simply stating that estimates are in good agreement with measured values obtained by dosimetry (Challoner et al., 1976; Leach et al., 1978; O. Larko and Diffey, 1983).

D.8. Estimates of UV Exposure from Artificial Light Sources

The literature search identified fifty studies that estimated UV exposure caused by the emissions of artificial light sources without performing human dosimetry. The majority (n=37) of the studies included in this section measured ambient UV at locations and orientations selected by anticipating the location(s) of exposure. The other type of study included in this section (n=13) isolated and measured the UV emissions from the artificial optical source of interest but did not select measurement locations based on the anticipated location of exposure. This section will refer to these types of studies as direct source test (DST) studies. Table D-14 provides a summary of the studies included in this section.

Table D-14 A summary of the studies that estimated UV exposure from emissions sourced by artificial optical sources.

Citation	Measurement Locations*	Optical Source	Measurement Device(s)	Study Subjects	Cal. Optical Source(s)
(Akbar-Khanzadeh and Jahangir-Blourchian, 2005)	LBA	UV-transilluminators	Radiometer	Lab tech	Unspecified
(Azizi, Golmohammadi and Aliabadi, 2016)	DST	CFL	Spectroradiometer	Unspecified	Unspecified
(Bonino *et al.*, 2009)	DST	Tanning Lamp	Spectroradiometer, Radiometer	Tanners	(Rad: INC), (Spec: LPM)
(Bonner, O'Hagan and Khazova, 2011)	LBA	Stage luminaries	Unknown	Performers and audience members	No mention
(Bower *et al.*, 2005)	LBA	Scattered UV laser radiation	Radiometer	Surgeon	Unspecified
(Cavatorta *et al.*, 2016)	LBA	CFL, UV-transilluminators, Other	Spectroradiometer	All persons within a hospital	DTHL
(Christensen, 2005)	LBA	Phototherapy Source	Radiometer	Phototherapy patients and providers	No mention
(Coleman *et al.*, 2010)	LBA	CFL, Phototherapy Source	Dosimeter, Spectroradiometer,	All persons within a hospital	(Rad: Unspecified), (Spec: DTHL)
(Dibowski and Esser, 2017)	LBA	High Flux Solar Simulator	Radiometer	SS Operators	Unspecified
(Dowdy and Sayre, 2013)	LBA	Nail polish lamps	Spectroradiometer	UV nail lamp users	QTHL
(Dowdy and Sayre, 2015)	LBA	Nail polish lamps	Spectroradiometer	UV nail lamp users	Unspecified
(Dumyahn and First, 1999)	LBA	UVGL	Radiometer	Unspecified	Unspecified
(Ellingson, 1986)	DST	CFL	Spectroradiometer	Unspecified	QTHL
(Eriksen *et al.*, 1987)	DST	Dental curing light	Spectroradiometer	Dentists and patients	QTHL
(Fantozzi *et al.*, 2017)	LBA	CFL	Radiometer	Hospital building occupants	Unspecified
(Gies, Roy and Elliott, 1985)	DST	CFL	Spectroradiometer, Radiometer	Tanners	(Rad: Tanning Lamp), (Spec: QTHL)
(Glassford and Burr, 2018)	LBA	Plasma arc cutter	Radiometer	Manufacturing workers	No mention
(Khazova and O'Hagan, 2008)	DST	CFL	Spectroradiometer	Unspecified	DTHL, QTHL
(Klein *et al.*, 2009)	DST	CFL	Spectroradiometer, broadband dosimeter	Photosensitive individuals	(Rad: No mention), (Spec: QTHL)
(Martin, Currie, and Pye, 1999)	LBA	Phototherapy lamp	Radiometer	Phototherapy patients and providers	(Rad: FL) (Spec: Unspecified)
(Meechan and Wilson, 2006)	LBA	UVGL	Radiometer	Lab techs	Unspecified
(Miller *et al.*, 2016)	DST	CFL	Radiometer, Spectroradiometer	Unspecified	(Rad: No mention), (Spec: DTHL, QTHL)
(Milonova *et al.*, 2016)	LBA	UVGL	Radiometer	Unspecified	No mention
(Nakashima, Utsunomiya, Takahashi, *et al.*, 2016)	LBA	Welding arc	Radiometer	Welders	Unspecified
(Nakashima, Utsunomiya, Fujii, *et al.*, 2016)	LBA	Welding arc	Radiometer	Welders	Unspecified
(Narbutt *et al.*, 2014)	LBA	Tanning lamp	Radiometer, Spectroradiometer	Phototherapy patients and providers	(Rad: Phototherapy lamp), (Spec: No mention)
(Nardell *et al.*, 2008)	LBA	UVGL	Radiometer	Shelter occupants	No mention
(Nilsen *et al.*, 2008)	DST	Tanning lamp	Radiometer, Spectroradiometer	Tanners	(Rad: tanning lamp), (Spec: QTHL, LPM)
(Nylander-French *et al.*, 1994)	LBA	UV curing lamp	Radiometer, Spectroradiometer	Manufacturing workers	(Rad: MPC), (Spec: No mention)
(O'Connor and O'Hare, 2006)	LBA	Phototherapy lamp	Radiometer	Phototherapy patients and providers	Unspecified
(Okuno, 1987)	LBA	Welding arc	Radiometer	Welders	Unspecified
(Okuno, Ojima and Saito, 2001)	LBA	Welding arc	Radiometer	Welders	Unspecified
(Ohowot *et al.*, 1997)	DST	Molten glass	Spectroradiometer	Glassblowers	Unspecified
(Peng, Lan, *et al.*, 2007)	LBA	Welding arc	Spectroradiometer	Welders	DTHL
(Peng, Liu, *et al.*, 2007)	LBA	Welding arc	Spectroradiometer	Welders	DTHL
(Petri and Karabetsos, 2014)	LBA	Tanning lamp	Radiometer	Tanners	(Rad: No mention), (Spec: No mention)
(Pinto *et al.*, 2015)	DST	Phototherapy lamp	Spectroradiometer	Phototherapy patients and providers	Unspecified
(Price *et al.*, 2016)	LBA	Dental curing light	Spectroradiometer	Dentists and patients	Unspecified
(Chou and Cullen, 1996)	LBA	Welding arc	Spectroradiometer	Welders	Unspecified
(Rybczynski and Wolska, 2016)	LBA	Welding arc	Spectroradiometer	Welders	DTHL
(Safari *et al.*, 2015)	DST	CFL	Radiometer	Unspecified	Unspecified
(Shipp *et al.*, 2014)	LBA	Nail polish lamps	Radiometer	UV nail lamp users	No mention
(Singh *et al.*, 2014)	LBA	Photocopier lamp	Radiometer	Photocopier users	No mention
(Sliney, 1995)	DST	Auto headlight lamp	Spectroradiometer	Unspecified	No mention
(Sliney, Gilbert and Lyon, 2016)	LBA	Insect light traps	Radiometer	Indoor workers	(Rad: ILT fixtures), (Spec: Unspecified)
(Snellman, Rantanen and Sundell, 2000)	LBA	Tanning lamps	Spectroradiometer	Phototherapy patients	No mention
(Surakka *et al.*, 1997)	LBA	UV curing lamp	Dosimeter, Spectroradiometer,	Manufacturing workers	(Rad: MPC), (Spec: LPM)
(Svenoe, Falk and Henriksen, 1995)	LBA	Tanning lamp	Spectroradiometer	Tanners	DTHL
(Wright *et al.*, 1996)	LBA	Tanning lamp	Radiometer	Tanners	Unspecified
(Zaffina *et al.*, 2012)	LBA	UVGL	Spectroradiometer	Pharmaceutical workers	No mention

* LBA - location by anticipation; DST – direct source test; INC - incandescent lamps; HPS - high-pressure sodium lamps; MH - metal halide lamps; FL - fluorescent lamps; CFL - compact fluorescent lamps; LED - light emitting diode; QTHL - quartz tungsten halogen lamp; LPM – low pressure mercury lamp; MPC - manufacturer provided calibration; DTHL - deuterium-halogen lamp.

D.8.a. Artificial Optical Sources

The most common artificial optical source measured by the studies listed in Table D-14 was CFLs (Gies, Roy and Elliott, 1985; Ellingson, 1986; Khazova and O'Hagan, 2008; Klein et al., 2009; Coleman et al., 2010; Safari et al., 2015; Azizi, Golmohammadi and Aliabadi, 2016; Cavatorta et al., 2016; Miller et al., 2016; Fantozzi et al., 2017). Other common sources that the listed studies measured included welding arcs (Okuno, 1987; Chou and Cullen, 1996; Okuno, Ojima and Saito, 2001; Peng, Lan, et al., 2007; Peng, Liu, et al., 2007; Nakashima, Utsunomiya, Fujii, et al., 2016; Nakashima,

Utsunomiya, Takahashi, et al., 2016; Rybczynski and Wolska, 2016), tanning lamps (Svenoe, Falk and Henriksen, 1995; Wright et al., 1996; Nilsen et al., 2008; Bonino et al., 2009; Petri and Karabetsos, 2014) phototherapy lamps (Martin, Currie and Pye, 1999; Snellman, Rantanen and Sundell, 2000; Christensen, 2005; O'Connor and O'Hare, 2006; Coleman et al., 2010; Narbutt et al., 2014; Pinto et al., 2015), and ultraviolet germicidal lamps (Dumyahn and First, 1999; Meechan and Wilson, 2006; Nardell et al., 2008; Zaffina et al., 2012; Milonova et al., 2016). Only a few studies measured the emissions from dental curing lights (Eriksen et al., 1987; Price et al., 2016), nail polish lamps (Dowdy and Sayre, 2013, 2015; Shipp et al., 2014), and UV curing lamps (Nylander-French et al., 1994; Surakka et al., 1997), and UV-transilluminators (Akbar-Khanzadeh and Jahangir-Blourchian, 2005; Cavatorta et al., 2016). Artificial optical sources measured by only a single study include auto headlight lamps (Sliney, Fast and Ricksand, 1995), a solar simulator (Dibowski and Esser, 2017), insect light traps (Sliney, Gilbert and Lyon, 2016), molten glass (Ohowot et al., 1997), a photocopier lamp (Singh et al., 2014), a plasma arc cutter (Glassford and Burr, 2018), and stage luminaries (Bonner, O'Hagan and Khazova, 2011).

D.8.b. Study Subjects

Table D-14 lists studies that estimated UV exposure in a variety of study subject types, and of those listed the most common study subjects were phototherapy patients and providers (Martin, Currie and Pye, 1999; Snellman, Rantanen and Sundell, 2000; Christensen, 2005; O'Connor and O'Hare, 2006; Coleman et al., 2010; Pinto et al., 2015), tanners (Gies, Roy and Elliott, 1985; Svenoe, Falk and Henriksen, 1995; Wright et al., 1996; Nilsen et al., 2008; Bonino et al., 2009; Petri and Karabetsos, 2014), and welders (Okuno, 1987; Okuno, Ojima and Saito, 2001; Peng, Lan, et al., 2007; Peng, Liu, et al., 2007; Nakashima, Utsunomiya, Fujii, et al., 2016; Nakashima, Utsunomiya, Takahashi, et al., 2016). Less common study subjects include glassblowers (Ohowot et al., 1997), dentists and dental patients (Eriksen et al., 1987; Price et al., 2016), building occupants (Peng, Lan, et al., 2007; Peng, Liu, et al., 2007; Nardell et al., 2008; Cavatorta et al., 2016; Sliney, Gilbert and Lyon, 2016; Fantozzi et al., 2017), lab technicians (Akbar-Khanzadeh and Jahangir-Blourchian, 2005; Meechan and Wilson, 2006; Dibowski and Esser, 2017), manufacturing workers (Nylander-French et al., 1994; Surakka et al., 1997; Glassford and Burr, 2018), performers and audience members (Bonner, O'Hagan and Khazova, 2011), pharmaceutical workers (Zaffina et al., 2012), photocopier users (Singh et al., 2014), photosensitive individuals (Klein et al., 2009), surgeons (Bower et al., 2005), and UV nail lamp users (Dowdy and Sayre, 2013, 2015; Shipp et al., 2014). Additionally, many studies did not specify a study subject (Ellingson, 1986; Sliney, Fast and Ricksand, 1995; Dumyahn and First, 1999; Khazova and O'Hagan, 2008; Safari et al., 2015; Azizi, Golmohammadi and Aliabadi, 2016; Miller et al., 2016; Milonova et al., 2016).

D.8.c. UV Measurement Devices

Of the studies listed in Table D-14, thirty-one measured UV using a broadband radiometer, twenty-seven measured UV using a spectroradiometer, and nine measured using both a spectroradiometer and a radiometer. Common broadband devices used by studies to measure UV include the International Light Technology 1400 radiometer (Nylander-French et al., 1994; Surakka et al., 1997; Dumyahn and First, 1999; Martin, Currie and Pye, 1999; Akbar-Khanzadeh and Jahangir-Blourchian, 2005; Bower et al., 2005; O'Connor and O'Hare, 2006; Nardell et al., 2008; Sliney, Gilbert and Lyon, 2016), the International Light Technology 1700 radiometer (Wright et al., 1996; Miller et al., 2016; Glassford and Burr, 2018), the Solar Light 2100 radiometer (Christensen, 2005; Nilsen et al., 2008; Bonino et al., 2009), and the Gigahertz-Optik X series radiometers (Petri and Karabetsos, 2014; Nakashima,

Utsunomiya, Fujii, et al., 2016; Nakashima, Utsunomiya, Takahashi, et al., 2016). Common spectroradiometer models used by studies to measure UV include the Mightex HRS-UV1-025 UV (Miller et al., 2016; Sliney, Gilbert and Lyon, 2016), various Ocean Optics USB series (Peng, Lan, et al., 2007; Peng, Liu, et al., 2007; Cavatorta et al., 2016; Price et al., 2016), various Optronics 700 series models (Gies, Roy and Elliott, 1985; Sliney, Fast and Ricksand, 1995; Snellman, Rantanen and Sundell, 2000; Bonino et al., 2009; Klein et al., 2009; Dowdy and Sayre, 2013), and a Licor-1800 portable scanning spectroradiometer (Chou and Cullen, 1996; Ohowot et al., 1997). Finally, some studies did not specify a make or model of the UV measurement instrumentation used (Svenoe, Falk and Henriksen, 1995; Bonner, O'Hagan and Khazova, 2011; Dowdy and Sayre, 2015; Safari et al., 2015).

D.8.d. Device Calibration

Table D-14 contains an overview of the instrumentation used during the calibration procedure. The table contains rows containing the term "unspecified", a term describing a study that described the UV measurement devices as "calibrated" but did not describe the method or instruments used to calibrate the device.

Twenty of the studies included in this section described measurement devices as "calibrated" but did not detail the calibration procedure (Okuno, 1987; Chou and Cullen, 1996; Dumyahn and First, 1999; Akbar-Khanzadeh and Jahangir-Blourchian, 2005; Bower *et al.*, 2005; Meechan and Wilson, 2006; O'Connor and O'Hare, 2006; Pinto *et al.*, 2015; Nakashima, Utsunomiya, Fujii, *et al.*, 2016; Nakashima, Utsunomiya, Takahashi, *et al.*, 2016; Price *et al.*, 2016; Dibowski and Esser, 2017; Fantozzi *et al.*, 2017). Among these, a common subset stated that the measurement device manufacturer provided the calibration (MPC), but provided no further details (Okuno, 1987; Dumyahn and First, 1999; Okuno, Ojima and Saito, 2001; Akbar-Khanzadeh and Jahangir-Blourchian, 2005; O'Connor and O'Hare, 2006; Nakashima, Utsunomiya, Fujii, *et al.*, 2016; Nakashima, Utsunomiya, Takahashi, *et al.*, 2016; Dibowski and Esser, 2017; Fantozzi *et al.*, 2017).

Twenty-three of the studies included in this section calibrated the UV measurement devices by using the DUT to measure a known reference spectrum source (Gies, Roy and Elliott, 1985; Ellingson, 1986; Eriksen *et al.*, 1987; Nylander-French *et al.*, 1994; Svenoe, Falk and Henriksen, 1995; Chou and Cullen, 1996; Ohowot *et al.*, 1997; Surakka *et al.*, 1997; Peng, Lan, *et al.*, 2007; Peng, Liu, *et al.*, 2007; Khazova and O'Hagan, 2008; Nilsen *et al.*, 2008; Bonino *et al.*, 2009; Klein *et al.*, 2009; Coleman *et al.*, 2010; Dowdy and Sayre, 2013, 2015; Pinto *et al.*, 2015; Azizi, Golmohammadi and Aliabadi, 2016; Cavatorta *et al.*, 2016; Miller *et al.*, 2016; Price *et al.*, 2016; Rybczynski and Wolska, 2016). Commonly measured reference spectrum sources were quartz tungsten halogen lamps (QTHL)(Gies, Roy and Elliott, 1985; ELLINGSON, 1986; Eriksen *et al.*, 1987; Khazova and O'Hagan, 2008; Nilsen *et al.*, 2008; Klein *et al.*, 2009; Dowdy and Sayre, 2013), deuterium-halogen (DTHL) lamps (Svenoe, Falk and Henriksen, 1995; Peng, Lan, *et al.*, 2007; Peng, Liu, *et al.*, 2007; Khazova and O'Hagan, 2008; Coleman *et al.*, 2010; Cavatorta *et al.*, 2016; Miller *et al.*, 2016; Rybczynski and Wolska, 2016) and the same artificial optical source generating the UV emissions in the field (Martin, Currie, and Pye, 1999; Nilsen *et al.*, 2008; Bonino *et al.*, 2009; Narbutt *et al.*, 2014; Sliney, Gilbert and Lyon, 2016). The latter five studies performed the calibration by comparing the DUT measurements of the artificial optical source emissions with those of a calibrated spectroradiometer.

Only a minority of the studies include in this section referenced following a standard calibration procedure to calibrate the UV measurement devices. The referenced calibration procedures included the

ASTM G138 calibration procedure (ASTM International, 2020a), and the NIST Handbook 150-2E calibration procedure (Faison and Brickenkamp, 2001). Additionally, Peng (Peng, Lan, *et al.*, 2007; Peng, Liu, *et al.*, 2007) referenced following the calibration procedure detailed in the user manual for the Ocean Optics DH-2000-CAL deuterium tungsten-halogen calibration light source. Finally, ten studies did not mention calibration at all (Sliney, Fast and Ricksand, 1995; Snellman, Rantanen and Sundell, 2000; Christensen, 2005; Peng, Liu, *et al.*, 2007; Nardell *et al.*, 2008; Bonner, O'Hagan and Khazova, 2011; Zaffina *et al.*, 2012; Shipp *et al.*, 2014; Singh *et al.*, 2014; Azizi, Golmohammadi and Aliabadi, 2016; Cavatorta *et al.*, 2016; Milonova *et al.*, 2016; Glassford and Burr, 2018).

Table D-15 Estimates of UV exposure from artificial optical sources.

Citation	Subjects	Optical Source	Health Weighting	Units as Published	Session Length (min)	Min (W/cm^2)	Max (W/cm^2)	Cent Tend Min (W/cm^2)	Cent Tend Max (W/cm^2)	Mean or Median (# of Groups)	Group Type
(Akbar-Khanzadeh and Jahangir-Blourchian, 2005)	Lab techs	UV-transilluminators	ACGIH	$\mu W/cm^2$	IRR	0.00E+00	3.00E-04	NP	NP	N/A	
(Azizi, Golmohammadi and Aliabadi, 2016)	Unspecified	CFL	ACGIH	W/m^2	IRR	NP	NP	4.00E-03		N/A	
(Bonino *et al.*, 2009)	Tanners	Stage luminaries	CIE	W/m^2	IRR	2.50E-05	8.30E-05	NP	NP	N/A	
(Bonner, O'Hagan and Khazova, 2011)	Performers, audience	Scattered UV laser radiation	ACGIH	mW/cm^2	IRR	NP	1.00E-04	NP	NP	N/A	
(Bower *et al.*, 2005)	Surgeons	CFL, UV-transilluminators, Other	ACGIH	mJ/cm^2	1440	NP	NP	1.55E-08		mean	
(Cavatorta *et al.*, 2016)	Hospital building occupants	CFL, Phototherapy lamp	ACGIH	W/m^2	IRR	0.00E+00	6.00E-04	NP	NP	N/A	
(Christensen, 2005)	Phototherapy patients and providers	High Flux Solar Simulator	CIE	$\mu W/cm^2$	IRR	0.00E+00	1.50E-05	NP	NP	N/A	
(Coleman *et al.*, 2010)	Phototherapy patients and providers, hospital building occupants	Nail polish lamps	ACGIH	W/m^2	IRR	0.00E+00	1.25E-06	NP	NP	N/A	
(Dibowski and Esser, 2017)	SS Operators	UVGL	ACGIH	W/m^2	IRR	4.00E-06	8.35E-05	NP	NP	N/A	
(Dowdy and Sayre, 2013)	UV nail lamp users	CFL	ACGIH	$\mu W/cm^2$	IRR	3.87E-07	1.68E-06	NP	NP	N/A	
(Dowdy and Sayre, 2015)	UV nail lamp users	Dental curing light	PAS	W/cm^2	IRR	3.03E-05	3.79E-06	NP	NP	N/A	
(Dumyahn and First, 1999)	Unspecified	CFL	ACGIH	$\mu W/cm^2$	IRR	NP	1.00E-05	NP	NP	N/A	
(Ellingson, 1986)	Unspecified	CFL	ACGIH	W/cm^2	IRR	1.30E-07	1.30E-07	NP	NP	N/A	
(Eriksen *et al.*, 1987)	Dentists and patients	Plasma arc cutter	ACGIH	$\mu W/cm^2$	IRR	NP	NP	NP	NP	N/A	
(Fantozzi *et al.*, 2017)	Hospital building occupants	CFL	ACGIH	W/m^2	IRR	3.00E-09	5.80E-04	NP	NP	N/A	
(Gies, Roy and Elliott, 1985)	Tanners	UVGL	ACGIH	W/m^2	IRR	1.70E-06	3.27E-05	NP	NP	N/A	
(Glassford and Burr, 2018)	Manufacturing workers	CFL	ACGIH	$\mu W/cm^2$	IRR	2.00E-08	6.00E-06	NP	NP	N/A	
(Khazova and O'Hagan, 2008)	Unspecified	UVGL	ACGIH	W/m^2	IRR	8.00E-08	5.00E-06	NP	NP	N/A	
(Klein *et al.*, 2009)	Photosensitive individuals	Welding arc	CIE	mW/cm^2	IRR	9.20E-10	3.17E-05	NP	NP	N/A	
(Martin, Currie, and Pye, 1999)	Phototherapy patients and providers	Welding arc	Unweighted	W/m^2	IRR	6.50E-03	1.20E-02	NP	NP	N/A	
(Meechan and Wilson, 2006)	Lab techs	UVGL	ACGIH	$\mu W/cm^2$	IRR	2.00E-07	1.18E-04	NP	NP	N/A	
(Miller *et al.*, 2016)	Unspecified	Phototherapy lamp	ACGIH	W/m^2	IRR	NP	1.00E-07	NP	NP	N/A	
(Milonova *et al.*, 2016)	Unspecified	Welding arc	ACGIH	$\mu W/cm^2$	IRR	4.10E-08	1.39E-07	6.00E-08	8.20E-08	mean (of 2)	Lamp tube off and on
(Nakashima, Utsunomiya, Takahashi, *et al.*, 2016)	Welders	Welding arc	ACGIH	mW/cm^2	IRR	5.10E-04	1.29E-02	NP	NP	N/A	
(Nakashima, Utsunomiya, Fujii, *et al.*, 2016)	Welders	Welding arc	ACGIH	mW/cm^2	IRR	9.10E-05	9.10E-04	NP	NP	N/A	
(Narbutt *et al.*, 2014)	Phototherapy patients and providers	Welding arc	Unweighted	mW/cm^2	IRR	1.00E-03	3.50E-03	NP	NP	N/A	
(Nardell *et al.*, 2008)	Shelter occupants	Phototherapy lamp	ACGIH	$\mu W/cm^2$	IRR	1.00E-08	1.30E-06	8.00E-08	3.20E-07	mean (of 7)	Three sites with old and new fixtures and one site with new fixtures
(Nilsen *et al.*, 2008)	Tanners	Dental curing light	CIE	W/m^2	IRR	0.00E+00	3.30E-05	NP	NP	N/A	
(Nylander-French *et al.*, 1994)	Manufacturing workers	Welding arc	CIE	mW/cm^2	IRR	2.00E-06	1.00E-01	NP	NP	N/A	
(O'Connor and O'Hare, 2006)	Phototherapy patients and providers	Auto headlight lamp	ACGIH	$\mu W/cm^2$	IRR	0.00E+00	9.40E-06	0.00E+00	2.48E-06	mean (of 6)	Different areas of a room
(Okuno, 1987)	Welders	Insect light traps	ACGIH	$\mu W/cm^2$	IRR	1.00E-05	4.20E-04	NP	NP	N/A	
(Okuno, Ojima and Saito, 2001)	Welders	UV curing lamp	ACGIH	W/m^2	IRR	2.80E-05	7.85E-04	NP	NP	N/A	
(Ohowot *et al.*, 1997)	Glassblowers	UVGL	Unweighted	$\mu W/cm^2$	IRR	1.36E-07	1.54E-07	NP	NP	N/A	
(Peng, Liu, *et al.*, 2007)	Welders	Tanning Lamp	ACGIH	$\mu W/cm^2$	IRR	NP	NP	1.10E-03		mean	
(Peng, Lan, *et al.*, 2007)	Welders	Phototherapy lamp	ACGIH	$\mu W/cm^2$	IRR	0.00E+00	1.19E-03	NP	NP	N/A	
(Petri and Karabetsos, 2014)	Tanners	CFL	CIE	W/m^2	IRR	9.00E-06	1.13E-04	5.40E-05		mean	
(Pinto *et al.*, 2015)	Phototherapy patients and providers	Tanning lamp	ACGIH	W/m^2	IRR	0.00E+00	1.00E-06	NP	NP	N/A	
(Price *et al.*, 2016)	Dentists and patients	Medium pressure mercury arc lamps	ACGIH	$\mu W/cm^2$	IRR	NP	NP	NP	NP	N/A	
(Chou and Cullen, 1996)	Welders	Tanning lamp	Unweighted	$\mu W/cm^2$	IRR	NP	8.80E-07	NP	NP	N/A	
(Rybczynski and Wolska, 2016)	Welders	Phototherapy lamp	ACGIH	W/m^2	IRR	2.64E-05	3.20E-05	2.90E-05		mean	
(Safari *et al.*, 2015)	Unspecified	Nail polish lamps	Unweighted	W/cm^2	IRR	0.00E+00	2.00E-02	NP	NP	N/A	
(Shipp *et al.*, 2014)	UV nail lamp users	Phototherapy lamp	Unweighted	mW/cm^2	IRR	6.00E-04	1.57E-02	1.06E-02	1.06E-02	median (of 17)	17 different lamps
(Singh *et al.*, 2014)	Photocopier users	Phototherapy lamp	Unweighted	mW/cm^2	IRR	1.00E-06	4.00E-06	NP	NP	N/A	
(Sliney, 1995)	Unspecified	Molten glass	ACGIH	mW/cm^2	IRR	NP	2.80E-07	NP	NP	N/A	
(Sliney, Gilbert and Lyon, 2016)	Indoor workers	Welding arc	ACGIH	$\mu W/cm^2$	IRR	2.00E-08	4.70E-06	NP	NP	N/A	
(Snellman, Rantanen and Sundell, 2000)	Phototherapy patients and providers	CFL	CIE	mW/cm^2	IRR	NP	NP	1.30E-05	9.50E-04	single	
(Surakka *et al.*, 1997)	Manufacturing workers	Nail polish lamps	ACGIH	$\mu W/cm^2$	IRR	NP	NP	2.00E-06	1.50E-03	median (of 2)	Two distances
(Svenoe, Falk and Henriksen, 1995)	Tanners	Photocopier lamp	Unweighted	W/m^2	IRR	2.50E-05	5.78E-04	NP	NP	N/A	
(Wright *et al.*, 1996)	Tanners	Tanning lamp	Unweighted	mW/cm^2	IRR	0.00E+00	8.50E-02	1.92E-02		mean	
(Zaffina *et al.*, 2012)	Pharmaceutical workers	Tanning lamp	ACGIH	W/m^2	IRR	1.50E-06	1.21E-05	NP	NP	N/A	

IRR - originally presented as irradiance, NP - the study did not publish this data., PAS* - Photocarcinogenic action spectrum

Table D-15 presents the minimum, maximum, and central tendency statistics converted from the original units of publication into units of effective irradiance. If the study originally published a single value of central tendency, the table presents only this single value. If the study did not present a single value of central tendency, but instead presented values of central tendency for each subject group, the table presents the converted minimum and maximum of these central tendency statistics as well as the number of subject groups.

Most of the studies included in section D.7. and D.8 published measurements weighted to the ACGIH action spectrum (n = 37). Of these, the highest published irradiance measurement value was 1.29E-02 effective W/cm^2 (Nakashima, Utsunomiya, Takahashi, *et al.*, 2016). This study estimated UV exposure in welders by measuring welding arc emissions at 500 mm from the source with a Gigahertz-Optik XD-45-HUV UV-hazard detector. Nine studies published welder UV exposure estimates weighted to the ACGIH action spectrum, and the mean of the maximum published UV exposure values for these studies was 1.93E-03 effective W/cm^2 (σ = 4.14E-03). This statistic is several magnitudes larger than the maximum values published by the two studies using dosimetry to investigate welder UV exposure, potentially indicating that location by anticipation methods may overestimate actual UV exposure (Shehade *et al.*, 1987; Zamanian *et al.*, 2015). However, neither study using dosimetry provided much detail on the welding materials and voltages used, factors that could drastically change the UV irradiance emitted by the arc. The next most common subject group investigated by the studies weighting with the ACGIH action spectrum was phototherapy patients and providers (n=3) and the mean of the maximum published UV exposure values for these studies was 3.88E-06 effective W/cm^2 (σ = 4.78E-06).

Only eight studies included in sections D.7 and D.8 published UV exposures weighted to the CIE action spectrum. Of these, Nylander-French (1994) published the highest irradiance measurement value of 1.0E-01 effective W/cm^2. The research team took this measurement inside a UV curing unit at the substrate passage level.

E. Specific Aims

The knowledge gaps detailed in the sections B and D include (1) the insufficient research into occupational hazards of cannabis farms, (2) the absence of research investigating cannabis farm worker UV exposure, (3) the absence of research investigating agricultural worker exposure to lamp emitted UV radiation, (4) the inability of current UV exposure models to estimate UV exposure from lamp emitted UV, (5) and the absence of wearable UV measurement technology capable of measuring UV at all health relevant wavelengths.

This thesis addresses the knowledge gaps with the following specific aims:

Aim 1
To provide needed research on occupational hazards within cannabis farms and address the absence of research on agricultural worker exposure to lamp emitted UV radiation, I will: (1a) Evaluate cannabis farm worker exposures to solar and lamp sourced UV by measuring UV intensities at five Washington State cannabis farms, and (1b) Measure worker exposure to UV radiation in five WA State cannabis farms using wearable UV dosimeters.

Aim 2
To address the inability of current of UV exposure models to estimate UV exposure in the agricultural environments of interest, I will adapt an existing visible light model to estimate UV irradiance at arbitrarily defined surfaces within a 3D space that is representative of the anticipated location of UV exposure.

Aim 3
To address the absence of a wearable UV measurement device capable of measuring UV at all health relevant wavelengths, I will: Develop a control system allowing a capable lab bench spectroradiometer to operate as a wearable dosimetric device.

Chapter 2: Ultraviolet radiation exposure in cannabis growing facilities

Key Words: Cultivation; Horticulture; Indoor; Marijuana; Non-ionizing radiation; UV
This chapter is accepted for publication in the Journal of Occupational and Environmental Hygiene

Abstract

Cultivation and processing of cannabis is becoming an important industry in the United States and Canada. The industry employs over 400,000 workers in the United States (U.S.) and is growing rapidly. Both natural sunlight and artificial lamp-generated radiation are commonly used to grow cannabis plants. These optical sources can contain both visible and ultraviolet radiation (UVR) wavelengths, and overexposure to UVR is associated with negative health effects. The severity of these adverse health effects is governed by the specific wavelengths and exposed dose of UVR, yet worker exposure to UVR within cannabis growing facilities has not been studied. In this study, worker exposure to UVR was assessed at five cannabis production facilities in Washington State, including indoor, outdoor, and shade house facilities. Lamp emission testing was performed at each facility and worker UVR exposures were measured for 87 work-shifts. Observations of worker activities and use of personal protective equipment in association with UVR exposure measurements were recorded. For lamp emission measurements, at three feet from the center of the lamp, the average irradiances were 4.09×10^{-4}, 6.95×10^{-8}, 6.76×10^{-9}, 3.96×10^{-9}, 1.98×10^{-9} effective W/cm^2 for germicidal lamps, metal halide lamps, high pressure sodium lamps, fluorescent lamps, and light emitting diodes, respectively. The average measured UVR exposure was 2.91×10^{-3} effective J/cm^2 (range: 1.54×10^{-6}, 1.57×10^{-2} effective J/cm^2). Thirty percent of the work-shifts monitored exceeded the American Conference for Governmental Industrial Hygienists (ACGIH) threshold limit value (TLV) of 0.003 effective J/cm^2. Exposures were highest for workers who spent all or part of the work-shift outdoors, and solar radiation was the primary source of worker UVR exposure for most of the work-shifts that exceeded the TLVs. Outdoor workers can reduce UVR exposures by applying sunscreen and wearing appropriate personal protective equipment. Although the artificial lighting used in the cannabis production facilities included in this study did not contribute substantially to the measured UV exposures, in many cases the lamp emissions would generate theoretical exposures at three feet from the center of the lamp that would exceed the TLV. Therefore employers should choose low UVR emitting lamps for indoor grow operations and should use engineering controls (e.g. door-interlocks to de-energize lamps) to prevent worker exposure to UVR from germicidal lamps.

Introduction

Laws permitting growth and possession of cannabis for medicinal and recreational use are currently changing rapidly in the United States (U.S.) and internationally (Carliner et al. 2017; Caulkins et al. 2018; Mahamad and Hammond 2019). While cultivation and use of cannabis is still considered illegal by the U.S. federal government, multiple states have legalized recreational or medical use of marijuana (Carliner et al. 2017). Canada has also recently legalized cannabis use (Mahamad and Hammond 2019). These changes have led to a dramatic expansion of the cannabis industry, which now employs approximately 420,000 workers in U.S., and job-growth is among the fastest of any industry in the U.S. (Borchardt 2017; Barcott et al. 2022). However, in part due to the history of cannabis as an illicit

substance, there are few peer reviewed studies that have investigated the occupational hazards faced by workers in this emerging industry.

Many cannabis production facilities grow crops using lamp-generated radiation, solar radiation, or a combination of both. A crop cycle typically begins by cloning mother plants and placing the clones in a nursery. Plants in nurseries generally only receive lamp-generated radiation, although some facilities use solar radiation in combination with lamp-generated radiation. Once the plants reach a desired size, workers move them into a "grow area" where the crop completes its growth and flowering stages of life. These grow areas vary between facilities, and include greenhouses, shade houses, indoor spaces, or outdoor spaces. Once in full bloom, the crop is harvested and hung to dry in a dark drying room. Finally, the dry product is taken from the drying room to a separate room or facility where the crop is processed into one of the many consumer cannabis products (Simpson 2017; WASAO 2018; Green et al. 2018).

Some lamp types used in the cannabis industry emit ultraviolet radiation (UVR). UVR wavelengths range from 100 to 400 nanometers (nm) and are further classified into UVA (315 to 400 nm), UVB (280 to 315 nm), and UVC (100 to 280 nm) (IARC 2018). The most common UVR overexposure injury is erythema (Hausser 1928; Coblentz et al. 1931), and the most severe erythema is caused by UVB (Hausser 1928; Ichihashi et al. 2003). Various organizations have developed weighting scales to quantify the wavelength dependence of skin damage caused by UVR (CIE 1999; IARC 2018; ACGIH 2022). Two commonly used weighting scales are those from the American Conference of Governmental Industrial Hygienists (ACGIH) and the International Commission on Illumination (CIE). All wavelengths of UVR are classified as a Group 1 carcinogen by the International Agency for Research on Cancer (IARC) (Surdu et al. 2013; IARC 2018). Additionally, IARC considers UVB "in the terrestrial solar spectrum to be mainly responsible for adverse health effects" (IARC 2018). UVB exposure has been associated with photokeratitis (Pitts and Tredici 1971), whereas both UVB and UVC overexposure causes keratoconjunctivitis (Pitts et al. 1977). Injury severity is influenced by eye motion, spectral profile, and angle of incoming radiation (ICNIRP, 1997).

The ACGIH has published threshold limit values (TLVs), most recently revised in 2022, that represent a 24-hour exposure threshold below which a typical worker should not develop adverse health effects (ACGIH 2022). There is no Federal Occupational Safety and Health Administration (OSHA) permissible exposure limit (PEL) for UVR exposure. The ACGIH 2010 TLVs are the basis for the Washington State Department of Labor and Industries (L&I) UVR PEL (WAC 2003), which restricts occupational exposure to UVR (from sources other than UVR lasers and the sun) to under 0.003 effective J/cm^2 (eff. J/cm^2) per day. This unit, used in both the ACGIH TLVs and the L&I regulations, is a health weighted measure of UVR exposure. The results presented are weighted to the recently published ACGIH 2022 TLV and corresponding action spectrum, which perfectly matches the ACGIH 2010 action spectrum at all wavelengths above 240 nm.

To maximize worker safety and industry productivity, scientific data must underpin cannabis regulation. In this context, the current study adds to the body of literature through the evaluation of ambient UVR irradiance and UVR exposure at five cannabis production facilities. The work presented here is one of the first studies to assess UVR irradiances in indoor cannabis cultivation facilities, and the first known application of wearable UVR dosimeters to measure worker exposure to UVR in this industry.

Methods

Study Setting and Subjects

UVR emissions from optical sources were measured and worker UVR exposure was monitored at five cannabis farms across Washington State during multiple visits throughout June to December of 2017. Farms were recruited through The Cannabis Alliance, a Washington State-based cannabis business organization. The study was advertised at a regular monthly meeting of The Cannabis Alliance and through their website and email listserve. Three of the farms evaluated in this study grew plants entirely indoors, one used both indoor and shade house spaces, and one used a combination of indoor, greenhouse, and outdoor space.

Only those workers directly involved in cannabis cultivation tasks were eligible to participate in the study. During the first visit to each farm, the study team met with all eligible workers present in order to recruit them to participate in the study. A total of 22 subjects (between 2-5 subjects per farm) consented to participate and were enrolled in the study. Enrolled subjects completed a questionnaire that provided information on specific job responsibilities, common work locations, and frequency of wearing personal protective equipment (PPE) such as sunglasses, hats, long sleeved shirts, and/or gloves while working.

During subsequent visits to all farms (3-6 visits per farm, total visits = 21), the research team collected personal full-shift UVR exposure measurements (n = 87 work shifts) on all enrolled subjects present using a wearable UVR dosimeter. The dosimeter was mounted on the back of each worker's neck, as that was expected to be the body part that received the highest exposure. Throughout each shift, one of the research technicians logged worker location, posture, use of PPE, and specific tasks completed. The technician updated the worker activity log approximately every 30 minutes. At the end of each shift, dosimeters were cleaned to ensure the any dirt or plant resin was removed from the optical surface and workers were consulted to ensure that tasks completed were correctly logged.

Devices

A radiometer was used to measure UVR emissions from optical sources and wearable dosimeters were used to measure worker exposure to UVR. The radiometer was the International Light Technologies (Peabody, MA) 2400 radiometer with sensor attachment (SED240/ACT5/W). The response function for this sensor emulates the ACGIH TLV weighting function and generates a response directly comparable to the 2010 ACGIH TLV and the L&I PEL. Radiometer sensitivity was calibrated by the instrument manufacturer using monochromatic radiation at 270 nm. The radiometer's spectral response function was determined by the instrument manufacturer every 2 nm between 200 and 400 nm using a calibrated laser driven light source (Energetiq Technology, Inc., Wilmington, MA, U.S.) and a Triax 180 spectrograph (Horiba Ltd., Kyoto, Japan) (See Figure 1). To account for spectral mismatch between the radiometer's spectral response and the 2022 ACGIH action spectrum, the CIE 220:2016 method (CIE 2016) was used to develop two spectral mismatch factors using the ASTM 1.5 (solar spectrum) and a germicidal lamp spectrum as reference spectra. The factor based on solar radiation (value = 0.272) was applied to measurements of emissions from MH, HPS, LED, and FL lamps. The other factor was applied to measurements of germicidal lamp emissions (value = 1.054). The radiometer's limit of detection (LOD) was 2.4×10^{-8} eff. W/cm^2 after application of the spectral mismatch factor for solar radiation.

Five wearable UVR dosimeters were purchased from [REDACTED]. The radiation sensor in these devices is an AlGaN photodiode with a spectral response function that is similar to the CIE action spectrum for inducing erythema in humans (Seckmeyer et al. 2012). The CIE function applies to wavelengths between 250 to 400 nm. The two functions and the spectral response function of our SED240/ACT5/W sensor are presented in Figure 1.

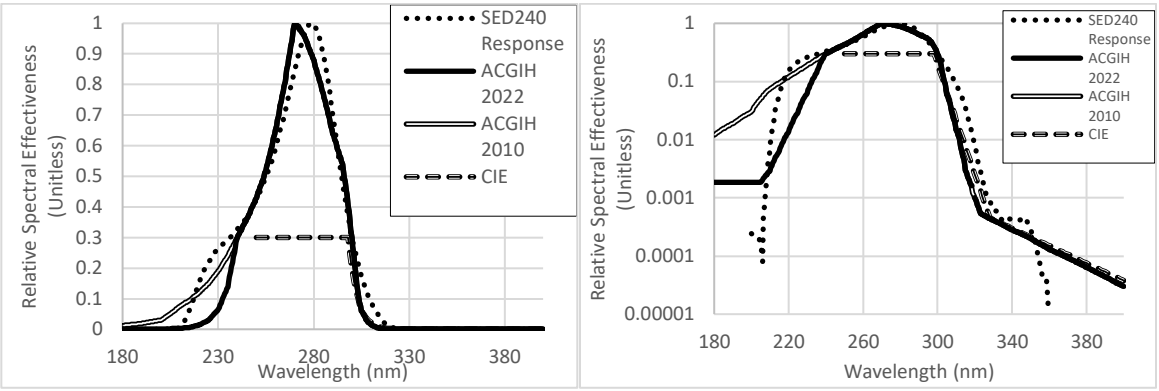

Figure 1. Comparison of the ACGIH 2010, ACGIH 2022, CIE and SED240/ACT5/W response functions presented in linear (top) and log (bottom) scales (ACGIH 2022; CIE 1999).

The dosimeter sensor is housed behind a polytetrafluoroethylene diffuser that approximates a cosine weighted angular response. The International Commission on Non-Ionizing Radiation Protection (ICNIRP) specifies that measurements of UVR exposure to the skin should be made over an angle of 180° using a detector with a cosine weighted angular response (ICNIRP 2007), whereas ACGIH specifies an unweighted angular response with the field of view restricted to 80°. Upon receiving radiation, the sensor generates a signal which is then amplified and sent to the processor. This processor digitizes the signal and records the data to the dosimeter's internal storage. The performance of the UVR dosimeters has previously been evaluated in comparison to a reference spectroradiometer (RS) that complied with the requirements for Network for the Detection of Atmospheric Composition Change instruments and with the requirements for type 2 instruments published by the World Meteorological Organization (CIE 2016). This validation study showed that after calibration, the UVR dosimeters showed mean absolute deviations of 15% (maximum 33%) from the RS measurements around noon during several test days in the northern hemisphere autumn. This dosimeter has also been used successfully in previous studies to measure personal exposure to UVR from the sun (Allen and McKenzie 2005). These devices have a limit of detection of roughly 2.97×10^{-8} eff. W/cm^2. However, the UVR irradiances at the indoor cannabis farms were often below the detection limit for these dosimeters. Therefore, after exposure monitoring at the first two facilities was complete, the research team purchased three additional enhanced sensitivity wearable UVR dosimeters of the same make and model as the regular dosimeters, but with the internal amplifier setting adjusted by the manufacturer to provide a limit of detection of roughly 1.04×10^{-8} eff. W/cm^2. These devices achieve a lower limit of detection by amplifying the sensor signal ten-fold compared to the other five devices, however, the upper limit of quantification is simultaneously reduced ten-fold. A sensitive device was co-located with a regular device on the back of a worker's neck at Facility Five due to the low light conditions present at that facility.

Calibration of UVR Dosimeter Response to Effective W/cm^2

The dosimeter's raw signal was converted to units of eff. W/cm^2 by generating and applying a conversion factor for each dosimeter. The data used to generate the conversion factor were obtained by co-location of the radiometer and dosimeters to measure solar radiation. Solar radiation was selected as the calibration spectrum because solar radiation encompasses a wide and continuous range of UVR wavelengths, has day-to-day consistency, and is the likely cause of many of the high exposures observed in this study. These measurement sessions lasted for a minimum of 20 min and included measurements at sunrise and sunset when UVR levels were changing rapidly, to capture a wide range of UVR irradiances for the calibration curve. Data were logged at a sampling rate of one measurement per sec, with the radiometer and all dosimeters oriented vertically. Three sessions used both the regular and enhanced sensitivity dosimeters and an additional three sessions only used the regular dosimeters. Spectral correction factors were applied to the radiometer measurement values. Outliers and measurements with a dosimeter response of zero were removed from the data set. Each dosimeter's data were plotted as the dependent variable against the radiometer data and a linear regression forced through zero was used to generate calibration coefficients for each dosimeter. Finally, limits of detection for each dosimeter (in eff. W/cm^2) were calculated from the calibration curve as described by Harris (2006) and verified by visual inspection of the calibration data.

Lamp Measurements

The farms visited employed a variety of lighting technologies, including germicidal lamps, high pressure sodium (HPS) lamps, ceramic Metal Halide (CMH) lamps, light emitting diodes (LED), and fluorescent lamps. The radiation emissions of each lamp make and model encountered at the five cannabis farms were measured. Emissions from various lamp models at a cannabis business convention (Cannacon) in Seattle, WA and at a specialty lamp store that supplies many of the local cannabis growers were also measured. These additional measurements provided a wider variety of lamp makes and models to better characterize the range of UVR emissions from the different lighting technologies used in cannabis cultivation. During measurement of lamp emissions, the sensor field of view was restricted with an optically absorbent 3 in by 1 ft pipe, which resulted in a field of view of 14.25 degrees. If the lamp emission irradiance at 3 ft was below the radiometer LOD, the same setup to measure the irradiance at 1 ft from the lamp center and used the inverse square law to estimate the emission irradiance at 3 ft.

Data Analysis

Lamp emission measurements were aggregated to calculate the mean emission irradiance for each of the five lamp types encountered during the study. For calculation of summary statistics, emissions measurements below the LOD were substituted with LOD/√2. As specified by the ACGIH TLV, the mean emission irradiances were then divided into the 0.003 eff. J/cm^2 to determine the corresponding time of overexposure for each lamp type.

Exposure monitoring summary statistics are presented by facility. A two sample, two tailed t-test assuming unequal variance was used to compare the mean average radiant exposure for indoor and outdoor shifts.

Data management and statistical analyses were performed using Microsoft Excel (Version 2013, Microsoft Corp., Redmond, WA, U.S.) and the R-programming language (Version 3.5.1, R Foundation for Statistical Computing, Vienna, Austria).

Results

Lamp Emission Measurements

The irradiance of UVR emissions varied by lamp type and are summarized in Table 1. Germicidal lamp models emitted the highest UVR irradiances by three orders of magnitude, with a mean of $4.09x10^{-4}$ eff. W/cm^2. The mean irradiances for CMH lamps, HPS lamps, fluorescent lamps, and LED lamps were $6.95x10^{-8}$, $6.76x10^{-9}$, $3.96x10^{-9}$, and $1.98x10^{-9}$ eff. W/cm^2, respectively. These values correspond to overexposure times of 0.12 min for germicidal lamp emissions and 720 min for metal halide lamp emissions. The corresponding overexposure durations for the other three lamp type emissions were over 1440 min (24 hr.) and therefore would not exceed the ACGIH TLV or the L&I PEL.

Table 1. UVR emissions (eff. W/cm^2) measured at three feet from the center of lamps.

Type	# of Lamp Types Tested	Min (eff. W/cm^2)	Max (eff. W/cm^2)	Mean (eff. W/cm^2)	SD (eff. W/cm^2)	Time to Exceed TLV (min)	Percentage at or above LOD
Germicidal	2	$2.34x10^{-4}$	$5.85x10^{-4}$	$4.09x10^{-4}$	$2.48x10^{-4}$	0.12	100
CMH	8	$3.30x10^{-9}$[B]	$1.59x10^{-7}$	$6.95x10^{-8}$	$7.39x10^{-8}$	720	100
HPS	9	<LOD[A]	$2.31x10^{-8}$[B]	$6.76x10^{-9}$ [B]	$7.56x10^{-9}$	Would not exceed	44
Fluorescent	7	<LOD[A]	$1.65x10^{-8}$[B]	$3.96x10^{-9}$ [B]	$5.53x10^{-9}$	Would not exceed	14
LED	14	<LOD[A]	$2.64x10^{-9}$[B]	$1.98x10^{-9}$	$2.79x10^{-10}$	Would not exceed	14

[A] One foot measurement below radiometer limit of detection.

[B] irradiance at three feet was below radiometer LOD of $2.4x10^{-8}$ (eff. W/cm^2). Value presented is estimated at three feet using the inverse square law, from measurements made at one foot from the lamp center.

Exposure Monitoring

Full shift UVR exposures were measured on 22 workers at the five facilities, for a total of 87 work shifts, as shown in Table 2. The average exposure accumulated during a work shift was $2.91x10^{-3}$ eff. J/cm^2 (range: $1.54x10^{-6}$ to $1.57x10^{-2}$ eff. J/cm^2; SD: $3.31x10^{-3}$ eff. J/cm^2). The average work shift was 438 min (range: 161 to 551 min; SD: 97 min). For 30% of the work shifts, the worker's accumulated UVR exposure exceeded the 0.003 eff. J/cm^2 ACGIH TLV.

Table 2. Summation statistics by facility.

Facility ID	Primary optical source	# of workers	# of shifts	% of shifts over TLV	Average Daily Radiant Exposure (eff. J/cm^2)	SD (eff. J/cm^2)	Max Radiant Exposure (eff. J/cm^2)	Shift Duration Mean (min)
1	HPS/LED	5	14	0	1.01×10^{-3}	7.28×10^{-4}	2.36×10^{-3}	463
2	LED	3	8	0	3.25×10^{-4}	4.90×10^{-4}	1.30×10^{-3}	475
3	Solar[A]	5	29	24%	2.61×10^{-3}	1.56×10^{-3}	7.31×10^{-3}	434
4	Solar[B]	5	29	66%	5.53×10^{-3}	4.25×10^{-3}	1.57×10^{-2}	446
5	HPS/Fluorescent	4	7	0	9.09×10^{-5}	5.32×10^{-5}	1.62×10^{-4}	305

[A] Greenhouse
[B] Outdoor

Facilities 1, 2, and 5 grow plants indoors and exclusively use lamp-generated radiation, while facilities 3 and 4 grow plants outdoors or in greenhouses. Plants grown outdoors only received solar radiation while plants grown in greenhouses received both solar and lamp-generated radiation. Work shifts performed in facilities that exclusively used lamp-generated radiation (n = 29) had a mean exposure of 5.98×10^{-4} eff. J/cm^2, which was significantly lower than shifts performed in facilities that primarily used solar radiation (n = 58; mean exposure of 3.58×10^{-3} eff. J/cm^2; $P < 0.01$).

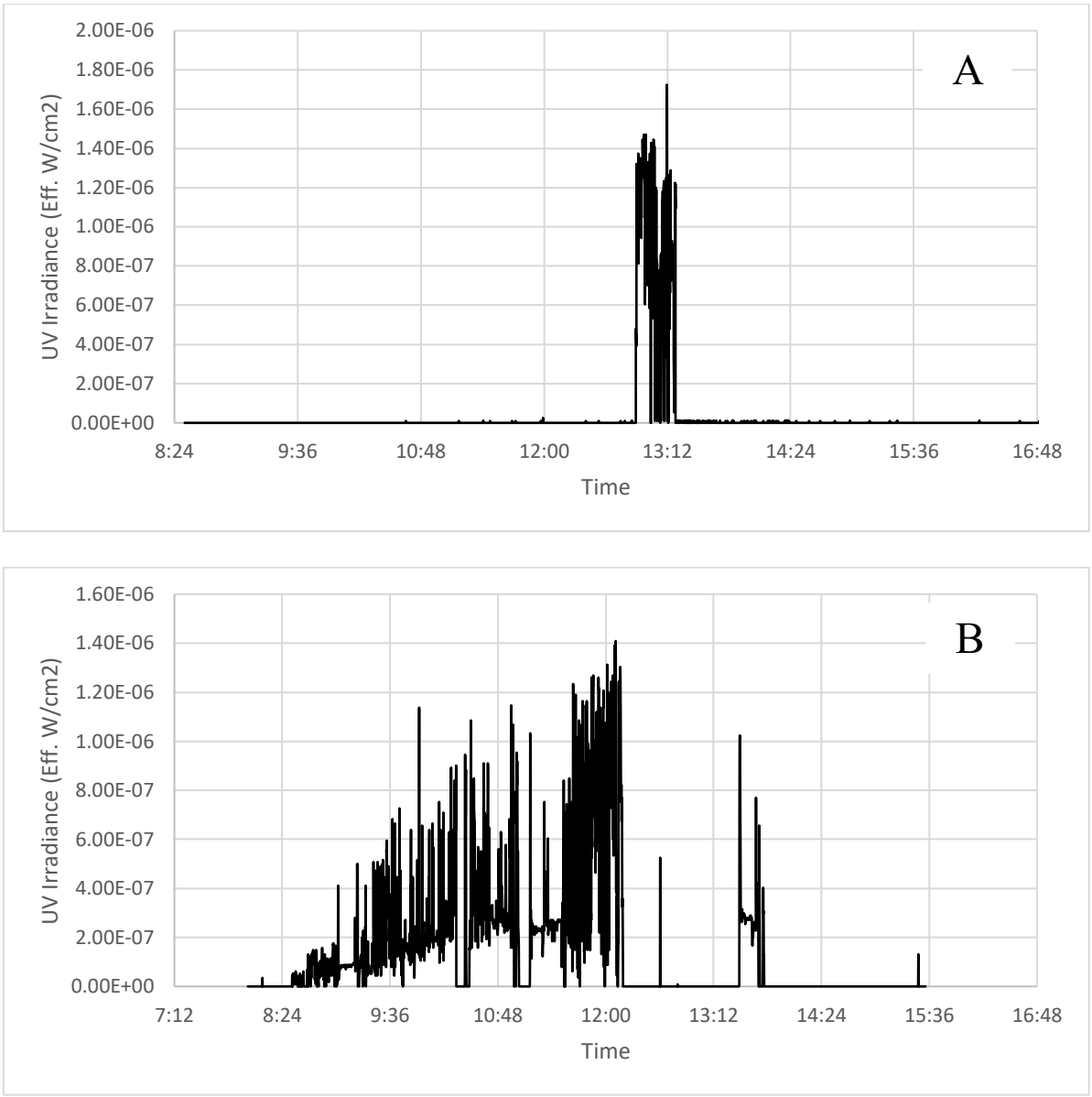

Figure 2. Typical time-series of workers' UVR exposures. Panel A: Worker at an indoor facility. Panel B: Worker at an outdoor facility.

Figure 2A illustrates a typical time series of UVR exposure during a single work shift for a worker at an indoor cannabis farm. This work shift contained one period of elevated UVR exposure between 12:50 and 13:20, which accounts for 99% of the total UVR exposure measured during this work shift. During this 30-minute interval, the subject's activity log indicates the worker was taking an outdoor lunch. Figure 2B illustrates a typical time series of UVR exposure during a single work shift for a worker at an outdoor cannabis farm. The time series illustrates a period of elevated UVR exposure between 8:30 am and 12:30 pm while the subject was working outside. The UVR irradiance tended to increase during this time period as the sun rose higher in the sky. After 12:30 pm this worker moved indoors to work trimming cannabis flower under regular fluorescent lighting. Their UVR exposures were largely undetectable during this time, except for a brief period between 13:30-13:40 when the worker took a break outdoors under a canvas sunshade.

Discussion

Lamp Emission Measurements

Powdery mildew is frequently encountered in cannabis farms (Scott and Punja 2021). However, the chemicals approved for use on cannabis in Washington State (WSDA 2018) are not especially effective in controlling powdery mildew. Consequently, germicidal lamps are being marketed to cannabis farms as a tool to control powdery mildew. Table 1 shows that germicidal lamps produce UVR at irradiances that could cause overexposure in under thirty sec. The irradiances measured create a health risk that is not well recognized in the cannabis industry, and germicidal lamp manufacturers do not consistently provide this information on lamp packaging (Solacure 2016)

Non germicidal lamps encountered during the study were LED, HPS, fluorescent, and MH lamps. MH lamps produced the highest levels of effective UVR among these four lamp categories on average, but at least one lamp of each type produced effective UVR at irradiances detectable by the radiometer. A variety of factors influence grower choice for lighting technologies, and lighting practices are not standardized across the industry. Use of solar radiation for cannabis cultivation is common in areas where climate and local regulations are conducive to growing cannabis outdoors, although in these settings, supplemental use of artificial light can extend the growing season. For indoor grows, a variety of factors influence the lighting technology used. These factors may include purchase and operating costs, availability of energy efficiency incentives that promote use of LED lamps, and individual grower beliefs about which lighting technology promotes desirable characteristics in their product.

Uncertainty Associated with UV Dosimeter Calibration

The UVR dosimeter measurements were calibrated with solar radiation using the ILT radiometer as the reference instrument to convert the dosimeter response into units that correspond to the ACGIH action spectrum, as described in the methods section. Figure 3 illustrates the calibration data for one dosimeter, aggregated from six calibration experiments undertaken on separate days. Linear relationships between the radiometer and the dosimeter were observed for all eight dosimeters, with the R^2 of the linear regression ranging between 0.80 to 0.87. Variation in the calibration relationship is likely due to variation in measurement angle, atmospheric conditions, and ambient temperature. Of these, measurement angle is probably the most significant source of variability because the radiometer and dosimeters have different angular response functions.

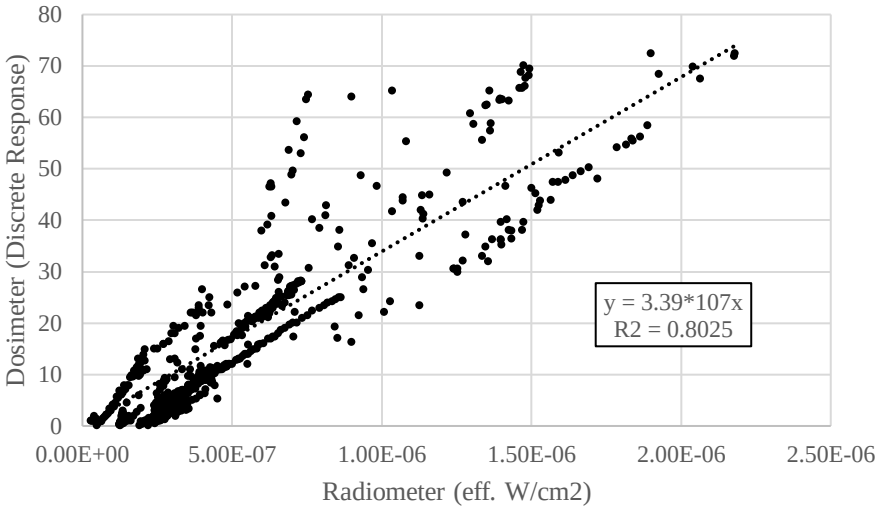

Figure 3. Plot of the calibration data for one dosimeter, aggregated across six calibration experiments, including the linear regression forced through zero. Each dot represents the average irradiance recorded over a one-minute interval.

Atmospheric conditions such as airborne particulate matter, cloud density, and humidity impact the day-to-day irradiance and spectrum of solar radiation. Variation in the solar spectrum may differentially affect device measurements because the radiometer has a different wavelength-dependent response function compared to the dosimeters. Changes in temperature may also have differentially affected instrument response, however, this effect is probably minimal because all sessions took place within the acceptable manufacturer provided temperature range.

Use of solar radiation to calibrate the dosimeters adds uncertainty to the calibration relationship when measuring UVR from non-solar sources. The spectra of lamp-generated radiation varies greatly by lamp make and model and can be very different from the solar spectrum. These spectral mismatches may cause bias in the dosimeter measurements of unknown magnitude and direction. Unfortunately, to our knowledge, no low-cost wearable UVR exposure sensors are commercially available that perfectly emulate the hazard function specified in the Washington State PEL, which is identical to that of the ACGIH 2010 TLV.

The dosimeter's cosine response and 180° field of view is appropriate for measurement of UV exposure to the skin, but not the eye, per the ICNRP guidance (ICNIRP 2007). The dosimeter measurement likely overestimates measurement of irradiance relative to the ACGIH prescription for measurement which stipulates an 80° field of view and no angular weighting. The Washington state regulation that specifies the PEL for nonionizing radiation does not specify either a field of view restriction, or an angular weighting for UV measurement (WAC 2003). The inconsistency amongst these various organizations in their guidance for measuring UVR exposure creates challenges for both UV dosimeter manufacturers and users.

Exposure Monitoring

Twenty-six of the 87 work shifts monitored (30%) had UVR exposures exceeding the ACGIH TLV. All 26 occurred at facilities where the primary optical source was solar radiation. Furthermore, the contribution of lamp generated radiation to exposures was not readily discernable. The UVR exposure time series for the indoor worker shown in Figure 2A illustrates this issue; 99% of the total UVR exposure for this work-shift occurred between 12:50 and 13:20 (Pacific Time Zone, U.S.), while the worker was on their lunch break outdoors and away from lamp-generated radiation. In contrast, during most of the work-shifts at this facility when the workers were indoors under artificial light, UVR exposures were undetectable. The portion of UVR exposure attributable to lamp-generated radiation is important from a regulatory compliance perspective, because the Washington State UVR PEL does not apply to solar radiation. In our data, UVR exposure attributable to solar radiation is not easily separable from the UVR exposure attributable to lamp-generated radiation because the granularity of our task activity logs was not adequate to capture each instance of solar radiation exposure. Incident radiation geometry may influence the target organ receiving UVR dose. The location and orientation of the human eyes are well adapted to the position of the sun overhead. However, the human eye is not adapted to optical sources in the plane of sight (Sliney 2001). Thus, indoor workers may receive a larger proportion of UVR dose to the eyes relative to the skin when compared to outdoor workers. In regard to effects of UVR exposure to the skin, health implications of any UVR dose received will vary based on individual susceptibility (skin phototypes) and adaptation to UVR exposure (e.g. tanning).

UVR exposure variability within and between shifts is likely due to a variety of environmental and personal factors. Environmental factors include variation in solar irradiance and cloud cover, worker location (outdoors vs indoors), use of various lamp models, radiation pathway interference, lamp height, and resin accumulation on dosimeter optical surfaces. The irradiance of lamp UVR emissions varied greatly within and between each of the five lamp types. Of the five lamp types, germicidal lamps emitted the highest effective UVR on average. In comparison, with the exception of one model, the LED lamps that were tested in this study emitted no detectable UVR, even at a measurement distance of 1 ft. However, given that UVR emitted from one LED model tested in this study, the data demonstrate that LEDs can be designed to produce UVR. Furthermore, some lamp manufacturers specifically market UVR-emitting LED lamps for use in cannabis cultivation. Forty lamp models were measured throughout the study, never encountering the same lamp model at multiple farms. The variation in lamp models likely creates a range of ambient UVR irradiances, which may increase the variability of UVR exposure over multiple shifts. Radiation pathway interference is caused by plant foliage and other objects in a growing area obstructing the path between the optical source and the dosimeter. A packed grow area is less porous to transmission of UVR and will likely reduce worker UVR exposure. In the indoor facilities, worker UVR exposures were affected by lamp height; the further away a lamp is from a worker, the lower the UVR exposure. Finally, the dosimeter optical surface may have accumulated cannabis resin or other interferences during a shift, decreasing sensor response. However, contamination of the dosimeter by cannabis resin was minimized by placing the dosimeters on the back of the worker's neck where direct contact with the cannabis plants was minimized compared to if the dosimeter were placed on the worker's wrist.

Personal factors that may have affected UVR exposure measurements include tasks performed, body position and orientation with respect to the light sources, use of PPE, and hair length. The tasks performed during a work shift influenced a workers' body position. For example, a worker may sit or crouch while pruning and stand while installing support nets. Body position influences proximity to the lamps and the body part orientation towards the optical source, both of which directly affect UVR

exposure. Finally, long hair may have obstructed the neck mounted dosimeters, reducing the measured UVR exposures.

Use of PPE such as long-sleeved clothing, hats, and sunglasses varied greatly by facility, ranging from shirtless to complete facial coverage via a ski mask. The PPE most commonly seen worn by the workers included hats, long sleeved clothing, headscarves, and sunglasses. Workers at facility #4 where plants were primarily grown outdoors typically wore the greatest amount of PPE (hats, scarves, sunglasses, long sleeved shirts, long trousers). The only worker-worn clothing that may have impacted our exposure measurements are wide brimmed hats or baseball hats worn backwards, as the hat brim had the potential to cast a shadow over the dosimeter. Workers wore a hat on 52% of work shifts. The mean UV exposure was 8.33×10^{-3} eff. J/cm^2 on work shifts where the workers wore a hat and 4.9×10^{-3} eff. J/cm^2 on work shifts where the workers did not wear a hat. This difference was statistically significant ($p = 0.031$) and may indicate that intense light conditions motivate a worker to opt to wear a hat. However, a paired t-test between the mean accumulated dose for hat wearers and non-hat wearers using only shifts with both groups represented ($n = 12$) did not show a significant difference between the two groups ($p = 0.57$). This suggests that wearing of hats by the workers was unlikely to have interference with the UV measurements.

Conclusions

This study's primary finding is that a significant proportion of cannabis cultivation workers experienced UVR exposures that exceeded the ACGIH TLV, and hence the workers are potentially at risk of adverse effects of overexposure to UVR. It is reasonable to assume that many other agricultural workers with outdoor jobs are similarly overexposed to UVR. All of the overexposures observed were associated with solar radiation. However several types of lamps used in cannabis facilities also emit UVR at levels high enough to cause exposures that exceed the ACGIH TLVs and the L&I PEL if workers were exposed for a long enough period of time. The risk of overexposure is greatly influenced by environmental and personal factors, including work location (indoors or outdoors), lamp type, and PPE use. Several of these risk factors are modifiable by employers and the workers. Outdoor workers should employ sensible sun-safe practices including wearing hats, scarves, sunglasses, long sleeved shirts, long trousers, and application of sunscreen regularly to exposed skin. Employers should provide workers with appropriate training on the hazards of UVR and should provide workers with shade from the sun where possible. Employers should also choose low UVR emitting lamps (e.g. LED and fluorescent) for indoor grows and use engineering controls (e.g. door-interlocks to de-energize lamps) to prevent worker exposure to UVR from germicidal lamps. Additionally, in view of the high variability observed in UVR emissions within each lamp class, it may be helpful for lamp manufacturers to specify spectral density functions for lamps. This would allow consumers to readily choose low UVR emitting lamps where appropriate.

This was a pilot study in a limited number of workplaces in a single state and thus may not be generalizable across the cannabis cultivation industry. As such, further research is needed to replicate the findings from this study and more fully understand the extent of UVR exposure and potential health hazards in this emerging industry. Additionally, grow lamp technology is advancing rapidly, with new lamp models released frequently. Newly introduced lamps to the market may produce high levels of UVR, and as such ongoing testing of UVR emissions may be needed. Finally, mismatches between a dosimeter's spectral response function and the ACGIH hazard function will cause bias in the dosimeter measurements of unknown magnitude and direction. Hence, exposure science would benefit greatly

from the development of an inexpensive wearable spectroradiometer, or an inexpensive wearable dosimeter weighted to the ACGIH hazard function since such a device would provide the platform for future research and assist U.S. employers in identifying and protecting workers from the hazard of UVR exposure.

Chapter 3: Wearable Spectroradiometer for Dosimetry

Maximilian Chmielinski[1], Martin Cohen[1], Michael Yost[1], Christopher D. Simpson[1]

[1] Department of Environmental and Occupational Health Sciences, Scholl of Public Health, University of Washington, Seattle WA

This chapter has been published in the journal Sensors: Chmielinski, M.J.; Cohen, M.A.; Yost, M.G.; Simpson, C.D. Wearable Spectroradiometer for Dosimetry. Sensors 2022, 22, 8829. https://doi.org/10.3390/s22228829

Abstract

Available wearable dosimeters suffer from spectral mismatch during the measurement of broadband UV and visible radiation in environments that receive radiation from multiple sources emitting differing spectra. We observed this type of multi-spectra environment in all five Washington State cannabis farms visited during a field study investigating worker exposure to ultraviolet radiation in 2018. Spectroradiometers do not suffer from spectral mismatch in these environments, however, an extensive literature review conducted at the time of writing did not identify any spectroradiometers that were directly deployable as wearable dosimetry devices. To close this research gap, we developed a microcontroller system and platform that allows for researchers to mount and deploy the Ocean Insight Flame-S Spectroradiometer as a wearable device for measurement of UV and visible wavelengths (300 to 700 nm). The platform validation consisted of comparing measurements taken under platform control with measurements taken with the spectrometer controlled by a personal computer running the software provided by the spectroradiometer manufacturer. Three Mann–Whitney U-Tests (two-tailed, 95% CI), one for each intensity condition, compared the central tendency between the total spectral power (TSP), the integral of a spectrum measurement, measured under both control schemas. An additional analysis of per pixel agreement and overall platform stability was performed. The three Mann–Whitney tests returned no significant difference between the set of TSPs for each filter condition. These results suggest that the spectroradiometer takes measurements of equivalent accuracy under both control schemas, and can be deployed as a wearable device for the measurement of wavelength resolved UV and visible radiation.

Introduction

Both natural sunlight and artificial lamp-generated radiation are commonly used in a variety of horticultural settings, including cannabis plants (Wallace and Both, 2016). These optical sources can contain both visible and ultraviolet (UV) wavelengths, however overexposure to ultraviolet radiation causes potential health risks. The most common UV overexposure injury is erythema (Hausser, 1928; Coblentz, Stair and Hogue, 1931) and the most severe erythema is caused by wavelengths between 280 and 315 nm (UVB) (Hausser, 1928; Ichihashi *et al.*, 2003). All UV wavelengths are classified as a Group 1 carcinogen by the International Agency for Research on Cancer (IARC) (IARC, 2012; Surdu *et al.*, 2013). Exposure of the eye to UV is associated with photokeratitis and keratoconjunctivitis. Injury severity is influenced by eye motion, spectral profile, and angle of incoming radiation. UVB exposure has been associated with photokeratitis (Pitts and Tredici, 1971), whereas both UVB and UVC overexposure has been causally linked to incidence of keratoconjunctivitis (Pitts, Cullen and

Hacker, 1977). Blue light (wavelengths ~ 380-550 nm can cause photochemical damage to the retina of the eye (ICNIRP, 2013) and may impact circadian rhythm, alertness and cognitive performance (Wong and Bahmani, 2022).

We previously observed that cannabis farm workers completed tasks under lamps that emitted UV radiation at four out of five cannabis farms in Washington State (Chmielinski *et al.*, 2018). While these observations confirm worker exposure to lamp emitted radiation, the severity and prevalence of agricultural worker overexposure to lamp emitted radiation is unstudied. A contributing reason as to why this research gap exists is because available wearable dosimeters cannot accurately measure exposure to broadband UV and visible radiation in an environment that contains light from multiple sources with different spectra (Gugg-Helminger, 2017), a condition observed at every cannabis farm we visited.

This inaccuracy results from the fact that radiation exposure is the sum of irradiance at each specific wavelength which is then integrated over the wavelength range and time period of interest. Wavelength-specific weightings, called action spectra or hazard spectra, which quantify the wavelength dependence of damage caused by UV radiation are then applied to the wavelength specific irradiance values in order to quantify the level of hazard that is present, and to determine compliance with occupational exposure limits. Broadband sensors perform well when the sensors are calibrated to a spectrum of interest (e.g., exposure to sunlight) and the environment of interest contains only this spectrum of interest. However, measurement of spectra that differ from that of the sensor calibration may lead to large measurement errors, named spectral mismatch errors (CIE, 2016).

Spectroradiometers do not suffer from spectral mismatch because they can measure wavelength resolved irradiance and hence can accurately measure radiation exposure in environments containing multiple sources with differing spectra. However, an extensive literature review did not identify any spectroradiometers that were directly deployable as wearable dosimetry devices. The ability of a wearable device to directly measure an individual's exposure to radiation is important, because some prior studies have shown that measurements of ambient irradiance using a fixed location device do not always provide reliable estimates of personal exposure (Sun *et al.*, 2014). The commercially available Ocean Insight Flame-S Spectroradiometer can measure UV and visible light with a spectrum spanning a broad range of wavelengths, but its design restricts its use to laboratory bench settings.

This manuscript describes the development and validation of a microcontroller system that allows for researchers to mount and deploy the Ocean Insight Flame-S Spectroradiometer as a wearable device for the accurate measurement of wavelength-resolved exposure to radiation across a broad range of UV and visible wavelengths (from 300 to 700 nm).

Materials and Methods

Platform

This platform uses the Flame-S Spectrometer with an attached CC-3-UV-S cosine corrector optical inlet (Ocean Insight, Orlando, FL, USA). The QP450-1-XSR optical fiber connects the optical inlet and the spectroradiometer (Ocean Insight, 2015) Although the Flame-S Spectrometer can nominally detect wavelengths down to 210nm, the standard version of this device suffers from spectral scatter during

measurements of broadband radiation, reducing its effective wavelength measurement range to approximately 300-700 nm, depending on the spectra of the measured source.

This platform, illustrated in Figure 1, uses the Arduino Due microcontroller board (Arduino, 2022) and the RS232 communications standard (TIA, 1997) to control the spectroradiometer. Additional peripherals include a HiLetgo ILI9341 2.8" thin-film-transistor (TFT) liquid crystal display (LCD) (HiLetgo, 2022), four non-latching momentary buttons, a 64 GB FAT32 SD card, a DS3231 I2C real-time clock (RTC)(Maxim Integrated, 2015) , and a CONXWAN B02P 26,800 mAh USB power bank (CONXWAN, 2022). The platform is currently housed in a 22cm x17cm x 11cm Zulkit hinged waterproof electrical box (Zulkit, 2022). The overall cost of the system is ~$4400 for the spectrometer, optical fiber and optical inlet, plus an additional $130 for the peripheral components to convert the spectrometer to a wearable device. As tested, the platform weighs 1,592 g. Figure S1 in the Supplemental Material provides a platform wiring diagram.

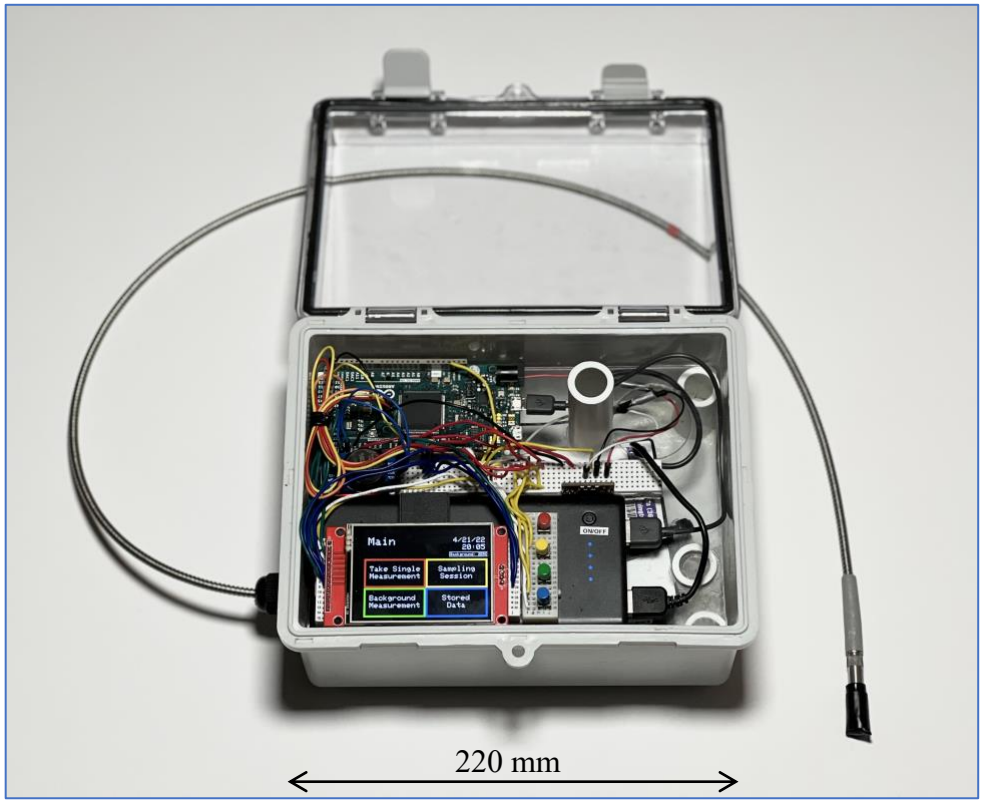

Figure 1: A top view of the wearable platform with hood open.

Test Source

The test source used to validate the performance of the spectroradiometer was a TriSOL TSS-300 Class AA+A solar simulator (OAI Inc., Milpitas, CA USA), located at the University of Washington Clean Energy Institute (WCET, 2022). This source generates a 300 mm × 300 mm square of radiation between 350 and 1200 nm. The working range of the collimated beam is 0.762 m, and the spatial uniformity is better than ±1%. The emitted irradiance matches that of the ASTM 173 1.5 air mass (AM)

solar spectrum to an accuracy of ±15% and a temporal stability of <2% (OAI, 2016). Prior to testing, the device underwent its 15-min warm up cycle.

Optical Bench

An optical bench holds the optical inlet to the spectrometer at orthogonal at approximately the center of the 300 mm × 300 mm illuminated region of the solar simulator at a distance of 0.2 m below the test source. Irradiance intensity was controlled by the installation of zero, one, or two UV fused silica 50 mm 2.0 optical density neutral density (ND) filters (Thorlabs, Newton, NJ USA) in front of the spectroradiometer optical inlet. The experimental set up is shown in Figure 2.

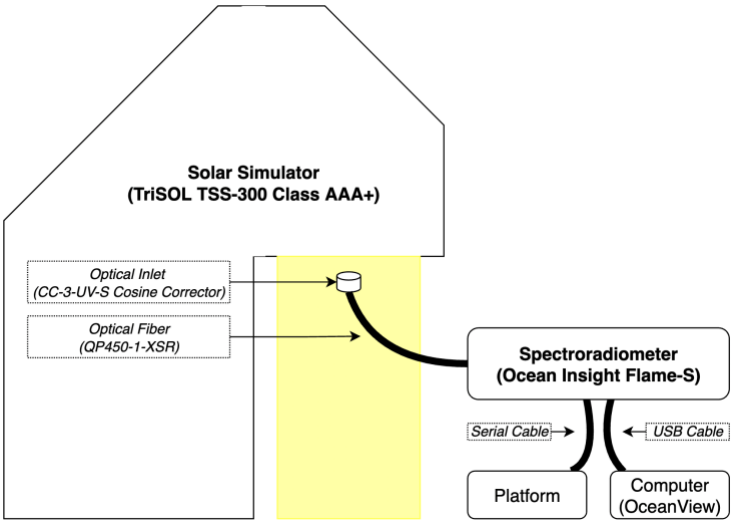

Figure 2: A simple block diagram of the testing setup.

Control Software

The manufacturer provided control software, OceanView (ver 1.6.7 Ocean Insight, Orlando, FL), allows for a computer running a Windows 10 or 11 operating system to control the spectroradiometer on the benchtop via USB 2.0 communication. In contrast, the Arduino Due board controls the spectroradiometer by sending commands and receiving data via the serial port. The Arduino operates using four states, consisting of a platform startup state, a spectroradiometer check state, a standby state, and a spectrum capture state. Should any state fail, the Arduino stops operation and sends an error code to the Serial port and, if initialized, the LCD screen (Chmielinski, 2022).

The platform startup state occurs automatically upon the Arduino connecting to power. In this state the Arduino begins serial communication and causes the initialization of all peripherals. Next, the spectroradiometer check state involves the Arduino sending a command to change the integration time set on the spectroradiometer from the factory default from 10 ms to 100 ms. When the Arduino receives a successful receipt of an electronic acknowledgement, an ‘ACK’, from the spectroradiometer, the Arduino transitions to the standby state (Chmielinski, 2022). In the standby state, the Arduino loads the control functions for the user interface to the LCD screens. Each control function is linked to one of the four momentary contact buttons on the platform. Upon the user pressing a button, the Arduino executes the associated function and moves the device into either the standby, spectroradiometer check, or the spectrum capture state.

During the spectrum capture, the Arduino sends a sequence of commands to the spectroradiometer that cause it to take a spectrum measurement, send spectrum data to the Arduino serial port, and have the Arduino save the data to the micro-SD card. Upon completion of this state, the Arduino moves into the standby state. The full source code for the firmware is accessible at the following repository: https://github.com/mxchml/Flame-Spectrocontroller (Chmielinski, 2022) accessed January 15th, 2023.

Both control schemas convert raw pixel signal to irradiance in $\mu W/(nm \times cm^2)$ through an identical five step computation consisting of a noise correction, a linearity correction, a pixel wavelength bound correction, an integration time application, and a calibration factor application. These processes are described in the Supplemental Materials of this submission.

Experiment #1: Platform Monitoring Sessions

The purpose of experiment #1 was to investigate the stability of the spectroradiometer measurement over a sustained duration while under platform control. For this purpose, the technician performed six monitoring sessions with the spectroradiometer under platform control to generate six sets of measurement data. During the six sessions, two sessions had zero neutral density (ND) filters installed, two had one ND filter installed, and two had two ND filters installed. For each session, the spectroradiometer was activated and the integration time was allowed to stabilize. After stabilization, the spectroradiometer was allowed to run for an arbitrary duration greater than one minute. All measurements taken prior to when the platform reached a stabilized integration time were not included in the analysis.

The adjustment of integration time between filter conditions, as well as the arbitrary sampling time beyond one minute resulted in the six datasets each comprising of a variable number of spectral measurements (n = 4 to 23).

Data Processing - Experiment #1
Each monitoring session comprised of a set of spectra (n = 4 to 23), and all spectra underwent integration by wavelength between the first pixel with a signal above threshold (varied by measurement, minimum was 353.313 nm) and 700 nm. This converted each spectrum to a value of total spectrum power (TSP) in units of mW/cm^2. The coefficient of variation (COV) and the percentage difference between the largest and smallest TSP, called the maximum percent power difference (MPPD), were calculated for each of the six sessions.

Experiment #2: Single Measurements Using Both Control Schemas

A priori we expect the spectra and signal intensities to be identical between the platform controller and the commercial product. However, differences between the two control schemes in the measured magnitude and/or the spectrum shape may occur due to differences in integration time and/or differential implementation of signal processing. Therefore, the purpose of experiment #2 is to validate agreement between measurements taken by under both control systems.

To generate a range of intensities at the detector, zero, one, or two ND filters were installed between the solar simulator and the spectroradiometer. For each number of installed filters, the spectroradiometer took a set of three measurements under platform control and a set of three measurements under OceanView control, resulting in a total of six sets that collectively contain eighteen measurements. The

technician switched the control schema by manually unplugging the spectroradiometer from the PC and connecting it to the Arduino controller platform.

Data Processing – Experiment #2

TSPs were calculated for each spectrum using the process described previously. Additionally, the average spectrum for each of the six sets was calculated by averaging the irradiance measured at each pixel.

Analysis

Mann Whitney U-Tests

Three Mann Whitney U-Tests (two-tailed, 95% CL) compared the central tendency of the TSPs calculated from the platform-controlled measurements to the TSPs calculated from the OceanView-controlled measurements for the zero, one, and two filter conditions. A two-tailed Mann Whitney U-Test at the 95% confidence level compared the central tendency of the set of COVs from the experiment #1 ($n = 6$) to the set of COVs from experiment #2 ($n = 6$).

Linear Regressions

For each of the three optical filter settings, a linear regression compared the average spectrum generated by the platform control with the average spectrum generated by OceanView control. The goodness of fit metric is the R^2 coefficient, while the slope of the regression line indicates quantitative agreement between the two spectrometer control schema.

For each pixel that measured above threshold for all filter conditions (n = 999), a linear regression based on three datapoints was performed. These three datapoints corresponded to the three-filter conditions, and each regression compared a pixel's average measurement under platform control to the average measurement under OceanView control. The 999 calculated slopes were plotted against the pixel wavelength to create a scatterplot visualizing how the agreement between platform / OceanView controlled measurements changes across wavelengths.

Results

Experiment #1

Table 1 presents the stability data generated from the six platform monitoring sessions and includes the number of installed filters, the number of samples, the duration of stable integration time measurement period, the COV, and the MPPD.

Table 1 Results from the platform monitoring sessions of the solar simulator emissions.

Filter	n	Stable Duration (s)	COV (%)	MPPD (%)
None	23	164	0.7	1.23
None	10	85	0.8	0.95
1x	11	98	0.2	0.20
1x	12	96	0.2	0.29
2x	4	100	0.1	0.11
2x	6	79	0.3	0.35

Experiment #2

Figure 3 presents six charts displaying the average spectrum measured for each irradiance condition. (upper row: platform-controlled acquisition, bottom row: OceanView controlled acquisition). Each spectrum is the average of three individual measurements.

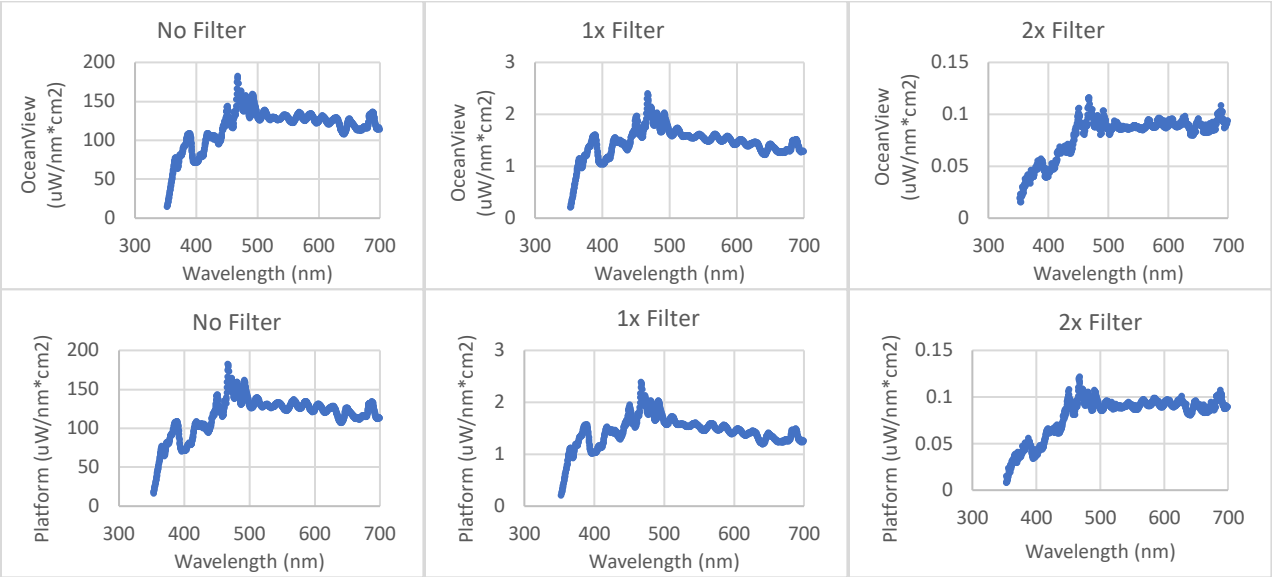

Figure 3: Each chart displays an average spectrum created by averaging three repeat spectral measurements. The top row shows the average spectrum of the platform-controlled measurements and the bottom row shows the average spectrum of the OceanView controlled measurements

All of the above plots begin at 353.313 nm. The lowest pixel irradiance measured above threshold was 13.7, 0.19, and 0.018 μW/(nm × cm^2) for the no filter, one filter and two filter conditions under OceanView control and 15.6, 0.20, and 0.007 μW/(nm × cm^2) for the no filter, one filter and two filter conditions under platform control, respectively. Table 2 presents summary statistics for these measurements.

Table 2 The mean total power average, standard deviation, coefficient of variation, integration time (IT) mean and standard deviation, and the results of the Mann-Whitney test comparing the TSP for the OceanView vs platform-controlled data.

Filter	OceanView						Mann - Whitney	Platform					
	n	Mean TSP (mW/cm^2)	SD (mW/cm^2)	COV	Mean IT (ms)	SD (ms)	U (p value)	n	Mean TSP (mW/cm^2)	SD (mW/cm^2)	COV	Mean IT (ms)	IT SD (ms)
None	3	40.3	0.055	0.001	6.32	0	3 (0.663)	3	40.3	0.102	0.002	5.3	0.58
1x	3	0.503	0.001	0.002	484	0	0 (0.081)	3	0.497	0.001	0.001	452	2.65
2x	3	0.028	<0.001	0.014	3329	0	2 (0.383)	3	0.028	<0.001	0.010	5000	0

Table 2 contains the mean total power averages, standard deviations, coefficients of variation, and integration time statistics summarizing the results from experiment #2. Under OceanView control, the maximum TSP measured for a single spectrum was 40.3 during the no filter condition and the minimum was 0.028 mW/cm^2 under the two-filter condition. Under platform control, the maximum TSP measured for a single spectrum was 40.3 during the no-filter condition and the minimum was

0.028 mW/cm^2 under the two-filter condition. The three Mann-Whitney tests returned no significant difference between the set of TSPs for each filter condition.

Figure 4 presents scatterplots and linear regression lines of the average spectra taken during OceanView control vs. average spectra taken during platform control.

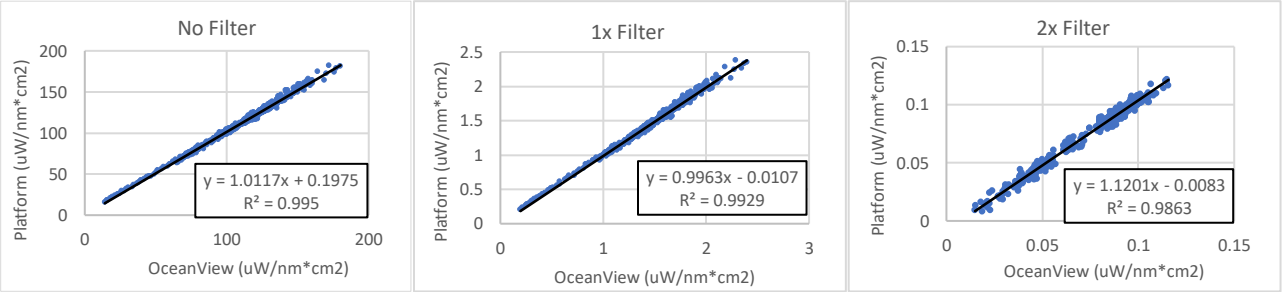

*Figure 4: Scatterplots of measurements taken during OceanView control on the x-axis and platform control on the y-axis, both in units of µW/nm*cm^2, for the three cycles. The plots also show the linear regression line, equation, and correlation coefficient.*

The slopes and slope confidence intervals for the no filter, one filter, and two filter regressions are 1.0117 ± 0.004, 0.9963 ± 0.005, and 1.1201 ± 0. 008. The slope closest to unity came from the one filter condition and had a value of 0.9963. The 2x filter regression resulted in the smallest y-intercept, with the intercept moving further from zero in the negative direction with each reduction in the number of filters present.

Figure 5 presents a plot of the slope of the linear regression calculated for each pixel's average Oceanview vs platform-controlled measurements.

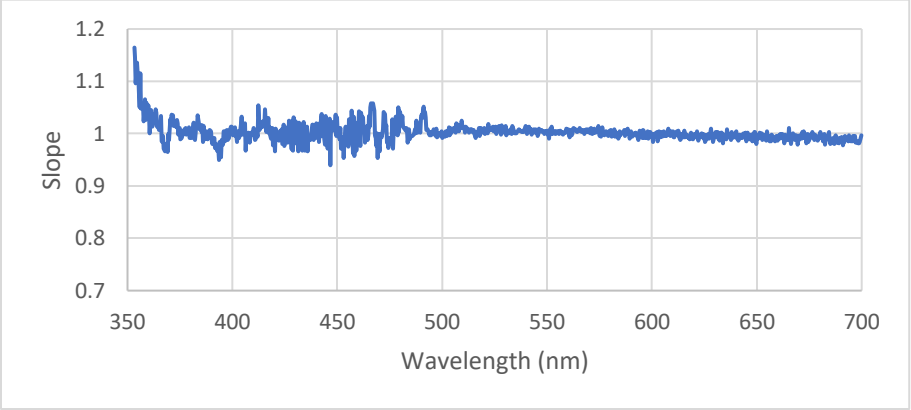

Figure 5: The slope of linear regressions for each pixel computed using three data points corresponding to platform- vs OceanView-controlled measurement during each of the three filter conditions.

The chart shows the regression slopes diverge from a value of unity at the wavelengths below approximately 370 nm, with the greatest divergence from unity occurring at 353 nm and having a value of 1.14.

Discussion

Each set of spectral measurements from experiment #1 had a low coefficient of variation and an MPPD that was below the solar simulator's reported 2% temporal stability. Furthermore, each set of measurements from experiment #2 taken under platform control had a low coefficient of variation. These results demonstrate stable spectroradiometer measurement when under platform control.

The experiment #2 Mann-Whitney tests did not show a statistically significant difference in the TSPs between the platform and OceanView controlled measurement sets. These results suggest that the accuracy of the TSPs of the measurements taken when the spectroradiometer operates under platform control is comparable to those taken while the spectroradiometer operates under OceanView control.

The linear regression results of Figure 5 showed excellent agreement across all pixels, especially those corresponding to wavelengths above ~370 nm. Below ~370 nm, Figure 5 shows the slopes positively tailing as the scatterplot approaches 353 nm. This tail indicates that the spectroradiometer under platform control takes increasingly higher irradiance measurements when compared to those taken under OceanView control as the wavelength of measurement decreases. The suspected cause of this disagreement is that electrical and thermal noise contribute a greater proportion of the total signal at wavelengths below 370nm, where the intensity of radiation emitted from the solar simulator source is low. Differences in the mean integration time may also have contributed to the differences in measurement noise between the control schema. However, the worst slope of 1.19 still indicates good agreement between the measurements under the two control schemas.

These results suggest that the accuracy of the spectra taken when the spectroradiometer operates under platform control are comparable to those taken while the spectroradiometer operates under OceanView control across all wavelengths between 353 nm and 700 nm. Agreement between measurements taken under both control schema suggest that the deployment of laboratory bench spectroradiometers using a simple lightweight control schema is a viable solution to the current dearth of available wearable spectroradiometric measurement technologies. Subsequently, we performed a comparison of instrument response to narrow band UVC radiation, under the two control schema. The radiation source for this test was an Ocean Optics mercury argon HG-2 calibration lamp. The difference in the measurement values was under 0.1% between the two control schema for all pixels between 253 and 255 nm. Additional testing with a broadband UVB and/or UVC optical source should be undertaken to further demonstrate the viability of this platform as a tool for measuring UVB and UVC exposure.

The usability of the device as a wearable sensor was evaluated by a Certified Industrial Hygienist (CIH) who manages a professional practice in the Washington DC area as well as a second CIH working for the University of Washington field group (DEOHS, 2022). As tested, the device is attached to a subject via a belt worn on the waist. The optical inlet was mounted on the frame of safety glasses, oriented to align with the subject's eye. The optical fiber connecting the inlet to the housing ran down the subject's back, sandwiched between an undershirt and an overshirt to prevent the fiber from snagging on objects in the environment.

The DC area CIH reported that the device performed well under a variety of conditions and that the user interface was intuitive and allowed him to operate the device without reference to a provided user manual. The UW CIH stated that the device was easy to use and comfortable to wear while walking,

however, discomfort was reported when sitting while wearing the device. He suggested exploring whether chest mounting strategies could improve comfort during sitting.

Supplemental Material for Chapter 3

Platform Circuit

Figure S1 displays the electrical connections between the Arduino Due, peripheral devices, and the spectroradiometer, RTC, and microSD interface. Table S1 details all labelled pins in this diagram.

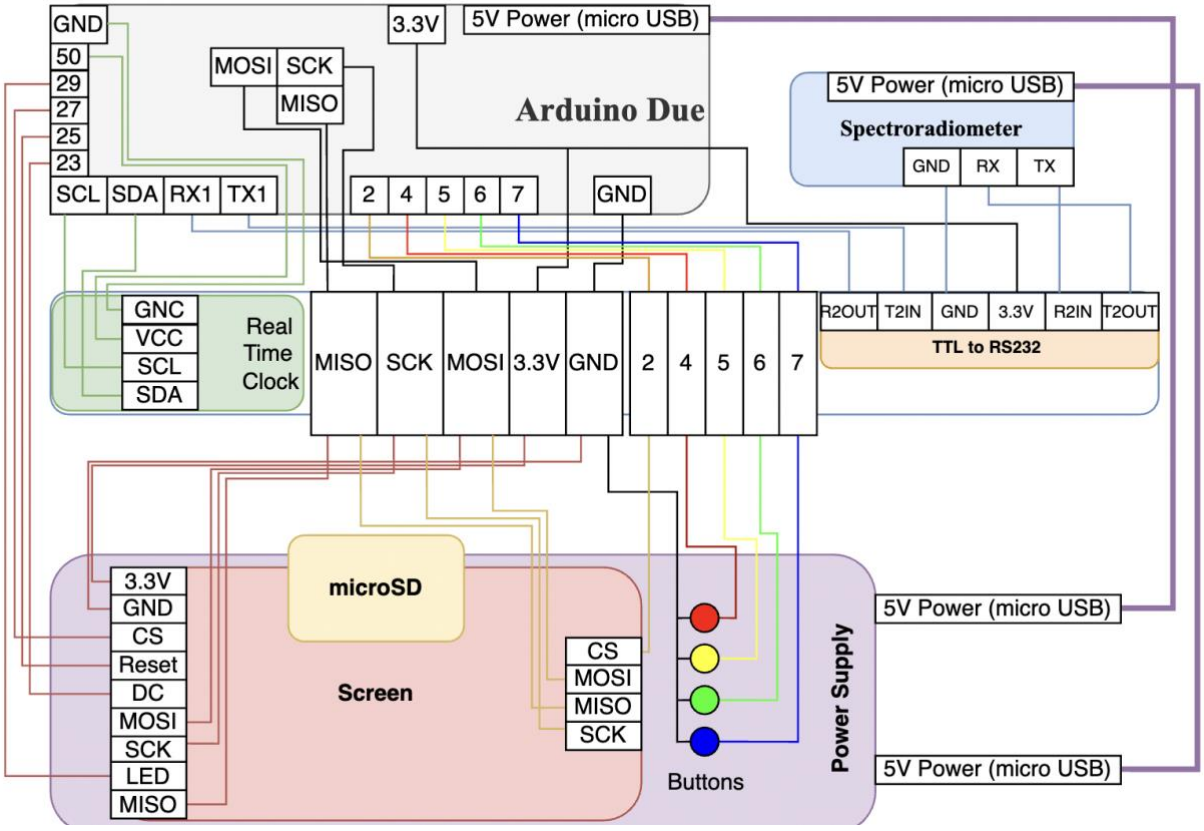

Figure S1: The wiring schematic for the platform.

Table S1: Descriptions for each pin label.

Label	Name	Description
5V Power (micro USB)	Power supply Connection	Connect the spectroradiometer and the Arduino Due to the power supply through micro USB ports
3.3V	Voltage High (3.3V)	Connects the peripheral to the 3.3V wire.
GND	Voltage Low (0V)	Connects the peripheral to the platform electrical ground.
MOSI	Master Out Slave In	Connection for the master device to send data to the slave device
MISO	Master In Slave Out	Connection for the slave device to send data back to the master device
SCK	Serial Clock	Line that carries the clock pulse generated by the master device
SDCS OR LCDCS	Chip Select (for SD card or LCD display)	Connection used by the master device to inform the slave device that it will send or request data. The SS/CS pin should be set to LOW to inform the slave that the master will send or request data. Otherwise, it is always HIGH
D/C	Data/Command pin	Switch on the TFT to send data to the SD card or the LCD display
TE	Tearing Effect	optional output from the display to synchronize data writes, avoiding the ‘Tearing Effect' that is seen when data is changed halfway through a display refresh
PWM	Pulse width modulation	Allows the input of a PWM signal to dim the backlight of the LCD display
RX	RS232 Data Receiving Pin	The Recommended Standard 232 pin that sends data from the device.
TX	RS232 Data Transmitting Pin	The Recommended Standard 232 pin that receives data from the device.
Pin #s	Arduino Pins	Multi-purpose pins that allow transmitting or receiving bits to and from the Arduino Due.
SDA	Serial Data Line	Data gets sent through this pin and gets synchronized with the clock signal on the SCL
SCL	Serial Clock Line	Receives the clock signal.

Peripheral Communication

Terminology

The platform primarily uses 16-bit data packets called ‘data words’ to communicate between the microcontroller and peripherals. This data structure can be described as two bytes, with 8-bits representing the large value called the most significant byte (MSB) and 8-bits representing the small value termed the least significant byte (LSB). In infrequent instances, this platform uses 32-bit data packets called double data words, which themselves can be described as two data words. As before, the

term for the 16-bits representing the large value is the most significant data word (MSW) and the term for the 16-bits representing the small value is the least significant word (LSW).

The rate at which information is transferred in a communication channel is called the baud rate. A baud rate of 115200 refers to a rate of 115200 bits per second.

RS-232 Standard

This platform uses the Recommended Standard 232 for 115200 baud rate communication between the Arduino Due and the spectroradiometer. The standard formally defines signals connecting between a data terminal equipment, in this case the Arduino Due, and a data connection equipment (the spectrometer). The standard represents bits as positive and negative voltages within a range of +3V to +15V and -3V to -15V (TIA, 1997). Researchers and engineers commonly opt to use the RS232 serial communication standard to control scientific equipment because of its simple implementation and adaptability.

Spectroradiometer Commands

The spectroradiometer firmware requires commands send via RS232 to begin with an ASCII character sometimes followed by binary data specifying an option. The spectroradiometer returns an electrical acknowledgement (ACK) upon receipt of a successful command and an electrical negative acknowledgement (NAK) upon receipt of an incorrect command.

Serial Peripheral Interface

The platform uses the Serial Peripheral Interface (SPI) for communication between the Arduino Due and the SD card reader/ TFT display. SPI is a synchronous serial communication protocol that provides two-way master-slave type communication between a microcontroller and its peripherals. SPI facilities this communication using synchronization bits and preset data transfer speeds. An SPI interface communicates using at least four lines, with an additional line required for each additional peripheral device.

Inter-Integrated Circuit Communication

The platform uses Inter-Integrated Circuit Communication (I2C) to communicate between the Arduino Due and the RTC. I2C consists of serial data line (SDL) and a serial clock line (SCL). The data to be transferred is sent through the SDA wire and is synchronized with the clock signal from SCL. The standard formally defines signals connecting between a master device, in this case the Arduino Due, and a slave device, in this case the RTC.

Spectroradiometer Quality Indices

This section presents the Ocean Optics Flame-S spectroradiometer quality indices, as provided by the instrument manufacturer (Ocean Insight 2021).

Table S2: The quality indices of the Ocean Insight Flame-S Spectroradiometer (Ocean Insight, 2021).

Quality Index	Description	
Wavelength uncertainty	<0.0001%	
Monochromatic pixel accuracy	at 210 nm:	16.2%
	at 250 nm:	10.8%
	at 300 nm:	10.4%
	at 350 nm:	11.4%
	at 400 nm:	8.0%
	at 450 nm:	5.8%
	at 500 nm:	4.6%
	at 550 nm:	3.8%
	at 600 nm:	3.4%
	at 650 nm:	3.0%
	at 700 nm:	2.8%
	at 750 nm:	2.8%
	at 800 nm:	2.8%
	at 850 nm:	2.8%
Spectral scatter	0.01%	
Slit scattering	<5%	
Signal to Noise (at saturation)	250:1	
Number of Pixels	2048	
Readout Noise	± 50 counts	
Pixel limit of detection	Min (200 nm):	6.72E-12 W
	Germicidal (254 nm):	1.59E-13 W
	Max (524 nm):	1.40E-14 W
Pixel saturation	Min (200 nm):	2.86E-02 W
	Germicidal (254 nm):	6.76E-04 W
	Max (524 nm):	5.98E-05 W
Sampling rate	1ms to 65s (platform range: 1ms to 5s)	

Optical Measurement Quality Indices

The primary quality indices that affect the measurement of UV radiation are the monochromatic pixel measurement uncertainty, spectral scatter, slit scattering, and signal to noise ratio (Nehir *et al.*, 2019). Monochromatic pixel measurement uncertainty is the uncertainty inherent for a single pixel in the measurement of a monochromatic source. Spectral scatter and slit scatter cause out of band signal to arrive at each pixel. Spectral scatter refers to the diffuse radiation arriving at evenly distributed intensity at all pixels, proportional to the total radiation intensity present at the optical inlet. Slit scatter refers to the radiation scattered by the entrance slit of the spectroradiometer. Spectroradiometers with large slit scattering error display large full width half maximum (FWHM) during measurement of monochromatic radiation, thus reducing the instrument's wavelength resolution.

Signal to noise ratio (SNR) is the signal intensity divided by the noise at a particular signal level. A spectroradiometer with a large signal to noise ratio can more accurately identify and measure a weak signal compared to one with a small signal to noise ratio (Ocean Insight, 2022).

The spectroradiometer contains eighteen pixels covered with an opaque material, called dark pixels, in addition to the 2048 optically active pixels. A manufacturer provided method to remove background noise generated by electrical and thermal fluctuations in the device subtracts the average signal generated by these dark pixels from the signal generated at each optically active pixel on the device. However, this method does not account for the noise introduced by spectral scatter (Ocean Insight 2015).

An uncorrectable source of noise originates in the detector's pre-amplifier during readout, aptly named readout noise. This spectroradiometer has a readout noise of ± 50 counts (Ocean Insight 2015).

The spectroradiometer has a variable limit of detection depending on the wavelength of the measured radiation. For an integration time at the device maximum integration time of 65 seconds, the device limit of detection ranges from 6.72E-12 W for 200 nm to 1.40E-14 W for radiation at 524 nm. The pixel saturation at the minimum integration time of 1ms is 2.86E-02 W at 200nm and 5.98E-05 W at 524 nm (Ocean Insight 2021).

Dynamic Integration Time Adjustment

The microcontroller adjusts the spectroradiometer integration time to target a pixel saturation level of 75%, adjusting based on the maximum number of signal counts collected for the previous collected measurement. The microcontroller first identifies the pixel with the maximum signal count, and uses it to generate a scaling multiplier with the following equation:

$$F = \frac{21363.6}{m}$$

Equation 1

Where m is the maximum pixel signal count from the previously taken spectrum and F is a factor applied to the previous integration time as follows:

$$I_o = FI_i$$

Equation 2

Where I_i is the previous integration time and I_o is the new integration time. If the new integration time exceeds 5 seconds, the microcontroller automatically sets the integration time to 5 seconds.

Processing Spectrum Data

Microcontroller Receipt of Data Words

Most Arduino libraries provide functions to handle bytes, not data words. To properly process data words sent by the spectroradiometer, the microcontroller applies a bit-wise operation to the data collected by the default Serial1.readBytes(buffer, size) function. This function collects a number of

bytes equal to the ‘size’ parameter and stores them into the ‘buffer’ array. The bit-wise operation involves instantiating a data word using the bit-shift operator <<. Example C++ code illustrates this bit-wise operation.

```
byte byte_buf[2];
Serial1.readBytes(byte_buf, 2);
word data_word_A =  byte_buf[1] | (word) byte_buf[0] << 8;
```

The first line of this code allocates two bytes of the microcontroller’s memory for the byte_buf array. The second line has the Serial1.readBytes function store the data word’s MSB in byte_buf[1] and its LSB in byte_buf[0]. The third line initializes a data word variable named ‘data_word_A‘ and uses the bit-shift operator to write the first 8-bits as the MSB and the second 8-bits as the LSB.

The microcontroller reads all 2056 data words sent by the spectroradiometer to flash memory. While the data exists in flash memory, the microcontroller performs several sequential processes to convert the data from raw signal counts into absolute irradiance in W/cm^2.

Linearity Correction

The microcontroller applies the manufacturer provided linearity correction calibration to each raw signal value in the spectrum. The value of each pixel undergoes the following function.

$$L_i = \frac{1}{F} C I_i \qquad (3$$

Where L_i is the signal count of pixel *i* with the linearity correction applied, *C* is a constant equal to 65,535/28000 to scale the spectroradiometer raw signal into the manufacturer software scale of 0 to 65535, I_i is the uncorrected signal count of pixel *i*, and F is the factor computed from:

$$\begin{aligned} F = \ & 0.884115 + I_i * 1.00742 * 10^{-5} \\ & - {I_i}^2 * 5.39901 * 10^{-10} \\ & + {I_i}^3 * 2.78301 * 10^{-14} \\ & - {I_i}^4 * 1.10510 * 10^{-18} \\ & + {I_i}^5 * \ 2.59529 * 10^{-23} \\ & - {I_i}^6 * 3.05861 * 10^{-28} \\ & + {I_i}^7 * 1.34544 * 10^{-33} \end{aligned} \qquad (4$$

Noise Correction

The manufacturer provided noise correction method averages the signal detected by each of 18 pixels, named dark pixels, that have an opaque coating that prevents the receipt of radiation signal. The average of these 18 pixels represents the average thermal and electrical noise inherent in a device measurement. The Arduino subtracts the average signal detected at these 18 pixels from the value measured at each of the other 2030 pixels present on the charge coupled diode.

Signal Thresholding

The microcontroller sets a pixel's corrected signal count value to zero if the value does not exceed a signal to a noise threshold. The threshold varies by wavelength band, and the noise value is the average computed during the previous noise correction process. For wavelengths under 315nm, the microcontroller requires the signal to be at least 66% larger than the noise. For wavelengths between 315 and 400nm, the signal needs to be at least 50% larger than the noise. For wavelengths between 400 and 871nm, the signal needs to be at least 10% larger than the noise.

Signal to Irradiance Conversion

The microcontroller uses manufacturer provided calibration factors along with the integration time, area of the spectroradiometer optical inlet, and the trapezoidal integration of the wavelength bounds to convert corrected signal counts into irradiance in μW/(cm^2*nm). To do so, the microcontroller uses the following function:

$$P_i = \frac{L_i * C_i}{0.119460 cm^2 * t * \Delta x_i} \quad (5$$

Where P_i is the power in mW/(nm*cm^2), the constant is the area of the cosine corrector inlet in cm^2, L_i is the spectral scatter corrected pixel signal count, C_i is the calibration factor of pixel *i* in uJ/count, *t* is the integration time in seconds, and Δx_i is the wavelength bound in nm.

Chapter 4: Non-Ionizing Radiation Modeling to Predict Ambient Irradiance in Work Areas at an Indoor Cannabis Farm.

Key Words: Non-ionizing radiation, Radiative transfer, Horticulture, Indoor, Marijuana, UV

This chapter has been submitted for publication in the Journal Annals of Workplace Exposures and Health

Abstract

Agricultural workers frequently experience potentially hazardous exposure to non-ionizing radiation from both solar and artificial sources, and measurement of this exposure can be expensive and impractical for large populations. This project develops and evaluates a vegetative radiative transfer model (VRTM) to predict irradiance in a grow room of an indoor cannabis farm. The model uses morphological characteristics of the crop, manufacturer provided lamp emissions data, and dimensional measurements of the grow room and hedgerows to predict irradiance. A linear regression comparing model predictions with the measurements taken by a visible light spectroradiometer had slopes within 23% of unity and R^2 values above 0.88 for visible (400 to 700nm), blue (400 to 500nm), green (500 to 600nm), and red (600 to 700nm) wavelength bands. The excellent agreement between the model and the measured irradiance in the cannabis farm grow room supports the potential of using VRTMs to predict irradiance and worker exposure in agricultural settings. Because there is no mechanistic difference between visible and other non-ionizing wavelengths of radiation in regards to mechanisms of radiative transfer, the model developed herein for visible wavelengths of radiation should be generalizable to other radiation bands including infrared and ultraviolet radiation.

Introduction

Considerable research has linked ultraviolet (UV) radiation and blue light exposure to various health hazards, including skin damage (Ichihashi *et al.*, 2003), eye damage (Pitts and Tredici, 1971), circadian rhythm disruption (Hatori *et al.*, 2017), immune system suppression (IARC, 2012), and various types of cancer (IARC, 2012). Outdoor agricultural worker exposure to UV radiation has been widely studied (Glanz, Buller and Saraiya, 2007) and exposures in the outdoor farmer population have been directly linked to negative health outcomes such as an increased risk of melanoma (Togawa *et al.*, 2021) and lip cancer (Acquavella *et al.*, 1998). In contrast only a few studies have documented indoor farm worker exposure to UV radiation from artificial lights (Chmielinski *et al.*, 2018). No research has yet studied the health outcomes of indoor farm worker radiation exposure, a gap due, in part, to the lack of exposure research on this topic. This research gap is becoming more important because of the increasing prevalence of supplemental lighting use across horticultural farms in the United States, evidenced by the 46% increase in the size of the grow lamp industry between 2016 and 2021 (Grandview Research, 2022). This growth is driven, in part, by new research showing the benefits of

supplemental lighting on crop yield benefits (Lu and Mitchell, 2016) and the rapidly decreasing costs of agricultural lamps (Morrow, 2008).

Direct measurements of personal exposure are often viewed as the gold standard for exposure assessment. However, collecting personal exposure measurements can be expensive, and may not be practical for large populations. In the absence of direct measurements, exposure models can be used to make predictions of personal exposure. Predictive exposure models can provide additional benefits, including (i) identifying potentially hazardous exposures *a priori*, for example during design of a facility or process and (ii) estimating the effect on worker exposure of changes in work processes or facilities. This project develops a model for predicting worker exposure to non-ionizing radiation – as a surrogate for exposure to UV radiation - in an indoor cannabis farm. Model performance is then evaluated via comparison with measurements of visible light irradiance in the cannabis farm made using a visible light spectroradiometer.

Methods

Dimensional Measurements

To create a 3D representation of the grow room, measurements of the location and dimensions of all lamps, hedgerows, and walls in the grow room using a DISTO D2 laser distance meter (Leica Geosystems; Heerbrugg, Switzerland). The DISTO D2 device had published measurement error of +/- 1.5mm, calibrated at distances of 0.64, 2.47, and 7.84 meters.

The grow room had a length, width, and height of 13.1m x 7.62m x 2.57m and contained fortyeight Vividrgo V2 (model ID: VGROHB 600W P26 MVOLT CLR PND BLK) lamps (Illumitex, Austin, TX). The room contained twenty-four wheeled hedgerow platforms, each of which held four cannabis plants contained within individual 5-gallon pots. The platforms had a width of 0.68m and a length of 2.75m, and the canopies on the platforms had dense vegetation between a height of 1.18m and 1.66m (see Figure 1 A,B). At the time of measurement, the plants were in the late stages of their flowering cycle, close to harvest. The Vividgro V2 lamps hung above the hedgerow platforms in parallel at a height of 2.16m. The room ceiling had a height of 2.57 m.

Optical Measurement

<u>Instrumentation</u>
Visible light measurements were taken using the Ocean Insight (Orlando, FL, USA) Flame-S spectroradiometer with a QP450-1-XSR fiber connecting a CC-3-UV-S cosine corrector optical inlet. The manufacturer provided a radiometric calibration performed using a DH-3P-CAL deuterium and tungsten halogen source traceable to the National Institute of Science and Technology. The calibration stated that the device wavelength uncertainty was <0.0001% and the irradiance measurement error ranged from 8.0% at 400nm to 2.8% at 700nm. The device was controlled by an in-house designed controller based on the Arduino Due platform allowing a technician to initiate an optical measurement with the push of a button (Chmielinski *et al.*, 2022). Irradiance measurements were recorded at integration times that resulted in 80% of pixel saturation at the peak wavelength. The optical inlet to the spectrometer was attached to a flexible arm that allowed precise control of the inlet position and orientation.

Measurement of emissions from an isolated lamp

Emissions from a single isolated lamp in the grow room were measured in order to verify the data contained in the manufacturer-provided Illuminating Engineering Society (IES) LM-79 report describing lamp emission intensity and angular distribution (BACL, 2015). The technician isolated a single lamp in plant row 21 near the center of the room using blackout curtains (Amazon Essentials, Seattle, WA), and the lid of an HDX 27 gallon storage tote. Spectroradiometric measurements were obtained as described in Appendix 2, section 2.c.v at a distance of 0.94 meters from the center of the lamp. All forty-eight lamps in the room remained active during these measurements.

Procedure for irradiance measurements in a grow room

Each optical measurement consisted of a positional and optical component. The laser distance meter was used to take horizontal and vertical positional measurements of the optical inlet at each measurement location.

On the first day of data collection, measurements were taken at heights slightly above (~1.66m from the floor), at the midpoint (~1.4m), and slightly below the plant canopy (~1.1m) in the aisles between plant platform '1' and the wall and between plant platforms '1' and '2' (). If the technician perceived a risk of contact between the optical inlet and vegetation, the height of the optical inlet was adjusted slightly ($\pm < 0.05$ m).

On the second day of data collection, the measurements were taken at heights of ~1.1 meter and ~1.66 meters in the aisles in between plant platforms labeled as '2', '3', '4', and '5' (Figure 1-C).
In the interest of time and to minimize crop disturbance, the technician decided to stop measurement about three fourths of the way down the aisles. Overall, a total of 57 measurements were collected at ~1.66 m, 25 measurements at ~1.4 m, and 78 measurements at ~1.1 m. Additionally, the technician took two sets of measurements directly below (n=7) and directly above (n=3) the plant canopy on plant platform '3' at heights of 0.87 and 1.81 meters, respectively.

Measurement of cannabis leaf transmittance and reflectance

Cannabis leaf transmittance and reflectance was measured on 20 cannabis leaves, as described in Appendix 3. These measurements were then used to calculate the absorptivity of the cannabis leaves in the visible wavelength range (400-700nm). The computed average adaxial absorptivity values were: red (600-700nm) 0.950, green (500-600nm) 0.937, and blue (400-500nm) 0.969, respectively.

Radiation Modelling

Vegetation radiative transfer models (VRTM) consist of methods to derive plant canopy optical properties from plant morphology and to characterize radiation propagation through those canopy representations (Goudriaan, 1977, 1988; Campbell and Norman, 2000; Xu and Wei, 2019). This project uses a VRTM based on an open-source backwards ray tracing simulation engine named the Radiance Lighting Simulation and Rendering System (*Radiance,* version 5.4) – an open-source lighting simulation software package (Ward, 1994) – to predict irradiance at selected locations in a single grow room at an indoor cannabis farm in Bellingham, WA.

Radiance uses backwards ray-tracing to solve an equation that outputs the radiance emitted, transmitted, or reflected at surfaces within a 3D space. The environment consists of a 3D space filled with 2D surface representations of real-world objects, called primitives, to which a user may assign optical properties. Simulations using *Radiance* generate rays from nodes in the 3D space (Ward and

Shakespeare, 1998). A node generates a user specified number of rays that propagate outward from the center of the node. Each node has an orientation and generates rays in that hemispherical direction with uneven hemispherical distribution. Peak ray generation density occurs close to the orientation of the node (Mardaljevic, 2011). The rays generated by the node do not interact with that node, other nodes, or other rays in the 3D space.

The model predicts irradiance in a 3D virtual representation of a real-world grow room. This 3D representation represents the geometry of real-world objects using the *Radiance* primitive named 'polygon' and the optical properties of the real-world objects using a variety of other 'material' primitives. The details of *Radiance* and VRTM structure may be found in Appendices 1 and 2, respectively.

Virtual Representation of Real World Grow Room

Geometric measurements of the grow room were used to define a virtual 3D space that contained representations for each lamp in the room (n = 48), polygons representing the walls, ceiling, and floor (n = 6), polygons representing HVAC components in the room (n = 18), polygons representing the hedgerows (n = 5304; 24 hedgerows x 221 primitives per hedgerow), and nodes that correspond to the real world measurement locations (Figure 1-D).

Lamps

The Vividgro V2 lamp manufacturer provides a LM-79 report that details both the lamp's emission' intensity and the angular profile. This data was translated into "light" and "brightdata" *Radiance* material primitives, characterizing the lamp emissions in the 3D space. The resulting red, green, and blue (RGB) emission intensities passed into the 'light' material primitive in W/m^2*sr are 74.06, 12.60, and 13.00. A two-dimensional table of angular adjustment factors and a lamp area correction were passed to the 'brightdata' material primitive. Appendix 2.c.v details the translation of the LM-79 report data to the RGB emission intensities and spatial adjustment factors.

Wall, Floor, and Object Reflectance

The polygons representing the walls, floor, and ceiling were assigned plastic material primitives with RGB diffuse reflectance values set to match those found in literature for the materials observed at the cannabis farm. Materials assigned to walls and ceiling received reflectance parameters matching that of conventional white paint, (Dornelles *et al.*, 2010a) and the material assigned to the floor received reflectance parameters matching that of 21 MPa concrete (Jin-Duk Lee *et al.*, 2012). The diffuse reflection values for the walls and ceiling were 0.95, 0.95, and 0.78 and for the floor were 0.36, 0.34, and 0.29 for the 600 to 700 nm, 500 to 600 nm, and 400 to 500 nm wavelength bands, respectively.

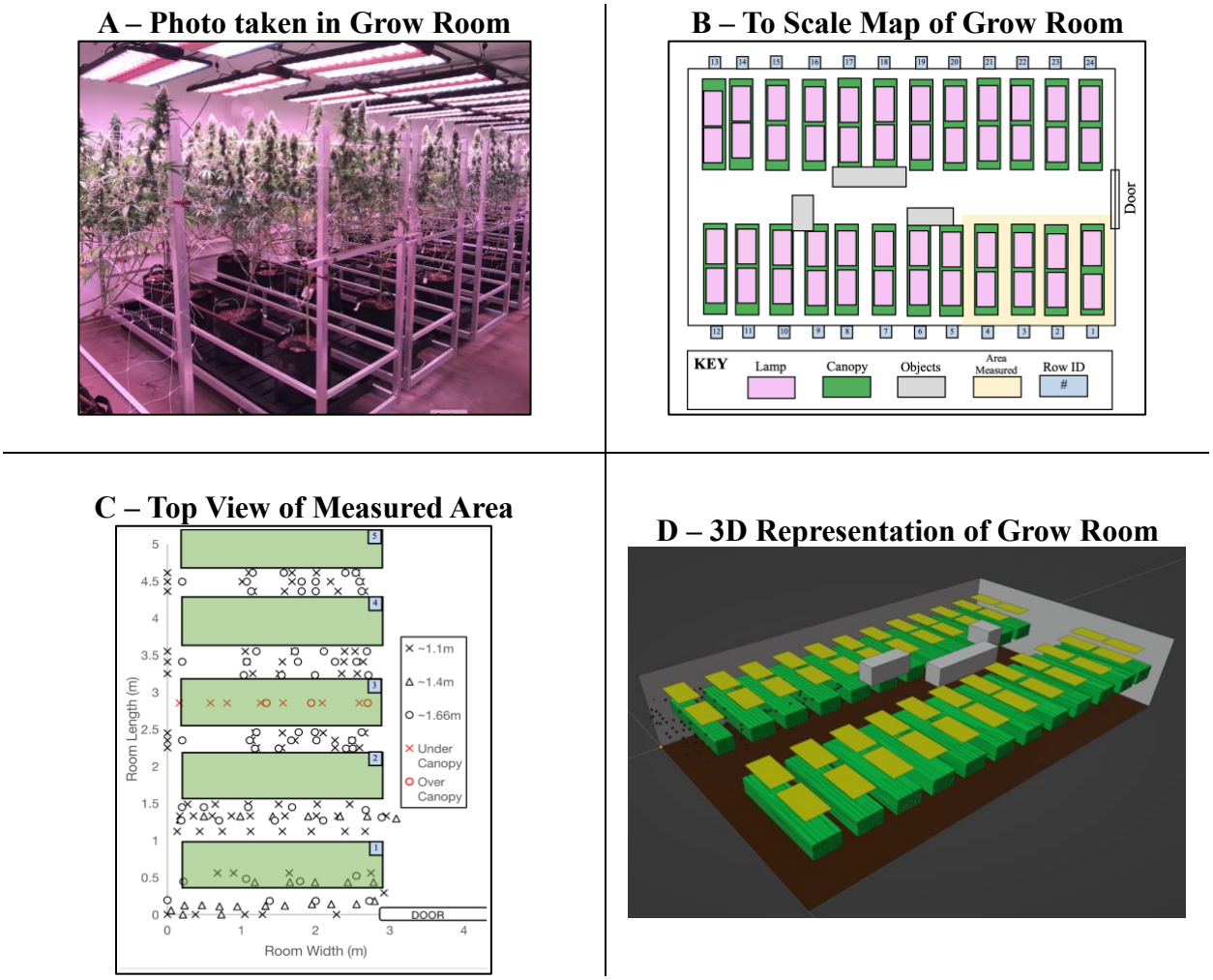

Figure 1 Various representations of the grow room including (A) a photograph taken in the room showing the wheeled rectangular hedgerow platforms and Vividgro V2 lamps hanging in parallel above,(B) a to scale top view of the grow room with "Objects" representing room HVAC and equipment,(C) a top view of the measured area in the grow room with measurement locations designated by marker symbols, (D) the virtual 3D space used for validation of the VTRM model with the 3D space consisting of the lamps (yellow), canopies (green), walls (grey), floor (brown), room objects (grey), and a ceiling (not visible) and the real-world locations of the spectroradiometric measurements represented as tiny black dots.

Optical properties of cannabis canopy

Leaf absorptivity, canopy leaf area index (L_I, the one-sided green leaf area per unit ground surface area), and two parameters related to the leaf area density (L_D, the ratio of the one-sided leaf area to a volume within the canopy) are needed to calculate optical extinction of the cannabis canopy. The two parameters related to L_D are the horizontal modifier u, and the fraction of canopy height at peak leaf density v. Since three of the four parameters could not be measured directly, the Nelder Mead algorithm implemented in python (Olsson and Nelson, 1975) was used to fit values for L_I, u and v. Appendix 2 provides further details on the four canopy parameters and Appendix 4 provides an overview of the of the Nelder Mead algorithm and fitting process.

Simulation implementation and statistical analysis

Python 3.10.3 (Python Software Foundation, 2023) provided the scripting environment for the VRTM. All executed *Radiance* simulations used the settings listed in Table 1-1 in Appendix 1. The algorithm ran for fifty iterations and the results section presents tabulations and summary statistics for the convergent parameter values and the resulting RMSE and R2 values. Heatmaps of the total irradiance measurements were generated using the 'autoKrige' function of the automap library to generate the 'geom_contour_filled' function of the ggplot2 library within R 4.1.3. (R Core Team, 2022)

Summary statistics were computed for the predictions at the same locations as that of the irradiance measurements. The relationship between the measured and predicted values was investigated using paired t-tests as well as linear regression. Summary statistics, t-tests, and linear regressions were run in Microsoft Excel for Mac (ver. 16.71) (Microsoft Corporation, 2023). Bubble plots were generated using R 4.1.3 to visualize the percent error between the measured and predicted values for locations below and above the canopy.

Results

Isolated Lamp Measurements

The lamp emissions generated from isolated lamp measurements were 96.1 (red), 13.85 (green), and 12.4 (blue) W/m^2*sr, respectively. The summation of the three wavelength bands yields a measured visible lamp emission of 122.3 W/m^2*sr.

Grow Room Measurements

Figure 2-A,B present heatmaps of the measurements taken under the canopy at a height of ~1.1 m and above the canopy at a height of ~1.66 m. Figure 2-C shows a bar chart of mean irradiance measurements in the grow room, grouped by measurement height and color coded by wavelength bound. Table 5-1 in Appendix 5 presents summary statistics of the irradiance measurements visualized in the referenced figures.

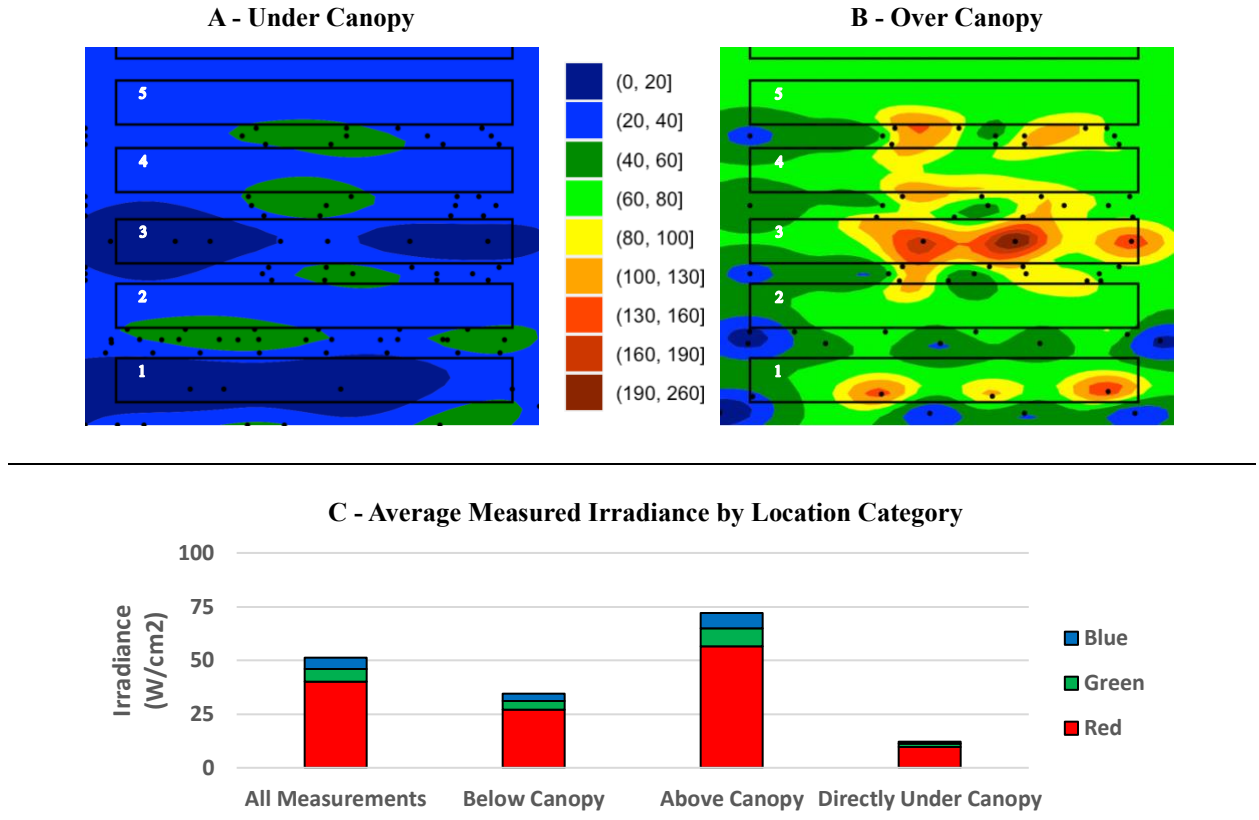

Figure 2 Visualizations of measured irradiance that include heatmaps of the irradiance measurements taken at heights (A) under the canopy and (B) above the canopy using a common scale in W/m^2 and (C) a bar chart of the averages of the irradiance measurements in W/m^2, grouped by spectral band and measurement height category.

The minimum, maximum, mean, and standard deviation of the above canopy measurements for all wavelength bands exceeded those generated from the measurements taken below the canopy by at least a factor of 2. Figure 2 presents heatmaps visualizing the irradiance distribution as constructed from measurements at heights below and above the canopy.

The heatmap constructed from measurements taken below the canopy indicates that measurements away from the center of an aisle between hedgerows have comparatively lower irradiance values than those taken in the aisle center. The second heatmap shows the inverse; the locations with the highest measurement values are those at the edge of the aisles or directly above each row of cannabis plants. The locations above hedgerow '3' are directly underneath the lamps.

Parameter Fitting

Table 1 presents values for the optical properties of the cannabis canopy fit by the fifty executions of the Nelder Mead algorithm (run on a VRTM that uses the lamps constructed from the manufacturer LM-79 report), together with R^2 and RSME values for the VRTM model fit.

The VRTM converged to the upper boundary for L_I 25 of 50 times, the upper boundary of the *v* modifier 37 times, the lower boundary of *v* a single time and the lower boundary of the *u* 11 times. The algorithm never converged to the lower boundary of L_I or the upper boundary of *u*. The minimum and maximum RMSE and R^2 differed by 4.85 and 0.003, respectively.

Table 1 Cannabis canopy parameters fit by Nelder Mead algorithm (run on a VRTM that uses the lamps constructed from the manufacturer LM-79 report), summary statistics for the RMSE and R^2 values from the runs, and the fit parameters corresponding to the VRTM with the lowest RMSE and the highest R^2

Parameter	L_I	Horizontal L_D Modifier (*u*)	Fraction of Height at Peak L_D (*v*)	RMSE (W/m^2)	R^2
Min	10.3	0.01	0.01	142.2	0.888
Max	15.0	6.10	1.00	147.1	0.892
Median	15.0	0.82	1.00	142.6	0.891
Mean	14.0	1.09	0.96	142.8	0.891
SD	1.57	1.15	0.15	0.8	0.001
Run with lowest RMSE	15.0	1.30	1.00	142.2	0.891
Run with best R^2	15.0	2.73	1.00	142.6	0.892

Irradiance Predictions

Table 5-2 in Appendix 5 presents summary statistics of the irradiance predictions, grouped by wavelength bound and by measurement height, for the predictions generated by the model run with the best RMSE.

Figure 3 presents scatter plots and linear regressions of the measurements vs predictions for the full visible light range as well as the RGB wavelength bands for the parameters associated with the model run that had the lowest RMSE.

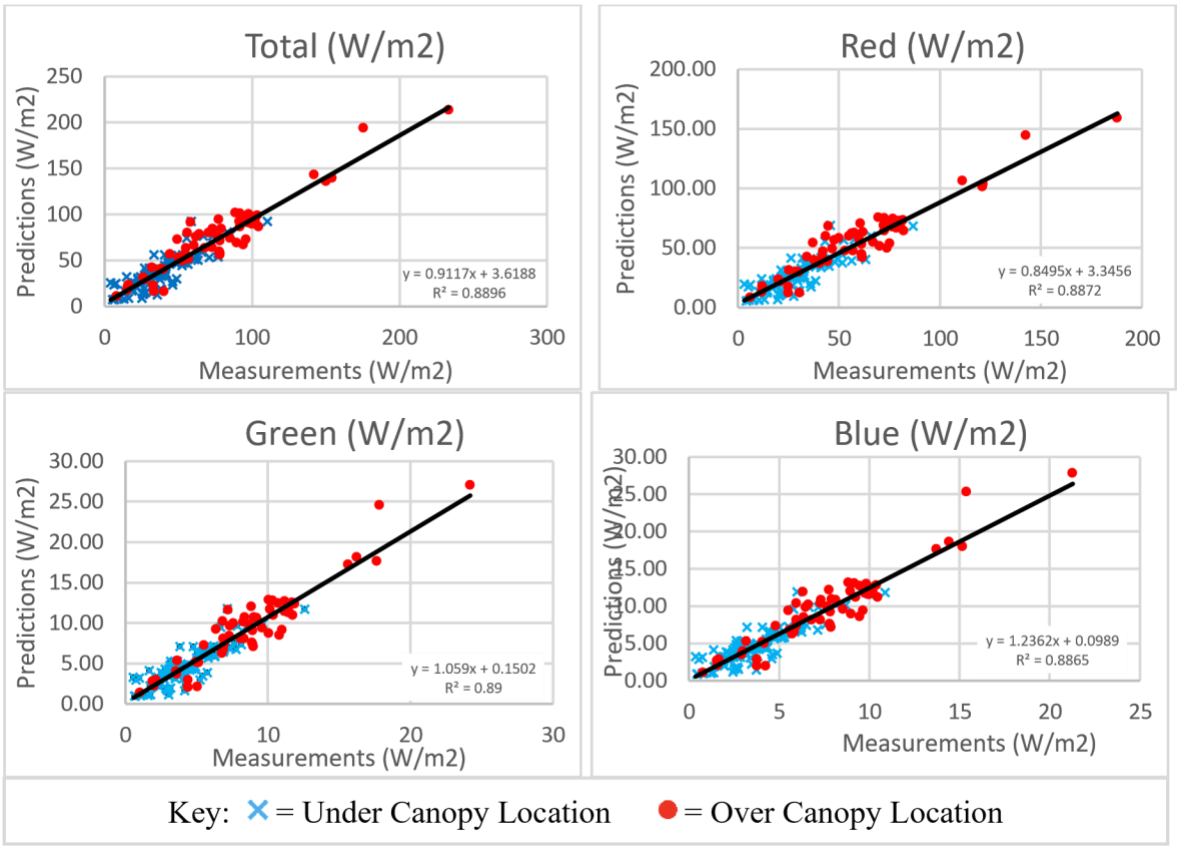

Figure 3 Scatterplots of the measurements vs predictions for the total, red, green, and blue wavelength bands. Each plot contains the results of a linear regression, and for each the top equation represents the linear fit for the locations under a height of 1.42 m, the middle equation represents the linear fit for the locations above 1.42 m, and the bottom equation represents the linear fit of all measurements.

The linear regressions show strong linear correlation between the measured and predicted values across all wavelength bands ($R^2 > 0.88$). The regression results show that the predictions underestimate the total and red irradiance and overestimate the green and blue irradiance. Figure 4 shows heatmaps and bubble plots of the predicted irradiances and percent error between the measured and predicted values.

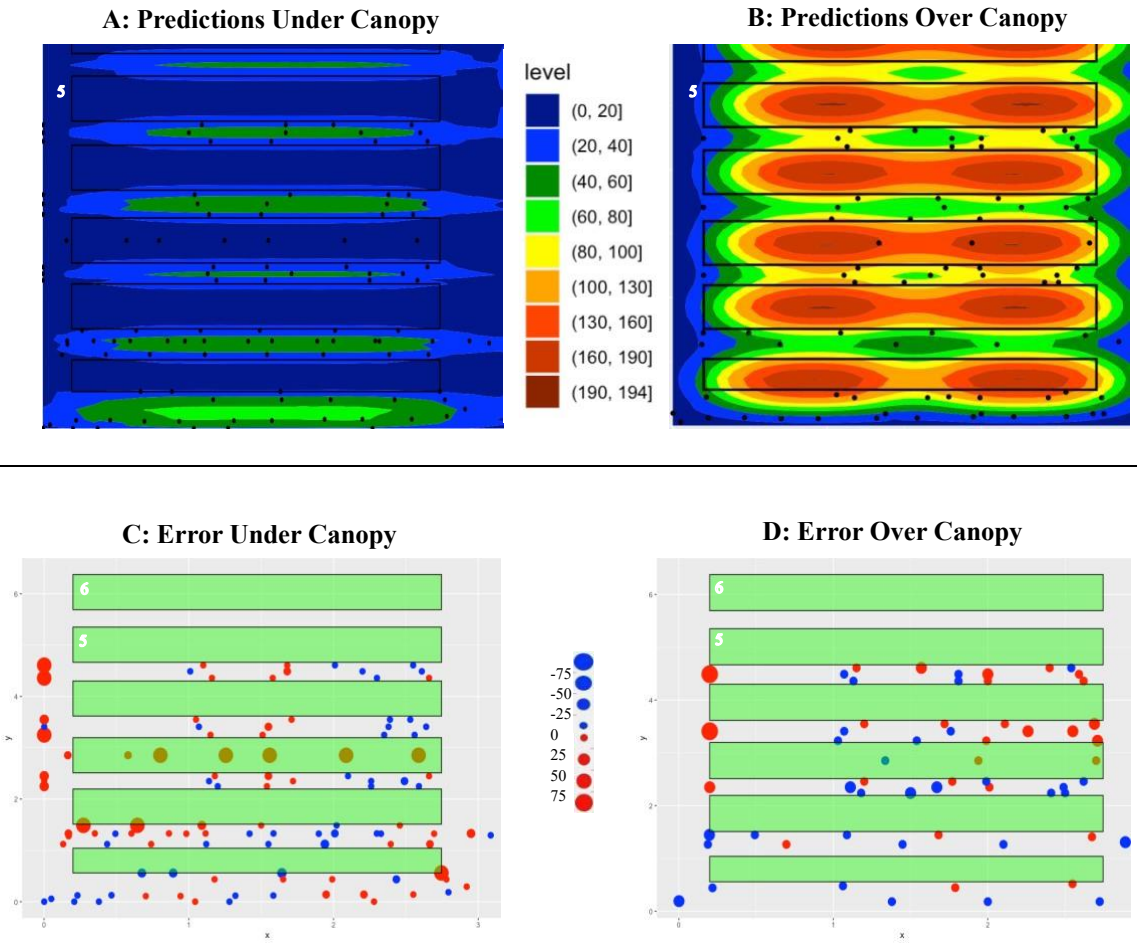

Figure 4 The top two graphics show simulation predictions at nodes set at 1.1 m (A) and 1.66m (B) using a common scale in W/m^2. The bottom graphics show bubble plots of the percent error between the measurements and model predictions. Bubbles colored blue show locations where the model has underestimated the measured value. Under canopy =1.1 m (C); Over Canopy = 1.66m (D)

The minimum and maximum percent error over all measurements was -84% to 185%. The mean of the percent error was 6.9% (sd = 38.18%).

Discussion

Isolated Lamp Measurements

The computed emission values for the isolated lamp differ from those listed in the LM-79 report by +29% in the red, +10% in the green, -5% in the blue, and +23% in the visible. The field team did encounter problems isolating a single lamp, as described in Appendix 2. It is possible that emissions from the surrounding lamps during measurement of emissions from the single isolated lamp may have resulted in overestimation of the measured emissions in the red and green bands for the isolated lamp. Emissions were only measured from a single lamp, and although all lamps in the room were the same make and model, research has shown that lamp aging can cause variable spectral degradation among identical lamps (Ke et al., 2018). Notably, and as discussed below, excellent R^2 values (>0.88) were

obtained between measured and predicted values of irradiance in the grow room for models using either lamp emissions based on the manufacturers LM-79 file, or models that used the measured emissions from the isolated lamp.

Room Irradiance Measurements and Modelling

The location with the largest measured irradiance was located directly under the lamp (233 W/m^2) at a height of 1.81 meters, while the measurement with the smallest measured irradiance was located slightly under the canopy (4.07 W/m^2) at a height of 1.07 meters. The mean irradiance of the measurements taken above the canopy is larger than those taken below the canopy. This is expected as measured irradiance should be greater when closer to the lamps.

The heatmaps of simulated irradiances (Figure 4) share some visual similarity with the heatmaps of measured irradiances (Figure 2). However, the measurement heatmaps contain visual discontinuities not seen in the prediction heatmap. These discontinuities probably result from spatial sparsity of measurement and use of kriging to interpolate irradiances in areas where measurements are sparse, especially in the areas proximal to left wall and hedgerows 2, 3, 4, and
5.

The large coefficient of variation (0.55) computed from the seven measurements taken directly under the canopy indicates that the canopy does not have a uniform leaf density distribution. This non-uniformity is likely a major source of error in the model agreement with the measurements below the canopy. The large coefficient of variation (0.53) computed from the measurements taken above the canopy probably results from measurement locations overlapping or not overlapping with a lamp's cone of illumination.

The results of the linear regressions show excellent agreement between the measured and predicted irradiance. The slope of the linear regressions for the total visible and red wavelength bands were 9% and 15% below unity, indicating underestimation, while the slope of the linear regressions for the green and blue wavelength bands were 6% and 23% above unity, indicating overestimation. Linear regressions of the under canopy and over canopy subsets returned slope values within 20% of the slope for all the data. A potential cause of this prediction error is the manufacturer LM-79 report underestimating lamp emissions in the red wavelength band while overestimating lamp emissions in the green and blue wavelength bands. Subsequent sections contain further discussion of the effect of discrepancies between the manufacturer data and the true lamp emissions.

Residual vs fitted plots of the linear regression models for total irradiance do not appear to show heteroscedasticity in the residual distribution for the under canopy, over canopy, and all data sets. This indicates that the equal variance assumption is likely satisfied for all three. All datapoints with residuals above 30 seem to display outlier behavior relative to the rest of the datapoints. Normal Q-Q plots of the three location classes show some minor tailing at the ends, indicating slight deviation from normality. The fitted model vs residual plots and the normal Q-Q plots are shown below as A and B.

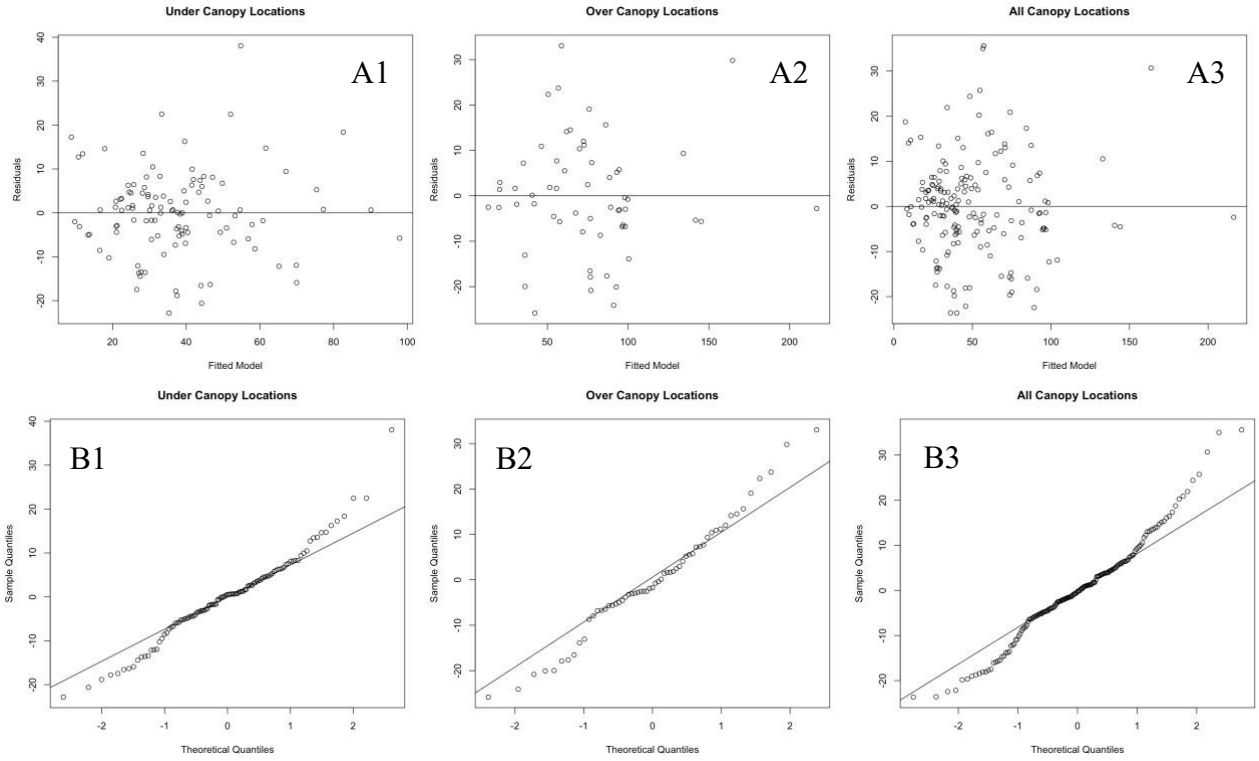

Figure 5 (A) Plots of the fitted model vs residuals for the under, over, and all locations. (B) Normal Q-Q plots of the three location classes show some minor tailing at the ends, indicating slight deviation from normality.

Due to the homoscedasticity in the residual distribution and the minor deviations from normality of the Q-Q plot, linear regression appears to be an appropriate method for the comparison between measured and predicted values.

Canopy Influence on Predictions

Model simulations both without the canopy included in the simulation, and with opaque canopies included in the simulation, to investigate the effect of canopy extinction on model fit. The no canopy simulation predictions greatly overestimated irradiance at locations below the plant canopy, resulting in poor linear regression fit ($R^2 < 0.2$). However, linear regressions using the predictions of the opaque canopy simulation had good agreement with the measurements ($R^2 > 0.87$). This performance is comparable to the base model, suggesting the real-world canopies have a large extinction effect on the lamp emissions. Appendix 5 (Figure 5-1, Figure 5-2) contains summary statistics, scatterplots and linear regression visualizations for both simulations.

Fitted Canopy Parameters

All algorithm runs converged to values of L_I above 10.2, and converged to the upper boundary of 15 for 25 of the 50 runs. An L_I value of 10.2 already describes a very thick canopy, and an L_I value of 15 is in the 99th percentile of the 2653 species reported in the Global Database of Fieldobserved Woody Tree

species (Lio and Ito, 2014). The distance between the convergent values and those published in literature casts doubt on the accuracy of the convergent L_I values.

The model runs converged to a *u* value of approximately 1.3, implying that leaf density decreases when moving away from the center of a canopy. The runs that converged to the boundary value of 0.01 had the worst RMSEs, implying that the horizontal L_D is not homogeneous throughout a canopy. This result is supported by the photo of the cannabis canopies presented in which illustrates higher leaf density towards the center of a cannabis canopy.

The runs converged to a value of *v* of 1, the top of the canopy. This suggests that the canopy thickness decreases as the position in the canopy gets lower. This result is somewhat supported by the photo of the canopies presented in Figure 1A, which shows canopies thinning out as the position in the canopy decreases. However, the same image shows the peak leaf area density occurring at a position below the top of the canopy, casting doubt on the accuracy of the fit value.

Taking measurements only outside the canopies likely limited the ability of the Nelder Mead algorithm to reliably fit the canopy parameters. The decision to restrict measurement to outside the canopy was intentional and motivated by preliminary attempts that resulted in the optical inlet becoming coated with plant resin. The coating necessitated immediate cleaning with disposable optical wipes, and the potentially equipment damaging experience underpinned the decision to avoid measurement of optical conditions inside the hedgerow itself. Notably, the observation that simulating canopies as fully opaque boxes yielded a model fit essentially identical to the model using fitted parameters describing the optical properties of the canopy L_I, *u* and *v* (Figure 3 vs Appendix Figure 5-2) demonstrates that the model is not especially sensitive to the values of L_I, *u* and *v*.

Effect of Wall and Floor Reflection on Irradiance Predictions

Four simulations were run to investigate the influence of wall and floor reflection on simulation predictions. The four simulations ran on 3D spaces that (1) had the walls set to 0% diffuse reflection, (2) had the walls set to 100% diffuse reflection, (3) had the floor set to 0% diffuse reflection, and (4) had the floor set to 100% diffuse reflection. Outside of the diffuse reflection change, all other 3D space properties matched that of the base model and the canopy parameters listed under best RMSE in Table 1. Linear regressions between the measurements vs predictions resulted in R^2 and slopes within 3% of those from the linear regressions shown in Figure 3, indicating that the wall and floor reflection have minimal effect on radiation transfer in the grow room. Table 5-3 in Appendix 5 presents these results.

Effect of Lamp Emissions on Irradiance Predictions

A simulation using lamp geometries assigned optical properties based on our direct measurement of emissions from a single isolated lamp and canopy parameters with the lowest RMSE listed in Table 1 resulted in an RMSE of 308. This RMSE value is approximately twice that of the base VRTM.

Linear regressions between the measurements and predictions returned slopes of 1.13, 1.12, 1.18, and 1.19 and R^2 values of 0.889, 0.886, 0.890, and 0.888 for the red, green, blue, and total visible wavelength bands, respectively (See Figure 5-3 in Appendix 5). These slopes are approximately 10-20% above unity for all four wavelength bands, suggesting the measured lamp emissions overestimate

the true lamp emissions. The slopes differ from the slopes listed in Figure 3 by +31%, +11%, -4%, and +24% respectively. These discrepancies are within ±2% of the discrepancies that compare the measured lamp emission values with the manufacturer provided data. The proportional discrepancies indicate that the lamp emission data has a direct and proportional effect on the irradiance predictions from the VRTM model, and are the likely cause of the model bias.

VRTM Applications to Worker Protection

Concerns related to worker health associated with exposure to lamp emitted UV underpin interest in using VRTMs to predict UV exposures. Although the current model was developed based on measurements of visible radiation, the underlying principles of the model are equally applicable to UV radiation. To extend this model to UV wavelengths, information on lamp emissions in the UV wavelength band would be required, together with information on cannabis leaf transmittance and reflectance in the UV band.

VRTM predictions can quickly identify existing work areas where the irradiance has an intensity sufficient to exceed a health criterion in a period shorter than that of a worker's scheduled shift in the area. The VRTM predictions provide a quantitative estimate of the degree of health criterion exceedance, and the combined awareness of location and severity can guide the implementation of administrative controls. The VRTM can be used as a prototyping environment to investigate the effectiveness of control strategies that eliminate, substitute, or otherwise barrier the optical hazard.

The current implementation of the VRTM is limited to predicting the irradiance in a work area, not estimating exposure directly. However, the VRTM's prediction capabilities may provide more accurate insights into irradiance received by workers than current dosimetry technologies allow. This is because currently available broadband dosimeters suffer from spectral mismatch when measuring radiance with a different spectrum than that of the dosimeter's calibration spectrum. Spectral mismatch can cause errors exceeding 1000%, especially in environments where multiple optical sources exist. VRTM predictions do not suffer from spectral mismatch error, provided manufacturer lamp emissions data is accurate and available.

Future research should investigate the use of VRTMs in the design of indoor farms to prevent hazardous optical conditions prior to construction and the viability of using static or dynamic 3D representations of workers as a surrogate of dosimetry monitoring.

Conclusion

The VRTM accurately predicted irradiances in the visible wavelength band in a grow room of an indoor cannabis farm using only manufacturer provided specifications for grow lamps, simple 3D representations of grow room objects and some information on the optical properties of those objects. Linear regressions between VRTM predictions and spectroradiometric measurements for the red, green, blue, and visible wavelength bands showed strong correlation ($R^2 > 0.89$). Model predictions were similar when using realistic optical properties of cannabis plants compared to treating cannabis hedgerows as opaque boxes. This finding implies that cannabis hedgerows are relatively dense and strongly attenuate radiation transfer in grow rooms. The canopy density may come as a consequence of legislation in Washington State that regulates cannabis farms based on the 2-dimensional surface area

of the plant canopy, which encourages a high density of cannabis plants to maximize production of cannabis flower.

Further research is needed to validate if the VRTM accuracy can be replicated in other indoor grow rooms and ones with thinner vegetation. The model was shown to be robust to changes in wall and floor reflectance, which indicates that wall and floor reflectance did not substantially influence radiative transfer within the room.

The use of a VRTM has several advantages over use of optical measurement devices in the context of indoor farm exposure characterization. An open-source simulation engine costs much less than the purchase, calibration, and maintenance costs of an appropriate measurement device. Use of a VRTM requires far less crop disturbance than optical measurements, and can predict irradiance at every location in the grow room in a relatively short period of time. Meanwhile, optical measurement of a small grow room with comparable spatial resolution to that of the VRTM capability will likely take days. Finally, VTRM predictions can be used to efficiently optimize design of a grow room before it is built to ensure optimal irradiance for plant growth while avoiding levels of irradiance that would be hazardous to workers in the facility.

Acknowledgements

This work was supported by the National Institute of Occupational Safety and Health (5 T42 OH008433) and by the National Institute of Environmental Health Sciences (P30ES007033). We would additionally like to thank the cannabis business owners for providing access to their facilities. The content is solely the responsibility of the authors and does not necessarily represent the official views of the United States Centers for Disease Control or the National Institutes of Health.

Appendix 1: Radiance 5.4 Lighting Simulation Engine

The *Radiance* simulation engine takes input files for geometry, materials, and the settings of the simulation. The geometry and material files have a file format called a '.rad' and settings of the simulation in a text format '.txt' or a windows command '.bat' batch file (Ward, 1994). Figure 11 presents a visualization of the system process flow.

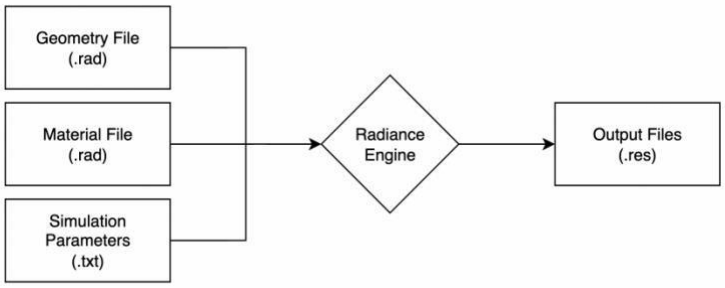

Figure 1-1 A flow chart of the Radiance engine system execution inputs and outputs.

A .rad file comprises of a list of data structures called primitives. Primitives act as the building blocks of any simulation and can represent surfaces, materials, patterns, or textures. Using multiple primitives allows the description of a real-world object in a scene, and the act of linking two primitives together is called the assignment of one primitive to another (Ward, 1994).

A surface primitive represents the location and dimension of an object's geometry. This project uses a surface primitive called the 'polygon', which represents a 2D surface in a 3D space. This primitive has a data structure consisting of a n by 3 matrix containing the x,y,z location of the vertices of the polygon. When the engine generates a polygon, the matrix row order determines the order of polygon vertex construction. The order of vertex construction determines the orientation of the polygon, with the front located according to the 'right-hand' rule in the order of vertex construction.

Assignment of a material primitive to a surface primitive describes how that surface will interact with a ray upon contact. Pattern assignment to material primitives causes deviations in material optical homogeneity. Texture assignment to surface primitives cause geometric perturbations in the surface smoothness (Ward, 1994).

(A) 1.a. Simulation Method

Simulations using *Radiance* generate rays from designated locations in the 3D space, called either nodes or pixels, depending on the simulation output. If the simulation output is irradiance at those locations, the small surfaces are called nodes. If the simulation output is the creation of a realistic rendered image, the small surfaces are called pixels, and the pixel layout usually takes the form of a grid with equidistant spacing. This project utilizes test surfaces consisting of nodes (Ward and Shakespeare, 1998).

A node generates a user-specified number of rays that propagate outward from the center of the node. Each node has an orientation and generates rays in that hemispherical direction with uneven hemispherical distribution. Peak ray generation density occurs close to the orientation of the node

(Mardaljevic, 2011). The rays generated by the node do not interact with that node, other nodes, or other rays in the 3D space.

When a newly generated ray intersects with a 2D surface in the 3D space, the engine forms a 'surface point' on the 2D surface. This surface point generates an additional user-specified number of rays that further propagate in the scene.

Figure 1-2 presents a visualization of a simple 3D space with a surface and a node. The solid line represents a ray originating at the node, and the lines with arrows represent the rays emitted by a newly created surface point.

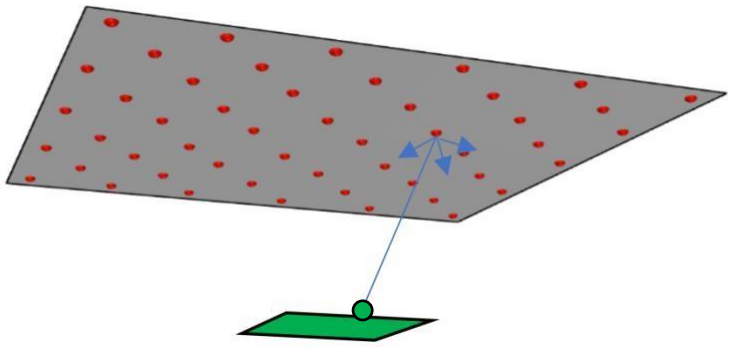

Figure 1-2 A simple 3D space with green point representing a node and an additional gray surface representing a ceiling. The node emits several rays, one of which is visualized as a blue line. Upon contact with the gray surface, the engine forms a surface point, visualized as red spheres. These points subsequently emit a user defined number of rays into the 3D space.

Upon the creation of a surface point, *Radiance* solves for the energy present at that surface point via the following equation:

$$E_{Surface\ point} = E_e(\theta_g, \phi_g) + \int_0^{2\pi} \int_0^{\pi/2} E_i(\theta_i, \phi_i)\, \rho(\theta_i, \phi_i, \theta_g, \phi_g) cos\theta_i sin\theta_i d\theta_i\, d\phi_i$$

Equation 1

Where:
$E_e(\theta_g, \phi_g)$ = the radiation emitted from the surface point
$E_i(\theta_i, \phi_i)$ = the incident radiance on the surface point
$\rho(\theta_i, \phi_i, \theta_g, \phi_g)$ = the bidirectional reflectance and transmittance distribution function
θ_i = the polar angle of incident radiation measured from the surface normal
ϕ_i = the azimuthal angle of incident radiation measured from the surface normal
θ_g = the polar angle for emitted radiation measured from the surface normal
ϕ_g = the azimuthal angle for emitted radiation measured about the surface normal

A simulation consists of solving Equation 1 at all surface points in a scene (Ward, 1994).

(A) 1.a.i. Color Weighting

Radiance uses a 3-wavelength band red, green, blue (RGB) structure to characterize the distribution of spectrum power (W/m^2). The red band contains the power between 600-700nm, green band contains the power between 500-600nm, and blue band contains the power between 400-500nm.

(A) 1.a.ii. Ray Interaction with Objects

When a ray contacts a surface without an assigned material primitive, the ray passes through the surface primitive as if it did not exist. Assignment of the material primitive to the surface primitive causes the surface to interact with the ray at the newly created surface point. This project uses the simulation engine to simulate three interactions: surface reflectance, surface transmittance, and volume extinction.

(A) 1.a.iii. Surface Reflectance and Transmittance

The simulation engine represents the total reflected and transmitted energy at a surface point as the sum of the specular (mirror) and diffuse (scattered) reflectance or transmittance.

(A) 1.a.iv. Diffuse Reflectance

The engine simulates diffuse reflectance by generating several new rays (controlled by the ambient divisions simulation parameter, see Table 1-1) at the surface point that propagate outward with peak generation density occurring close to the normal of the primitive's surface (Mardaljevic, 2011). The engine calculates the proportion of reflected energy for each of the newly generated rays according to a Lambertian relationship for each of the three-color wavelength bands:

$$\varepsilon_{vf,i}(\theta) = \rho_{d,i} * \cos(\theta)$$
$$for\ i = red, green, blue$$

Equation 2

Where $_{vf,i}$ is the proportion of red, green, or blue energy reflected along the new ray, θ is the angle between the incident and the new ray, and $\rho_{d,i}$ is the user defined red, green, or blue diffuse reflectance parameter of the material primitive (Ward, 2004).

(A) 1.a.v. Diffuse Transmittance

The engine treats diffuse transmittance similarly to diffuse reflectance, with the same generation of a user-controlled number of new rays at the surface point. These rays propagate outward with peak generation density occurring close to the normal of the node surface, except in the direction opposite that of reflectance. The engine calculates the proportion of transmitted energy for each of the newly generated ray according to a Lambertian relationship for each of the three-color wavelength band:

$$\varepsilon_{vf,i}(\theta) = \tau_{d,i} * cos(\theta)$$
$$for\ i = red, green, blue$$

Equation 3

Where $\varepsilon_{vf,i}$ is the proportion of red, green, or blue energy transmitted along the newly generated ray, θ is the angle between the incident and the new ray, and $\tau_{d,i}$ is the user defined red, green, or blue diffuse transmittance parameter of the material primitive (Ward, 2004).

(A) 1.a.vi. Specular Reflectance

The engine simulates specular reflectance by generating a single ray at the mirror angle to the incident ray and assigning that ray three values representing the proportion of red, green, and blue energy reflected according to the following equation:

$$_{vf,i} = \rho_{d,i} * (1 - \rho_s)$$
$$for\ i = red, green, blue$$

Equation 4

Where $_{vf,i}$ is the proportion of red, green, or blue energy reflected along the new ray, $\rho_{d,i}$ is the user defined red, green, or blue diffuse reflectance parameter of the material primitive, and ρ_s is the user defined specular reflectance factor of the material (Ward, 2004).

(A) 1.a.vii. Specular Transmittance

The engine simulates specular transmittance by generating a single ray in the direction of the incident ray. It then assigns the newly generated ray three values representing the proportion of red, green, and blue energy reflected according to the following equation:

$$v_{f,i} = \tau_{d,i} * (1 - \tau_s)$$
$$for\ i = red, green, blue$$

Equation 5

Where $v_{f,i}$ is the proportion of red, green, or blue energy reflected along the new ray, $\tau_{d,i}$ is the user defined red, green, or blue diffuse transmittance parameter of the material primitive, and τ_s is the user defined specular transmittance factor of the material (Ward, 2004).

(A) 1.a.viii. Reflectance Roughness Parameter

Many material primitives allow the user to input a roughness scalar parameter. This parameter simulates the root mean square slope of surface facets, with a value of 0 corresponding to a perfectly smooth surface, and a value of 1 corresponding to very rough surface. This project uses a zero value for the roughness parameter, causing no deviation in the behavior of specular and diffuse reflectance as discussed in the preceding sections.

(A) 1.a.ix. Volume Extinction

The *Radiance* engine does not have a primitive that represents a volume in the 3D space. Instead, the engine computes volume extinction through the assignment of the material primitive called 'mist.' Assignment of this material requires creating an enclosed geometry consisting of polygon primitives and assigning the same mist primitive multiple times to each of the enclosing surfaces. A 'mist' primitive represents optical extinction as red, green, and blue scalar values in units of 1/meters (n = 3), representing a constant proportional loss of energy over one meter (Ward and Shakespeare, 1998).

The engine performs the computation of extinction at points on the pseudo-boundaries of the volume. A pseudo-boundary point refers to a point along a ray where it either (1) intersects one of the surfaces forming the boundary of the volume assigned the 'mist' primitive, (2) intersects with the boundary of a separate volume assigned a 'mist' primitive, or (3) contacts an optical surface within the volume assigned a 'mist' primitive. The engine uses the following formula to compute volume extinction through the 'mist' primitive:

$$I_F = I_I e^{-kd}$$

Equation 6

Where I_F is the final energy after computation of volume extinction, I_I is the initial energy prior to volume interaction, k is the volume extinction coefficient, and d is the distance traveled within the medium.

(A) 1.a.x. Simulation Parameters

Radiance allows adjustment of eighteen parameters that impact the simulation runtime and the accuracy of the simulation results (Ward and Shakespeare, 1998). A sensitivity analysis conducted by Dubois (2001) showed that of these 18 parameters, ambient bounces, ambient division, ambient super-sampling, ambient accuracy, and ambient resolution have the largest impact on irradiance accuracy.

We have opted to use simulation parameters that match or exceed the values published by several studies that previously explored the influence of simulation parameter setting on simulation accuracy (Dubois, 2001; Li, Lau and Lam, 2004; Ruppertsberg and Bloj, 2006; Erlendsson, 2014) Simulations using these parameters almost universally generated irradiance predictions with errors under 10% compared to measured values. Table 1-1 presents these initial simulation parameters alongside recommended parameter value 'bundles' published by the *Radiance* user manual.

Table 1-1 The VRTM simulation parameter settings used in the current study, alongside the recommended parameter value 'bundles' published by the Radiance user manual.

Parameter	***Radiance* Recommended "Bundles"**				**VRTM**
	Min	**Fast**	**Accurate**	**Max**	
ambient accuracy	0.5	0.2	0.15	0	0.1
ambient bounces	0	0	2	8	6
ambient divisions	0	32	512	4096	4096
ambient resolution	8	32	128	0	128
ambient super-samples	0	32	256	1024	1024
anti-aliasing jitter	0	0.6	0.9	1	0.9
direct certainty	0	0.25	0.5	1	0.75
direct pretest density	32	64	512	0	512
direct relays	0	1	3	6	3
direct thresholding	1	0.5	0.05	0	0.15
limit reflectance	0	4	8	16	8
limit weight	0.05	0.01	0.002	0	0.005
pixel sampling rate	16	8	4	1	1
sampling threshold	1	0.15	0.05	0	0.05
source jitter	0	0	0.7	1	0.7
source sub structuring	0	0.5	0.15	0.02	0.05
specular jitter	0	0.3	0.7	1	1
specular threshold	1	0.85	0.15	0	0.15

Ward (1997) provides descriptions of all parameters listed in Table 1-1 in the documentation for a *Radiance* sub-program named 'rtrace', available online as of April 1st, 2023.

Appendix 2: Vegetative Radiative Transfer Model (VRTM)

(A) 2.a. Overview

This project implements a VRTM that predicts irradiance in a grow room from a real-world cannabis farm located in Bellingham, Washington. The VRTM takes inputs representing the 3D geometry of the grow room and contains geometric representations of real-world objects within the room and the optical properties of those objects. The VRTM outputs RGB irradiance in W/m^2 at nodes located at the user's discretion.

As described in the previous section, the VRTM consists of three general steps: (1) creation of virtual representations of real-world objects, (2) assignment of optical properties to these virtual objects, and (3) running the simulation engine. The first two general steps consist of several subprocesses which convert real-world dimensional and optical properties to simulation engine primitives.

Some sub-processes depend on parameters that we do not have the capability to directly measure in the real-world. These parameters are the leaf area index (L_I, the one-sided green leaf area per unit ground surface area), and two parameters related to the leaf area density (L_D, the ratio of the one-sided leaf area to the canopy volume). These parameters are a horizontal L_D modifier u, and a fraction of height at peak leaf density v. To circumvent this issue, we use the Nelder Mead Simplex optimization algorithm to fit the unmeasurable parameters using the root mean squared error computed from predicted and measured irradiance in a real world grow farm. Figure 2-1 presents a flowchart of the VRTM process flow, and Table 2-1 describes the input variables for the VRTM.

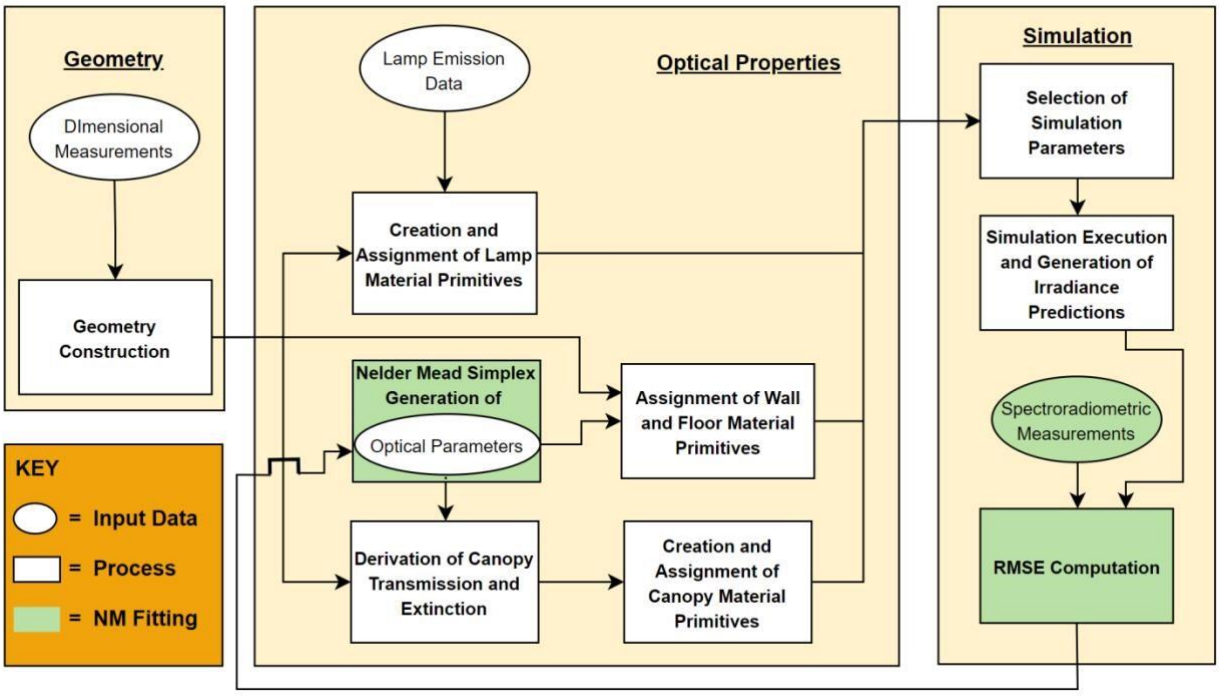

Figure 2-1 The VRTM consists of three general steps: creating virtual objects from real-world measurements, assigning optical properties to those virtual objects, and running a Radiance simulation. The items with green shading show the implementation of a Nelder Mead Simplex algorithm for fitting parameters that we do not have the capability to directly measure.

Table 2-1 A list and description of all inputs to the VRTM.

Input	Contents	Input Format	NM Fitted	Description
3D Space	Multiple *Radiance* 'polygon' primitives together forming virtual objects	File type: .rad	No	A file that contains a virtual representation of the x, y, z locations and dimensions of cannabis hedgerows, lamps, floor, ceiling, walls, and the work area in a cannabis farm
Lamp Emissions	A 'light' primitive containing three values for RGB emission intensity and a 'brightdata' primitive that contains a 2D matrix of angles and emission intensity factors.	File type: .rad	No	Two inputs that together represent a lamp's emission intensity and angular distribution.
Canopy Leaf Absorptivity	Three scalar values representing leaf RGB absorptivity	Float	No	The VRTM uses each canopy's dimensions, L_I, leaf angle parameter, and leaf absorptivity to construct a 'mist' primitive to represent canopy absorption and a 'BRTDfunc' primitive to represent canopy reflectance.
Canopy (L_I)	Scalar value for leaf area index for canopies	Float	Yes	
Horizontal L_D modifier (u)	Scalar value that flattens or steepens the horizontal L_D	Float	Yes	
Fraction of height at peak L_D (v)	The fraction of the canopy height where the vertical L_D reaches its maximum	Float	Yes	

(A) 2.b. Geometry

(A) 2.b.i. Virtual Canopy

A number of previous studies performing vegetative radiative transfer modeling have represented plant canopies as simple geometric shapes with either homogenous or heterogenous optical properties (Jackson and Palmer, 1972; Mann *et al.*, 1980; Cohen and Fuchs, 1987; Gijzen and Goudriaan, 1989; Kim and Lieth, 2002; Annandale *et al.*, 2004; Oyarzun, Stöckle and Whiting, 2007; Pieri, 2010; Colaizzi, Evett, *et al.*, 2012; Colaizzi, Schwartz, *et al.*, 2012; Parry *et al.*, 2019). This project represents the canopy as a simple cubic object divided into 36 segments, with the divisions within the cube allowing the representation of a heterogenous volume extinction within the canopy.

Radiance 'polygon' primitives form the building blocks of the cannabis hedgerow. The dimensions of the hedgerow object match the real-world measurements of the top, bottom, and sides of a hedgerow. Six rows of six identical rectangular columns form the inside of each hedgerow. Each of the thirty-six rectangular columns comprises of six polygon primitives. Finally, five polygon primitives encapsulate the internal columns. Each segment receives the assignment of a different 'mist' primitive with RGB

extinction parameters dependent on the L_D at that location. Figure 2-2 visualizes the cannabis hedgerow geometry.

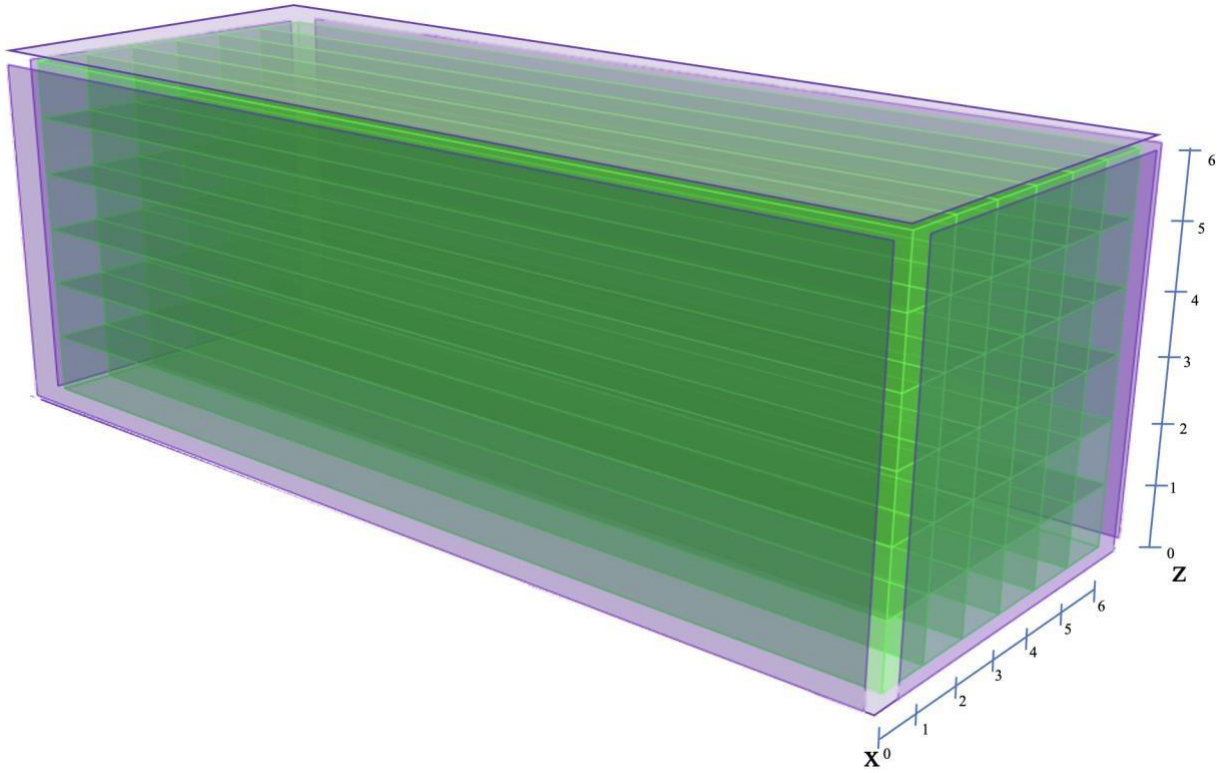

Figure 2-2 The hedgerow comprises of six polygons that span the top and sides of the hedgerow (purple surfaces) and 36 rectangular columns (green surfaces). Note, the purple surfaces appear offset from the green surfaces for illustration purposes only. During simulation, these surfaces overlap.

(A) 2.b.ii. Virtual Lamps, walls, floors, and ceiling

The 3D space represents the geometry of a real-world lamp using a single 2D polygon primitive. The size of the polygon surface matches the horizontal dimensions of each LED array. The 3D space represents location and dimensions of real-world walls, floors, and ceilings using the 'polygon' surface primitive.

(A) 2.c. Object Optical Properties

The VRTM derives canopy reflectance and extinction using methods published by Campbell et al. (2000), Xu and Wei (2019), and Goudriann et al. (1988). The VRTM uses nine parameters to derive canopy reflectance and extinction. These parameters are the hedgerow dimensions (length, width, and height), the leaf red, green, and blue absorptivity, the leaf area index (L_I), and two parameters related to L_D (*u,* and *v)*.

(A) 2.c.i. Leaf Absorptivity

Leaf absorptivity is the fraction of the incident irradiance absorbed by a leaf. We measured the reflectance and transmittance of twenty cannabis leaves, then calculated the average leaf

absorptivity (procedure and calculations described in Appendix 3). The calculated absorptivity values used in the VRTM, using the adaxial reflectance measurements, were 0.950, 0.937, and 0.969 in the red, green, and blue wavelength bands.

(A) 2.c.ii. Leaf Angle Distribution (*s*)

The *s* conceptualizes the angular distribution of the leaves as if one moves, without rotation, a canopy's leaves from their original position to the surface of an ellipsoidal of variable height ratio. This ratio, represented as *s* in subsequent equations, is the quotient of the ellipsoidal width to height, equivalently described as the vertical to horizontal projections of leaf angles in a canopy. Figure 2-3 provides a visualization for two canopies, one with a vertically skewed *s* and one with a spherical *s*.

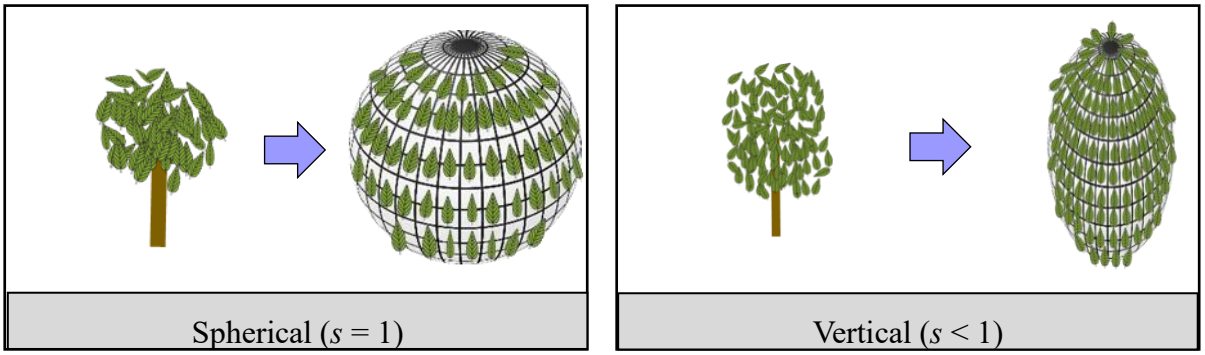

Figure 2-3 A simple visualization for two canopies, one having a spherical s (left) and one having a vertically skewed s (right). Within each box, the left graphic presents leaves randomly distributed representing how one would find them on a canopy and the right graphic presents translated (unrotated and same size) leaves moved to the surface of an ellipsoid.

The *s* parameter allows computation of K, the proportion of the leaf projected area (shadow area cast on a surface normal to the light ray) to the hemispherical surface area of the ellipsoid. Campbell et al. (1990) refers to this proportion as the canopy extinction coefficient, and presents the following equation for computation:

$$K\,(s,\psi) = \frac{\sqrt{s^2+sin^2(\psi)}}{s+1.774(s+1.182)^{-0.733}}$$

Equation 7

In the equation above, Ψ is the angle of the incoming radiation measured from the angle of the canopy normal.

No existing literature published measured values of *s* for cannabis. In the absence of existing estimates of *s*, studies commonly assume a spherical leaf angle distribution (*s* = 1) (Zou *et al.*, 2014). The only identified work modeling cannabis canopy optical properties assumed a spherical leaf angle density (Daughtry and Walthall, 1998), and this project does the same.

(A) 2.c.iii. Canopy Extinction

As described previously, *Radiance* characterizes volume extinction through assignment of the material primitive called 'mist.' We assigned a unique mist material to each of the volumes of the

thirty-six rectangular columns in a canopy (Figure 2-2). Each 'mist' primitive consists of a scalar red, green, and blue extinction value derived by equating the conditions on the left and right of the Figure 2-4 visualization.

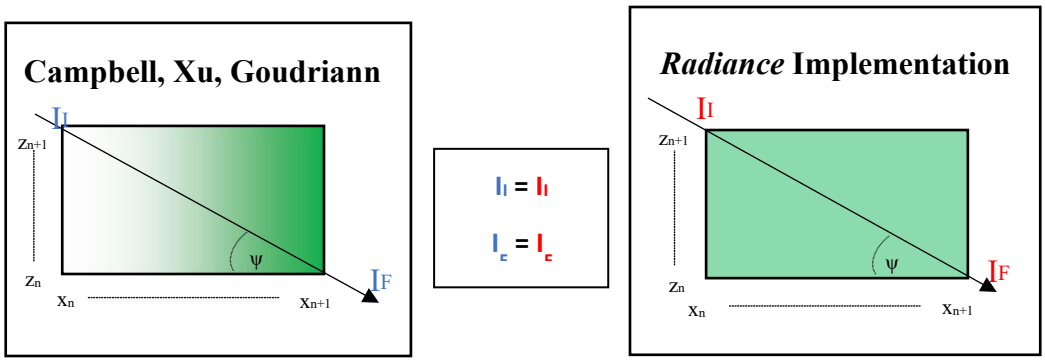

Figure 2-4 The left figure illustrates the extinction coefficient gradient computed using the methods fully described by the Campbell et al. (2000). *The right figure illustrates the uniform extinction implemented by the 'mist' primitive. The equality of* I_F *between the figures governs the computation of the scalar values passed to the 'mist' primitive.*

The left and right boxes of Figure 2-4 visualize the left and right side the following equation:

Campbell, Xu, Goudriann		***Radiance***
$t_i = exp(-\sqrt{\alpha_i} * K(\psi) * L_D(L_I, x_n, x_{n+1}, z_n, z_{n+1}, u, v))$	=	$exp(-k_i * d)$

$$n = 0, 1, 2, \ldots, 6$$
$$i = red, green, and\ blue$$
$$tan(\psi) = (z_{n+1} - z_n) / (x_{n+1} - x_n)$$

Equation 8

Where t_i is the proportion of incident energy transmitted, k_i is the 'mist' primitive optical extinction for the red, green, or blue color wavelength band, α_i is the red, green or blue leaf absorptivity, K is the ratio of the projected leaf angle area to the hemispherical surface area of the spheroid, ψ is the angle between the cube diagonal and horizontal, $L_D(L_I, x_n, x_{n+1}, z_n, z_{n+1})$ is the L_D traversed by the ray, x_n and x_{n+1} are the horizontal positions of the rectangular column, z_n and z_{n+1} are the vertical positions of the column, u is the horizontal L_D modifier, v is the height of the peak vertical leaf area density, and d is the length of the cross-sectional diagonal of a single rectangular column.

Each of the thirty-six rectangular columns has the same diagonal length but a distinct value for L_D, computed according to the following equation:

$$L_D(L_I, x_n, x_{n+1}, z_n, z_{n+1}, u, v) = \int_{x_n}^{x_{n+1}} L_{DH}(L_I, x, u)dx + \int_{z_n}^{z_{n+1}} L_{DV}(L_I, z, v)dz$$
$$for\ n = 0, 1, 2, \ldots, 6$$

Equation 9

Where $L_{DH}(L_I, x, u)$ is the horizontal L_D function:

$$L_{DH}(L_I, x) = L_I * \frac{\pi}{2W} * \sin\left(\frac{x\pi}{W}\right)^u$$

Equation 10

Where W is the width of the hedgerow, x is the horizontal position defined from [0,W], and *u* is the horizontal density distribution modifier defined from [0,1].

$L_{DV}(L_I, z, v)$ is the function describing the vertical L_D:

$$L_{DV}(L_I, z) = \frac{L_I * \left(\frac{H}{v/H}\right)^2 * \left({}^{z}/_{H}\right)^2}{{}^{1}/_{2} * \sqrt{{}^{1}/_{2} * \sqrt{\frac{\pi}{\left(\frac{H}{v/H}\right)^2}} * \operatorname{erf}\left(\sqrt{\left(\frac{H}{v/H}\right)^2}\right) - e^{-\left(\frac{H}{v/H}\right)^2}}} * e^{-\left(\frac{H}{v/H}\right)^2 * \left(\frac{z}{v/H}\right)^2}$$

Equation 11

Where H is the height of the canopy, *v* is the proportion of the total height at which the vertical density reaches its maximum, z is the vertical position defined from the bottom of the hedgerow to the top of the hedgerow, and 'erf' is a Gauss error function. Note, the lower bound of z may not be equal to zero. The relationships presented by Equation 10 and Equation 11 are visualized in Figure 2-5 for a hypothetical canopy with a L_I of 8, a width of 0.5 m, a height of 0.9 m, a height at which the vertical density reaches its maximum at 0.5 m, and the canopy starting at a height of zero.

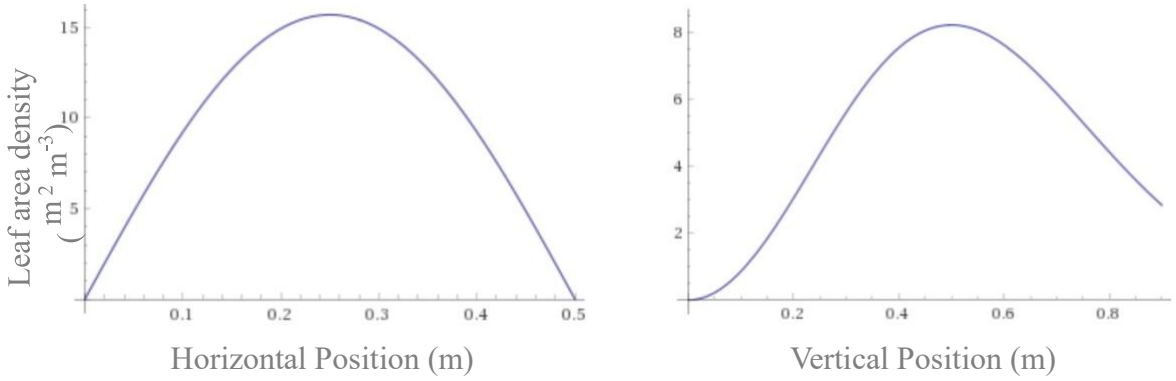

Figure 2-5 The L_D vs the horizontal (left) and vertical (right) position.

By solving Equation 8 for the mist extinction parameter, the equation becomes:

$$\frac{\sqrt{\alpha_i} * K(\psi) * L_D(L_I, x_n, x_{n+1}, z_n, z_{n+1}, u, v)}{d} = k_i$$

$$n = 0, 1, 2, \ldots., 6$$
$$i = red, green, and\ blue$$

Equation 12

Figure 2-6 provides a visual representation of the green extinction values computed for each of the 36 canopy segments. The canopy has a height of 1.66m and width of 1.18m, a L_I of 14.6, a horizontal L_D distribution modifier of 0.48, a vertical leaf distribution modifier of 0.92, and RGB leaf optical absorptivity values of 0.950, 0.937, 0.969 respectively. The leaf optical absorptivity values were computed using the measured adaxial reflectance values computed as shown in Section (A) 3.d

19.10	23.66	25.46	25.46	23.66	19.10
18.20	22.76	24.56	24.56	22.76	18.20
15.69	20.25	22.06	22.06	20.25	15.69
12.21	16.77	18.57	18.57	16.77	12.21
8.84	13.40	15.21	15.21	13.40	8.84
6.78	11.34	13.15	13.15	11.34	6.78

Figure 2-6 Green extinction coefficients (unitless) for each of the 36 cubes within a canopy, as if a ray had taken the path along the diagonal of each cube.

(A) 2.c.iv. Canopy Reflectance

The six polygon primitives illustrated as the purple surfaces in Figure 2-4 facilitate hedgerow reflectance through the construction and assignment of the BRTDfunc material primitive. A polygon assigned the BRTDfunc material primitive differentially interacts with an incident ray depending on whether the ray initially contacts the front or back of the polygon primitive. The VRTM treats the front of the polygon surface as the side facing away from the canopy volume.

The VRTM constructs the BRTDfunc by setting the values for front and rear RGB diffuse reflectance (n = 6), and front and rear RGB specular transmittance (n = 6).

The VRTM sets the value of the front RGB diffuse reflectance to represent the reflectance of a canopy as computed below:

$$\rho_i = \frac{1 - \sqrt{a_i}}{1 + \sqrt{a_i}}$$
$$i = red, green, and\ blue$$

Equation 13

Where ρ_i is the hemi-spherical reflectance for a deep canopy with horizontal leaves. When using the measured cannabis leaf absorptivity using adaxial leaf reflectance, Equation 13 results in canopy reflectance values of 0.013, 0.016, 0.008 for the red, green, and blue color wavelength band computed using the measured adaxial reflectance values.

The VRTM sets the values of specular reflectance to zero and both the front and rear RGB specular transmittance to unity. These values simulate no interaction if the ray contacts the polygon from the internal canopy side but causes the creation of a surface point if the ray makes contact from the

outward facing side. This surface point generates a single ray of equivalent intensity and direction to that of the incident ray, which proceeds into the canopy. Additionally, this surface point generates a user specified number of rays that simulate the canopy's diffuse reflectance.

(A) 2.c.v. Lamp Emissions

The VRTM simulates lamp emissions through the construction and assignment of a 'light' material primitive to a polygon primitive. The 'light' material primitive represents a lamp's emissions as the red, green, and blue radiance in $W/(m^2*sr)$. A polygon assigned the 'light' material emits light with an even intensity in all directions. The VRTM simulates the lamp emission angular distribution through the creation and assignment of a 'brightdata' pattern primitive to the light material primitive. When a ray contacts the polygon surface, the engine uses the resulting incident angle to interpolate the lamp emission intensity from the dataset and applies the resulting factor to the RGB emission intensity.

Most commonly, lamp manufacturers provide lamp emissions data in the form of an '.ies' data file or an IES LM-79 report. Both contain datasets that detail a lamp's emission intensity data and emission angular distribution data.

Conversion of LM-79 Report Data to Radiance Primitives for the Vividgro V2 Lamp

We used a manufacturer-provided IES LM-79 report for the Vividgro V2 lamp as well as dimensional drawings of the lamp to define the *Radiance* 'light' and 'brightdata' primitives. The LM-79 report contained a table of emitted radiant power in mW from 400 to 700nm at 5 nm resolution (BACL, 2015). Conversion of mW to mW/sr involved integrating the values for the 400 to 500nm, 500 to 600nm, and 600 to 700 nm wavelength bands and then dividing by 4π to convert the integration results to units of power emitted per steradian. These RGB mW/sr values were then divided by the emissive area of the lamp ($0.65m^2$) and 1000 to get the final values in W/m^2*sr, resulting in RGB emissions of 74.06, 12.60, and 13.00.

The manufacturer data presents the LED emission angular distribution as a two-dimensional table containing emission angle and candela emitted at that angle. The 'brightdata' material primitive contains a similar two-dimensional table, with the manufacturer's candela values replaced by a normalization of the candela data from 0 to 1.

Validation of IES File Representation of Lamps

To validate the manufacturer-provided lamp emission data, we measured irradiances from an isolated Vividgro V-2 lamp at seven locations and compared those measurements to irradiances at the same locations predicted by *Radiance* using the manufacturer-provided ies file. The lamp was first optically isolated from the other lamps in the grow room using large blackout curtains (Figure 2-8). We then measured irradiance at seven positions one meter below the lamp with the spectroradiometer optical inlet oriented normal to the lamp beam axis, as illustrated in Figure 27. The positions included (1) in line with the center of the lamp, (2) in line with the 75% beam angle, (3) in line with the 50% beam angle, and (4) in line with the 25% beam angle. These positions correspond to beam angles specified in the IES file.

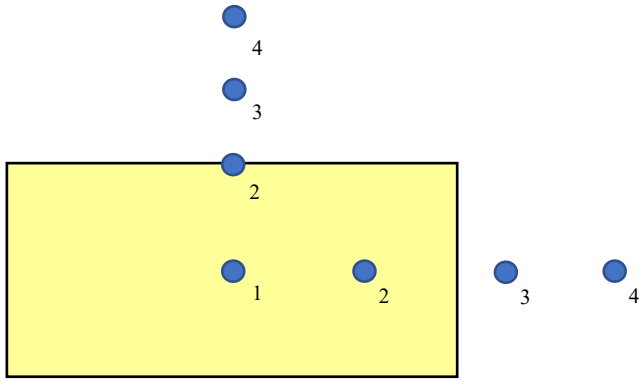

Figure 2-7 The image presents a bottom view of the lamp. The technician took 7 irradiance measurements at one meter below the lamp emissive surface.

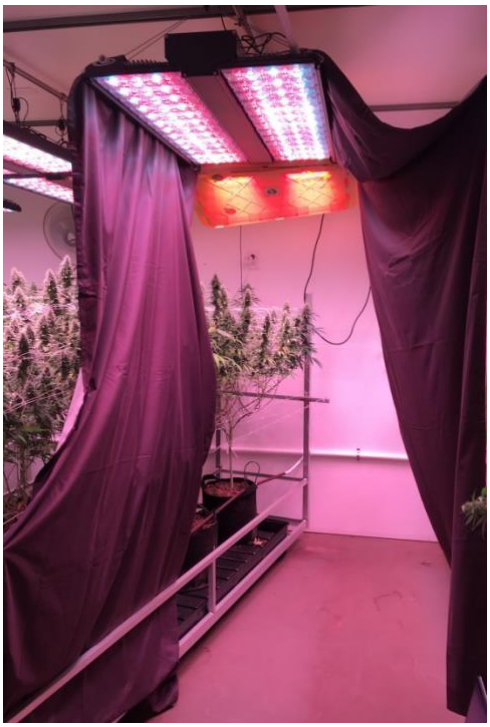

Figure 2-8 The setup for the optically isolated lamp measurements. All other lamps in the room remained on during these measurements.

The input 3D space for the validation simulation contains seven nodes located in the same position as the real-world measurements. Additionally, the 3D space contains one 'polygon' primitive representing the lamp, one 'light' primitive containing the manufacturer provided lamp emission intensity, and one 'brightdata' primitive containing the manufacturer provided emission angular distribution profile.

Validation of the manufacturer provided emission intensity consists of comparing the measured irradiance at each of the seven locations specified in Figure 2-7 to the irradiance predicted by the simulation at the corresponding node. Both the predicted and measured sets are normalized from 0 to 1.

In addition, to evaluate the importance of discrepancies between the measured lamp irradiances and those predicted by using the manufacturer-provided ies file to the VRTM, new 'light' and 'brightdata' primitives were constructed, using the validation measurements.

Construction of the new 'light' material primitive, specifically three new RGB emission intensity values, uses the following equation:

$$I_{e,i} = 4\pi I_{m,i} d^2$$
$$i = red, green, and\ blue$$

Equation 14

Where $I_{e,i}$ is the RGB irradiance emitted from the lamp in watts, $I_{m,i}$ is the measured RGB power in W/m^2 at position 1, and *d* is the distance between the lamp and the measurement. This computed power is then divided by π and the lamp area get a result in W/m^2*sr.

The 'brightdata' primitive receives a 3D matrix generated from the seven irradiance measurements. This matrix has two rows containing the zenith and azimuth angles of the emission, and a third row containing a scalar factor. The scalar factor is computed according to the following equation:

$$a_o(\theta) = a_i * \cos(\theta) * \frac{d_i^2}{1^2}$$

Equation 15

Where $a_o(\theta)$ is the factor associated with the emission at an angle of θ, a_i is the normalized measurement value, and d_i is the straight-line distance between the measurement and the lamp (Dornelles *et al.*, 2010).

Wall, Floor, and Ceiling Reflectance

The VRTM assigns a single 'plastic' material primitive to all polygons representing real-world walls, ceiling, and room objects and a separate single 'plastic' material primitive for the floor. For the walls, ceiling, and room objects we used values for RGB diffuse reflectance of 0.95, 0.95, and 0.78 to match that of reflective white paint (Dornelles *et al.*, 2010) and for the floor we used values for RGB diffuse reflectance of 0.36, 0.34, 0.29, matching that of 21 MPa concrete (J.-D Lee *et al.*, 2012).

(A) 2.d. Source Code

Source code for the VRTM Implementation is located at the following URL: https://github.com/mxchml/Vegetative-Radiative-Transfer-Model-.

Appendix 3: Measurement of Cannabis Leaf Reflectance and Transmittance

We measured cannabis leaf transmittance and reflectance at a cannabis farm located in Port Townsend, WA, using an optical bench installed in the mid-seat area of a 2020 Dodge Caravan minivan. The optical source for both the transmittance and reflectance testing was a ceramic metal halide (CMH) lamp (Phillips 315W T12 - 3100K Agro) attached to a Nanolux Summit System ballast. Figure 3-1 presents a spectrum of the test source emissions as measured with the spectroradiometer setup used for leaf transmittance testing.

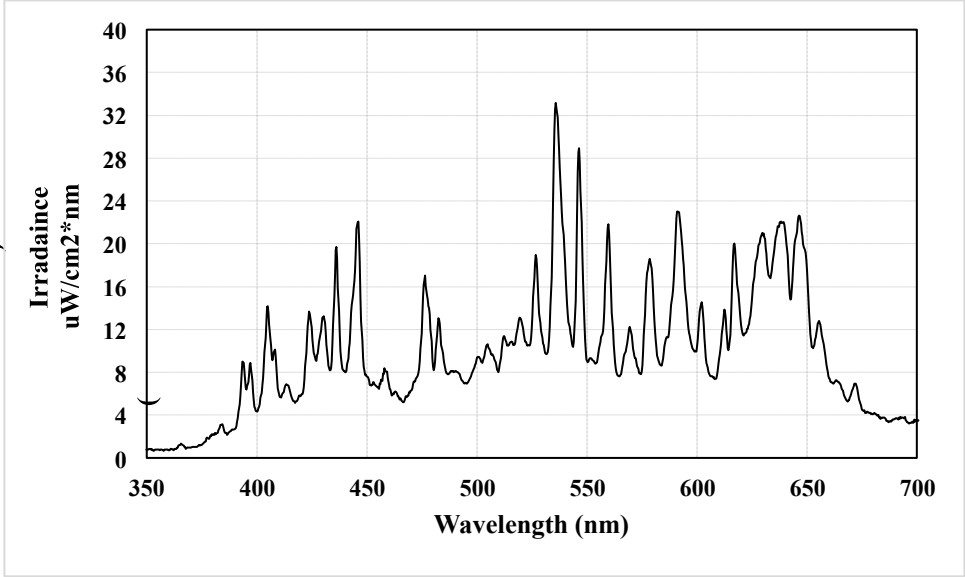

Figure 3-1 A spectrum of the Phillips 315 T12 Agro lamp as measured by an Ocean Insight Flame-S spectroradiometer.

(A) 3.a.i. Literature Review

To contextualize the cannabis leaf transmittance and reflectance measurement values, we conducted a search within the Ecological Spectral Information System (EcoSIS) (Wagner, Merz and Townsend, 2018) for datasets that contain both leaf spectral transmittance and leaf spectral reflectance in the visible wavelength range. A query comprised of the measurement qualities “transmittance” and “reflectance” along with the target type of “leaf” was entered to the search query.

The query returned seven datasets, of which we kept six (Hosgood *et al.*, 1995; Jacquemound *et al.*, 2003; Serbin, 2014; Serbin, DuBois, *et al.*, 2019; Serbin, Meng, *et al.*, 2019; Kothari *et al.*, 2022) for analysis, omitting one (Herrmann, Karmieli and Yermiyah, 2014) because it did not present species names consistent with the other datasets. We merged the leaf reflectance and transmittance data from the six into a single dataset, henceforth referred to as the dataset of published data. This dataset served as the comparison group for the cannabis leaf measurements.

The dataset of published data contains 9278 spectral measurements consisting of 286 species with leaf transmittance data and 311 species with leaf reflectance data. *Acer pseudoplatanus* (Sycamore Maple) had the most representation with 181 measurements for both refection and transmittance data, while 27 species had only one transmittance measurement and 20 species had only one reflectance measurement.

The average proportion reflected for the 400 to 700 nm range was 0.074 (sd = 0.027) and the average proportion transmitted was 0.050 (sd = 0.033). The minimum proportion reflected was 0.027 and the maximum was 0.46. Table 3-1 presents descriptive statistics of the dataset of published data.

Table 3-1 Descriptive statistics for the dataset of published data.

Optical Property	Species Count	Statistic	Proportion of Radiation			
			Blue (400 to 500 nm)	Green (500 to 600 nm)	Red (600 to 700 nm)	Visible (400 to 700 nm)
Reflectance (n = 5,671)	311	Min	0.013	0.032	0.021	0.027
		Mean (sd)	0.051 (0.019)	0.102 (0.037)	0.069 (0.031)	0.074 (0.027)
		Max	0.375	0.504	0.522	0.460
Transmittance (n =3,607)	286	Min	-0.001	0.000	0.000	0.000
		Mean (sd)	0.016 (0.018)	0.084 (0.048)	0.051 (0.039)	0.050 (0.033)
		Max	0.396	0.508	0.508	0.471

(A) 3.b. Leaf Transmittance Testing

(A) 3.b.i. Methods Measurement Setup

The optical bench used for transmittance testing had two mounts, one for a crocodile clamp holding the leaf under test and one for a ring clamp attached to the optical inlet. The optical inlet comprised of a field of view (FOV) limiter and a cosine corrector. The FOV limiter comprised of a three-inch long 1/8" x 1/8" brass pipe fitting, which had three layers of black paint (Behr Premium Paint and Primer - Black Matte, Behr Paint Company, Santa Ana, CA, USA) coating the interior. The cosine corrector (model: CC-3-UV-Vis) tightly slotted into the FOV limiter, and an optical fiber (QP450-1-XSR; Ocean Insight, Orlando, FL, USA) connected the optical inlet to an Ocean Insight Flame–S UV-Vis Spectroradiometer (Ocean Insight, Orlando, FL, USA).

The Ocean Insight Flame – S spectroradiometer can nominally detect wavelengths down to 210nm, however, the standard version of this device suffers from spectral scatter during measurement of broadband radiation, reducing its effective wavelength measurement range to approximately 300 to 700 nm, depending on the spectra of the measured source. We used the calibrated manufacturer software, OceanView 1.6.7, as the controlling software for the device. Figure 3-2 presents a 2D representation of this optical bench during a leaf transmittance test. Blackout curtains surrounded the optical bench during testing and the lamp warm up period was thirty minutes.

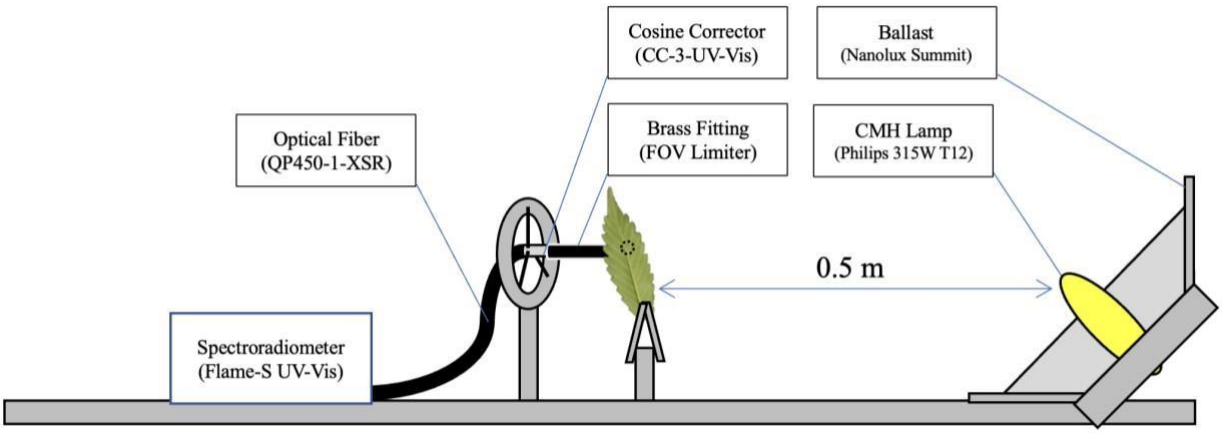

Figure 3-2 2D representation of the optical bench used for leaf transmittance testing.

The setup for a single leaf measurement consisted of using the crocodile clamps to fix the leaf flush with the opening of the FOV limiter fitting. After leaf installation, the spectroradiometer control software took approximately 30 seconds to automatically adjust the integration time such that the peak spectrum irradiance occurred at 85% of spectroradiometer pixel saturation. Upon integration time stabilization, the technician commanded the spectroradiometer to take a measurement using a laptop connected via micro-USB. Twenty leaves underwent the transmittance testing from twenty different cannabis plant cultivars. Twelve leaves were taken from plants in the flowering stage and eight were taken from plants in the growth stage of a cannabis plant life cycle. In order to assure stability of the transmittance measurements, five measurements were taken for a single leaf and these five repeats occurred throughout the survey period between 10:00 and 14:00 PCT.

Prior to collection of the first transmittance measurement and after approximately every three leaves, we commanded the spectroradiometer to take an ambient radiation measurement, a measurement without any leaf present. We took a total of eleven ambient measurements, the first with integration times of 27ms and the rest with an integration time of 30ms. The period between each the ambient radiation measurement was approximately five to ten minutes. The coefficient of variation (COV) for the wavelength of maximum signal (536 nm) was 1.2%, and the repeat ambient measurements demonstrated no consistent instrument drift across the measurement period.

Analysis

We imported all data into Microsoft Excel (ver. 16.71; Microsoft Corp., Redmond, WA, USA) and used this software for all data processing. We computed the fraction of radiation transmitted through the leaf for each wavelength according to the following equation:

$$\%T_i = \frac{I}{I_o} * 100$$

Equation 16

Where T_i is the proportion of transmitted light at wavelength i expressed as a percentage, I_o is the raw signal measured at wavelength i from the ambient light measurement, and I is the raw signal measured at wavelength i from the leaf measurement. Data were then aggregated into blue (400 to 500nm), green (500 to 600nm), and red (600 to 700nm) wavelength bands. Finally, we computed descriptive statistics to describe the measurements collectively and compared them to those in the dataset for published data.

The descriptive statistics computed included the minimum, mean, maximum, standard deviation, and coefficient of variation for each wavelength bands.

(A) 3.b.ii. Results and discussion

Figure 3-3 presents the minimum, maximum, and average proportion of radiation transmitted though the leaves (n = 20) at each wavelength.

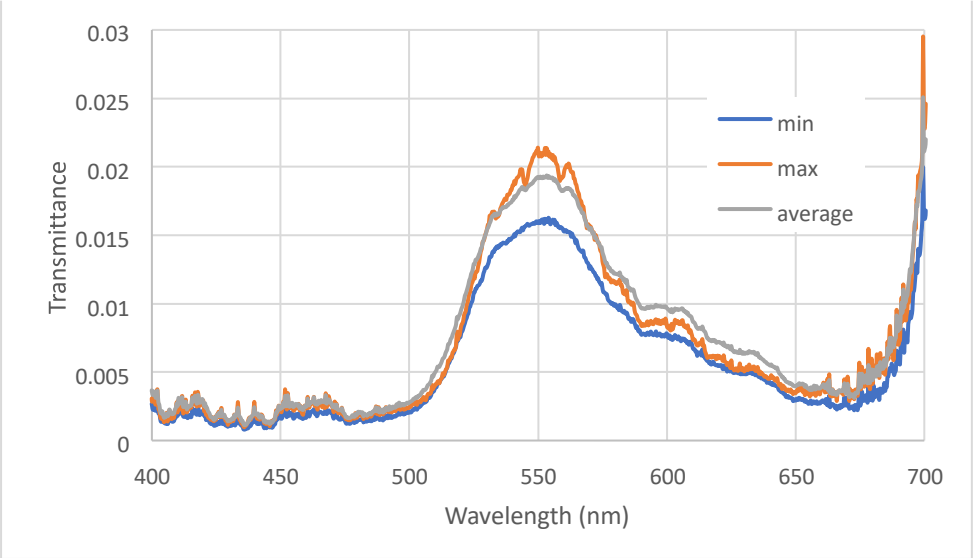

Figure 3-3 The minimum, maximum, and average of the measured leaf transmittance (n=20).

The average transmittance across the entire 400 to 700 wavelength range is 0.007 (sd = 0.002). The average proportion transmitted in the red (400 to 500), green (500 to 600), and blue (600 to 700) wavelength ranges is 0.006 (sd = 0.000), 0.012 (sd = 0.004), and 0.002 (sd = 0.006), respectively.

Table 3-2 Descriptive statistics for the cannabis leaf transmittance measurements.

Optical Property	Statistic	Proportion of Radiation			
		Blue (400 to 500 nm)	**Green (500 to 600 nm)**	**Red (600 to 700 nm)**	**Visible (400 to 700 nm)**
Transmittance (n = 20)	Min	0.001	0.007	0.003	0.003
	Mean (sd)	0.002 (0.001)	0.010 (0.004)	0.006 (0.002)	0.007 (0.002)
	Max	0.003	0.019	0.01	0.011

The average transmittance across the entire 400 to 700 wavelength range for the flowering cannabis plants is 0.007 (sd = 0.002), while the average transmittance for the same wavelength range for the vegetative state cannabis plants is 0.006 (sd = 0.002). A two-sided t-test of unequal variance at the 95% confidence interval showed no significant difference between the average transmittance measured between the two groups (p = 0.302)

The highest transmittance occurred at 699nm and has a value of 0.03. In the green wavelength range (500 to 600nm), the maximum transmittance occurred at 554 nm (average transmittance at the 554nm is 0.019 (sd = 0.005).

When comparing the transmittance values of the five measurements of a single leaf, the average COV was 6%, and the leaf transmittance did not change consistently during the ~90-minute period over which these repeat measures were taken.

The average measured leaf transmittance for the 400 to 700 nm wavelength band was 0.007, which places our measurements of the cannabis leaf in the 1.1% percentile of transmittance among the measurements in the dataset of published data. All twenty cannabis measurements fell within the range of the published values, with the minimum and maximum measured cannabis leaf transmittance (400 to 700nm) falling into the 0.001% and 3.8% percentiles, respectively. At the species level, cannabis leaves had the second least transmittance out of the 286 species represented, after *Phoradendron leucarpum*. The low transmittance values indicate that the measured cannabis leaves absorb and reflect a large proportion of incident radiation when compared to the plant species listed in the three datasets.

The average measured green to red ratio among the cannabis transmittance measurements is 1.98 (sd = 0.17), which indicates that on average cannabis leaves transmit a greater proportion of radiation in the green wavelength range putting the cannabis leaf as the 226th out of 286 species represented in the dataset with published values.

(A) 3.c. Leaf Reflectance Measurement

(A) 3.c.i. Methods

The optical bench used for leaf reflectance testing had two mounts, one for a crocodile clamp holding the leaf under test and one that contained threads for the screw attachment of a full size digital single reflex lens (DSLR) camera. The measurement device used for this test was an EOS 30D digital camera (Canon, Ota, Japan) with the following settings: 20mm focal length, f/4 aperture, 1/160 exposure time and an ISO of 100.

The optical source was the same Phillips 315W T12 – 3100K Agro lamp attached to the Nanolux Summit System ballast as in the leaf transmittance testing. The optical bench was positioned such that the lamp and the camera had a 45 deg offset.

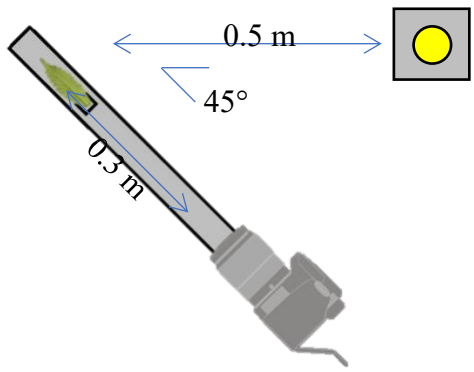

Figure 3-4 A top view of the optical bench as setup during the leaf reflectance testing.

The setup for a single leaf measurement consisted of using the crocodile clamps to fix the leaf with its upper (adaxial) surface perpendicular to and facing the camera axis. Once installed, the technician imaged the leaf, then flipped the leaf to the reverse (abaxial) side and took another image. Prior to each image capture, the technician fixed and imaged a Macbeth Colorchecker chart (Pascale, 2006) to the

crocodile clamp. In total, reflectance measurements were collected on leaves from 20 cannabis plants. Fourteen leaves were taken from plants in the flowering stage and six were taken from plants in the growth stage of a cannabis plant life cycle.

We imported all images from the camera SD card into the HDRshop software package (Tchou and Debevec, 2001). In HDR shop, we cropped each leaf image to the pixels representing the leaf and each Macbeth ColorChecker chart to the pixels representing the chart. The cropped images were saved as high dynamic range (HDR) files. The *Radiance* program macbethcal took each Macbeth chart HDR file and generated a color mapping function. The *Radiance* program pcomb then used this color mapping function to color correct the HDR images containing the leaf adaxial and abaxial sides. Each pixel in the corrected images represents estimates of the proportion of light reflected in the red, green, and blue color bands.

(A) 3.c.ii. Reflectance measurements results and discussion

Table 3-3 presents the adaxial and abaxial minimum, maximum, and average proportion of radiation reflected for the red, green, and blue color wavelength band (n = 20).

Table 3-3 Descriptive statistics for the cannabis leaf adaxial reflectance measurements.

Optical Property	Statistic	Proportion of Radiation			
		Blue (400 to 500 nm)	**Green (500 to 600 nm)**	**Red (600 to 700 nm)**	**Visible (400 to 700 nm)**
Adaxial (n = 20)	Min	0.021	0.031	0.028	0.027
	Mean (sd)	0.029 (0.007)	0.050 (0.024)	0.044 (0.019)	0.041 (0.016)
	Max	0.042	0.125	0.105	0.087
Abaxial (n = 20)	Min	0.037	0.076	0.068	0.060
	Mean (sd)	0.044 (0.006)	0.104 (0.023)	0.091 (0.021)	0.080 (0.016)
	Max	0.053	0.175	0.158	0.128
Average (n = 20)	Min	0.031	0.055	0.050	0.045
	Mean (sd)	0.036 (0.005)	0.077 (0.023)	0.067 (0.019)	0.060 (0.015)
	Max	0.047	0.150	0.132	0.108

The average adaxial reflectance across the visible wavelength range for the flowering cannabis plants is 0.045 (sd = 0.019), while the average reflectance for the same wavelength range for the vegetative cannabis plants is 0.034 (sd = 0.006). A two-sided t-test of unequal variance at the 95% confidence interval showed no significant difference between the average reflectance measured between the two groups (p = 0.141).

The average abaxial reflectance for the visible wavelength range for the flowering cannabis plants is 0.083 (sd = 0.018), while the average reflectance for the same wavelength range for the vegetative cannabis plants is 0.075 (sd = 0.011). A two-sided t-test of unequal variance at the 95% confidence interval showed no significant difference between the average reflectance measured between the two groups (p = 0.357)

The average reflectance for the visible wavelength range for the flowering plants is 0.064 (sd = 0.018), while the average reflectance for the same wavelength range for the vegetative plants is 0.055 (sd = 0.007). A two-sided t-test of unequal variance at the 95% confidence interval showed no significant difference between the average reflectance measured between the two groups (p = 0.128)

The average measured leaf reflectance for the 400 to 700 nm wavelength band was 0.060 (sd = 0.015) which places our measurements of the cannabis leaf in the 36.2% percentile of reflectance among the measurements in the dataset of published data. All twenty cannabis measurements fell within the range of the published values, with the minimum and maximum measured cannabis leaf reflectance (400 to 700nm) falling to the 29.4% and 90.5% percentiles, respectively.

The average measured green to red ratio among the cannabis reflectance measurements is 1.14 (sd = 0.02), putting the cannabis leaf as the 10th out of 311 species represented in the dataset with published values. This suggests that on average cannabis leaves transmit a greater proportion of radiation in the red wavelength range than most species in the dataset of published values.

(A) 3.d. Computation of Leaf Absorptivity for Use in the VRTM

The computation of leaf absorptivity was performed according to the following equation.

$$1 - (r_i + t_i) = a_i$$
$$i = red, green, and\ blue$$

Equation 17

Where r_i is the average adaxial reflectance for the red, green, or blue wavelength bands and t_i is the average transmittance for the red, green, or blue wavelength bands. The values of r_i are 0.029, 0.050, and 0.044 for the blue, green, and red wavelength bands, respectively. The values of t_i are 0.036, 0.077, and 0.067 for the blue, green, and red wavelength bands, respectively. The computed blue, green, and red leaf absorptivity are 0.969, 0.937, and 0.950, respectively.

Appendix 4: Nelder Mead Algorithm

Each iteration of the algorithm goes through three steps: ordering, calculating a centroid, and transformation.

(A) 4.a.i. Ordering and Centroid Computation

Ordering determines the worst (f_h), second worst (f_s), and best vertex (f_l) in the simplex based on the function output values for each of the Simplex's vertices. For a minimization problem, the best vertex has the smallest function value, and vice versa for a maximization problem. Calculation of the centroid involves removing the worst vertex from the working simplex and computing the centroid with the remaining vertices. After computation of the centroid, the transformation step begins.

(A) 4.a.ii. Working Simplex Transformation

The transformation step computes a new simplex based on the current working simplex. The transformation step contains a series of sub-steps, with all but the first sub-step dependent on the result of the previous sub-step. The sub-steps consist of computation of the reflection vertex, computation of the expansion vertex, computation of the contraction vertex, or shrinking the simplex.

Each iteration transformation begins with computation of the reflection vertex:

$$x_r = c + \alpha(c - x_h)$$

Equation 18

Where x_r = the reflection vertex, c = the centroid, α is the scalar reflection parameter (usually 1), and x_h is the worst vertex.

If $f_l \leq f_r < f_s$ the iteration terminates and x_r is accepted. However, if $f_r < f_l$ is true, the expansion vertex is computed or if $f_r \geq f_s$ is true, the contraction sub-step is performed.

The expansion vertex is computed according to the following equation:

$$x_e = c + \gamma(x_r - c)$$

Equation 19

Where x_e is the expansion vertex, c is the centroid, γ is the scalar expansion parameter, x_r is the reflection vertex. If $f_e < f_r$, the iteration terminates and x_e is accepted. Otherwise, the iteration terminates and x_r is accepted.

The contraction sub-step consists of either an outside if simplex contraction if $f_s \leq f_r < f_h$ is true or an inside simplex contraction if $f_r \geq f_h$ is true. The outside contraction vertex is computed according to the following equation:

$$x_c = c + \beta(x_r - c)$$

Equation 20

Where x_c is the contraction vertex, c is the centroid, β is the scalar contraction parameter and x_r is the reflection vertex. If $f_c \leq f_r$ the iteration terminates and x_c is accepted. Otherwise, the shrink transformation is performed.

The inside contraction vertex is computed according to the following equation:

$$x_c = c + \beta(x_h - c)$$

Equation 21

Where x_c is the contraction vertex, c is the centroid, β is the scalar contraction parameter and x_h is the worst vertex. If $f_c < f_h$ the iteration terminates and x_c is accepted. Otherwise, the shrink transformation is performed.

The shrink transformation computes n-1 new vertices, replacing all vertices of the working simplex except for the best vertex. The new vertices are computed by passing each of the non-best vertices to the following equation:

$$x_{j(new)} = x_l + \delta(x_j - x_l)$$
$$For: j = 0, \ldots, n, \ with \ j \neq l$$

Equation 22

Where $x_{j(new)}$ are the new vertices, x_l is the best vertex, δ is the scalar shrink parameter, x_j is the location to pass the working simplex vertices.

(A) 4.a.iii. Termination

This implementation of the Nelder Mead Simplex algorithm uses the same termination tests as that described in the MATLAB Language Reference Manual. The algorithm terminates once the working simplex meets one of the following termination conditions:

Domain Convergence

$$|x_i - x_{i+1}| < T * (1 + |x_i|)$$

Equation 23

Where x_i is the value for the current iteration, x_{i+1} is the value of the previous iteration, and T is a scaling factor that determines a threshold under which the absolute value of the difference between x_i and x_{i+1} must fall under. This implementation of T uses the Matlab default of 10^{-4}.

Function-Value Convergence

$$|f(x_i) - f(x_{i+1} + 1)| < U$$

Equation 24

Where $f(x_i)$ is the RMSE of the current iteration, $f(x_{i+1} + 1)$ is the RMSE of the previous iteration, and U is the threshold under which the absolute value of the difference between $f(x_i)$ and $f(x_{i+1} + 1)$ must fall under. This implementation of U uses the Matlab default of 10^{-4}.

Iterations Limit Reached
This implementation uses a limit of 500 iterations.

(A) 4.a.iv. Local Minimum Avoidance

The current implementation checks for local minima through a simple random seed restart. First, this process randomly selects a vertex dimension using the python ‘randint’ function to generate a uniformly distributed random integer bounded by the number of parameters. The program then generates and insets a new seed into that parameter space for each vertex.

Appendix 5: Additional Results

Table 5-1 Summary statistics of the irradiance measurements in W/m², grouped by spectral band and measurement height.

Grouping	Band ID	Min (W/m²)	Max (W/m²)	Mean (W/m²)	SD (W/m²)
All Measurements (n=170)	Red	3.12	187	40.2	26.9
	Green	0.57	24.1	5.89	3.68
	Blue	0.38	21.2	5.11	3.26
	Total Visible	4.07	233	51.2	33.8
Below Canopy <= 1.41 m (n = 110)	Red	3.12	67.2	27.1	12.6
	Green	0.57	9.63	3.96	1.84
	Blue	0.38	8.7	3.43	1.67
	Total Visible	4.07	85.5	34.5	16.1
Above Canopy >= 1.67 (n = 60)	Red	6.27	187	56.6	30.8
	Green	1.03	24.1	8.29	3.99
	Blue	0.79	21.2	7.22	3.55
	Total Visible	8.08	233	72.1	38.3
Directly Under Canopy (n = 7)	Red	4.02	19.7	9.76	5.32
	Green	0.66	3.05	1.43	0.83
	Blue	0.46	2.45	1.09	0.69
	Total Visible	5.18	25.2	12.2	6.82

Table 5-2 Summary statistics of the irradiance predictions in W/m², grouped by spectral band and measurement height.

Grouping	Band ID	Min (W/m²)	Max (W/m²)	Mean (W/m²)	SD (W/m²)
All Measurements (n=170)	Red	5.80	159	37.7	24.3
	Green	0.99	27.1	6.40	4.14
	Blue	0.88	27.8	6.44	4.29
	Total Visible	7.73	214	50.5	32.7
Below Canopy <= 1.41 m (n = 110)	Red	5.80	69.16	27.62	13.8
	Green	0.99	11.76	4.70	2.35
	Blue	0.88	11.91	4.67	2.43
	Total Visible	7.73	92.83	37.00	18.6
Above Canopy >= 1.67 (n = 60)	Red	8.41	159	56.0	28.5
	Green	1.42	27.1	9.53	4.84
	Blue	1.11	27.8	9.68	5.03
	Total Visible	10.9	214	75.2	38.3
Directly Under Canopy (n = 7)	Red	5.80	6.79	6.27	0.37
	Green	0.99	1.17	1.07	0.07
	Blue	0.88	1.15	1.03	0.10
	Total Visible	7.73	9.11	8.37	0.53

Table 5-3 Summary statistics of the simulation with no canopies predictions in W/m², grouped by spectral band and measurement height, for the model run with the best RMSE (i.e. L_I = 15, u=1.3, v = 1).

Grouping	Band ID	Min (W/m²)	Max (W/m²)	Mean (W/m²)	SD (W/m²)
All Measurements (n=170)	Red	5.80	159	37.7	24.3
	Green	0.99	27.1	6.40	4.14
	Blue	0.88	27.8	6.44	4.29
	Visible	7.73	214	50.5	32.7
Below Canopy <= 1.41 m (n = 110)	Red	5.80	69.2	27.6	13.8
	Green	0.99	11.8	4.70	2.35
	Blue	0.88	11.9	4.67	2.43
	Visible	7.73	92.8	37.0	18.6
Above Canopy >= 1.67 (n = 60)	Red	8.41	159	56.0	28.5
	Green	1.42	27.1	9.53	4.84
	Blue	1.11	27.8	9.68	5.03
	Visible	10.9	214	75.2	38.3
Directly Under Canopy (n = 7)	Red	5.80	6.79	6.27	0.37
	Green	0.99	1.17	1.07	0.07
	Blue	0.88	1.15	1.03	0.10
	Visible	7.73	9.11	8.37	0.53

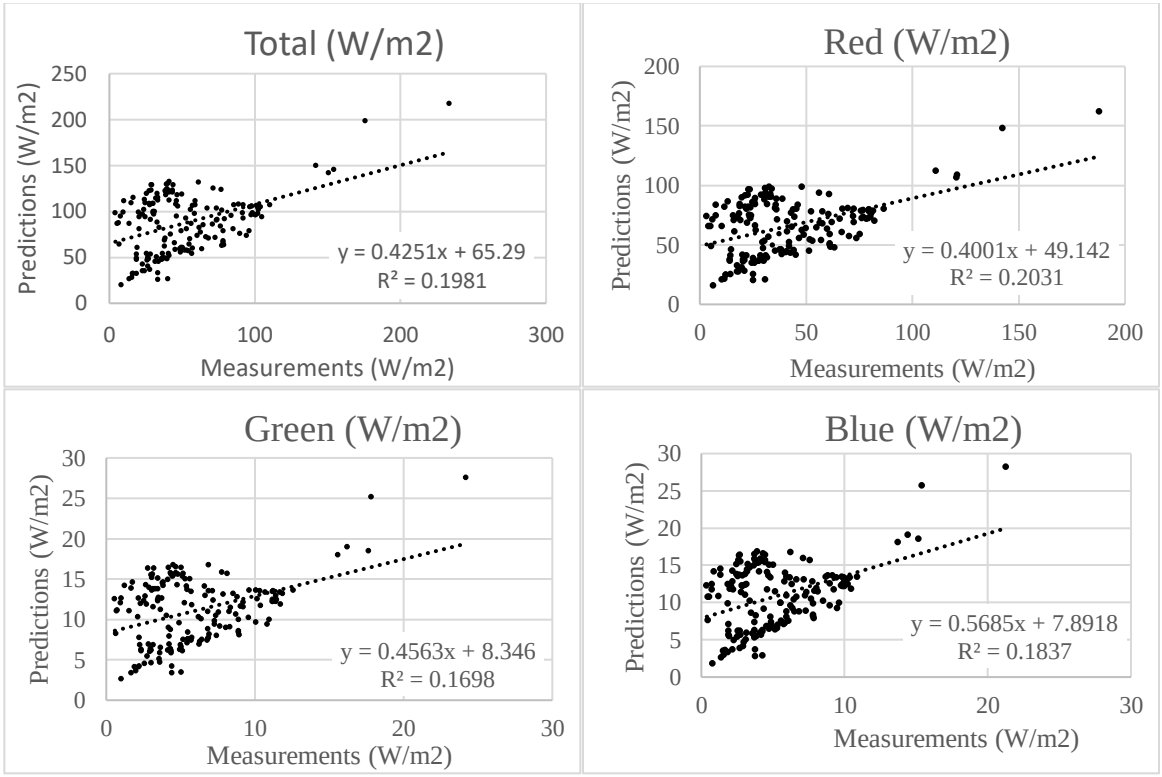

Figure 5-1 Results from a simulation run without plant canopies.

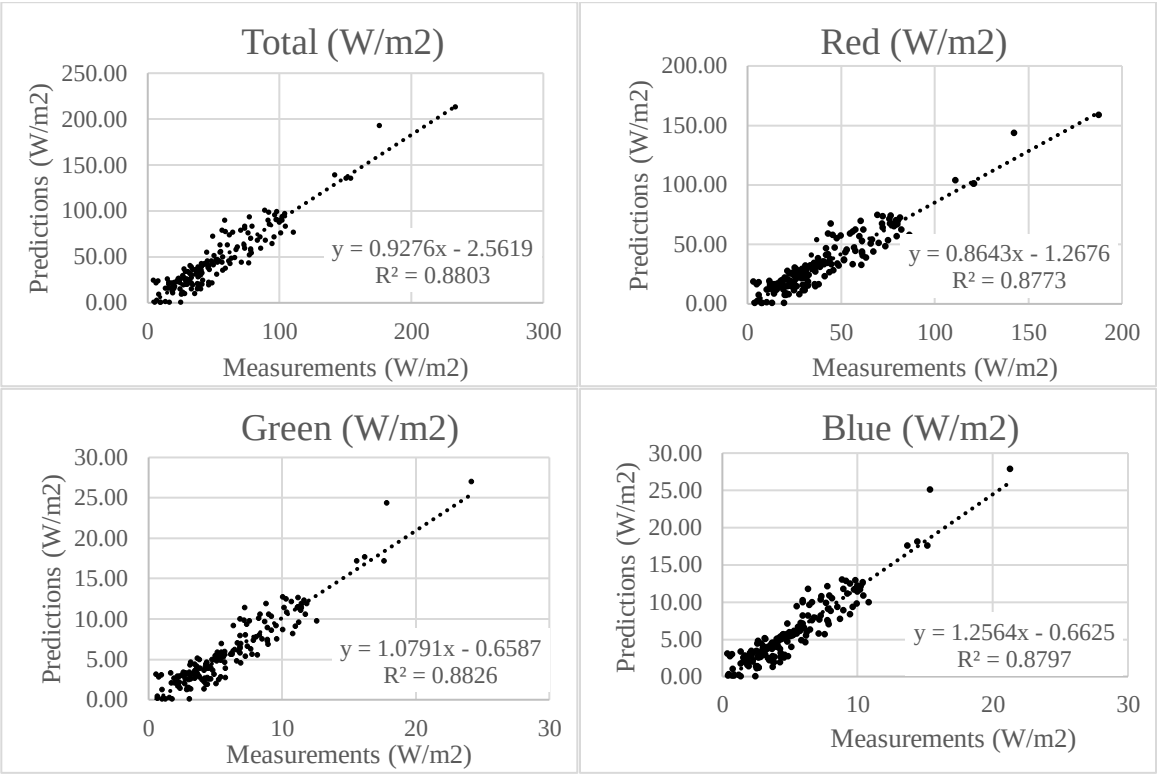

Figure 5-2 Results from a simulation run with cannabis plant represented as opaque hedgerows.

Table 5-4 The results of linear regression performed on measurement vs predictions on four simulations run with the parameters that had the best RMSE of the original set, except with the wall or floor diffuse reflectance changed.

Parameter		Total Visible	Red	Green	Blue
Base model	Slope	0.92	0.87	1.07	1.25
	R^2	0.89	0.86	0.89	0.89
	Intercept	2.22	2.32	-0.03	-0.10
Wall = 0	Slope	0.91	0.86	1.09	1.27
	R^2	0.88	0.87	0.88	0.88
	Intercept	3.62	-0.19	-0.70	-0.58
Floor = 0	Slope	0.92	0.86	1.07	1.25
	R^2	0.88	0.88	0.89	0.88
	Intercept	3.62	2.72	-0.39	-0.34
Wall = 1	Slope	0.92	0.86	1.07	1.25
	R^2	0.89	0.86	0.89	0.89
	Intercept	2.44	2.39	-0.03	0.06
Floor = 1	Slope	0.91	0.85	1.07	1.25
	R^2	0.88	0.88	0.89	0.88
	Intercept	3.62	6.86	0.12	0.065

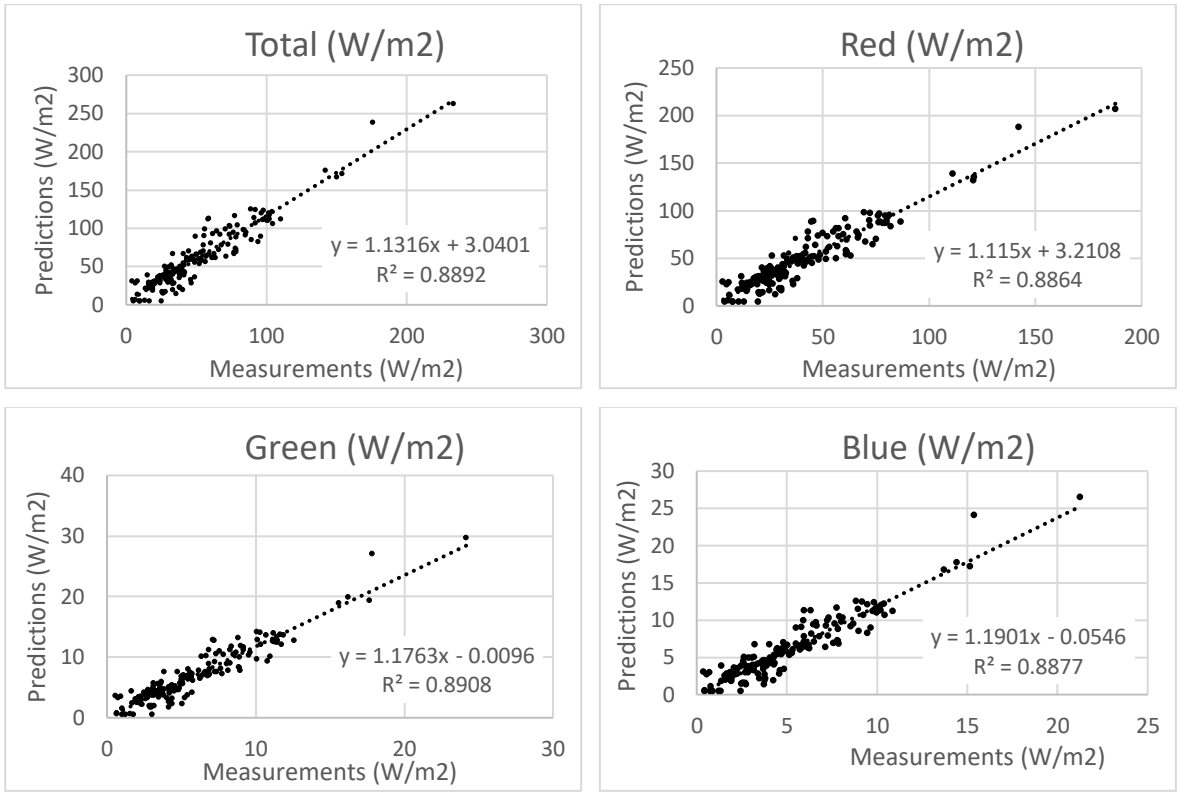

Figure 5-3 Results from a simulation run with lamp geometries assigned the measured isolated lamp material primitive constructed from lamp emission measurements.

References

[ACGIH] American Conference of Governmental Industrial Hygienists (2020) Ultraviolet Radiation TLV Documentation. Cincinnati, OH, USA

[ACGIH] American Conference of Governmental Industrial Hygienists (2023) TLVs and BEIs. Cincinnati, OH, USA: Available at: https://www.acgih.org/tlv-bei-guidelines/tlv-physical-agents-introduction.

[ASTM] American Society for Testing and Materials (2014) 'Solar Constant and Zero Air Mass Solar Spectral Irradiance', E490-00a, pp. 1–16. Available at: https://doi.org/10.1520/E0490-00AR14.2.

[ASTM] American Society for Testing and Materials (2018) 'Standard Test Method for Transfer of Calibration from Reference to Field Radiometers', American Society for Testing and Materials, ASTM-E824. Available at: https://doi.org/10.1520/E0824-10R18E01.

[ASTM] American Society for Testing and Materials (2020a) 'Standard Test Method for Calibration of a Spectroradiometer Using a Standard Source', American Society for Testing and Materials, G138-12(2020)e1. Available at: https://doi.org/10.1520/G0138-12R20E01.

[ASTM] American Society for Testing and Materials (2020b) 'Standard Test Method for Calibration of Narrow- and Broad-Band Ultraviolet Radiometers Using a Spectroradiometer', American Society for Testing and Materials, G130. Available at: https://doi.org/10.1520/G0130-12R20.

[BACL] Bay Area Compliance Laboratories (2015) IES LM-79-08 Test Report for the Vividgro V2 Grow Light Model: VGROHB 600W P26 MVOLT CLR PND BLK. Guangdong, CN. Available at: https://greencreative.com/wp-content/uploads/PKS180801080-10-1-GREENCREATIVE-90HIDHB-850-BYP-EX39-LM-79-final.pdf (Accessed: 30 March 2023).

[CDA] Canadian Dermatology Association (2020) Photoaging. Available at: https://dermatology.ca/public-patients/skin/photoaging/ (Accessed: 16 April 2023).

[CDPHE] Colorado Department of Public Health and the Environment (2017) 'Guide to Worker Safety and Health in the Marijuana Industry'. Available at: https://deohs.washington.edu/sites/default/files/documents/Guide-to-Worker-Safety-and-Health-in-the-Marijuana-Industry_FULL-REPORT.pdf (Accessed: 6 April 2023).

[CDPHE] Colorado Department of Public Health and the Environment (2019) Marijuana occupational safety and health. Available at: https://www.colorado.gov/pacific/cdphe/marijuana-occupational-safety-and-health.

[CIE] International Commission on Illumination (1984) 'The Spectroradiometric Measurement of Light Sources', CIE 63-1984. Available at: https://cie.co.at/publications/spectroradiometric-measurement-light-sources (Accessed: 6 April 2023).

[CIE] International Commission on Illumination (1999) ‘CIE S007/E-1998 Erythema reference action spectrum and standard erythema dose’, Color Research & Application, 24(2), p. 158. Available at: https://doi.org/10.1002/(SICI)1520-6378(199904)24:2<158::AID-COL11>3.0.CO;2-4.

[CIE] International Commission on Illumination (2011) ‘Spectral Responsivity Measurement of Detectors, Radiometers AND Photometers’, CIE 202:2011.

[CIE] International Commission on Illumination (2016) ‘Characterization of the Performance of Illuminance Meters and Luminance Meters’, ISO/CIE 19476:2014.

[DEOHS] University of Washington Department of Environmental and Occupational Health Sciences (2022) Field Research and Consultation Group. Available at: https://deohs.washington.edu/frcg (Accessed: 18 September 2022).

[IARC] International Agency for Research on Cancer (2012) ‘Solar and Ultraviolet Radiation’, in Monographs on the Evaluation of Carcinogenic Risks to Humans. pp. 35–101. Available at: https://monographs.iarc.who.int/wp-content/uploads/2018/06/mono100D-6.pdf (Accessed: 16 April 2023).

[IARC] International Agency for Research on Cancer. (2018) Solar and Ultraviolet Radiation. IARC Monographs, 100D(6), 35–101. Available at: https://monographs.iarc.fr/wp-content/uploads/2018/06/mono100D-6.pdf [Accessed: 29 April 2023]

[ICNIRP] International Commission on Non-Ionizing Radiation Protection (2004) ‘Guidelines on limits of exposure to ultraviolet radiation of wavelengths between 180 nm and 400 nm (incoherent optical radiation)’, Health Physics, 87(2), pp. 171–186. Available at: https://doi.org/10.1097/00004032-200408000-00006.

[ICNIRP] International Commission on Non-Ionizing Radiation Protection (2007) ‘Protecting Workers from UV Radiation.’, Munich: . Available at: https://www.icnirp.org/cms/upload/publications/ICNIRPUVWorkers.pdf (Accessed: 29 March 2023).

[ICNIRP] International Commission on Non-Ionizing Radiation Protection (2013) ‘Guidelines on limits of exposure to incoherent visible and infrared radiation’, Health Physics, 105(1), pp. 74–96. Available at: https://doi.org/10.1097/HP.0b013e318289a611.

[ICNIRP] International Commission on Non-Ionizing Radiation Protection. (1997) Guidelines on limits of exposure to broad-band incoherent optical radiation (0.38 to 3 mm). Health Phys. 73(3):539-54.

[ILT] International Light Technologies (2019) Light Measurement Input Optics. Available at: https://www.intl-lighttech.com/product-group/light-measurement-input-optics (Accessed: 15 September 2019).

[TIA] Telecommunications Industry Association (1997) TIA/EIA-232 Standard Interface Between Data Terminal Equipment and Data Circuit-Terminating Equipment Employing Serial Binary Data Interchange.

[WAC] Washington State Administrative Code (2003) Non-Ionizing Radiation WAC 296-62-09005. Available at: https://app.leg.wa.gov/wac/default.aspx?cite=296-62-09005 [Accessed: 7 May, 2023]

[WAC] Washington State Administrative Code (2022) 'Quality assurance and quality control.', Code: 314-55-102. Available at: https://app.leg.wa.gov/wac/default.aspx?cite=314-55-102 [Accessed: 7 May, 2023]

[WASAO] Washington State Auditor Office (2018) Marijuana Producer Process Maps. Available at: https://www.sao.wa.gov/wp-content/uploads/2018/11/ar1022033.pdf. [Accessed 20 March 302023]

[WCET] University of Washington Clean Energy Institute (2022) OAI Solar Simulator, University of Washington Clean Energy Testbeds. Available at: https://www.wcet.washington.edu/tools/oai-solar-sim/ (Accessed: 13 July 2022).

[WSDA] Washington State Department of Agriculture (2018) Pesticide and Fertilizer Use for the Production of Marijuana in Washington. Available at: https://agr.wa.gov/departments/marijuana/pesticide-use; [accessed on 30 March 2023].

ABC 7 News (2023) 'Bay Area cannabis industry leaders concerned for public safety amid string of violent incidents', ABC 7 News. Available at: https://abc7news.com/bay-area-cannabis-shops-san-francisco-armed-robberies-public-safety/13094915/ [accessed on 29 April 2023]

Acquavella, J. et al. (1998) 'Cancer Among Farmers: A Meta-Analysis', Annals of Epidemiology, 8(1), pp. 64–74. Available at: https://doi.org/10.1016/s1047-2797(97)00120-8.

Airey, D.K. et al. (1997) 'An estimate of the total UV-B exposure for outdoor workers during a south-east Queensland summer', (July 1996). Available at: 10.1097/00004032-199704000-00005

Airey, D.K., Wong, J.C.F. and Fleming, R.A. (1995) 'A comparison of human‐and headform‐based measurements of solar ultraviolet B dose', Photodermatology, Photoimmunology & Photomedicine, 11(4), pp. 155‐158. Available at: https://doi.org/10.1111/j.1600-0781.1995.tb00158.x.

Akbar-Khanzadeh, F. and Jahangir-Blourchian, M. (2005) 'Ultraviolet radiation exposure from UV-transilluminators', Journal of Occupational and Environmental Hygiene, 2(10), pp. 493–496. Available at: https://doi.org/10.1080/15459620500274211.

Allen M, McKenzie R. (2005) Enhanced UV exposure on a ski-field compared with exposures at sea level. Photochemical & Photobiological Sciences : Official Journal of the European Photochemistry Association and the European Society for Photobiology, 4(5), 429–437. Available at: https://doi.org/10.1039/b418942f

Alshamrani, A.Z. (2018) 'Cataracts Pathophysiology and Managements', The Egyptian Journal of Hospital Medicine, 70(1), pp. 151–154. Available at: https://doi.org/10.12816/0042978.

Annandale, J.G. et al. (2004) 'Two-dimensional solar radiation interception model for hedgerow fruit trees', Agricultural and Forest Meteorology, 121(3), pp. 207–225. Available at: https://doi.org/https://doi.org/10.1016/j.agrformet.2003.08.004.

Antoine, M. et al. (2007) ‘Effective exposure to solar UV in building workers: Influence of local and individual factors’, Journal of Exposure Science and Environmental Epidemiology, 17(1), pp. 58–68. Available at: https://doi.org/10.1038/sj.jes.7500521.

Arduino (2022) Arduino Due. Available at: https://docs.arduino.cc/hardware/due (Accessed: 31 May 2022).

Armstrong, B.K. and Kricker, A. (2001) ‘The epidemiology of UV induced skin cancer.’, Journal of Photochemistry and Photobiology. B, Biology, 63(1–3), pp. 8–18. Available at: https://doi.org/10.1016/s1011-1344(01)00198-1.

Ascherio, A., Munger, K.L. and Simon, K.C. (2010) ‘Vitamin D and multiple sclerosis.’, The Lancet. Neurology, 9(6), pp. 599–612. Available at: https://doi.org/10.1016/S1474-4422(10)70086-7.

Atmaca, L.S., Idil, A. and Can, D. (1995) ‘Early and late visual prognosis in solar retinopathy’, Graefe’s Archive for Clinical and Experimental Ophthalmology, 233(12), pp. 801–804. Available at: https://doi.org/10.1007/BF00184094.

Azizi, M., Golmohammadi, R. and Aliabadi, M. (2016) ‘Comparative analysis of lighting characteristics and ultraviolet emissions from commercial compact fluorescent and incandescent lamps’, Journal of Research in Health Sciences, 16(4), pp. 200–205. Available at: https://www.scopus.com/inward/record.uri?eid=2-s2.0-85008155453&partnerID=40&md5=5be9a1f41a10e64a5b459ec97e7015c1.

AZOM (2016) The Basic Working Principle of a Spectrometer, AZO Materials. Available at: https://www.azom.com/article.aspx?ArticleID=13364 (Accessed: 7 April 2022).

Baisakhiya, S. and Chaudhry, M. (2013) ‘Acute Solar Retinopathy’, Delhi Journal of Ophthalmology, 23, pp. 285–287. Available at: https://doi.org/10.7869/djo.2012.85.

Barcott, B. et al. (2022) Jobs Report 2022: Legal cannabis now supports 428,059 American jobs. Available at: https://leafly-cms-production.imgix.net/wp-content/uploads/2022/02/22132544/LeaflyJobsReport2022.pdf (Accessed: 16 April 2023).

Beck, N., Balanay, J.A.G. and Johnson, T. (2017) ‘Assessment of occupational exposure to heat stress and solar ultraviolet radiation among groundskeepers in an eastern North Carolina university setting’, Journal of Occupational and Environmental Hygiene, 15(2), pp. 105–116. Available at: https://doi.org/10.1080/15459624.2017.1392530.

Beckman, S. et al. (2023) ‘California cannabis cultivation and processing workers: A qualitative analysis of physiological exposures and health effects’, American Journal of Industrial Medicine, 66(1), pp. 75–84. Available at: https://doi.org/10.1002/ajim.23442.

Beckman, S., Langer, C.E. and Schenker, M.B. (2023) ‘A Pilot Study of Respiratory and Dermal Symptoms in California Cannabis Cultivation Workers’, Journal of Agromedicine, 28(1), pp. 28–35. Available at: https://doi.org/10.1080/1059924X.2022.2141407.

Bernstein, E.F. et al. (1996) 'Chronic sun exposure alters both the content and distribution of dermal glycosaminoglycans', British Journal of Dermatology, 135(2), pp. 255–262. Available at: https://doi.org/10.1111/j.1365-2133.1996.tb01156.x.

Bodekær, M. et al. (2014) 'UVR exposure and vitamin D in a rural population. A study of outdoor working farmers, their spouses and children', Photochemical and Photobiological Sciences, 13(11), pp. 1598–1606. Available at: https://doi.org/10.1039/c4pp00188e.

Bodekær, M. et al. (2015) 'Personal UVR exposure of farming families in four European countries', Journal of Photochemistry and Photobiology B: Biology, 153, pp. 267–275. Available at: https://doi.org/10.1016/j.jphotobiol.2015.10.002.

Boldeman, C. et al. (2004) 'Swedish pre-school children's UVR exposure - A comparison between two outdoor environments', Photodermatology Photoimmunology & Photomedicine, 20(1), pp. 2–8. Available at: https://doi.org/10.1111/j.1600-0781.2004.00069.x

Boldemann, C. et al. (2006) 'Impact of preschool environment upon children's physical activity and sun exposure', Preventive Medicine, 42(4), pp. 301–308. Available at: https://doi.org/https://doi.org/10.1016/j.ypmed.2005.12.006.

Bonino, A. et al. (2009) 'Tanning lamps ultraviolet emissions and compliance with technical standards', Radiation Protection Dosimetry, 137(3–4), pp. 197–200. Available at: https://doi.org/10.1093/rpd/ncp243.

Bonner, R., O'Hagan, J.B. and Khazova, M. (2011) 'Assessment of personal exposures to optical radiation in large entertainment venues', Radiation Protection Dosimetry, 149(3), pp. 225–237. Available at: https://doi.org/10.1093/rpd/ncr232.

Borchardt D. (2017) Marijuana Industry Projected To Create More Jobs Than Manufacturing By 2020. Forbes. https://www.forbes.com/sites/debraborchardt/2017/02/22/marijuana-industry-projected-to-create-more-jobs-than-manufacturing-by-2020/?sh=29865ee93fa9 [accessed on 30 March 2023].

Botto, N. and Warshaw, E. (2008) 'Solar urticaria', Journal of American Dermatology, 59(6), pp. 909–920. Available at: https://doi.org/10.1016/j.jaad.2008.08.020.

Bouillon, R. et al. (2006) 'Action spectrum for the production of previtamin D3 in human skin', International Commission on Illumination, CIE 174:2006, pp. 1–12. Available at: https://www.researchgate.net/publication/288863467_Action_spectrum_for_the_production_of_previtamin_D3_in_human_skin (Accessed: 16 April 2023).

Bower, K.S. et al. (2005) 'Scattered laser radiation and broadband actinic ultraviolet plasma emissions during LADARVision excimer refractive surgery', Journal of Cataract and Refractive Surgery, 31(8), pp. 1506–1511. Available at: https://doi.org/10.1016/j.jcrs.2005.01.023.

Brewer, A.W., Mcelroy, C.T. and Kerr, J.B. (1973) 'Nitrogen Dioxide Concentrations in the Atmosphere', Nature, 246(5429), pp. 129–133. Available at: https://doi.org/10.1038/246129a0.

Brown, C.E. et al. (2020) ‘Evaluation of an Occupational Safety and Health Training for Cannabis Cultivation Workers’, Annals of Work Exposures and Health, 64(7), pp. 765–769. Available at: https://doi.org/10.1093/annweh/wxaa026.

Campbell, G.S. (1986) ‘Extinction coefficients for radiation in plant canopies calculated using an ellipsoidal inclination angle distribution’, Agricultural and Forest Meteorology, 36(4), pp. 317–321. Available at: https://doi.org/https://doi.org/10.1016/0168-1923(86)90010-9.

Campbell, G.S. (1990) ‘Derivation of an angle density function for canopies with ellipsoidal leaf angle distributions’, Agricultural and Forest Meteorology, 49(3), pp. 173–176. Available at: https://doi.org/10.1016/0168-1923(90)90030-a.

Campbell, G.S. and Norman, J.M. (2000) ‘Chapter 15: The Light Environment of Plant Canopies’, in An Introduction to Environmental Biophysics. Springer Science and Business Media, pp. 247–278. Available at: https://doi.org/10.1007/978-1-4612-1626-1_15.

Carliner H, Brown QL, Sarvet AL, Hasin DS. (2017) Cannabis use, attitudes, and legal status in the U.S.: A review. In Preventive Medicine (Vol. 104, pp. 13–23). Academic Press Inc. Available at: https://doi.org/10.1016/j.ypmed.2017.07.008

Casale, G.R. et al. (2015) ‘Extreme UV index and solar exposures at Plateau Rosà (3500 m a.s.l.) in Valle d’Aosta Region, Italy’, Science of The Total Environment, 512–513, pp. 622–630. Available at: https://doi.org/10.1016/J.SCITOTENV.2015.01.049.

Caulkins, J.P. et al. (2018) ‘Big data on a big new market: Insights from Washington State’s legal cannabis market’, International Journal of Drug Policy, 57, pp. 86–94. Available at: https://doi.org/10.1016/j.drugpo.2018.03.031.

Cavatorta, C. et al. (2016) ‘A survey of sources of incoherent artificial optical radiation in a hospital environment in accordance with European Directive 2006/25/EC: Evaluation of the related exposure risk’, Journal of Radiological Protection, 36(1), pp. 144–162. Available at: https://doi.org/10.1088/0952-4746/36/1/144.

Challoner, A.V.J. et al. (1976) ‘Personnel monitoring of exposure to ultraviolet radiation’, Clinical and Experimental Dermatology, 1(2), pp. 175–179. Available at: https://doi.org/10.1111/j.1365-2230.1976.tb01413.x.

Chandra, P. et al. (2007) ‘Treatment of vitamin D deficiency with UV light in patients with malabsorption syndromes: a case series.’, Photodermatology, Photoimmunology & Photomedicine, 23(5), pp. 179–185. Available at: https://doi.org/10.1111/j.1600-0781.2007.00302.x.

Chandra, S. et al. (2011) ‘Photosynthetic response of Cannabis sativa L., an important medicinal plant, to elevated levels of CO2’, Physiology and Molecular Biology of Plants, 17(3), pp. 291–295. Available at: https://doi.org/10.1007/s12298-011-0066-6.

Chandrasekhar, S. (1960) Radiative Transfer. New York: Dover Publications.

Chatterjee, A., Milton, R.C. and Thyle, S. (1982) 'Prevalence and aetiology of cataract in Punjab.', The British Journal of Ophthalmology, 66(1), pp. 35–42. Available at: https://doi.org/10.1136/bjo.66.1.35.

Chen, P. et al. (2010) 'Meta-analysis of vitamin D, calcium and the prevention of breast cancer.', Breast Cancer Research and Treatment, 121(2), pp. 469–477. Available at: https://doi.org/10.1007/s10549-009-0593-9.

Cheng, I. et al. (2015) 'An Observational Study of Personal Ultraviolet Dosimetry and Acute Diffuse Reflectance Skin Changes at Extreme Altitude', Wilderness & Environmental Medicine, 24(4), pp. 390–396. Available at: https://doi.org/10.13140/RG.2.1.4098.0646.

Chmielinski, M. (2022) Source Code for the Arduino Controller of the Ocean Insight Flame-Spectroradiometer, Github. Available at: https://github.com/mxchml/Flame-Spectrocontroller (Accessed: 1 August 2022).

Chmielinski, M. et al. (2018) 'Measuring Worker Exposures to Bulb Generated Ultraviolet Radiation in the Cannabis Industry', in American Industrial Hygiene Conference and Exposition (AIHce). Philadelphia.

Chmielinski, M. et al. (2022) 'Wearable Spectroradiometer for Dosimetry', Sensors, 22(22). Available at: https://doi.org/10.3390/s22228829.

Chodick, G. et al. (2008) 'Agreement between diary records of time spent outdoors and personal ultraviolet radiation dose measurements', Photochemistry and Photobiology, 84(3), pp. 713–718. Available at: https://doi.org/10.1111/j.1751-1097.2007.00236.x.

Chorley, A. et al. (2014) 'Measurements of pilots' occupational solar UV exposure', Photochemistry and Photobiology, 90(4), pp. 935-940 Available at: https://doi.org/10.1111/php.12269.

Chorley, A.C. et al. (2016) 'Occupational Ocular UV Exposure in Civilian Aircrew', Aerospace Medicine and Human Performance, 87(1), pp. 32–39. Available at: https://doi.org/10.3357/AMHP.4404.2016.

Chou, B.R. and Cullen, A.P. (1996) 'Ocular Hazards of Industrial Spot Welding', Optometry and Vision Science, 73(6). Available at: https://doi.org/10.1097/00006324-199606000-00011.

Christensen, T. (2005) 'Protection against ultraviolet and visible radiation use in medical therapy', Perinatology, 7(1), pp. 43–48. Available at: https://www.scopus.com/inward/record.uri?eid=2-s2.0-22944467467&partnerID=40&md5=44e5529d1a24733bb330e2e559260324.

Chubarova, N.E. et al. (2011) 'Aerosol and radiation characteristics of the atmosphere during forest and peat fires in 1972, 2002, and 2010 in the region of Moscow', Izvestiya, Atmospheric and Oceanic Physics, 47(6), pp. 729–738. Available at: https://doi.org/10.1134/S0001433811060028.

Coblentz, W.W., Stair, R. and Hogue, J.M. (1931) 'The Spectral Erythemic Reaction of the Human Skin to Ultra-Violet Radiation', Proceedings of the National Academy of Sciences of the United States of America, 17(6), pp. 401–405. Available at: http://www.jstor.org/stable/86213.

Cockell, C. et al. (2002) ‘Human exposure to ultraviolet radiation at the Antipodes – a comparison between an Antarctic and Arctic location’, Polar Biology, 25, pp. 492–499. Available at: https://doi.org/10.1007/s00300-002-0381-z.

Cockell, C.S. et al. (2001) ‘Exposure of arctic field scientists to ultraviolet radiation evaluated using personal dosimeters’, Photochemistry and Photobiology, 74(4), pp. 570–578. Available at: https://doi.org/10.1562/0031-8655(2001)074<0570:EOAFST>2.0.CO;2.

Cohen, S. and Fuchs, M. (1987) ‘The distribution of leaf area, radiation, photosynthesis and transpiration in a Shamouti orange hedgerow orchard. Part I. Leaf area and radiation’, Agricultural and Forest Meteorology, 40(2), pp. 123–144. Available at: https://doi.org/https://doi.org/10.1016/0168-1923(87)90002-5.

Colaizzi, P.D., Evett, S.R., et al. (2012) ‘Radiation Model for Row Crops: I. Geometric View Factors and Parameter Optimization’, Agronomy Journal, 104(2), pp. 225–240. Available at: https://doi.org/https://doi.org/10.2134/agronj2011.0082.

Colaizzi, P.D., Schwartz, R.C., et al. (2012) ‘Radiation Model for Row Crops: II. Model Evaluation’, Agronomy Journal, 104(2), pp. 241–255. Available at: https://doi.org/10.2134/agronj2011.0083.

Coleman, A. et al. (2010) ‘A survey of the optical hazards associated with hospital light sources with reference to the Control of Artificial Optical Radiation at Work Regulations 2010’, Journal of Radiological Protection, 30(3), p. 469. Available at: https://doi.org/10.1088/0952-4746/30/3/004.

Collman, G.W. et al. (1988) ‘Sunlight and other risk factors for cataracts: an epidemiologic study.’, American Journal of Public Health, 78(11), pp. 1459–1462. Available at: https://doi.org/10.2105/ajph.78.11.1459.

CONXWAN (2022) CONXWAN 18W Battery Pack, Amazon Store. Available at: https://www.amazon.com/Portable-Charger-26800mAh-Capacity-External/dp/B08729Z2JX.

Couch, J. et al. (2017) ‘Evaluation of Potential Hazards during Harvesting and Processing Cannabis at an Outdoor Organic Farm’, Health Hazard Evaluation Report No. 2015-0111-3271. Available at: https://www.cdc.gov/niosh/hhe/reports/pdfs/2015-0111-3271.pdf. (Accessed: 18 April 2023).

Couch, J.R. et al. (2020) ‘Review of NIOSH Cannabis-Related Health Hazard Evaluations and Research’, Annals of Work Exposures and Health, 64(7), pp. 693–704. Available at: https://doi.org/10.1093/annweh/wxaa013.

Couch, J.R., Burton, N.C., Victory, K.R., Green, B.J., Lemons, A.R., Nayak, A.P. and Beezhold, Donald H. (2019) ‘Endotoxin exposures during harvesting and processing cannabis at an outdoor cannabis farm’, Aerobiologia, 35(2), pp. 367–371. Available at: https://doi.org/10.1007/s10453-018-09552-0.

Couch, J.R., Grimes, G.R., et al. (2019) ‘Potential occupational and respiratory hazards in a Minnesota cannabis cultivation and processing facility’, American Journal of Industrial Medicine, 62(10), pp. 874–882. Available at: https://doi.org/10.1002/ajim.23025.

Cullen, A. (2002) ‘Photokeratitis and Other Phototoxic Effects on the Cornea and Conjunctiva’, International Journal of Toxicology, 21, pp. 455–464. Available at: https://doi.org/10.1080/10915810290169882.

Cust, A.E. et al. (2018) ‘Validation of Questionnaire and Diary Measures of Time Outdoors Against an Objective Measure of Personal Ultraviolet Radiation Exposure’, Photochemistry and Photobiology, 94(4), pp. 815–820. Available at: https://doi.org/10.1111/php.12893.

Dadvand, P. et al. (2011) ‘Measurement errors in the assessment of exposure to solar ultraviolet radiation and its impact on risk estimates in epidemiological studies.’, Photochemical & Photobiological Sciences: Official Journal of the European Photochemistry Association and the European Society for Photobiology, 10(7), pp. 1161–1168. Available at: https://doi.org/10.1039/c0pp00333f.

Damian, D.L., Barnetson, R.S. and Halliday, G.M. (2001) ‘Effects of low-dose ultraviolet radiation on in vivo human cutaneous recall responses.’, The Australasian Journal of Dermatology, 42(3), pp. 161–167. Available at: https://doi.org/10.1046/j.1440-0960.2001.00507.x.

Daughtry, C.S.T. and Walthall, C.L. (1998) ‘Spectral Discrimination of Cannabis Sativa L. Leaves and Canopies’, Remote Sensing of Environment, 64(2), pp. 192–201. Available at: https://doi.org/10.1016/S0034-4257(98)00002-9.

Davidson, M. et al. (2018) ‘Occupational health and safety in cannabis production: an Australian perspective’, International Journal of Occupational and Environmental Health, 24(3–4), pp. 75–85. Available at: https://doi.org/10.1080/10773525.2018.1517234.

Dawe, R.S. and Ibbotson, S.H. (2014) ‘Drug-induced photosensitivity.’, Dermatologic Clinics, 32(3), pp. 363–8, ix. Available at: https://doi.org/10.1016/j.det.2014.03.014.

de Paula Corrêa, M. and C.M. Pires, L. (2013) ‘Doses of erythemal ultraviolet radiation observed in Brazil’, International Journal of Dermatology, 52(8), pp. 966–973. Available at: https://doi.org/10.1111/j.1365-4632.2012.05834.x.

Decuyper, I.I. et al. (2020) ‘Occupational Allergies to Cannabis’, The Journal of Allergy and Clinical Immunology: In Practice, 8(10), pp. 3331–3338. Available at: https://doi.org/https://doi.org/10.1016/j.jaip.2020.09.003.

DeV., A.G. (1965) ‘Pterygium Throughout the World.’, Archives of Ophthalmology, 74(2), p. 288. Available at: https://doi.org/10.1001/archopht.1965.00970040290034.

di Sarra, A. et al. (2002) ‘Effects of desert dust and ozone on the ultraviolet irradiance at the Mediterranean island of Lampedusa during PAUR II’, Journal of Geophysical Research: Atmospheres, 107(D18), p. PAU 2-1-PAU 2-14. Available at: https://doi.org/10.1029/2000JD000139.

Dibowski, G. and Esser, K. (2017) ‘Hazards Caused by UV Rays of Xenon Light Based High Performance Solar Simulators’, Safety and Health at Work, 8(3), pp. 237–245. Available at: https://doi.org/10.1016/J.SHAW.2016.12.002.

Dickerson, R., Stenchikov, G. and Civerolo, K. (1997) 'The impact of aerosol on solar UV radiation and photochemical smog Radiation and Photochemical Smog', Science. Available at: https://doi.org/10.1126/science.278.5339.827.

Diffey, B. (2008) 'A Behavioral Model for Estimating Population Exposure to Solar Ultraviolet Radiation', Photochemistry and Photobiology, 84(2), pp. 371–375. Available at: https://doi.org/https://doi.org/10.1111/j.1751-1097.2007.00271.x.

Diffey, B. et al. (1986) 'Personal monitoring of exposure to ultraviolet radiation in the car manufacturing industry', Annals of Occupational Hygiene, 30(2), pp. 163–170. Available at: https://doi.org/10.1093/annhyg/30.2.163.

Diffey, B.L. (1992) 'Stratospheric ozone depletion and the risk of non-melanoma skin cancer in a British population', Physics in Medicine and Biology, 37(12), pp. 2267–2279. Available at: https://doi.org/10.1088/0031-9155/37/12/008.

Diffey, B.L. (2002) 'Sources and measurement of ultraviolet radiation', Methods, 28(1), pp. 4–13. Available at: https://doi.org/10.1016/S1046-2023(02)00204-9.

Diffey, B.L. and Saunders, P.J. (1995) 'Behavior outdoors and its effects on personal ultraviolet exposure rate measured using and ambulatory datalogging dosimeter', Photochemistry and Photobiology, 61(6), pp. 615–618. Available at: https://doi.org/10.1111/j.1751-1097.1995.tb09877.x.

Dornelles, K. et al. (2010) 'Spectral behaviour of cool paints produced in Brazil for roof paint and their impact on the thermal comfort and energy use in buildings designed for hot climates', in Adapting to Change: New Thinking on Comfort. Windsor. Available at: https://doi.org/10.13140/RG.2.1.4104.8802.

Dowdy, J.C. and Sayre, R.M. (2013) 'Photobiological Safety Evaluation of UV Nail Lamps', Photochemistry and Photobiology, 89(4), pp. 961–967. Available at: https://doi.org/10.1111/php.12075.

Dowdy, J.C. and Sayre, R.M. (2015) 'Nail curing UV lamps: Trivial exposure not cause for public alarm.', Journal of the American Academy of Dermatology, 73(5), pp. 185–6. Available at: https://doi.org/10.1016/j.jaad.2015.06.064.

Downs, N. et al. (2008) 'Modelling ultraviolet exposures in a school environment', Photochemical & Photobiological Sciences, 7(6), pp. 700–710. Available at: https://doi.org/10.1039/B801685B.

Downs, N., Harrison, S. and Parisi, A. (2015) 'Queensland Teacher Sun Survey: Measurements and Procedures for Recording Occupational UV Exposures in Townsville and Toowoomba', Annals of the Australasian College of Tropical Medicine, 16(2). Available at: https://research.usq.edu.au/item/q31y8/queensland-teacher-sun-survey-measurements-and-procedures-for-recording-occupational-uv-exposures-in-townsville-and-toowoomba (Accessed: 18 April 2023).

Downs, N.J. et al. (2009) 'Measurements of the upper body ultraviolet exposure to golfers: Non-melanoma skin cancer risk, and the potential benefits of exposure to sunlight', Photodermatology Photoimmunology and Photomedicine, 25(6), pp. 317–324. Available at: https://doi.org/10.1111/j.1600-0781.2009.00472.x.

Downs, N.J. et al. (2016) ‘Solar ultraviolet and the occupational radiant exposure of Queensland school teachers: A comparative study between teaching classifications and behavior patterns’, Journal of Photochemistry and Photobiology B: Biology, 158, pp. 105–112. Available at: https://doi.org/10.1016/J.JPHOTOBIOL.2016.02.018.

Downs, N.J., Parisi, A. V and Igoe, D. (2014) ‘Measurements of occupational ultraviolet exposure and the implications of timetabled yard duty for schoolteachers in Queensland, Australia: Preliminary results’, Journal of Photochemistry and Photobiology B: Biology, 131, pp. 84–89. Available at: https://doi.org/https://doi.org/10.1016/j.jphotobiol.2014.01.012.

Dubois, M.-C. (2001) Impact of shading devices on daylight quality in offices - Simulations with radiance. Lund Institute of Technology. Available at: https://www.lth.se/fileadmin/byggnadskonstruktion/publications/Report3062.pdf (Accessed: 31 March 2023).

Dumyahn, T. and First, M. (1999) ‘Characterization of Ultraviolet Upper Room Air Disinfection Devices’, American Industrial Hygiene Association Journal, 60(2), pp. 219–227. Available at: https://doi.org/10.1080/00028899908984439.

Duncan, D.D. et al. (1997) ‘Visible and ultraviolet-B ocular-ambient exposure ratios for a general population. Salisbury Eye Evaluation Project Team.’, Investigative Ophthalmology & Visual Science, 38(5), pp. 1003–1011.

Ehrlich, T., Simpson, C. and Busch Isaksen, T. (2020) ‘Sociopolitical Externalities Impacting Worker Health in Washington State’s Cannabis Industry’, Annals of Work Exposures and Health, 64(7), pp. 683–692. Available at: https://doi.org/10.1093/annweh/wxz083.

Ellingson, O.L. (1986) ‘The characterization of a black light device: a hazard evaluation process’, American Industrial Hygiene Association Journal, 47(8), pp. 488–490. Available at: https://doi.org/10.1080/15298668691390089.

Eltis, M. (2011) ‘Pingueculae and their clinical implications’, Clinical and Refractive Optometry, 22, pp. 10–13. Available at: https://www.researchgate.net/publication/287883966_Pingueculae_and_their_clinical_implications (Accessed: 16 April 2023).

Engel, A., Johnson, M.L. and Haynes, S.G. (1988) ‘Health effects of sunlight exposure in the United States. Results from the first National Health and Nutrition Examination Survey, 1971-1974.’, Archives of Dermatology, 124(1), pp. 72–79.

Eriksen, P. et al. (1987) ‘Optical hazard evaluation of dental curing lights*’, Community Dentistry and Oral Epidemiology, 15(4), pp. 197–201. Available at: https://doi.org/10.1111/j.1600-0528.1987.tb00518.x.

Erlendsson, Ö. (2014) Daylight optimization: A parametric study of atrium design. Lisans Tezi: School of Architecture and the Built Environment. Available at: http://kth.divaportal.org/smash/get/diva2:723644/FULLTEXT01.pdf (Accessed: 31 March 2023).

Evoy, R. and Kincl, L. (2020) ‘Evaluation of Pesticides Found in Oregon Cannabis from 2016 to 2017’, Annals of Work Exposures and Health, 64(7), pp. 770–774. Available at: https://doi.org/10.1093/annweh/wxz075.

Eykelbosh, A. (2018) ‘Cannabis Legalization and Environmental Health’, in NCCEH Environmental Health Seminar Series. National Collaborating Centre for Environmental Health.

Faison, C. and Brickenkamp, C. (2001) ‘NIST Handbook 150-2E National Voluntary Laboratory Accreditation Program Calibration Laboratories Technical Guide for Optical Radiation Measurements’. Handbook (NIST HB), National Institute of Standards and Technology, Gaithersburg, MD. Available at: https://tsapps.nist.gov/publication/get_pdf.cfm?pub_id=905613.

Fantozzi, F. et al. (2017) ‘Risk assessment arising from exposure to artificial optical radiation: Results of an extensive evaluation campaign in the hospitals of Tuscany (Italy)’, 2017 IEEE International Conference on Environment and Electrical Engineering and 2017 IEEE Industrial and Commercial Power Systems Europe (EEEIC / I&CPS Europe). Available at: https://doi.org/10.1109/EEEIC.2017.7977447.

Farag, S. and Kayser, O. (2017) ‘The Cannabis Plant: Botanical Aspects’, in V.R. Preedy (ed.) Handbook of Cannabis and Related Pathologies. San Diego: Academic Press, pp. 3–12. Available at: https://doi.org/https://doi.org/10.1016/B978-0-12-800756-3.00001-6.

Fartasch, M. et al. (2012) ‘The relationship between occupational sun exposure and non-melanoma skin cancer: clinical basics, epidemiology, occupational disease evaluation, and prevention.’, Deutsches Arzteblatt International, 109(43), pp. 715–720. Available at: https://doi.org/10.3238/arztebl.2012.0715.

Feister, U. et al. (2015) ‘Validation of modeled daily erythemal exposure along tropical and subtropical shipping routes by ship-based and satellite-based measurements’, Journal of Geophysical Research: Atmospheres Research, 120(9), pp. 4117–4131. Available at: https://doi.org/10.1002/2014JD023005.Received.

Feister, U., Meyer, G. and Kirst, U. (2013) ‘Solar UV exposure of seafarers along subtropical and tropical shipping Routes’, Photochemistry and Photobiology, 89(6), pp. 1497–1506. Available at: https://doi.org/10.1111/php.12144.

Fioletov, V.E. et al. (1998) ‘Influence of volcanic sulfur dioxide on spectral UV irradiance as measured by Brewer Spectrophotometers’, Geophysical Research Letters, 25(10), pp. 1665–1668. Available at: https://doi.org/10.1029/98GL51305.

Fioletov, V.E. et al. (2001) ‘Long-term variations of UV-B irradiance over Canada estimated from Brewer observations and derived from ozone and pyranometer measurements’, Journal of Geophysical Research: Atmospheres, 106(D19), pp. 23009–23027. Available at: https://doi.org/10.1029/2001JD000367.

Fioletov, V.E. et al. (2010) ‘Estimated ultraviolet exposure levels for a sufficient vitamin D status in North America’, Journal of Photochemistry and Photobiology B: Biology, 100(2), pp. 57–66. Available at: https://doi.org/10.1016/j.jphotobiol.2010.05.002.

Firnhaber, J.M. (2012) ‘Diagnosis and Treatment of Basal Cell and Squamous Cell Carcinoma’, American Family Physician, 86(2), pp. 161–168.

First, M.W. et al. (2005) ‘Monitoring human exposures to upper-room germicidal ultraviolet irradiation’, Journal of Occupational and Environmental Hygiene, 2(5), pp. 285–292. Available at: https://doi.org/10.1080/15459620590952224.

Flesch, P. (2006) Light and Light Sources: High-Intensity Discharge Lamps. Berlin, DE: Springer. Available at: https://doi.org/10.1007/978-3-540-32685-4.

Garssen, J. et al. (1998) ‘Estimation of the effect of increasing UVB exposure on the human immune system and related resistance to infectious diseases and tumors.’, Journal of Photochemistry and Photobiology. B, Biology, 42(3), pp. 167–179. Available at: https://doi.org/10.1016/s1011-1344(97)00122-x.

Garssen, J. et al. (1999) ‘UVB exposure-induced systemic modulation of Th1- and Th2-mediated immune responses.’, Immunology, 97(3), pp. 506–514. Available at: https://doi.org/10.1046/j.1365-2567.1999.00801.x.

Geiss, O. and Rembges, D. (2003) ‘Manual for Polysulfone Dosimeters: Characterization, Handling, and Application as Personal UV Exposure Devices’, European Commission Joint Research Center, EUR 20981 EN. Available at: https://publications.jrc.ec.europa.eu/repository/bitstream/JRC26555/EUR%2020981%20EN.pdf

Ghodsian, N. (2019) ‘Health Effects of Exposure to Cannabis in Workers in an Indoor Growing Facility’, Thesis (Master’s)--University of Washington. Available at: https://digital.lib.washington.edu/researchworks/bitstream/handle/1773/44222/Ghodsian_washington_0250O_20433.pdf?sequence=1&isAllowed=y [Accessed on May 7, 2023]

Gichuhi, S. and Sagoo, M.S. (2016) ‘Squamous cell carcinoma of the conjunctiva’, Community Eye Health, 29(95), pp. 52–53. Available at: https://pubmed.ncbi.nlm.nih.gov/28289320.

Gies, H.P. et al. (1995) ‘Solar UVR Exposures of Three Groups of Outdoor Workers on the Sunshine Coast, Queensland’, Photochemistry and Photobiology, 62(6), pp. 1015–1021. Available at: https://doi.org/https://doi.org/10.1111/j.1751-1097.1995.tb02402.x.

Gies, H.P., Roy, C.R. and Elliott, G. (1985) Spectral irradiance measurements and hazard evaluations of sunbeds and sunlamps. Australian Radiation Lab. Available at: https://inis.iaea.org/collection/NCLCollectionStore/_Public/16/077/16077493.pdf?r=1 (Accessed: 17 April 2023).

Gies, P. and Wright, J. (2003) ‘Measured Solar Ultraviolet Radiation Exposures of Outdoor Workers in Queensland in the Building and Construction Industry’, Photochemistry and Photobiology, 78(4), pp. 342–348. Available at: https://doi.org/10.1562/0031-8655(2003)078<0342:MSUREO>2.0.CO;2.

Gies, P. et al. (2009) ‘Measured occupational solar UVR exposures of lifeguards in pool settings’, American Journal of Industrial Medicine, 52(8), pp. 645–653. Available at: https://doi.org/10.1002/ajim.20722.

Gijzen, H. and Goudriaan, J. (1989) ‘A flexible and explanatory model of light distribution and photosynthesis in row crops’, Agricultural and Forest Meteorology, 48(1), pp. 1–20. Available at: https://doi.org/https://doi.org/10.1016/0168-1923(89)90004-X.

Gilbert, R. et al. (2012) ‘Associations of circulating 25-hydroxyvitamin D with prostate cancer diagnosis, stage and grade.’, International Journal of Cancer, 131(5), pp. 1187–1196. Available at: https://doi.org/10.1002/ijc.27327.

Giménez, V.B. et al. (2015) ‘Maximum Incident Erythemally Effective UV Exposure Received by Construction Workers, in Valencia, Spain’, Photochemistry and Photobiology, 91(6), pp. 1505–1509. Available at: https://doi.org/10.1111/php.12530.

Glanz, K., Buller, D.B. and Saraiya, M. (2007) ‘Reducing ultraviolet radiation exposure among outdoor workers: State of the evidence and recommendations’, Environmental Health, 6(22). Available at: https://doi.org/10.1186/1476-069X-6-22.

Glassford, E. and Burr, G. (2018) ‘Evaluating optical hazards from plasma arc cutting’, Journal of Occupational and Environmental Hygiene, 15(1), pp. D1–D7. Available at: https://doi.org/10.1080/15459624.2017.1388511.

Goudriaan, J. (1977) Crop Micrometeorology: a Simulation Study. ProQuest Dissertations Publishing. Available at: https://library.wur.nl/WebQuery/wurpubs/fulltext/166537 (Accessed: 16 April 2023).

Goudriaan, J. (1988) ‘The bare bones of leaf-angle distribution in radiation models for canopy photosynthesis and energy exchange.’, Agricultural and Forest Meteorology, 43(2), pp. 155–169. Available at: https://doi.org/10.1016/0168-1923(88)90089-5.

Grandahl, K. et al. (2017) ‘Solar UV exposure among outdoor workers in Denmark measured with personal UV-B dosimeters: technical and practical feasibility’, BioMedical Engineering OnLine, 16(1), p. 119. Available at: https://doi.org/10.1186/s12938-017-0410-3.

Grandahl, K. et al. (2018) ‘Measurements of Solar Ultraviolet Radiation Exposure at Work and at Leisure in Danish Workers’, Photochemistry and Photobiology, 94(4), pp. 807–814. Available at: https://doi.org/10.1111/php.12920.

Grandview Research (2022) Grow Light Market Analysis By Application (Indoor Farming, Vertical Farming, Commercial Greenhouse). San Francisco. Available at: www.grandviewresearch.com/industry-analysis/grow-light-market (Accessed: 5 February 2023).

Green, B.J. et al. (2018) ‘Microbial hazards during harvesting and processing at an outdoor United States cannabis farm.’, Journal of Occupational and Environmental Hygiene, 15(5), pp. 430–440. Available at: https://doi.org/10.1080/15459624.2018.1432863.

Green, G. (2010) The Cannabis Grow Bible. 2nd ed. Green Candy Press.

Gugg-Helminger, A. (2017) ‘CIE 220:2016-Characterization and Calibration Method of UV Radiometers’, IUVA News, 19(2), pp. 18–23. Available at: www.gigahertz-optik.de.

Guo, S. et al. (2014) ‘Sun exposure and vitamin D status as northeast Asian migrants become acculturated to life in Australia’, Photochemistry and Photobiology, 90(6), pp. 1455–1461. Available at: https://doi.org/10.1111/php.12349.

Guy, C.Y. and Diab, R.D. (2002) ‘A Health Risk Assessment of Ultraviolet Radiation in Durban’, South African Geographical Journal, 84(2), pp. 208–213. Available at: https://doi.org/10.1080/03736245.2002.9713772.

Harris D. (2006) Quantitative Chemical Analysis (7th ed.). W. H. Freeman. ISBN: 9780716766827

Hart, P.H. and Norval, M. (2018) ‘Ultraviolet radiation-induced immunosuppression and its relevance for skin carcinogenesis.’, Photochemical & Photobiological Sciences : Official journal of the European Photochemistry Association and the European Society for Photobiology, 17(12), pp. 1872–1884. Available at: https://doi.org/10.1039/c7pp00312a.

Hatori, M. et al. (2017) ‘Global rise of potential health hazards caused by blue light-induced circadian disruption in modern aging societies’, Aging and Mechanisms of Disease, 3(1). Available at: https://doi.org/10.1038/s41514-017-0010-2.

Hausser, K.W. (1928) ‘Influence of wavelength in radiation biology’, Strahlentherapie, (28), pp. 25–44.

Hawes, M. and Cohen, M. (2013) ‘Method of drying cannabis materials’, USPTO. USA: United States Patent and Trademark Office. Available at: https://patents.google.com/patent/US20150096189A1/en (Accessed: 16 April 2023).

Herbert, H. (2007) ‘Polymorphous light eruption’, Photodermatology, Photoimmunology & Photomedicine, 24(2007), pp. 155–161. Available at: https://doi.org/10.1111/j.1600-0781.2008.00343.x.

Herlihy, E. et al. (1994) ‘Personal dosimetry of solar UV radiation for different outdoor activities’, Photochemistry and Photobiology, 60(3), pp. 288–294. Available at: https://doi.org/10.1111/j.1751-1097.1994.tb05106.x.

Herrmann, I., Karmieli, A. and Yermiyah, U. (2014) ‘Fresh and Dry Pepper Leaf Spectra with Associated Potassium and Nitrogen Measurements.’, Ecological Spectral Information System. Available at: https://ecosis.org/package/fresh-and-dry-pepper-leaf-spectra-with-associatedpotassium-and-nitrogen-measurements (Accessed: 10 January 2023).

Herzinger, T. et al. (2011) ‘IgE-Mediated Hypersensitivity Reactions to Cannabis in Laboratory Personnel’, International Archives of Allergy and Immunology, 156, pp. 423–426. Available at: https://doi.org/10.1159/000324444.

Heuvelink, E. et al. (2006) ‘Horticultural Lighting in the Netherlands : New Developments’, Acta Horticulturae, 711(1), pp. 25–34. Available at: https://doi.org/10.17660/ActaHortic.2006.711.1.

HiLetgo (2022) SPI TFT LCD Display Touch Panel ILI9341. Available at: http://www.hiletgo.com/ProductDetail/2157216.html (Accessed: 31 May 2022).

Hiller, R., Giacometti, L. and Yuen, K. (1977) ‘Sunlight and cataract: an epidemiologic investigation’, American Journal of Epidemiology, 105(5), pp. 450–459. Available at: https://doi.org/10.1093/oxfordjournals.aje.a112404.

HORIBA (2020) Introduction to the detectors techniques. Available at: https://www.horiba.com/en_en/technology/measurement-and-control-techniques/spectroscopy/detectors/.

Hosgood, B. et al. (1995) ‘Leaf optical properties experiment 93 (LOPEX93)’, Report EUR,16095. Available at: https://data.ecosis.org/dataset/13aef0ce-dd6f-4b35-91d9-28932e506c41/resource/4029b5d3-2b84-46e3-8fd8-c801d86cf6f1/download/leaf-opticalproperties-experiment-93-lopex93.pdf (Accessed: 31 March 2023).

Howard, J. and Osborne, J. (2020) ‘Cannabis and work: Need for more research’, American Journal of Industrial Medicine, 63(11), pp. 963–972.

Hoy, W.E. (1996) ‘Nonmelanoma skin carcinoma in Albuquerque, New Mexico: experience of a major health care provider.’, Cancer, 77(12), pp. 2489–2495. Available at: https://doi.org/10.1002/(SICI)1097-0142(19960615)77:12<2489::AID-CNCR11>3.0.CO;2-O.

Huché-Thélier, L. et al. (2016) ‘Light signaling and plant responses to blue and UV radiations — Perspectives for applications in horticulture’, Environmental and Experimental Botany, 121, pp. 22–38. Available at: https://doi.org/10.1016/j.envexpbot.2015.06.009.

Ichihashi, M. et al. (2003) ‘UV-induced skin damage’, Toxicology, 189(1–2), pp. 21–39. Available at: https://doi.org/10.1016/S0300-483X(03)00150-1.

Idorn, L.W. et al. (2013) ‘Sun behavior after cutaneous malignant melanoma: A study based on ultraviolet radiation measurements and sun diary data’, British Journal of Dermatology, 168(2), pp. 367–373. Available at: https://doi.org/10.1111/bjd.12066.

Idorn, L.W. et al. (2014) ‘A 3-year follow-up of sun behavior in patients with cutaneous malignant melanoma’, JAMA Dermatology, 150(2), pp. 163–168. Available at: https://doi.org/10.1001/jamadermatol.2013.5098.

Jackson, J.E. and Palmer, J.W. (1972) ‘Interception of light by model hedgerow orchards in relation to latitude, time of year and hedgerow configuration and orientation’, Journal of Applied Ecology, 9(2), pp. 341–357. Available at: https://doi.org/10.2307/2402436.

Jackson, S. and Storey, A. (2000) ‘E6 proteins from diverse cutaneous HPV types inhibit apoptosis in response to UV damage.’, Oncogene, 19(4), pp. 592–598. Available at: https://doi.org/10.1038/sj.onc.1203339.

Jackson, S.A. (1980) ‘A film badge dosimeter for UVA radiation.’, Journal of Biomedical Engineering, 2(1), pp. 63–64. Available at: https://doi.org/10.1016/0141-5425(80)90095-3.

Jacquemound, S. et al. (2003) ‘ANGERS Leaf Optical Properties Database’, Ecological Spectral Information System. Available at: https://ecosis.org/package/angers-leaf-optical-propertiesdatabase--2003- (Accessed: 10 January 2023).

Jagger, J. (1985) Solar-UV actions on living cells. United States: Praeger Publishers. Available at: http://inis.iaea.org/search/search.aspx?orig_q=RN:20015429.

Jokela, K. et al. (1995) ‘Increased UV Exposure in Finland in 1993’, Photochemistry and Photobiology, 62(1), pp. 101–107. Available at: https://doi.org/10.1111/j.1751-1097.1995.tb05245.x.

Josefsson, W. and Landelius, T. (2000) ‘Effect of clouds on UV irradiance: As estimated from cloud amount, cloud type, precipitation, global radiation and sunshine duration’, Journal of Geophysical Research: Atmospheres, 105(D4), pp. 4927–4935. Available at: https://doi.org/10.1029/1999JD900255.

Kambayashi, H. et al. (2001) ‘Epidermal changes caused by chronic low-dose UV irradiation induce wrinkle formation in hairless mouse.’, Journal of Dermatological Science, 27 Suppl 1, pp. S19-25. Available at: https://doi.org/10.1016/s0923-1811(01)00113-x.

Kang, S. et al. (2022) Fitzpatrick’s Dermatology in General Medicine. 9e ed. New York, NY: McGraw-Hill Health Professionals Division.

Ke, H. et al. (2018) ‘Study on the chromaticity of LED lamps given by online test during accelerated aging under thermal stress’, Optik, 164, pp. 510–518. Available at: https://doi.org/10.1016/j.ijleo.2018.02.120.

Kenleigh, D. (2022) ‘Cannabis Allergy in Occupationally Exposed Cannabis Workers, Recreational Users and Non-Users’, Thesis (Master’s)--University of Washington.

Kerr, A. and Ferguson, J. (2010) ‘Photoallergic contact dermatitis’, Photodermatology, Photoimmunology & Photomedicine, 26(1), pp. 56–65.

Kerr, J.B. and Fioletov, V.E. (2008) ‘Surface ultraviolet radiation’, Atmosphere-Ocean, 5900(June), pp. 159–184. Available at: https://doi.org/10.3137/ao.460108.

Khazova, M. and O’Hagan, J.B. (2008) ‘Optical radiation emissions from compact fluorescent lamps’, Radiation Protection Dosimetry, 131(4), pp. 521–525. Available at: https://doi.org/10.1093/rpd/ncn234.

Kim, S.-H. and Lieth, J.H. (2002) ‘Modeling photosynthesis of heterogeneous rose crop canopies in the greenhouse’, Acta horticulturae, 593, pp. 121–128. Available at: https://doi.org/10.17660/ActaHortic.2002.593.15.

Kimlin, M G et al. (2002) ‘Understanding the UVA environment at a sub-tropical site and its consequent impact on human UVA exposure’, Photochemical and Photobiological Sciences, 1(7), pp. 478–482. Available at: https://doi.org/10.1039/b200844k.

Kimlin, M. and Parisi, A. (2001) ‘Usage of real-time ultraviolet radiation data to modify the daily erythemal exposure of primary schoolchildren’, Photodermatology, Photoimmunology &

Photomedicine, 17(3), pp. 130–135. Available at: https://doi.org/https://doi.org/10.1034/j.1600-0781.2001.170305.x.

Kimlin, M. G. et al. (2002) 'Comparison of the solar spectral ultraviolet irradiance in motor vehicles with windows in an open and closed position', International Journal of Biometeorology, 46(3), pp. 150–156. Available at: https://doi.org/10.1007/s00484-002-0131-5.

Kimlin, M.G. and Parisi, A. V (1999) 'Ultraviolet radiation penetrating vehicle glass: A field based comparative study', Physics in Medicine and Biology, 44(4), pp. 917–926. Available at: https://doi.org/10.1088/0031-9155/44/4/008.

Kimlin, M.G. et al. (2006) 'Anatomical distribution of solar ultraviolet exposures among cyclists', Journal of Photochemistry and Photobiology B: Biology, 85(1), pp. 23–27. Available at: https://doi.org/https://doi.org/10.1016/j.jphotobiol.2006.04.004.

Kimlin, M.G. et al. (2019) 'Personal ultraviolet Radiation exposure in a cohort of Chinese mother and child pairs: The Chinese families and children study 11 Medical and Health Sciences 1117 Public Health and Health Services', BMC Public Health, 19(1). Available at: https://doi.org/10.1186/s12889-019-6610-y.

Kimlin, M.G., Parisi, A. V and Wong, J.C.F. (1999) 'Home Workers and Ultraviolet Radiation Exposure', in Proceedings of the 2nd Internet Conference on Photochemistry and Photobiology.

Kimlin, M.G., Parisi, A. V. and Wong, J.C.F. (1998) 'Quantification of personal solar UV exposure of outdoor workers, indoor workers and adolescents at two locations in Southeast Queensland', Photodermatology Photoimmunology and Photomedicine, 14(1), pp. 7–11. Available at: https://doi.org/10.1111/j.1600-0781.1998.tb00002.x.

Kirchhoff, V.W.J.H. et al. (2001) 'UV-B optical thickness observations of the atmosphere', Journal of Geophysical Research: Atmospheres, 106(D3), pp. 2963–2973. Available at: https://doi.org/10.1029/2000JD900506.

Klein, R.S. et al. (2009) 'Analysis of compact fluorescent lights for use by patients with photosensitive conditions', Photochemistry and Photobiology, 85(4), pp. 1004–1010. Available at: https://doi.org/10.1111/j.1751-1097.2009.00540.x.

Knuschke, P. and Barth, J. (1996) 'Biologically weighted personal UV dosimetry', Journal of Photochemistry and Photobiology B: Biology, 36(1), pp. 77–83. Available at: https://doi.org/10.1016/1011-1344(95)07223-3.

Koronakis, P.S. et al. (2002) 'Interrelations of UV-global/global/diffuse solar irradiance components and UV-global attenuation on air pollution episode days in Athens, Greece', Atmospheric Environment, 36(19), pp. 3173–3181. Available at: https://doi.org/https://doi.org/10.1016/S1352-2310(02)00233-9.

Køster, B. et al. (2017) 'The validated sun exposure questionnaire: association of objective and subjective measures of sun exposure in a Danish population-based sample', British Journal of Dermatology, 176(2), pp. 446–456. Available at: https://doi.org/10.1111/bjd.14861.

Kothari, S. et al. (2022) ‘CABO 2018-2019 Leaf-Level Spectra. Dataset.’, Ecological Spectral Information System. Available at: https://ecosis.org/package/cabo-2018-2019-leaf-level-spectra (Accessed: 10 January 2023).

Kozai, T., Fujiwara, K. and Runkle, E.S. (2016) LED Lighting for Urban Agriculture. Available at: https://doi.org/DOI 10.1007/978-981-10-1848-0.

Kricker, A. et al. (1995) ‘Does intermittent sun exposure cause basal cell carcinoma? a case-control study in Western Australia.’, International Journal of Cancer, 60(4), pp. 489–494. Available at: https://doi.org/10.1002/ijc.2910600411.

Kripke, M.L. and Fisher, M.S. (1976) ‘Immunologic parameters of ultraviolet carcinogenesis.’, Journal of the National Cancer Institute, 57(1), pp. 211–215. Available at: https://doi.org/10.1093/jnci/57.1.211.

Krueger, A.J. et al. (1995) ‘Volcanic sulfur dioxide measurements from the total ozone mapping spectrometer instruments’, Journal of Geophysical Research: Atmospheres, 100(D7), pp. 14057–14076. Available at: https://doi.org/https://doi.org/10.1029/95JD01222.

Kuusk, A. et al. (2018) Canopy Radiative Transfer Modeling, Comprehensive Remote Sensing. Elsevier. Available at: https://doi.org/10.1016/B978-0-12-409548-9.10534-2.

Langford, I.H., Bentham, G. and McDonald, A.-L. (1998) ‘Multi-level modelling of geographically aggregated health data: a case study on malignant melanoma mortality and UV exposure in the European Community’, Statistics in Medicine, 17(1), pp. 41–57. Available at: https://doi.org/10.1002/(SICI)1097-0258(19980115)17:1<41::AID-SIM712>3.0.CO;2-0.

Larko, O and Diffey, B.L. (1983) ‘Natural UV-B radiation received by people with outdoor, indoor, and mixed occupations and UV-B treatment of psoriasis’, Clinical and Experimental Dermatology, 8(3), pp. 279–285. Available at: https://doi.org/https://doi.org/10.1111/j.1365-2230.1983.tb01780.x.

Lazarjani, M.P. et al. (2021) ‘Processing and extraction methods of medicinal cannabis: a narrative review’, Journal of Cannabis Research, 3(1), p. 32. Available at: https://doi.org/10.1186/s42238-021-00087-9.

Leach, J.F. et al. (1978) ‘Measurement of the ultraviolet doses received by office workers’, Clinical and Experimental Dermatology, 3(1), pp. 77–79. Available at: https://doi.org/10.1111/j.1365-2230.1978.tb01463.x.

Lee, Jin-Duk et al. (2012) ‘Analysis of Concrete Reflectance Characteristics Using Spectrometer and VNIR Hyperspectral Camera’, International Archives of the Photogrammetry, Remote Sensing and Spatial Information Sciences, pp. 127–130. Available at: https://doi.org/10.5194/isprsarchives-XXXIX-B7-127-2012.

Lekalakala, P. et al. (2015) ‘Oculocutaneous Albinism and Squamous Cell Carcinoma of the Skin of the Head and Neck in Sub-Saharan Africa’, Journal of Skin Cancer, 2015, p. 167847. Available at: https://doi.org/10.1155/2015/167847.

Li, D.H.W., Lau, C.C.S. and Lam, J.C. (2004) 'Predicting daylight illuminance by computer simulation techniques', Lighting Research & Technology, 36(2), pp. 113–129. Available at: https://doi.org/10.1191/1365782804li108oa.

Liljendahl, T.S. et al. (2012) 'Quantification of ultraviolet radiation-induced DNA damage in the urine of Swedish adults and children following exposure to sunlight', Biomarkers, 17(7), pp. 634–641. Available at: https://doi.org/10.3109/1354750X.2012.709881.

Liljendahl, T.S. et al. (2013) 'Urinary levels of thymine dimer as a biomarker of exposure to ultraviolet radiation in humans during outdoor activities in the summer', Mutagenesis, 28(3), pp. 249–256. Available at: https://doi.org/10.1093/mutage/ges077.

Lio, A. and Ito, A. (2014) 'A Global Database of Field-observed Leaf Area Index in Woody Plant Species', Oak Ridge National Laboratory Distributed Active Archive Center. Oak Ridge, Tennessee, USA. Available at: https://doi.org/http://dx.doi.org/10.3334/ORNLDAAC/1231.

Logue, M.E. and Zlotoff, B.J. (2015) 'Reflections on smart phones, tablets, and ultraviolet (UV) light: Should we worry? An observational study', Journal of the American Academy of Dermatology, 73(3), pp. 526–528. Available at: https://doi.org/10.1016/j.jaad.2015.06.027.

Lu, N. and Mitchell, C. (2016) 'Supplemental Lighting for Greenhouse Grown Fruiting Vegetables', in LED Lighting for Urban Agriculture, pp. 219–230.

Lucas, R. (2010) Environmental Burden of Disease Series, No. 17 - Solar Ultraviolet Radiation. World Health Organization. Available at: https://apps.who.int/iris/handle/10665/339523 (Accessed: 16 April 2023).

Mackenzie, F.D. et al. (1992) 'Risk Analysis in the Development of Pterygia', Ophthalmology, 99(7), pp. 1056–1061. Available at: https://doi.org/https://doi.org/10.1016/S0161-6420(92)31850-0.

Mackenzie, L.A. and Bell, F.W. (1973), The construction and development of a grating monochromator and its application to the study of the reaction of the skin to light. British Journal of Dermatology, 89(3), pp. 251–264. https://doi.org/10.1111/j.1365-2133.1973.tb02972.x

Madsen, C. and Zhao, J. (1999) Optical Filter Design and Analysis: A Signal Processing Approach. Wiley-Interscience. Available at: https://learning.oreilly.com/library/view/optical-filter-design/9780471183730/.

Mahamad, S. and Hammond, D. (2019) 'Retail price and availability of illicit cannabis in Canada', Addictive Behaviors, 90, pp. 402–408. Available at: https://doi.org/https://doi.org/10.1016/j.addbeh.2018.12.001.

Majano, R. (2020) 'Cultivating a Safe Work Environment: Measuring and Addressing Sexual Harassment in Cannabis Dispensaries', Master's Thesis -- University of California Los Angeles.

Majmudar, V., Azam, N.A.M. and Finch, T. (2006) 'Contact urticaria to Cannabis sativa', Contact Dermatitis, 54(2), p. 127. Available at: https://doi.org/https://doi.org/10.1111/j.0105-1873.2006.0560h.x.

Makgabutlane, M. and Wright, C.Y. (2015) ‘Real-time measurement of outdoor worker’s exposure to solar ultraviolet radiation in Pretoria, South Africa’, South African Journal of Science, 111(5–6). Available at: https://doi.org/10.17159/sajs.2015/20140133.

Mann, J.E. et al. (1980) ‘Light Penetration in a Row-Crop with Random Plant Spacing’, Agronomy Journal, 72(1). Available at: https://doi.org/10.2134/agronj1980.00021962007200010026x.

Mardaljevic, J. (2011) ‘Ambient Calculation: Crash Course’, in 10th Annual International Radiance Workshop. Berkeley, CA: Berkeley Lab. Available at: https://www.radianceonline.org/community/workshops/2011-berkeleyca/presentations/day1/JM_AmbientCalculation.pdf (Accessed: 31 March 2023).

María-Antonia Serrano Javier Cañada, J.C.M. et al. (2012) ‘Solar UV exposure of children in a summer school in Valencia, Spain’, International Journal of Biometeorology, 56(2), pp. 371–377. Available at: https://doi.org/10.1007/s00484-011-0440-7.

María-Antonia Serrano, Javier Cañadab, J.C.M. et al. (2011) ‘Solar UV exposure of primary schoolchildren in Valencia, Spain’, Photochemical and Photobiological Sciences, 10(4), pp. 523–530. Available at: https://doi.org/10.1039/c0pp00153h.

Martin, C.J., Currie, G.D. and Pye, S.D. (1999) ‘The importance of radiometer angular response for ultraviolet phototherapy dosimetry’, Physics in Medicine and Biology, 44(4), pp. 843–855. Available at: https://doi.org/10.1088/0031-9155/44/4/003.

Martyny, J.W., Serrano, K.A., Schaeffer, J.W. and Van Dyke, M. V (2013) ‘Potential exposures associated with indoor marijuana growing operations.’, Journal of Occupational and Environmental Hygiene, 10(11), pp. 622–639. Available at: https://doi.org/10.1080/15459624.2013.831986.

Maxim Integrated (2015) DS3231 Specifications Sheet, Maxim Integrated. San Jose. Available at: https://datasheets.maximintegrated.com/en/ds/DS3231.pdf (Accessed: 31 May 2022).

McCarty, C.A. et al. (1996) ‘Ocular exposure to UV-B in sunlight: the Melbourne visual impairment project model.’, Bulletin of the World Health Organization, 74(4), pp. 353–360.

McPartland, J.M., Hegman, W. and Long, T. (2019) ‘Cannabis in Asia: its center of origin and early cultivation, based on a synthesis of subfossil pollen and archaeobotanical studies’, Vegetation History and Archaeobotany, 28(6), pp. 691–702. Available at: https://doi.org/10.1007/s00334-019-00731-8.

Meechan, P.J. and Wilson, C. (2006) ‘Use of Ultraviolet Lights in Biological Safety Cabinets: A Contrarian View’, Applied Biosafety, 11(4), pp. 222–227. Available at: https://doi.org/10.1177/153567600601100412.

Meroli, S. (2012) Active Pixel Sensor Vs CCD. Who is the clear winner? Available at: https://meroli.web.cern.ch/lecture_cmos_vs_ccd_pixel_sensor.html (Accessed: 6 April 2023).

Microsoft Corporation (2023) Microsoft Excel Version 16.71. Redmond, WA.

Miller, S. et al. (2016) ‘Interlaboratory Evaluation of Ultraviolet Radiation Emissions from Compact Fluorescent Lamps’, Photochemistry and Photobiology, 92(2), pp. 348–354. Available at: https://doi.org/10.1111/php.12573.

Miller, S.A. et al. (2006) ‘Reduction of the UV burden to indoor tanners through new exposure schedules: a pilot study’, Photodermatology, Photoimmunology & Photomedicine, 22(2), pp. 59–66. Available at: https://doi.org/10.1111/j.1600-0781.2006.00206.x.

Milonova, S. et al. (2016) ‘Occupant UV exposure measurements for upper-room ultraviolet germicidal irradiation’, Journal of Photochemistry and Photobiology B: Biology, 159, pp. 88–92. Available at: https://doi.org/10.1016/j.jphotobiol.2016.03.009.

Moehrle, M. and Garbe, C. (2000) ‘Personal UV Dosimetry by Bacillus subtilis Spore Films’, Dermatology, 200(1), pp. 1–5. Available at: https://doi.org/10.1159/000018306.

Moehrle, M. et al. (2000) ‘Extreme UV exposure of professional cyclists’, Dermatology, 201(1), pp. 44–45. Available at: https://doi.org/10.1159/000018428.

Moehrle, M. et al. (2003) ‘Continuous long-term monitoring of UV radiation in professional mountain guides reveals extremely high exposure’, International Journal of Cancer, 103(6), pp. 775–778. Available at: https://doi.org/10.1002/ijc.10884.

Moehrle, M., Korn, M. and Garbe, C. (2000) ‘Bacillus subtilis spore film dosimeters in personal dosimetry for occupational solar ultraviolet exposure’, International Archives of Occupational and Environmental Health, 73(8), pp. 575–580. Available at: https://doi.org/10.1007/s004200000183.

Moehrle, M., Soballa, M. and Korn, M. (2003) ‘UV exposure in cars’, Photodermatology Photoimmunology and Photomedicine, 19(4), pp. 175–181. Available at: https://doi.org/10.1034/j.1600-0781.2003.00031.x.

Moise, A.F. et al. (1999) ‘Solar ultraviolet radiation exposure of infants and small children’, Photodermatology, Photoimmunology & Photomedicine, 15(3‐4), pp. 109‐114. Available at: https://doi.org/10.1111/j.1600-0781.1999.tb00069.x.

Moise, A.F., Büttner, P.G. and Harrison, S.L. (1999) ‘Sun Exposure at School’, Photochemistry and Photobiology, 70(2), pp. 269–274. Available at: https://doi.org/https://doi.org/10.1111/j.1751-1097.1999.tb07999.x.

Moise, A.F., Gies, H.P. and Harrison, S.L. (1999) ‘Estimation of the Annual Solar UVR Exposure Dose of Infants and Small Children in Tropical Queensland, Australia’, 69(4), pp. 457–463.

Monticelli, D. de F. et al. (2022) ‘Cannabis Cultivation Facilities: A Review of Their Air Quality Impacts from the Occupational to Community Scale’, Environmental Science & Technology, 56(5), pp. 2880–2896. Available at: https://doi.org/10.1021/acs.est.1c06372.

Moran, D.J. and Hollows, F.C. (1984) ‘Pterygium and ultraviolet radiation: a positive correlation’, The British Journal of Ophthalmology, 68(5), pp. 343–346. Available at: https://doi.org/10.1136/bjo.68.5.343.

Morrow, R.C. (2008) ‘LED Lighting in Horticulture’, HortScience, 43(7). Available at: https://doi.org/10.21273/HORTSCI.43.7.1947.

Mottus, M. and Sulev, M. (2006) ‘Radiation fluxes and canopy transmittance : Models and measurements inside a willow canopy’, Journal of Geophysical Research, 111, pp. 1–11. Available at: https://doi.org/10.1029/2005JD005932.

Munakata, N. (1999) ‘Comparative measurements of solar UV radiation with spore dosimetry at three European and two Japanese sites’, Journal of Photochemistry and Photobiology B: Biology, 53(1), pp. 7–11. Available at: https://doi.org/https://doi.org/10.1016/S1011-1344(99)00114-1.

Myneni, R.B., Ross, J. and Asrar, G. (1989) ‘A review on the theory of photon transport in leaf canopies’, Agricultural and Forest Meteorology, 45(1), pp. 1–153. Available at: https://doi.org/https://doi.org/10.1016/0168-1923(89)90002-6.

Nakashima, H., Utsunomiya, A., Fujii, N., et al. (2016) ‘Hazard of ultraviolet radiation emitted in gas tungsten arc welding of aluminum alloys’, Industrial Health, 54(2), pp. 149–156. Available at: https://doi.org/10.2486/indhealth.2015-0141.

Nakashima, H., Utsunomiya, A., Takahashi, J., et al. (2016) ‘Hazard of ultraviolet radiation emitted in gas metal arc welding of mild steel’, Journal of Occupational Health, 58(5), pp. 452–459. Available at: https://doi.org/10.1539/joh.16-0065-OA.

Narbutt, J. et al. (2014) ‘System for monitoring UV radiation level in phototherapy cabins in Poland’, Archives of Medical Science, 10(6), pp. 1244–1254. Available at: https://doi.org/10.5114/aoms.2014.47834.

Nardell, E.A. et al. (2008) ‘Safety of Upper-Room Ultraviolet Germicidal Air Disinfection for Room Occupants: Results from the Tuberculosis Ultraviolet Shelter Study’, Public Health Reports, 123(1), pp. 52–60. Available at: https://doi.org/10.1177/003335490812300108.

Nardini, G., Neri, D. and Paroncini, M. (2014) ‘Measured anatomical distributions of solar UVR on strawberry production workers in Italy’, Journal of Agricultural Safety and Health, 20(2), pp. 67–78. Available at: https://doi.org/10.13031/jash.20.10189.

Neckel, H. and Labs, D. (1984) ‘The solar radiation between 3300 and 12500 Å’, Solar Physics, 90(2), pp. 205–258. Available at: https://doi.org/10.1007/BF00173953.

Nehir, M. et al. (2019) ‘Improving optical measurements: Non-linearity compensation of compact charge-coupled device (CCD) spectrometers’, Sensors, 19(12). Available at: https://doi.org/10.3390/s19122833.

Newton, R. et al. (1996) ‘Effect of ambient solar ultraviolet radiation on incidence of squamous-cell carcinoma of the eye.’, Lancet, 347(9013), pp. 1450–1451. Available at: https://doi.org/10.1016/s0140-6736(96)91685-2.

Nicholas G. Reed, S.W.& D.H.S. et al. (2009) ‘Intercomparison of instruments used for safety and performance measurements of ultraviolet germicidal irradiation lamps’, Journal of Occupational and Environmental Hygiene, 6(5), pp. 289–297. Available at: https://doi.org/10.1080/15459620902801041.

Nilsen, L.T.N. et al. (2008) ‘Trends in UV irradiance of tanning devices in Norway: 1983-2005’, Photochemistry and Photobiology, 84(5), pp. 1100–1108. Available at: https://doi.org/10.1111/j.1751-1097.2008.00330.x.

Norval, M. (2006) ‘The effect of ultraviolet radiation on human viral infections’, Photochemistry and Photobiology, 82(6), pp. 1495–1504. Available at: https://doi.org/10.1111/j.1751-1097.2006.tb09805.x.

Noxon, J.F. (1975) ‘Nitrogen dioxide in the stratosphere and troposphere measured by ground-based absorption spectroscopy.’, Science, 189(4202), pp. 547–549. Available at: https://doi.org/10.1126/science.189.4202.547.

Nylander-French, L.A. et al. (1994) ‘Assessment of Worker Exposure in the Processing of Ultraviolet Radiation-Cured Acrylate Lacquer- Coated Wood Products’, 0898. Available at: https://doi.org/10.1080/1047322X.1994.10388443.

O’Connor, U.M. and O’Hare, N.J. (2006) ‘Environmental risk analysis of ultraviolet phototherapy centres in Ireland’, Irish Journal of Medical Science, 175(2), pp. 63–67. Available at: https://doi.org/10.1007/BF03167953.

OAI (2016) Trisol Solar Simulator for Class AAA Performance Technical Specifications. San Jose, CA.

Ocean Insight (2015) Flame Miniature Spectrometer User Manual. Orlando. Available at: https://www.egr.msu.edu/psp/sites/default/files/content/Flame-Manual.pdf (Accessed: 31 May 2022).

Ocean Insight (2021) Flame-S Radiometric Calibration Report. Orlando.

Ocean Insight (2022) Glossary on Spectroscopy and Technical Terms. Available at: https://www.oceaninsight.com/knowledge-hub/glossary/ (Accessed: 8 August 2022).

Ohowot, O.M. et al. (1997) ‘Occupational exposure to optical radiation and the ocular health status of glassblowers’, Ophthalmic and Physiological Optics, 17(6), pp. 483–491. Available at: https://doi.org/10.1111/j.1475-1313.1997.tb00087.x.

Okuno, T. (1987) ‘Measurement of Ultraviolet Radiation from Welding Arcs’, Industrial health, 25(3), pp. 147–156. Available at: https://doi.org/10.2486/indhealth.25.147.

Okuno, T., Ojima, J. and Saito, H. (2001) ‘Ultraviolet radiation emitted by CO2 arc welding’, Annals of Occupational Hygiene, 45(7), pp. 597–601. Available at: https://doi.org/10.1016/S0003-4878(01)00023-0.

Olsson, D.M. and Nelson, L.S. (1975) ‘The nelder-mead simplex procedure for function minimization’, Technometrics, 17(1), pp. 45–51. Available at: https://doi.org/10.1080/00401706.1975.10489269.

Ono, M., Munakata, N. and Watanabe, S. (2005) 'UV Exposure of Elementary School Children in Five Japanese Cities¶', Photochemistry and Photobiology, 81(2), pp. 437–445. Available at: https://doi.org/10.1111/j.1751-1097.2005.tb00205.x.

Østerlind, A. et al. (1988) 'The Danish case-control study of cutaneous malignant melanoma. II. Importance of UV-light exposure', International Journal of Cancer, 42(3), pp. 319–324. Available at: https://doi.org/10.1002/ijc.2910420303.

Otanez, M. and Grewal, J. (2021) 'Health and Safety in the Legal Cannabis Industry Before and During COVID-19', New Solutions - A Journal of Environmental and Occupational Health Policy, 30(4), pp. 311–323. Available at: https://doi.org/10.1177/1048291120976134.

Oyarzun, R.A., Stöckle, C.O. and Whiting, M.D. (2007) 'A simple approach to modeling radiation interception by fruit-tree orchards', Agricultural and Forest Meteorology, 142(1), pp. 12–24. Available at: https://doi.org/https://doi.org/10.1016/j.agrformet.2006.10.004.

Parisi, A. and Kimlin, M. (1999) 'Effects of simple measures to reduce the occupational solar UV exposure of outdoor workers', Journal of Occupational Health and Safety - Australia and New Zealand, 15(3), pp. 267–272.

Parisi, A. V and Kimlin, M.G. (1999) 'Effect of meal break times on solar UV exposure of schoolchildren in a southeast Queensland summer month', Environmetrics, 11(5), pp. 452–459. Available at: https://doi.org/10.1002/1099-095X(200009/10)11:5<563::AID-ENV414>3.0.CO;2-8.

Parisi, A. V and Kimlin, M.G. (2000) 'Estimate of Annual Ultraviolet-A Exposures in Cars in Australia', Radiation Protection Dosimetry, 90(4), pp. 409–416. Available at: https://doi.org/10.1093/oxfordjournals.rpd.a033167.

Parisi, A. V and Wong, J.C.F. (1997) 'The erythemal ultraviolet exposure for humans in greenhouses', Physics in Medicine and Biology, 42(12), pp. 2331–2339. Available at: https://doi.org/10.1088/0031-9155/42/12/002.

Parisi, A. V and Wong, J.C.F. (2000) 'An estimation of biological hazards due to solar radiation', Journal of Photochemistry and Photobiology B: Biology, 54(2–3), pp. 126–130. Available at: https://doi.org/10.1016/S1011-1344(00)00006-3.

Parisi, A. V et al. (1999) 'Lifetime ultraviolet exposure estimates for selected population groups in south-east Queensland', Physics in Medicine and Biology, 44(12), pp. 2947–2953. Available at: https://doi.org/10.1088/0031-9155/44/12/307.

Parisi, A. V, Kimlin, M.G., et al. (2000) 'Field-based measurements of personal erythemal ultraviolet exposure through a common summer garment', Photodermatology Photoimmunology and Photomedicine, 16(16), pp. 134–138.

Parisi, A. V, Meldrum, L.R., Kimlin, M.G., et al. (2000) 'Evaluation of differences in ultraviolet exposure during weekend and weekday activities', Physics in Medicine & Biology, 45(45), p. 2253. Available at: https://doi.org/10.1088/0031-9155/45/8/314.

Parisi, A. V, Meldrum, L.R., Wong, J.C.F., et al. (2000) ‘Effect of childhood and adolescent ultraviolet exposures on cumulative exposure in South East Queensland schools.’, Photodermatology, Photoimmunology & Photomedicine, 16(1), pp. 19–24. Available at: https://doi.org/10.1034/j.1600-0781.2000.160106.x.

Parisi, A. V. and Wong, J.C.F.F. (1998) ‘Quantitative evaluation of the personal erythemal ultraviolet exposure in a car’, Photodermatology Photoimmunology and Photomedicine, 14(1), pp. 12–16. Available at: https://doi.org/10.1111/j.1600-0781.1998.tb00003.x.

Parisi, A. V. et al. (2000) ‘Reduction in the Personal Annual Solar Erythemal Ultraviolet Exposure Provided by Australian Gum Trees’, Radiation Protection Dosimetry, 92(4), pp. 307–312. Available at: https://doi.org/10.1093/oxfordjournals.rpd.a033297.

Parry, C.K. et al. (2019) ‘An intercomparison of radiation partitioning models in vineyard canopies’, Irrigation Science, pp. 239–252. Available at: https://doi.org/10.1007/s00271-019-00621-x.

Pascale, D. (2006) ‘RGB coordinates of the Macbeth ColorChecker’, The BabelColor Company. Available at: http://kronometric.org/phot/lighting/Macbeth%20ColorChecker%20Tables.pdf (Accessed: 31 March 2023).

Pe’er, J. (2005) ‘Ocular surface squamous neoplasia.’, Ophthalmology clinics of North America, 18(1), pp. 1–13, vii. Available at: https://doi.org/10.1016/j.ohc.2004.08.001.

Peng, C.-Y., Lan, C.-H., et al. (2007) ‘Exposure assessment of aluminum arc welding radiation’, Health Physics, 93(4), pp. 298–306. Available at: https://doi.org/10.1097/01.HP.0000267862.44497.a4.

Peng, C.-Y., Liu, H.-H., et al. (2007) ‘Evaluation and monitoring of UVR in shield metal arc welding processing’, Health Physics, 93(2), pp. 101–108. Available at: https://doi.org/10.1097/01.HP.0000259903.64054.84.

Pereira, F., Larriba, M.J. and Muñoz, A. (2012) ‘Vitamin D and colon cancer.’, Endocrine-Related Cancer, 19(3), pp. R51-71. Available at: https://doi.org/10.1530/ERC-11-0388.

Perkins, E.S. (1985) ‘The association between pinguecula, sunlight and cataract.’, Ophthalmic Research, 17(6), pp. 325–330. Available at: https://doi.org/10.1159/000265395.

Peters, C.E. et al. (2016) ‘Levels of Occupational Exposure to Solar Ultraviolet Radiation in Vancouver, Canada’, Annals of Occupational Hygiene, 60(7), pp. 825–835. Available at: https://doi.org/10.1093/annhyg/mew037.

Peters, C.E. et al. (2019) ‘Solar Ultraviolet Radiation Exposure among Outdoor Workers in Three Canadian Provinces’, Annals of Work Exposures and Health, 63(6), pp. 679–688. Available at: https://doi.org/10.1093/annweh/wxz044.

Petersen, B. et al. (2013) ‘Determinants of personal ultraviolet-radiation exposure doses on a sun holiday’, British Journal of Dermatology, 168(5), pp. 1073–1079. Available at: https://doi.org/10.1111/bjd.12211.

Petersen, B. et al. (2015) ‘Sun behavior and personal UVR exposure among Europeans on short term holidays’, Journal of Photochemistry and Photobiology B: Biology, 151, pp. 264–269. Available at: https://doi.org/https://doi.org/10.1016/j.jphotobiol.2015.08.022.

Petri, A. and Karabetsos, E. (2014) ‘Effective ultraviolet irradiance measurements from artificial tanning devices in Greece’, Radiation Protection Dosimetry, 167(4), pp. 490–501. Available at: https://doi.org/10.1093/rpd/ncu346.

Phalen, R.N. (2020) ‘Cannabis’, in Patty’s Industrial Hygiene, pp. 1–23. Available at: https://doi.org/https://doi.org/10.1002/0471435139.hyg142.

Pieri, P. (2010) ‘Modelling radiative balance in a row-crop canopy: Cross-row distribution of net radiation at the soil surface and energy available to clusters in a vineyard’, Ecological Modelling, 221(5), pp. 802–811. Available at: https://doi.org/https://doi.org/10.1016/j.ecolmodel.2009.07.028.

Pile, H. and Crane, J. (2020) Actinic Prurigo, StatPearls Publishing. Available at: https://www.ncbi.nlm.nih.gov/books/NBK499957/.

Pinto, I. et al. (2015) ‘Blue Light and Ultraviolet Radiation Exposure from Infant Phototherapy Equipment’, Journal of Occupational and Environmental Hygiene, 12(9), pp. 603–610. Available at: https://doi.org/10.1080/15459624.2015.1029611.

Pittas, A.G. and Dawson-Hughes, B. (2010) ‘Vitamin D and diabetes’, The Journal of Steroid Biochemistry and Molecular Biology. 2010/03/18, 121(1–2), pp. 425–429. Available at: https://doi.org/10.1016/j.jsbmb.2010.03.042.

Pitts, D.G. and Tredici, T.J. (1971) ‘The effects of ultraviolet on the eye.’, American Industrial Hygiene Association Journal, 32(4), pp. 235–246. Available at: https://doi.org/10.1080/0002889718506444.

Pitts, D.G., Cullen, A.P. and Hacker, P.D. (1977) ‘Ocular effects of ultraviolet radiation from 295 to 365 nm.’, Investigative Ophthalmology and Visual Science, 16(10), pp. 932–939.

Pola, E.C., Masanganise, R. and Rusakaniko, S. (2003) ‘The trend of ocular surface squamous neoplasia among ocular surface tumor biopsies submitted for histology from Sekuru Kaguvi Eye Unit, Harare between 1996 and 2000.’, The Central African Journal of Medicine, 49(1–2), pp. 1–4.

Ponsonby, A.-L., Lucas, R.M. and van der Mei, I.A.F. (2005) ‘UVR, vitamin D and three autoimmune diseases--multiple sclerosis, type 1 diabetes, rheumatoid arthritis.’, Photochemistry and Photobiology, 81(6), pp. 1267–1275. Available at: https://doi.org/10.1562/2005-02-15-IR-441.

Price, R.B.T. et al. (2016) ‘The dental curing light: A potential health risk’, Journal of Occupational and Environmental Hygiene, 13(8), pp. 639–646. Available at: https://doi.org/10.1080/15459624.2016.1165822.

Python Software Foundation (2023) Python 3.11.1 Documentation. Available at: https://docs.python.org/3/ (Accessed: 1 January 2023).

Quintern, L.E. et al. (1997) ‘Characterization and application of UV detector spore films: the sensitivity curve of a new detector system provides good similarity to the action spectrum for UV-induced erythema in human skin’, Journal of Photochemistry and Photobiology B: Biology, 37(1), pp. 158–166. Available at: https://doi.org/https://doi.org/10.1016/S1011-1344(96)04414-4.

R Core Team (2022) R: A language and environment for statistical computing. Available at: https://www.R-project.org/ (Accessed: 1 January 2023).

Rafieepour, A. et al. (2015) ‘Seasonal variation in exposure level of types A and B ultraviolet radiation: An environmental skin carcinogen’, Annals of Medical and Health Sciences Research, 5(2), p. 129. Available at: https://doi.org/10.4103/2141-9248.153623.

Reed, S. et al. (2018) ‘Occupational Respiratory Hazards in the Emerging Medicinal Cannabis Industry in Australia’, in Conference Proceedings of the 32nd International Congress on Occupational Health.

Regili, A. et al. (2016) ‘SimUVEx v2 : A Numeric Model to Predict Anatomical Solar Ultraviolet Exposure’, in 2016 SAI Computing Conference (SAI). London, UK, pp. 1344–1348. Available at: https://doi.org/10.1109/SAI.2016.7556156.

Root, K.S. et al. (2020) ‘Application of the Environmental Relative Moldiness Index in Indoor Marijuana Grow Operations’, Annals of Work Exposures and Health, 64(7), pp. 728–744. Available at: https://doi.org/10.1093/annweh/wxaa071.

Rosenthal, F.S. et al. (1991) ‘Ocular and facial skin exposure to ultraviolet radiation in sunlight: A personal exposure model with application to a worker population’, Health Physics, 61(I), pp. 77–86. Available at: https://doi.org/10.1097/00004032-199107000-00008.

Roy, C. et al. (1998) ‘Solar UVR Exposures of Primary School Children at Three Locations in Queensland’, Photochemistry and Photobiology, 68(1), pp. 78–83. Available at: https://doi.org/10.1562/0031-8655(1998)0682.3.co;2.

Ruppertsberg, A. and Bloj, M. (2006) ‘Rendering complex scenes for psychophysics using RADIANCE: How accurate can you get?’, Journal of the Optical Society of America. A, Optics, image science, and vision, 23, pp. 759–768. Available at: https://doi.org/10.1364/JOSAA.23.000759.

Russell, J. (2020) ‘Re: Safety of Cannabis-Associated Air Contaminants and Emissions’, Canadian Medical Association Journal - Memo. Available at: https://www.cmaj.ca/content/re-safety-cannabis-associated-air-contaminants-and-emissions

Rybczyński, A. Wolska, A. (2016) ‘Selected measurement problems during the evaluation of occupational exposure to UV radiation emitted by the welding arc’, 2016 IEEE Lighting Conference of the Visegrad Countries (Lumen V4), Karpacz, Poland, pp. 1-7, doi: 10.1109/LUMENV.2016.7745535.

Sabburg, J. and Wong, J. (2000) ‘The effect of clouds on enhancing UVB irradiance at the Earth’s surface: A one year study’, Geophysical Research Letters, 27(20), pp. 3337–3340. Available at: https://doi.org/10.1029/2000GL011683.

Sack, C. et al. (2020) ‘Allergic and Respiratory Symptoms in Employees of Indoor Cannabis Grow Facilities’, Annals of Work Exposures and Health, 64(7), pp. 754–764. Available at: https://doi.org/10.1093/annweh/wxaa050.

Sack, C., Simpson, C. and Pacheco, K. (2023) ‘The Emerging Spectrum of Respiratory Diseases in the US Cannabis Industry’, in Seminars in Respiratory and Critical Care Medicine. Thieme Medical Publishers, Inc.

Safari, S. et al. (2015) ‘Ultraviolet Radiation Emissions and Illuminance in Different Brands of Compact Fluorescent Lamps’, International Journal of Photoenergy, pp. 1–6. Available at: https://doi.org/10.1155/2015/504674.

Saldanha, A. (2022) ‘Armed robberies at WA pot shops hit decade high’, The Seattle Times.

Scheeline, A. (2017) ‘How to Design a Spectrometer’, Applied Spectroscopy, 71(10), pp. 2237–2252. Available at: https://doi.org/10.1177/0003702817720468.

Schenker, M.B. and Beckman, S. (2023) ‘Cannabis industry worker health and safety: time for action’, Journal of Agromedicine, 28(1), pp. 14–17.

Schenker, M.B. and Langer, C.E. (2021) ‘Health and safety of cannabis workers’, The Routledge Handbook of Post-Prohibition Cannabis Research, pp. 135–143.

Schennetten, K., Meier, M.M. and Scheibinger, M. (2019) ‘Measurement of UV radiation in commercial aircraft’, Journal of Radiological Protection, 39(1), pp. 85–96. Available at: https://doi.org/10.1088/1361-6498/aaf2a7.

Schmalwieser, A W et al. (2010) ‘UV exposition during typical lifestyle behavior in an urban environment’, Photochemistry and Photobiology, 86(3), pp. 711–715. Available at: https://doi.org/10.1111/j.1751-1097.2010.00714.x.

Schmalwieser, Alois W et al. (2010) ‘Facial Solar UV Exposure of Austrian Farmers During Occupation’, Photochemistry and Photobiology, 86(6), pp. 1404–1413. Available at: https://doi.org/10.1111/j.1751-1097.2010.00812.x.

Schmid, K.L. et al. (2013) ‘Assessment of Daily Light and Ultraviolet Exposure in Young Adults’, Optometry and Vision Science Journal, 90(2), pp. 148–155.

Schwander, H. et al. (2002) ‘Modification of spectral UV irradiance by clouds’, Journal of Geophysical Research: Atmospheres, 107(D16), p. AAC 7-1-AAC 7-12. Available at: https://doi.org/10.1029/2001JD001297.

Scott C, Punja ZK. 2021. Evaluation of disease management approaches for powdery mildew on Cannabis sativa L. (marijuana) plants. Canadian Journal of Plant Pathology, 43(3), 394–412. https://doi.org/10.1080/07060661.2020.1836026

Seckmeyer G, Klingebiel M, Riechelmann S, Lohse I, McKenzie RL, ben Liley J, Allen, M. W., Siani, A.-M., & Casale, G. R. (2012) A Critical Assessment of Two Types of Personal UV Dosimeters. Photochemistry and Photobiology, 88(1), 215–222. https://doi.org/10.1111/j.1751-1097.2011.01018.x

Sehgal, V. et al. (2014) 'Basal Cell Carcinoma: Pathophysiology', SKINmed, 12, pp. 176–181.

Selgrade, M.K., Repacholi, M.H. and Koren, H.S. (1997) 'Ultraviolet radiation-induced immune modulation: potential consequences for infectious, allergic, and autoimmune disease', Environmental Health Perspectives, 105(3), pp. 332–334. Available at: https://doi.org/10.1289/ehp.97105332.

Serbin, S. (2014) 'Fresh Leaf Spectra to Estimate Leaf Morphology and Biochemistry for Northern Temperate Forests', Ecological Spectral Information System. Available at: https://doi.org/10.21232/C2WC75.

Serbin, S., DuBois, S., et al. (2019) 'UW-BNL NASA HyspIRI Airborne Campaign Leaf and Canopy Spectra and Trait Data. Data set. ', Ecological Spectral Information System (EcoSIS). Available at: https://ecosis.org/package/uw-bnl-nasa-hyspiri-airborne-campaign-leaf-andcanopy-spectra-and-trait-data (Accessed: 31 March 2023).

Serbin, S., Meng, R., et al. (2019) 'NGEE Tropics GLiHT Puerto Rico Campaign Leaf Spectral Reflectance and Transmittance March 2017. Data set. ', Ecological Spectral Information System. Available at: https://ecosis.org/package/ngee-tropics-gliht-puerto-rico-campaign-leaf-spectralreflectance-and-transmittance-march-2017 (Accessed: 10 January 2023).

Serra, H. et al. (2018) 'Pterygium: A Complex and Multifactorial Ocular Surface Disease. A Review on its Pathogenic Aspects', Rare Diseases, Avid Science, pp. 1–37. Available at: https://doi.org/10.29290/RARD.1.2.2018.2-37.

Serrano, M.-A. et al. (2013) 'Erythemal ultraviolet solar radiation doses received by young skiers', Photochemical & Photobiological Sciences, 12(11), pp. 1976–1983. Available at: https://doi.org/10.1039/C3PP50154J.

Serrano, M.-A. et al. (2014) 'Occupational UV Exposure of Environmental Agents in Valencia, Spain', Photochemistry and Photobiology, 90(4), pp. 911-918. Available at: https://doi.org/10.1111/php.12252.

Serrano, M.-A.A. et al. (2014) 'Personal UV exposure for different Outdoor sports', Photochemical and Photobiological Sciences, 13(4), pp. 671–679. Available at: https://doi.org/10.1039/c3pp50348h.

Serrano, M.-A.A., Cañada, J. and Moreno, J.C. (2013) 'Solar UV exposure in construction workers in Valencia, Spain', Journal of Exposure Science and Environmental Epidemiology, 23(5), pp. 525–530. Available at: https://doi.org/10.1038/jes.2012.58.

Serrano, M.A. et al. (2009) 'Erythemal Ultraviolet Exposure in Two Groups of Outdoor Workers', Photochemistry and Photobiology, 85(6), pp. 1468–1473. Available at: https://doi.org/10.1111/j.1751-1097.2009.00609.x.

Serrano, M.A., Cañada, J. and Moreno, J.C. (2010) 'Erythemal Ultraviolet Exposure of Cyclists in Valencia, Spain', Photochemistry and Photobiology, 86(3), pp. 716–721. Available at: https://doi.org/10.1111/j.1751-1097.2009.00693.x.

Serrano, M.A.M.-A., Cañada, J. and Moreno, J.C. (2011) 'Ultraviolet exposure for different outdoor sports in Valencia, Spain', Photodermatology Photoimmunology and Photomedicine, 27(6), pp. 311–317. Available at: https://doi.org/10.1111/j.1600-0781.2011.00620.x.

Shehade, S.A. et al. (1987) 'Photodermatitis due to spot welding', British Journal of Dermatology, 117(1), pp. 117–119. Available at: https://doi.org/10.1111/j.1365-2133.1987.tb04100.x.

Shenenberger, D.W. (2012) 'Cutaneous malignant melanoma: a primary care perspective.', American Family Physician, 85(2), pp. 161–168.

Shipp, L.R. et al. (2014) 'Further investigation into the risk of skin cancer associated with the use of UV nail lamps', JAMA Dermatology, 150(7), pp. 775–776. Available at: https://doi.org/10.1001/jamadermatol.2013.8740.

Siani, A.M. et al. (2008) 'Personal UV exposure in high albedo alpine sites', Atmospheric Chemistry and Physics, 8(14), pp. 3749–3760. Available at: https://doi.org/10.5194/acp-8-3749-2008.

Siani, A.M. et al. (2009) 'Short-term UV exposure of sunbathers at a Mediterranean sea site', Photochemistry and Photobiology, 85(1), pp. 171–177. Available at: https://doi.org/10.1111/j.1751-1097.2008.00413.x.

Siani, A.M. et al. (2011) 'Occupational Exposures to Solar Ultraviolet Radiation of Vineyard Workers in Tuscany (Italy)', Photochemistry and Photobiology, 87(4), pp. 925–934. Available at: https://doi.org/10.1111/j.1751-1097.2011.00934.x.

Silvey, B. (2019) 'Characterization of Occupational Exposure to Airborne Contaminants in an Indoor Cannabis Production Facility', Thesis (Master's)--University of Washington. Available at: https://digital.lib.washington.edu/researchworks/handle/1773/44207?show=full (Accessed: 10 April 2023).

Silvey, B., Seto, E., Gipe, A., Ghodsian, N. and Simpson, Christopher D. (2020) 'Occupational Exposure to Particulate Matter and Volatile Organic Compounds in Two Indoor Cannabis Production Facilities', Annals of Work Exposures and Health, 64(7), pp. 715–727. Available at: https://doi.org/10.1093/annweh/wxaa067.

Simpson, C. (2017) 'Something Old, Something New', International Society of Exposure Science Newsletter, 3, pp. 11–14. Available at: https://deohs.washington.edu/pnash/sites/deohs.washington.edu.pnash/files/2022PNASHYear-endReport_Yost%207544_rev11.10.22.pdf (Accessed: 16 April 2023).

Simpson, C. (2020) 'Occupational Health and Safety in the Cannabis Industry', Annals of Work Exposures and Health, 64(7), pp. 677–678. Available at: https://doi.org/10.1093/annweh/wxaa068.

Singer, R.S. et al. (1994) ‘Association of Asymmetrical Facial Photodamage With Automobile Driving’, Archives of Dermatology, 130(1), pp. 121–123. Available at: https://doi.org/10.1001/archderm.1994.01690010127031.

Singh, B.P. et al. (2014) ‘An assessment of ozone levels, UV radiation and their occupational health hazard estimation during photocopying operation’, Journal of Hazardous Materials, 275, pp. 55–62. Available at: https://doi.org/10.1016/J.JHAZMAT.2014.04.049.

Sisto, R. et al. (2009) ‘Quantitative evaluation of personal exposure to UV radiation of workers and general public’, Radiation Protection Dosimetry, 137(3–4), pp. 193–196. Available at: https://doi.org/10.1093/rpd/ncp234.

Sleijffers, A. et al. (2001) ‘Influence of Ultraviolet B Exposure on Immune Responses Following Hepatitis B Vaccination in Human Volunteers’, Journal of Investigative Dermatology, 117(5), pp. 1144–1150. Available at: https://doi.org/https://doi.org/10.1046/j.0022-202x.2001.01542.x.

Sliney DH. 2001. Photoprotection of the eye-UV radiation and sunglasses. In Journal of Photochemistry and Photobiology B: Biology. 64(2-3).

Sliney, D.H. (1972) ‘The Merits of an Envelope Action Spectrum for Ultraviolet Radiation Exposure Criteria’, American Industrial Hygiene Association Journal, 33(10), pp. 644–653. Available at: https://doi.org/10.1080/0002889728506722.

Sliney, D.H. (1995) ‘UV radiation ocular exposure dosimetry’, Journal of Photochemistry and Photobiology B: Biology, 31(1), pp. 69–77. Available at: https://doi.org/https://doi.org/10.1016/1011-1344(95)07171-5.

Sliney, D.H., Fast, P. and Ricksand, A. (1995) ‘Optical radiation hazards analysis of ultraviolet headlamps’, Applied Optics, 34(22), pp. 4912–4922. Available at: https://doi.org/10.1364/AO.34.004912.

Sliney, D.H., Gilbert, D.W. and Lyon, T. (2016) ‘Ultraviolet safety assessments of insect light traps’, Journal of Occupational and Environmental Hygiene, 13(6), pp. 413–424. Available at: https://doi.org/10.1080/15459624.2015.1125489.

Snellman, E., Rantanen, T. and Sundell, J. (2000) ‘Cumulative UV radiation dose and outcome in clinical practice: Effectiveness of trioxsalen bath PUVA with minimal UVA exposure’, Photodermatology Photoimmunology and Photomedicine, 16(5), pp. 207–210. Available at: https://doi.org/10.1034/j.1600-0781.2000.160503.x.

Solacure. (2016) Flower Power F40. Solacure.Com. http://www.solacure.com/flowerpower.html. [Accessed on 23 May 2022].

Song, G.G., Bae, S.C., and Lee, Y.H. (2012) ‘Association between vitamin D intake and the risk of rheumatoid arthritis: a meta-analysis.’, Clinical Rheumatology, 31(12), pp. 1733–1739. Available at: https://doi.org/10.1007/s10067-012-2080-7.

Stern, R.S. (1999) ‘The mysteries of geographic variability in nonmelanoma skin cancer incidence.’, Archives of Dermatology. United States, pp. 843–844. Available at: https://doi.org/10.1001/archderm.135.7.843.

Stewart, D.W. et al. (2003) ‘Canopy Structure, Light Interception, and Photosynthesis in Maize’, Agronomy Journal, 95(6), pp. 1465–1474. Available at: https://doi.org/https://doi.org/10.2134/agronj2003.1465.

Stone, D. (2014) ‘Cannabis, pesticides and conflicting laws: The dilemma for legalized States and implications for public health’, Regulatory Toxicology and Pharmacology, 69(3), pp. 284–288.

Sun, J. et al. (2014) ‘The relationship between ambient ultraviolet radiation (UVR) and objectively measured personal UVR exposure dose is modified by season and latitude’, Photochemical and Photobiological Sciences, 13(12), pp. 1711–1718. Available at: https://doi.org/10.1039/c4pp00322e.

Surakka, J. et al. (1997) ‘Assessment of ultraviolet radiation exposure in the wood surface coating industry’, Applied Occupational and Environmental Hygiene, 12(4), pp. 261–270. Available at: https://doi.org/10.1080/1047322X.1997.10389502.

Surdu, S. et al. (2013) ‘Occupational Exposure to Ultraviolet Radiation and Risk of Non-Melanoma Skin Cancer in a Multinational European Study’, PLoS ONE, 8(4). Available at: https://doi.org/10.1371/journal.pone.0062359.

Svenoe, T., Falk, E.S. and Henriksen, K. (1995) ‘Irradiances and health risks associated with the use of UV lamps and sunbeds’, European Review for Medical and Pharmacological Sciences, 17(2–3), pp. 53–62.

Sweet, S. (2016) ‘The Energy Intensity of Lighting Used for the Production of Recreational Cannabis in Washington State and Implications for Energy Efficiency’, Master’s Thesis - Evergreen State College. Available at: https://archives.evergreen.edu/masterstheses/Accession86-10MES/Sweet_SMESthesis2016.pdf (Accessed: 16 April 2023).

Talat, N. et al. (2010) ‘Vitamin d deficiency and tuberculosis progression’, Emerging Infectious Diseases, 16(5), pp. 853–855. Available at: https://doi.org/10.3201/eid1605.091693.

Taylor, H.A. (1971) Analytical methods techniques for actinometry in Analytical photochemistry and photochemical analysis. Edited by J.M.F.M. Dekker. New York.

Taylor, H.R. (1980) ‘The prevalence of corneal disease and cataracts in Australian Aborigines in northwestern Australia’, Australian Journal of Opthalmology, 8(4), pp. 289–301. Available at: https://doi.org/10.1111/j.1442-9071.1980.tb00285.x.

Taylor, H.R. et al. (1989) ‘Corneal Changes Associated With Chronic UV Irradiation’, Archives of Ophthalmology, 107(10), pp. 1481–1484. Available at: https://doi.org/10.1001/archopht.1989.01070020555039.

Tchou, C. and Debevec, P. (2001) ‘HDR Shop’, SIGGRAPH 2001 Conference Abstracts and Applications. Available at:

https://citeseerx.ist.psu.edu/document?repid=rep1&type=pdf&doi=ed1d2b09ddd486a4aae36615d327bd46a323fbd5 (Accessed: 31 March 2023).

Thieden, E. et al. (2005) 'Ultraviolet exposure patterns of Irish and Danish gardeners during work and leisure', British Journal of Dermatology, 153(4), pp. 795–801. Available at: https://doi.org/10.1111/j.1365-2133.2005.06797.x.

Thieden, E. et al. (2013) 'People maintain their sun exposure behavior in a 5-7-year follow-up study using personal electronic UVR dosimeters', Photochemical and Photobiological Sciences, 12(1), pp. 111–116. Available at: https://doi.org/10.1039/c2pp25138h.

Thieden, E. et al. (2019) 'Adult UVR exposure changes with life stage-a 14-year follow-up study using personal electronic UVR dosimeters', Photochemical and Photobiological Sciences, 18(2), pp. 467–476. Available at: https://doi.org/10.1039/C8PP00365C.

Thieden, E., Ågren, M.S. and Wulf, H.C. (2000) 'The wrist is a reliable body site for personal dosimetry of ultraviolet radiation', Photodermatology Photoimmunology and Photomedicine, 16(2), pp. 57–61. Available at: https://doi.org/10.1034/j.1600-0781.2000.d01-4.x.

Thieden, E., Ågren, M.S. and Wulf, H.C. (2001) 'Solar UVR exposures of indoor workers in a Working and a Holiday Period assessed by personal dosimeters and sun exposure diaries', Photodermatology, Photoimmunology & Photomedicine, 17(6), pp. 249–255.

Thieden, E., Philipsen, P.A., and Wulf, H.C. (2006) 'Ultraviolet radiation exposure pattern in winter compared with summer based on time-stamped personal dosimeter readings', British Journal of Dermatology, 154(1), pp. 133–138. Available at: https://doi.org/10.1111/j.1365-2133.2005.06961.x.

Thieden, E., Philipsen, Peter A, et al. (2004) 'UV radiation exposure related to age, sex, occupation, and sun behavior based on time-stamped personal dosimeter readings.', Archives of Dermatology, 140(2), pp. 197–203. Available at: https://doi.org/10.1001/archderm.140.2.197.

Thieden, E., Philipsen, Peter A., et al. (2004) 'Proportion of lifetime UV dose received by children, teenagers and adults based on time-stamped personal dosimetry', Journal of Investigative Dermatology, 123(6), pp. 1147–1150. Available at: https://doi.org/10.1111/j.0022-202X.2004.23466.x.

Thieden, Elisabeth, Philipsen, Peter A, et al. (2005) 'Sunburn Related to UV Radiation Exposure, Age, Sex, Occupation, and Sun Bed Use Based on Time-Stamped Personal Dosimetry and Sun Behavior Diaries', Archives of Dermatology, 141(4), pp. 482–488. Available at: https://doi.org/10.1001/archderm.141.4.482.

Thieden, Elisabeth, Philipsen, Peter A., et al. (2005) 'Sunscreen use related to UV exposure, age, sex, and occupation based on personal dosimeter readings and sun-exposure behavior diaries', Archives of Dermatology, 141(8), pp. 967–973. Available at: https://doi.org/10.1001/archderm.141.8.967.

Thimijan, R.W. and Heins, R.D. (1983) 'Photometric, Radiometric, and Quantum Light Units of Measure: A Review of Procedures for Interconversion', HortScience, 18(6), pp. 818–822. Available at: https://doi.org/10.21273/HORTSCI.18.6.818.

Togawa, K. et al. (2021) ‘Cancer incidence in agricultural workers: Findings from an international consortium of agricultural cohort studies (AGRICOH)’, Environment International, 157. Available at: https://doi.org/10.1016/j.envint.2021.106825.

Trask, C., Koehncke, N. and Trask, D. (2021) ‘High Risk? Indoor Cannabis Producers’ Perceptions of Occupational Health and Safety’, Journal of Agromedicine, 26(4), pp. 361–373. Available at: https://doi.org/10.1080/1059924X.2020.1795031.

Urashima, M. et al. (2010) ‘Randomized trial of vitamin D supplementation to prevent seasonal influenza A in schoolchildren.’, The American Journal of Clinical Nutrition, 91(5), pp. 1255–1260. Available at: https://doi.org/10.3945/ajcn.2009.29094.

Vanos, J.K. et al. (2017) ‘Schoolyard Shade and Sun Exposure: Assessment of Personal Monitoring During Children’s Physical Activity’, Photochemistry and Photobiology, 93(4), pp. 1123–1132. Available at: https://doi.org/10.1111/php.12721.

Verdebout, J. (2010) ‘Estimating natural UV personal exposure with radiative transfer calculations’, Radiation Protection Dosimetry, 141(3), pp. 275–282. Available at: https://doi.org/10.1093/rpd/ncq186.

Vernez, D. et al. (2011) ‘A Numeric Model to Simulate Solar Individual Ultraviolet Exposure’, Photochemistry and Photobiology, 87(3), pp. 721–728. Available at: https://doi.org/10.1111/j.1751-1097.2011.00895.x.

Victory, K.R. et al. (2018) ‘Notes from the field: occupational hazards associated with harvesting and processing Cannabis—Washington, 2015–2016’, Morbidity and Mortality Weekly Report, 67(8), p. 259.

Vishvakarman, D. and Wong, J.C.F. (2003a) ‘Accuracy of annual erythema exposure estimation using different numbers of ambient exposure fractions in the human exposure model’, Photodermatology, Photoimmunology & Photomedicine, 19(3), pp. 128–133. Available at: https://doi.org/https://doi.org/10.1034/j.1600-0781.2003.00021.x.

Vishvakarman, D. and Wong, J.C.F. (2003b) ‘Description of the use of a risk estimation model to assess the increased risk of non-melanoma skin cancer among outdoor workers in Central Queensland, Australia’, Photodermatology, Photoimmunology & Photomedicine, 19(2), pp. 81–88. Available at: https://doi.org/https://doi.org/10.1034/j.1600-0781.2003.00012.x.

Vishvakarman, D., Wong, J.C.F. and Boreham, B.W. (2001) ‘Annual occupational exposure to ultraviolet radiation in central Queensland’, Health Physics, 81(5), pp. 536–544. Available at: https://doi.org/10.1097/00004032-200111000-00008.

Wagner, E., Merz, J. and Townsend, P.A. (2018) ‘Ecological spectral information system: an open spectral library’, in American Geophysical Union Fall Meeting Abstracts. Washington DC. Available at: https://ui.adsabs.harvard.edu/abs/2018AGUFM.B41L2878W/abstract (Accessed: 31 March 2023).

Wainwright, L., Parisi, A. and Schouten, P. (2013) ‘Characterization and evaluation of a miniaturized polyphenylene oxide dosimeter for ultraviolet exposures’, Journal of Photochemistry and Photobiology B: Biology, 120, pp. 98–103. Available at: https://doi.org/10.1016/j.jphotobiol.2013.02.003.

Wainwright, L.K., Parisi, A. V and Downs, N.J. (2017) 'Concurrent evaluation of personal damaging and beneficial UV exposures over an extended period', Journal of Photochemistry and Photobiology B: Biology, 170, pp. 188–196. Available at: https://doi.org/10.1016/j.jphotobiol.2017.04.013.

Wallace, C. and Both, A.J. (2016) 'Evaluating operating characteristics of light sources for horticultural applications', Acta Horticulturae, 1134, pp. 435–443. Available at: https://doi.org/10.17660/ActaHortic.2016.1134.55.

Walters, K.M., Fisher, G.G. and Tenney, L. (2018) 'An overview of health and safety in the Colorado cannabis industry', American Journal of Industrial Medicine, 61(6), pp. 451–461. Available at: https://doi.org/10.1002/ajim.22834.

Wang, Z. et al. (2015) 'Agricultural and Forest Meteorology Radiation interception and utilization by wheat / maize strip intercropping systems', Agricultural and Forest Meteorology, 204, pp. 58–66. Available at: https://doi.org/10.1016/j.agrformet.2015.02.004.

Ward, E. (1997) 'RTRACE Documentation'. Radsite. Available at: https://www.radianceonline.org/learning/documentation/manual-pages/pdfs/rtrace.pdf (Accessed: 31 March 2023).

Ward, G. (2004) 'Behavior of Materials in Radiance', Lawrence Berkley Laboratory. Available at: https://floyd.lbl.gov/radiance/refer/materials.pdf (Accessed: 30 March 2023).

Ward, G. and Shakespeare, R. (1998) Rendering with Radiance: the art and science of lighting visualization. San Francisco, CA, USA: Morgan Kaufmann Publishers.

Ward, G.J. (1994) 'The RADIANCE Lighting Simulation and Rendering System', in SIGGRAPH 1994: 21st Annual Conference on Computer Graphics and Interactive Techniques, pp. 459–472.

Weaver, B.A. (2008) Solar Ultraviolet Radiation Exposure in Outdoor Work Environment at Bowling Green, Ohio. Available at: http://rave.ohiolink.edu/etdc/view?acc_num=mco1211995092.

Weihs, P. et al. (2013) 'Measurements of personal UV exposure on different parts of the body during various activities', Photochemistry and Photobiology, 89(4), pp. 1004–1007. Available at: https://doi.org/10.1111/php.12085.

Welles, C.C. et al. (2014) 'Vitamin D deficiency and cardiovascular events in patients with coronary heart disease: data from the Heart and Soul Study.', American Journal of Epidemiology, 179(11), pp. 1279–1287. Available at: https://doi.org/10.1093/aje/kwu059.

Williams, C., Thompstone, J. and Wilkinson, M. (2008) 'Work-related contact urticaria to Cannabis sativa', Contact Dermatitis, 58(1), pp. 62–63. Available at: https://doi.org/https://doi.org/10.1111/j.1600-0536.2007.01169.x.

Wilson, A.D. and Lyall, H. (1986) 'Design of an ultraviolet radiometer. 2. Detector optical characteristics.', Applied Optics, 25(24), p. 4540. Available at: https://doi.org/10.1364/ao.25.004540.

Wittlich, M. et al. (2016) ‘An approximation of occupational lifetime UVR exposure: algorithm for retrospective assessment and current measurements’, Journal of the European Academy of Dermatology and Venereology, 30(S3), pp. 27–33. Available at: https://doi.org/https://doi.org/10.1111/jdv.13607.

Wolska, A. (2013) ‘Occupational exposure to solar ultraviolet radiation of polish outdoor workers: Risk estimation method and criterion’, International Journal of Occupational Safety and Ergonomics, 19(1), pp. 107–116. Available at: https://doi.org/10.1080/10803548.2013.11076970.

Wong, C.F. et al. (1992) ‘Measurement of human exposure to ultraviolet-b solar radiation using a cr-39 dosimeter’, Health Physics, 63(4), pp. 457–461. Available at: https://doi.org/10.1097/00004032-199210000-00011.

Wong, N.A. and Bahmani, H. (2022) ‘A review of the current state of research on artificial blue light safety as it applies to digital devices’, Heliyon, 8(8). Available at: https://doi.org/10.1016/j.heliyon.2022.e10282.

Woods, T. and Rottman, G. (2002) ‘Solar Ultraviolet Variability Over Time Periods of Aeronomic Interest’, Washington DC American Geophysical Union Geophysical Monograph Series, 1 January. Available at: https://doi.org/10.1029/130GM14.

Woods, T.N. et al. (1996) ‘Validation of the UARS solar ultraviolet irradiances: Comparison with the ATLAS 1 and 2 measurements’, Journal of Geophysical Research: Atmospheres, 101(D6), pp. 9541–9569. Available at: https://doi.org/10.1029/96JD00225.

Wright, A.L. et al. (1996) ‘Survey of the variation in ultraviolet outputs from ultraviolet A sunbeds in Bradford’, Photodermatology Photoimmunology and Photomedicine, 12(1), pp. 12–16. Available at: https://doi.org/10.1111/j.1600-0781.1996.tb00237.x.

Wright, C.Y. et al. (2013) ‘Sunburn risk among children and outdoor workers in South Africa and Reunion Island coastal sites’, Photochemistry and Photobiology, 89(5), pp. 1226–1233. Available at: https://doi.org/10.1111/php.12123.

Wright, C.Y., Coetzee, G. and Ncongwane, K. (2011) ‘Ambient solar UV radiation and seasonal trends in potential sunburn risk among schoolchildren in South Africa’, SAJCH South African Journal of Child Health, 5(2), pp. 33–38.

Xiang, F. et al. (2015) ‘Weekend personal ultraviolet radiation exposure in four cities in Australia: Influence of temperature, humidity and ambient ultraviolet radiation’, Journal of Photochemistry and Photobiology B: Biology, 143, pp. 74–81. Available at: https://doi.org/https://doi.org/10.1016/j.jphotobiol.2014.12.029.

Xu, L. and Wei, R. (2019) ‘Optimal greenhouse lighting scheduling using canopy light distribution model : A simulation study on tomatoes’, Lighting Research & Technology. Available at: https://doi.org/10.1177/1477153519825995.

Yam, J.C.S. and Kwok, A.K.H. (2014) ‘Ultraviolet light and ocular diseases’, International Ophthalmology, (34), pp. 383–400. Available at: https://doi.org/10.1007/s10792-013-9791-x.

Yoshikawa, T. et al. (1990) ‘Susceptibility to effects of UVB radiation on induction of contact hypersensitivity as a risk factor for skin cancer in humans.’, The Journal of Investigative Dermatology, 95(5), pp. 530–536. Available at: https://doi.org/10.1111/1523-1747.ep12504877.

Ysasi, G.G. et al. (2014) ‘Ultraviolet Erythematic Radiation Dose Received by Golfers in Winter, in Valencia’, Photochemistry and Photobiology, 90(5), pp. 1170–1173. Available at: https://doi.org/10.1111/php.12295.

Ysasi, G.G. et al. (2018) ‘Analysis of Erythemal UVB Dose Received Inside a Car in Valencia, Spain’, Photochemistry and Photobiology, 94(2), pp. 390–397. Available at: https://doi.org/10.1111/php.12865.

Zaffina, S. et al. (2012) ‘Accidental Exposure to UV Radiation Produced by Germicidal Lamp: Case Report and Risk Assessment’, Photochemistry and Photobiology, 88(4), pp. 1001–1004. Available at: https://doi.org/10.1111/j.1751-1097.2012.01151.x.

Zamanian, Z. et al. (2015) ‘Assessment of Health Consequences of Steel Industry Welders’ Occupational Exposure to Ultraviolet Radiation.’, International Journal of Preventive Medicine, 6(1), p. 123. Available at: https://doi.org/10.4103/2008-7802.172379.

Zou, X. et al. (2014) ‘Photographic measurement of leaf angles in field crops’, Agricultural and Forest Meteorology, 184, pp. 137–146. Available at: https://doi.org/https://doi.org/10.1016/j.agrformet.2013.09.010.

Zulkit (2022) Zulkit Junction Box, Amazon Store. Available at: https://www.amazon.com/Zulkit-Waterproof-Electrical-Transparent-220x170x110/dp/B07RVN91WB?th=1 (Accessed: 31 May 2022).